MOTION AND WAVE LOAD ANALYSES OF LARGE OFFSHORE STRUCTURES AND SPECIAL VESSELS IN WAVES

A Thesis Submitted for the Degree of Doctor of Philosophy

by

Xiong-Jian Wu

Department of Mechanical Engineering
Brunel, The University of West London
Uxbridge, Middlesex UB8 3PH
United Kingdom

June 1990

TEXT
CUT OFF IN THE
ORIGINAL

To my Wife, my Children and my Parents

ABSTRACT

Predictions of the environmental loading and induced motional and structural responses are among the most important aspects in the overall design process of offshore structures and ships. In this thesis, attention is focused on the wave loads and excited bodily motion responses of large offshore structures and special vessels.

With the aim of improving the existing theoretical methods to provide techniques of theoretical effectiveness, computational efficiency, and engineering practicality in marine and offshore applications, the thesis concentrates upon describing fundamental and essential aspects in the physical phenomenon associated with wave-structure interactions and deriving new methods and techniques to analyse offshore structures and unconventional ships of practical interest.

The total wave force arising from such a wave-structural interaction is assumed to be a simple superposition of the potential and the viscous flow force components. The linear potential forces are solved by the Green function integral equation whilst the viscous forces are estimated based on the Morison's damping formula.

Forms of the Green function integral equation and the associated Green function are given systematically for various practical cases. The relevant two-dimensional versions are then derived by a transformation procedure. Techniques are developed to solve the integral equation numerically including the interior integral formulation and, in particular, to tackle the mathematical difficulties at irregular frequencies.

In applying the integral equations to solve problems with various offshore structures and special vessels, some modified, improved or simplified methods are proposed. At first, simplified method is derived for predictions of the surge, sway and yaw motions of elongated bodies of full sectional geometry or structures with shallow draft. Then, a new shallow draft theory is described for both three- and two-dimensional cases with inclusion of the finite draft effect. Furthermore, a three-dimensional strip method is formulated where the end effects of the body are fully taken into account. Finally, an approximation to the horizontal mean drift forces of multi-column offshore structures are presented.

Some new findings are also discussed including the multiple resonances occurring in the motions of multi-hulled marine structures due to the wave-body interaction, the mutual cancellation effect of the diffraction and the radiation forces arising from a full shaped slender body, and so on.

Further to those verification studies for individual methods developed, more comprehensive example investigations are given related to two industrial applications. One is a derrick barge semi-submersible with zero forward speed; and the other, a SWATH ship with considerable speed.

By correlation of all the proposed approaches with available analytical, numerical and experimental data, the thesis tries to demonstrate a principle that as long as principal physical aspects in the wave-structure interaction problem are properly treated, an appropriately modified or simplified method works, performs well and, sometimes, even better.

CONTENTS

1. INTRODUCTION

With the development of offshore operation and ocean exploration, the invention, design and construction of new ranges of unconventional shaped marine structures for both high workability and cost economy are largely demanded. The design of a new marine structure depends mainly on knowledge and experience gained from some complementary practice, i.e. model tests, theoretical analysis, field measurements and former design. construction and operation processes. To ensure safety, operability, economy and designed life duration of a marine structure to withstand specific ocean environmental effects (i.e. waves, winds, currents, seabed, beach, ice, neighbouring offshore structures or service vessels, etc.), theoretical estimates on motion responses and wave loads (which is called seakeeping analysis in naval architecture) play an increasingly important role in the overall design process. This trend is continuing as computer facilities and software packages with their increased capability become relatively less expensive to run whilst experimental facilities, model tests and labour costs appear more and more expensive and difficult to maintain.

In general, the body motion and wave loading analysis of large marine structures deals with the predictions of operational performance of such structures at a site in a seaway or undergoing sea transportation. This involves, for instance, rigid body motions, detailed fluid pressure distributions, resultant local shearing forces and global bending moments, extreme sea loads and motions, slamming and deck wetness associated with relative motions and velocities, accelerations and subjective motions with respect to crew and machinery performance, resultant forces on attached structures (e.g. pipeline stress, taut tension and mooring forces), etc. All of these individual aspects require a method to estimate the wave-structure interaction. Therefore, development, improvement and application of numerical techniques for analysing such an interaction becomes one of the daily activities of naval and offshore hydrodynamicists and other related researchers or

engineers.

There exist various marine and offshore structures designated for different tasks. In this thesis, however, attention is focused on interaction problems between waves and large offshore structures of complicated but realistic configurations possessing massive and full shaped floater(s) and/or multiple sub-members, e.g. a large mobile or fixed platform and a twin-hull vessel. The structures are either stationary, moving slowly or subject to current of low speed. Neither fast slender monohull ships and fixed framed platforms nor idealised geometries and topics of only pure mathematical interest will be cited. The waves and motions in this study are restricted, as is usually assumed in ordinary seakeeping analysis, to a range of low and intermediate frequencies. That is, it excludes high frequency problems, for example, those already covered by flexible mode oscillations in hydroelasticity (Bishop and Price 1979), earthquake induced responses (see OMAE 1986) and shock wave effects due to underwater explosions (Keil 1961). The sea is assumed of an infinite or intermediate depth to exclude the necessity of using a shallow water approximation.

1.1. General Review

1.1.1. Separation of force components

Generally speaking, in the interaction phenomenon between water waves and a large body of complicated configuration, the wave slope may be steep, the body motion excursion can be large and there may unavoidably exist flow separation, vorticity or breaking waves. Therefore, from a pure theoretical point of view the Navier-Stokes equation (Stokes 1951) for an incompressible fluid with constant viscosity seems most appropriate. Just like a rough sea obstructing the voyage of a ship the mathematical free-surface condition constantly produces an obstacle to the

development of a more sophisticated theory. The Navier-Stokes equation together with the com plicated free-surface and body boundary conditions (Wehausen and Laitone 1960) are too difficul to solve at present, and to my knowledge there is no published work so far implementing a full application of this approach to an interaction problem of waves and a real offshore structure. By using supercomputers and a tremendous amount of computing time, the Navier-Stokes equation was very recently investigated by Miyata and Nishimura (1985). This work, however, adopts an inconsistent treatment by ignoring the viscosity in the boundary conditions on the free-surface and the body surface and the approach may have a long way to go before it becomes readily available for engineering applications.

In the past to advance technology engineers and scientists set up principles of simplification which are widely used even today. One of these, the principle of linear superposition remains a key element in present advancements. According to Lighthill (1979,1986), Kelvin was the first who provided the principle of motion separation, which enables an analysis of the flow around a body into a linear superposition of

(a) *the potential flow satisfying the boundary conditions; and*

(b) *a residual vortex motion satisfying zero boundary conditions in infinity and the normal velocity on the body surface.*

Equivalent to an assumption of ignoring the cross-coupling terms between the potential flow and the vortex motion components, this principle provides one of the most basic foundations used in contemporary naval and offshore hydrodynamics, whether one realises it or not. Thus to obtain the total fluid loading F_{Tj} relating to the jth motion mode or direction, one needs only a careful evaluation of F_j, the potential flow force of (a) and a rough estimate of F_{vj}, the drag force of (b), i.e.

$$F_{Tj} = F_j + F_{vj} \tag{1.1}$$

The component potential flow (a) representing a full nonlinear potential flow problem (Longuet-Higgins and Cokelet 1976) is of great complexity and numerical techniques of practical use are still under development. To avoid such a direct solution, a perturbation procedure with respect to a small parameter ε (chosen as the wave slope) is used to derive systematically equations in various orders of ε (Peter and Stoker 1957, John 1949, Wehausen and Laitone 1960). The resultant first-order equations, involving a linearised free-surface condition, form the linear (or the first-order) diffraction theory formulation, whilst those in respect to order two construct the second-order diffraction problem (Ogilvie 1983) and so on. Consequently, the potential force in Equation (1.1) can be rewritten as a linear combination of potential force components in various order, that is,

$$F_j = F_j^{(1)} + F_j^{(2)} + \cdots + F_j^{(n)} + 0(\varepsilon^{n+1}) \tag{1.2}$$

Empirical formula for the drag force of (b) is available, known as the drag terms in the Morison equation due to the landmark contribution made by Morison, O'Brien, Johnson and Schaaf (1950). Alternatively, a more refined vortex method may be applied (see Stansby and Isaacson 1986). Thus, correct to the second-order, the total wave loading now takes the form

$$F_{Tj} = F_j^{(1)} + F_j^{(2)} + F_{vj} \tag{1.3}$$

1.1.2. Wave model

It is common practice to derive a water wave model from a potential theory governed by the Laplace equation and relevantboundary conditions. Various wave theories have been established including the sinusoidal (or infinitesimal, or small amplitude) wave theory, the Stokes finite amplitude wave theory, nonlinear shallow water wave theories of cnoidal, hyperbolic and solitary waves, and so on (see the review by Sarpakaya and Isaacson 1981). Among these, the sinusoidal wave (Airy 1845) is most relevant to this context due to its suitability in linear analysis and for

linear superposition in a modern spectral analysis.

Applying the statistical theory of noise in electronics by Rice (1944, 1945), Longuet-Higgens (1952) first introduced a spectral representation of an irregular sea by the sum of a large number of regular, sinusoidal waves. Moreover, a three-dimensional or multi-directional wave spectrum can also be modelled (St. Denis and Pierson 1953, Price and Bishop 1974). In engineering practice the phenomenon of wave-current interaction has been poorly understood except for the resultant frequency of encounter (see §4.9.3 in Sarpakaya and Isaacson 1981) and recent research activities are beginning to account for the current effect on a wave spectrum. Related works have been reported by Tung and Huang (1976), Mathiesen (1984), Sakai, Hirosue and Iwagaki (1981), etc., and a thorough review is given by Peregrine and Jonsson (1983).

Based on the spectral technique St. Denis and Pierson (1953) pioneered the probabilistic theory of ship motions which enables predictions of motions and wave loads on a marine structure in a real seaway to be derived from data relating to individual regular waves (also see Price and Bishop 1974). Therefore, concentration can now be focused on analysing solutions in regular waves only.

1.1.3. Force regime and validity of method

The real flow-body interaction is a rather complicated phenomenon changeable from condition to condition and any existing theoretical model may only be valid in a certain range of application. The validation of wave loading prediction methods have been discussed comprehensively by researchers with scientific backgrounds akin to ocean engineering, for example, Dean (1970), Hogben, Miller, Searle and Ward (1977) and Garrison (1978).

For the problem of a fixed circular cylinder in waves let us denote δ to represent the fluid particle orbit diameter, H the wave height, λ the wave length and D the typical member diameter.

A rough guideline describing the force regime is given by Standing, Dacunha and Matten (1981) and this is summarised as follows:

(i) *First-order forces*

(1a) drag dominant when $\delta /D > 1.0$, using estimation method for inertia and drag forces,

(1b) diffraction dominant when $D/\lambda > 0.2$, using diffraction theory,

(1c) inertia dominant when $\delta /D < 1.0$ and $D/\lambda < 0.2$, using either of the two methods as stated in (1a) and (1b).

(ii) *Mean second-order forces*

(2a) drag dominant when $(H/D)^3 > 60\,(H/\lambda)^2$,

(2b) diffraction dominant when $(D/\lambda)^3 > (1/60)\,(H/\lambda)$,

(2c) less clear when the first-order forces are inertia dominant as defined in (1c).

These rough conclusions, shedding some light on the fluid-structure fundamental problem, are shown diagrammatically in Figure 1.1 where the limit of occurrence of breaking waves is also indicated.

1.1.4. First-order forces and motions

Again, the principle of linear superposition enables the total wave potential solution to be determined by the linear summation of the incident wave, the diffraction wave due to the interference of the fixed body with the incident wave, the radiation wave with respect to each independent mode of the body oscillatory motions and a steady wave field if forward speed or current exists.

1.1.4a. Force and motion predictions

(i) *Methods for slender ships*

In the literature the Froude-Krylov theory was the first available linear theory to predict wave forces and the excited motions of a slender ship. This was developed by Froude, W. (1861), Froude, R.E. (1896) and Krylov (1896a, b). Their hypothesis assumed that the existence of the body does not change the incident wave field if the beam and draft of the body are both small compared with the wave length and this resulted in the so-called Froude-Krylov force due to the incident wave only. Today this simplified approach receives little research attention except its application by practical naval architects and offshore engineers for simple structures. It was very recently that Wu and Price (1986a, 1989) applied, and then proved, a similar idea to predict all the three horizontal modes of motion of either a long but full-shaped body or a shallow draft structure, other than the more restrictive slender ship forms (see §4).

The first strip theory pioneered by Korvin-Kroukovsky (1955), treating a whole ship as a number of two-dimensional strips and taking account of the diffraction effect by an artificial relative velocity concept, is one of the milestones in the development of modern seakeeping analysis though, nowadays, it has almost been replaced by more rigorous and more powerful new strip theories. Of these new strip methods, the STF method of Salvesen, Tuck and Faltinsen (1970) for slender ships, includes predictions of five rigid body motions with the exception of the surge; deals with the forward speed effect by the formulae of Ogilvie and Tuck (1969); satisfies the symmetric relations of the cross-coupling hydrodynamic coefficients proved by Timman and Newman (1962) and obtains the diffraction forces by the Haskind relationship (Newman 1965) in terms of radiation potential solutions from the close-fit method of Frank (1967). In spite of its critical high frequency assumption, theoretical predictions are generally in good agreement with model test data for slender ships. This technique has been extended by Beck and Troesch (1980) to exclude

the use of the Haskind relationship, by Lee (1976) to study SWATH ships (small waterplane area twin hull ships), by Wu and Price (1986b) for possible application to a drydock with zero forward speed in a semi-submerged condition, and so on. The lack of surge motion prediction in the method may be complemented by the Froude-Krylov hypothesis as used by Grim (1963) and proved by Wu and Price (1989).

In developing a strip theory it also necessitates the adoption of two geometric assumptions, i.e. the infinite length and negligible ends effect, but as pointed out by Ogilvie (1974) the ship ends cause many difficulties and this situation has not been thoroughly studied. It is particularly the case when offshore structures are considered, since, in most cases these have blunt ends. Furthermore, Ursell (1968) concluded that an infinitely long cylinder is not a satisfactory approximation to a ship of finite length in head seas. In a motion analysis, the strip theory may provide acceptable predictions for ships with low length/beam ratios down to L/B = 2.5 (p. 404, ITTC 1987). However, as far as the shearing forces and bending moments are concerned the STF strip method overestimates these loads for bodies with full-shaped ends because of the cumulative error contribution of sectional forces by the Haskind relationship (Ogilvie 1974). From a design point of view perhaps this does not matter since the predicted data are on the safe side, i.e. an over-estimate.

In addition, the STF strip method also assumes high frequencies and ignores, in the formulation, the free-surface integral due to the forward speed. These may lead to errors in the motion predictions for high speed vessels (e.g. the reported erroneous resonant heave response for a container ship by O'Dea and Jones, 1983). Nevertheless, new methods for ship motion analysis based on more sophisticated mathematical formulations do not usually seem to give much better results than the strip theory (Seakeeping Committee report, ITTC 1987) and the STF strip method remains the most popular used in the seakeeping analysis of ships.

A competitor to the STF approach is the unified slender body theory (Newman and Sclavounos 1980, Sclavounos 1984), which is exclusive of the high frequency limitation and devoid of the head sea singularity inherent in the diffraction problem of a strip theory (Ogilvie 1974). It seems that the unified slender body theory gives more accurate force estimates but no better motion predictions. Borresen and Faltinsen (1984) extended this approach to shallow water and found little improvement over the strip method. Another interesting extension of this slender body theory was made by Breit and Sclavounos (1986) to a twin-hull body.

(ii) *Methods for vertically-walled bodies*

Large circular cylinders are extensively used in offshore engineering, for example, offshore piles and columns of a platform. An analytic close form solution of first-order forces and moments for a free-surface piercing circular cylinder has been derived by Havelock (1940a) for deep water, by Omer and Hull (1949) for shallow water and by MacCamy and Fuchs (1954) in general cases. If a large spacing assumption (Milne-Thomson 1968, Okusu 1974) is further applied, wave forces for an array of multiple circular cylinders can be approximately formulated (McIver and Evans 1984) and exact expressions for these forces on such an array may be found by the method of Kagemoto and Yue (1986).

For a vertical body of arbitrary waterplane geometry, Hwang and Tuck (1970) presented a two-dimensional method to solve the diffraction force in the horizontal plane, which may be referred to as the two-dimensional horizontal plane method analogous to the two-dimensional vertical plane method in a strip theory. Furthermore, this approach is also applicable to a numerical solution of multiple vertical bodies of arbitrary waterline geometry (Isaacson 1978).

(iii) *Shallow draft theories*

Shallow draft bodies are very popular in offshore operations, for instance, barges (p.433-435, ITTC 1987), ocean production units, crane barges, and platforms. The shallow draft feature makes it possible to derive an effective and efficient shallow draft theory. Unfortunately, theoretical developments have lagged behind practical needs. The original shallow draft theory presented by MacCamy (1961) is a two-dimensional version and Kim (1963) extended it to three-dimensional cases. The body is idealised by a simple plate and this greatly reduces the computing time requirement. This original version, however, is unable to predict the horizontal motions of surge, sway and yaw and has no draft correction to take care of the effect of finite draft of a real shallow draft structure. Therefore, according to Odabasi and Hearn (1978), the application of this method is extremely limited and it has not been used for seakeeping analysis of displacement type vessels.

Very recently, a new shallow draft theory was proposed by Wu and Price (1986a), which includes a draft correction and is able to predict all the six rigid body motions. Full details of the method are given in §6.

(iv) *Three-dimensional approaches*

Three-dimensional diffraction analysis of motions and wave loads of realistic marine structures became available only when modern computers allowed full solutions of the three-dimensional hydrodynamic coefficients and wave exciting forces to be derived. In the field of numerical hydrodynamics, the panel collocation technique of Hess and Smith (1964) provided a major breakthrough by approximating the continuous body surface with a finite number of discretised flat panel element and replacing the governing equation by a set of simultaneous linear equations for each discrete panel which are readily solvable by matrix manipulation. Further to the constant panel technique, high order panel methods were subsequently developed (Hess 1973, 1980).

Various three-dimensional diffraction computer codes have been developed in the 1970s for structures with zero forward speed, see Garrison, Rao and Snider (1970), Faltinsen and Michelsen (1974), Hogben and Standing (1974), Ootmerssen (1976, 1979), Garrison (1978), Inglis and Price (1979, 1980). Alongside these singularity approaches, the finite element technique based methods (Zienkiewicz, Bettess and Kelly 1978) offer an alternative, especially in shallow water of varying seabed topography. Furthermore, hybrid approaches combining a close domain finite element representation and an outer region boundary integral idealisation have been developed (Yue, Chen and Mei 1978, Euvrard, Jami, Lenoir and Martin 1981, Eatock Taylor and Zietsman 1982). In this thesis, however, focus is limited to the singularity based methods only.

In the case of slender ships with forward speed, a three-dimensional motion theory is described by Chang (1977) whose numerical data, however, showed no remarkable improvement over the simple strip theory. The most comprehensive numerical investigation so far is found in the work of Inglis and Price (1982a, b) who also suggest the application of simplified formulae to tackle the forward speed effect similar to those in the strip theories. Such a simplification is further extended by Beukelman, Huijsmans and Keuning (1984) for a ship in shallow water. Closely related to the prediction of the second-order wave drift forces in a current, recently, two low speed approximations describing the behaviour of a full body in a current are proposed respectively by Huijsmans and Hermans (1985) and Zhao and Faltinsen (1988). Despite the existence of a large number of three-dimensional computational packages, so far, no theoretical complete numerical procedure for a full-shaped body with forward speed or/and under current is available.

1.1.4b. Wave potential solutions

To supply sufficient information to the motion and wave loads analysis methods as stated in 1.1.4a., the first-order boundary value problem governing the wave-structure interaction needs to

be solved. Analytical solutions can be derived for some simple geometries and these were of great interest in early years when modern computer facilities were not available. Nowadays, these solutions are of limited application when analysing realistic structures other than to provide useful guidelines to check updated numerical procedures or programs. However, numerical computation experience indicates that most of the existing computational packages produce satisfactory data for these simple and idealised bodies, but give results showing large discrepancies for realistic structures of complicated configuration (Eatock Taylor and Jefferys 1986).

Numerical solution methods fall mainly into three categories. Namely, the singularity approach (or the Green function integral equation method), the finite element technique and a combination method as mentioned in 1.1.4a. The first singularity technique developed is the two-dimensional multipole expansion method of Ursell (1949a, b) originally used to analyse the hydrodynamic behaviour of a circular cylinder in deep water. This was extended by Tasai (1959) and Porter (1960) incorporating a conformal mapping process to deal with more realistic ship sections and further extended by Wang and Wahab (1971) for the heave motion of twin circular cylinders. Such a solution technique is still adopted in the strip method program SCORES (Raff 1972). Accuracy of this approach largely relies upon the precision of mapping of a given cross-section into a perfect circle and difficulties arise when tackling complicated sectional forms (Takagi, Furukawa and Takagi 1983).

The current singularity distribution method can be expressed in three alternative forms, i.e. the source, the dipole and a mixed distribution (Yeung 1982). The dipole technique if in a double derivative form may be difficult to evaluate unless proper approximations are introduced (Colton and Kress 1983). The boundary integral equation are expressible in an exterior, surface or interior integral formulation correspondingly to the chosen field point located outside , on or inside the body surface. The surface and exterior integral equations are commonly used and a recent investi-

gation carried out by Wu (1987) suggests the applicability of the interior formulation.

It was Frank (1967) who provided the first source method program for the potential solution of arbitrary two-dimensional sections and known subsequently as the Frank's close-fit method. This was incorporated into the STF strip theory program (Salvesen, Tuck and Faltinsen 1970) for general motion and wave loading analysis of ships. In marine hydrodynamics the singularity distribution technique seems to be the most favourable solution method adopted. Since the 1970s, after the pioneering work of Hess and Smith (1964), research has focused on finding an efficient numerical formula for the three-dimensional Green function in order to reduce computational efforts. Various contributions have been made to the zero forward speed case by Kim (1965, 1966), Monacella (1966), Hogben and Standing (1974), Faltinsen and Michelsen (1974), Hearn (1977), Noblesse (1982), Endo (1983), Pidcock (1985), Newman (1985), Telste and Noblesse (1986). In the cases of an oscillating body with forward speed or in current, the Green function representing a pulsating, translating source (Wehausen and Laitone 1961, Chang 1977) is very complicated. Several alternative forms of numerical evaluation have been investigated, e.g. by Inglis and Price (1980) and Guevel and Bougis (1982). An urgent task remains to innovate a fast algorithm to evaluate this Green function.

For a generalisation to a full-shaped body but with a limitation of lower speeds, a fast algorithm was proposed by Huijsmans and Hermans (1985) and Huijsmans (1986). Their method is based on a non-rigorous expansion form of the forward speed Green function and the integral equation with respect to a small parameter, speed U, and the theory is correct to the order of O(U). In the solution the effect from the steady wave field (Eggers 1981, Brandsma and Hermans 1985) has been taken care of. Under a similar restriction, Zhao and Faltinsen (1988) use a more consistent model, remaining correct to order O(U), by matching a near field simple source distribution and far field multipoles of a simplified pulsating, translating source (Grekas 1981).

The development of a complete motion and wave loading analysis method, however, solely depends upon the availability of a complete solution technique for a full three-dimensional body with speed, i.e. neither the limitation of a slender body nor the restriction to low speeds. Such a theory and solution can be optimistically expected to emerge in the very near future.

More comprehensive reviews of the recent development of the first-order diffraction theories can be found by Ogilvie and Beck (1973), Odabasi and Hearn (1978), Newman (1983), the Seakeeping Committee Report of ITTC (1987) for the general motion and sea loading problems; Mei (1978) and Yeung (1982) for the numerical techniques available; and Sarpkaya and Isaacson (1981), Hogben, Miller, Searle and Ward (1977), Standing (1981) and the Ocean Engineering Committee Report of ITTC (1987) for more offshore related structures.

1.1.5. Second-order forces and motions

The second-order solution leads to the mean drift forces, forces due to frequency sum and forces due to frequency difference (Pinkster 1979, Standing and Dacunha 1982, Ogilvie 1983). As defined by the perturbation process corresponding to the incident wave amplitude (Wehausen and Laitone 1960) these second-order wave forces are an order smaller than the first-order ones and serve to complement them. However, these forces play very important roles in offshore practice, for example, the slowly varying drift forces due to frequency difference of waves cause low frequency resonances of a moored or guyed offshore structure in surge, sway and yaw or a small waterplane area vessel in heave, roll and pitch, whilst the rapidly varying forces due to frequency sum may excite high frequency resonances of a TLP in heave, roll and pitch.

The second-order forces are attributed to two kinds of contributions, namely,

(i) products of first-order quantities from the first-order potential and motion solutions (§1.1.4), and

(ii) the second-order potential solutions.

1.1.5a. Mean drift forces

In a time average, components (i) give rise to the mean drift forces whilst component (ii) gives simple set-down forces in the vertical plane but no contribution in the horizontal plane. To this problem Maruo (1960) and Newman (1967) have made important contributions. The mean wave drift forces and moment can be estimated by either a near field approach (Pinkster 1979) or a far field one as described by Newman (1967) for the deep water case and by Faltinsen and Michelsen (1974) for shallow water. As far as large offshore platforms are concerned both of the these approaches are computing time consuming. Since these forces are closely related to the design of the mooring or dynamic positioning systems applied to offshore structures, an engineering estimation method rather than complicated mathematical proof is urgently required. This promoted a joint project undertaken by several Dutch offshore companies and research organisations to develop a practical prediction technique for the calculation of the mean drift forces on semi-submersibles and some preliminary results were reported by Angwin (1986).

1.1.5b. Sum frequency forces

Superharmonic resonances of TLPs at frequencies double or triple the frequency of the incident wave have been confirmed in model tests (Yoneya and Yoshita 1983, Pinkster and Boom 1983). In regular waves, the two-dimensional double frequency problem has been studies by Lee (1968), Potash (1971), Papanikolau (1984) for radiation problems, and by Soding (1976), Kyozuka (1982), Miao and Liu (1986) for diffraction problems. In solving the second-order diffraction potential, besides the treatment of the inhomogeneous free-surface condition, difficulties exist to find a proper radiation condition. For the three-dimensional second-order diffraction potential solution, Molin (1979, 1986) presented a more complete analysis and

proposed a likely form of the radiation condition. For a free-surface piercing circular cylinder, recent studies are reported by Qiu and Wang (1986), Eatock Taylor and Hung (1987) and Liu (1988). In regular waves, sum frequency wave forces have been investigated by Loken (1986) and Hertjard and Nielsen (1986).

1.1.5c. Difference frequency forces

In irregular waves, both components (i) and (ii) (p.11) contribute to the slowly varying drift forces (also to the sum frequency forces) inducing slow drift motions of a moored structure. This is of major concern in offshore operations and a large number of studies have been reported, e.g. by Hau and Blenkarn (1970), Remery and Hermans (1971), Newman (1974), Ootmerssen (1976), Faltinsen and Loken (1978, 1979) and Standing and Dacunha (1982). Pinkster (1979) conducted a comprehensive investigation on slow drift forces and motions of three-dimensional bodies and presented related formulations as well as experimental verifications. A thorough review can be found in Standing, Dacunha and Matten (1981).

A full evaluation of the slow drift force is a troublesome task because it requires the second-order potential solution of which general solution methods are still under development, as discussed in 1.1.5b. To overcome this difficulty, Lighthill (1979) derived a very useful formula expressing the total second-order force in terms of first-order quantities by making use of Green's theorem and Haskind reciprocal relations. Lighthill's formula involves an integral over the entire free-surface and usually some approximation is required for its evaluation. An exact application of this approach was achieved by Matsui (1986) who also proposed an approximation to ignore the free-surface integral. A comparison of his results with various approximate methods of Bowers (1976), Newman (1974) and Pinkster (1979) seems encouraging, at least for the example of an articulated cylinder.

It is particularly worthwhile mentioning Newman's approximation (1974). This much simplified approach needs only the calculation of the mean drift forces in regular waves, requires much less computing time and results in predictions of slow drift force and motion of acceptable accuracy (Nass 1986) in practical problems. Therefore, this simplified method is widely used in offshore engineering, especially, when today's numerical techniques and experimental measurements for the slow drift forces show some degree of uncertainty.

When slow drift resonant motion occurs, fluid damping (including the contributions of wave damping, frictional damping and viscous damping due to drag) plays a significant role. But at low frequencies the first-order wave damping is nearly zero, the frictional term is small and the drag force proportional to the square of the frequency is small, too. Thus, a damping term significant to the slow drift motion was identified as the second-order low frequency wave damping (Wickers and Sluij 1979, Wickers 1982). This damping value was formulated by Wickers and Huijsmans (1984) exclusive of current and by Wickers (1986) inclusive of current as the derivative of the mean horizontal drift force with respect to the moving speed. This formula was also applied by Hearn, Tong and Lau (1978), but confusingly they showed that a much more sophisticated three-dimensional forward speed approach produced much poorer results.

The conventional slow drift motion theories as described above contain theoretical weaknesses. First of all, the theory is inconsistent since the large excursion of the slow motion is contradictory to the small motion amplitudes assumption necessary in the perturbation procedure in order to decompose the first- and the second-order quantities. Secondly, the additionally introduced low frequency damping contribution may be an indication of the incompleteness of the current slow drift motion analysis. A possible consistent theory has been studied by Triantafyllou (1982) who suggests that the slow motion potential is of first-order and satisfies linear boundary conditions.

1.1.6. Full nonlinear potential analysis

The powerful small amplitude perturbation method may be invalid when dealing with steep waves, in particular, when breaking waves appear. These may necessitate a full nonlinear potential flow analysis. A finite difference time stepping procedure coupled with the boundary element method solution is currently under development for time domain analysis of a steep wave-large body interaction. This technique was first adopted by Longuet-Higgins and Cokelet (1976), followed by Faltinsen (1977) in two-dimensional cases and by Isaacson (1982) in three-dimensional problems. Lin, Newman and Yue (1984) paid particular emphasis on handling two principal difficulties. One is the singular flow at the intersection of the body and the free-surface and the other, to find an appropriate radiation condition at infinity. Although it seems to be a much simpler approach compared to Miyata and Nishimura's nonlinear viscous flow model (1985) the technique is still so complicated that there is no reported engineering application in offshore structures other than to a simple circular cylinder.

1.1.7. Drag forces

The separated flow component (b) (§1.1.1) of a residual vortex motion around an arbitrary body should satisfy the free-surface and the oscillatory body boundary condition (or transformed to a reverse problem of a fixed body in an oscillatory flow). Solution of this problem is very difficult to obtain and considerable efforts have been made to develop a numerical model of vortex flow and drag due to eddy making. Good progress has been achieved mainly in simple two-dimensional cases particularly in the vortex flow around circular cylinders (Leonard 1980, Sarpakaya and Isaacson 1981, the Ocean Engineering Committee Report of ITTC 1987). For two-dimensional ship sections Ikeda and Tanaka (1983) proposed a discrete vortex method which is also applied by Muller (1985) for cross-sections with bilge keel and by Downie, Bearman and

Graham (1984) for rectangular barge sections. Alternatively Aarsenes, Faltinsen and Pettersen (1985) present a vortex tracking method for ship sections.

Where the drag force due to viscosity is concerned, little else can be offered to practical engineers and designers beyond the routine estimation tools obtained from Morison equation. Morison, O'Brien, Johnson and Schaaf's formula (1950) is based on experimental measurements of a circular cylinder in an oscillatory flow and separates the total force into two independent components, i.e. an inertia and a drag force. The inertia coefficient C_M and drag coefficient C_D are dependent on both the Reynolds number (Re) and the Keulegan-Carpenter number ($Kc = U_m T/D$ with U_m denoting the amplitude of the velocity, T, the flow period and D, the diameter) but are always set down as constant values in design applications as suggested by classification societies for simple geometries (e.g. Bureau Veritas 1975).

Since the members of most semi-submersibles fall into the inertia or drag force dominant regime, the Morison equation method is theoretically reasonable to predict motion responses and wave loads of semi-submersibles (Hooft 1971) and the taut tension and motions of TLPs (Yoneya and Yoshita 1983). The accuracy of this simple technique is further confirmed in an international investigation by Takagi et al (1985). For large offshore structures and unconventional vessels with massive underwater floaters, the wave diffraction effect is of significance taking care of the interaction between multiple large sub-members but the Morison drag forces are also of certain importance, especially, when resonant motions occur (Lee 1976, Wu and Price 1986c).

In conclusion, the linear combination of more accurately described potential forces derived from a sophisticated diffraction analysis (§1.1.4-5) and rough estimates of drag forces from Morison equation (§1.1.7) with appropriate C_D values corresponding to structural geometry may be appropriate practically when describing the dynamic behaviour of large offshore structures and unconventional vessels, especially in our present stage of technological development, as

discussed by Lighthill (1979, 1986), see §1.1.1.

1.2. Existing Problems

As can be seen from the brief review describing the motion and wave loading analysis in §1.1, in the last forty years, great efforts have been spent and good progress achieved in deriving numerical solutions of problems mathematically formulated in the 1940s or so (e.g. Kochin 1939, Havelock 1940b, John 1950, etc) and also in the practical implementation of these numerical techniques to solve problems arising in naval and offshore practice. However, much work remains to be done.

1.2.1. Uncertainty in numerical investigations

It is not uncommon to find in the naval literature descriptions of numerical methods relating to the evaluation of hydrodynamic coefficients, wave loads and motion responses supplemented by mathematical derivations displaying the rigour of the methods as well as examples illustrating the validity and advantage of the approach proposed. It is quite often that bodies of simple or analytically defined geometries are selected for example calculations in order to verify a theory and very few presentations include comments on the troubles of implementation, practicality of the method to more complicated structures, deviation of solutions, limitations and even failure of the methods. In recent years such problems have attracted great attention and both individual and organised investigations have been reported.

In computing hydrodynamic coefficients Berhault (1978) found big differences among different numerical techniques used. From the ITTC organised investigation into a semi-submersible, Takagi et al (1985) reported that results provided by individual investigators show

(i) similar results for surge and sway motions and these are in good agreement with experimental data (reasoning may be found in §5),

(ii) great scatter around the heave resonant frequency; in particular, data derived from a three-dimensional diffraction theory are not necessarily better than the simplest Morison equation,

(iii) poor agreement of roll and pitch response in long wave periods, especially, around the natural periods.

Moreover, Eatock Taylor and Jefferys (1986) summarised the ISSC organised studies on a TLP and revealed severe discrepancies in the data generated by various methods and programs. It is also interesting to observe that the predicted surge, sway and yaw responses are again in reasonable correlation despite serious variations in relative added mass data, e.g. the ratio of the largest and the smallest values of the surge added mass surprisingly exceeds 1.7.

Besides the objective complexity of the flow phenomenon, avoidable human error and unavoidable factors in numerical treatment and in computational programming, all these comparative studies bear evidence of uncertainties in our theoretical approaches and imply that our so-called exact solutions or sophisticated theories are merely approximations to the real physical phenomenon, similar to simplified techniques, though at different levels of sophistication. Large offshore structures and unconventional vessels are physical objects of great complexity and the flow regime associated with the body-structure interaction of interest seems partially or totally beyond the diffraction dominated regime. Therefore, the argument of Paulling (1981) stands that

it is unlikely that a single unified computational procedure can be developed to satisfactorily treat all aspects of the response. In stead, a menu of programmes must be assembled to treat the various members and types of forces.

1.2.2. Uncertainties over theoretical approach

The following discussions give prominence to some areas which appear to hide weaknesses in our theories. The list is not complete but the topics discussed are of special concern and interest.

1.2.2a. Fluid damping

To determine the resonant motion response a more precise theoretical prediction or estimation of the fluid damping is essential. This consists of various contributions (see p. 492-495, ITTC Report 1987) of which the wave damping due to radiation waves and the drag damping due to vorticity may usually be two major components. For a lightly damped mode like the roll motion of a ship and motion resonances at low frequency in offshore structures, fluid damping due to drag (§1.1.7) is considerably important but more accurate techniques remain under development. Furthermore, the resonant motion amplitude is large and the force arising through the coupling between the potential flow (a) and vortex motion (b) (§1.1.1) is likely to have significant effect, too. There is no available theoretical method to evaluate this contribution except to solve directly the extremely complicated Navier-Stokes equation.

Because of theoretical difficulties, sometimes, measured damping coefficients are used to gain the required accuracy in the resonant motion predictions, for example, the roll damping of ships (Mathiesen 1988), a fast container ship (O'Dea and Jones 1983) and a small waterplane area vessel (Smith 1983).

1.2.2b. Theory of uniqueness

Before commencing the application of the wave-body interaction theories (§1.1), a primary pre requisite is the establishment of a uniqueness proof. For a linearised three-dimensional wave-body interaction problem in a finite water depth John (1950) proved uniqueness when

applying the Green function integral equation to any floating body embodied by a vertical bound through its waterline. In the two-dimensional deep water case Ursell (1950) proved uniqueness for a submerged circular cylinder. Recently, Simon and Ursell (1984) tried to find the uniqueness for a two-dimensional floating body in deep water confined by a conical bound through its waterline points up to an angle 45^o away from the vertical. Regrettably, no generalisation of the uniqueness proof has so far been derived. Of course, the geometries of large offshore structures and unconventional vessels are outside the bounds of these existing uniqueness proofs and therefore, we are in fact applying linear diffraction theories by Green function integral methods with the presumed existence of uniqueness proof.

1.1.2c. Mathematical problem in singularity methods

(i) *Irregular frequency problem*

The singularity methods are the most popular in use to solve linear wave-body interaction problems but these techniques suffer from mathematical failure at discrete irregular frequencies (John 1950). These irregular frequencies distributed in the high frequency range cause erroneous results for predicted data at frequencies, especially in a second-order analysis and in a hydroelastic modelling.

Great attention has been paid to eliminate this difficulty and various solutions are proposed (see §4). Of these Ursell's two-dimensional multipole potential solution is of significance (1981). In principle, Ursell's solution is applicable to three-dimensional cases and an alternative form is proposed in §4 . Wu and Price (1986d,1987) proposed an alternative Green function form which was shown capable of removing the irregular frequencies from arbitrary mono-, twin- and multihulled sections.

(ii) *Intersecting angle problem*

The second problem arises at the points of intersection when a concaved body intersects the free-surface at a small angle since there exist a logarithmic singularity (Haraguchi and Ohmatsu 1983). This singularity may be eliminated by suitable practical modifications. For this Haraguchi and Ohmatsu (1983) adopted additional elements on the free-surface connected with the intersecting points and found the treatment effective for a circular section at various draft values.

From the physical point of view, it is inappropriate to apply a linear wave theory to a very shallow layer of flow above the body wall slope because the problem appears to be highly non-linear and thus verification may rely on comparisons with experimental data only. After a comparative study with model tests Takagi, Kurukawa and Takagi (1983) revealed that Haraguchi's computational results considerably differ from the experimental measurements, and a modified Green function technique incorporating a slightly changed geometry by substituting the intersecting part with a small arc may give more satisfactory answers.

(iii) *Ill-conditioning problem*

In solving the Green function integral equation additional ill-conditioning frequencies have been found apart from the two identified groups, i.e. the resonant frequencies due to the exterior water waves and the irregular frequencies related to the interior problem. The reasoning is not clear so far and it is most likely that there exists a third kind of ill-conditioning frequency of theoretical and numerical interest.

1.2.3. Numerical convergence and error estimate

In the application of a singularity method in a discretised integral equation form, the global solution errors may come from the following major sources:

(i) error due to panel discretisation,

(ii) error due to evaluation of the kernel function integrals, and

(iii) error due to solution of the matrix equation,

besides the human errors arising from numerical manipulation and computer programming.

In numerical mathematics, convergence problems and asymptotic error estimates for the Fredholm integral equation of the second kind have been developed, for instance, by Wendland (1983), Arnold and Wendland (1983) and Delves and Walsh (1974). Although numerous contributions applying the singularity techniques are published every year, parallel approaches have not been established in the naval field. Perhaps this is of secondary importance since there is no uniqueness proof as well.

For a smoothly-shaped body with no sharp angle at the intersection with the free-surface or a body in deep submergence a uniqueness proof is available and coincidently, rapid numerical convergence can readily be achieved and good agreement is always shown by the various equivalent computer codes. On the contrary, no uniqueness theory exists to cover complicated geometries, such as a TLP and a semi-submersible, and correspondingly no good correlation can be observed in the data resulting from the different computer programs.

Apart from a smoothly shaped body or a ship form it looks unlikely that there exists a general formula to guide panel discretisation in order to achieve rapid convergence and to ensure small error in the solution. It should be emphasised that a body may possess multiple geometric singularities, e.g. at corners and sharp joints, where the potential solutions tend to infinity. Panel arrangement around these region may have significant influences and solutions by very fine meshes do not necessarily create improvements. Contrarily, distribution of larger panels neighbouring these singular lines or a simple replacement of these by small arcs are likely to result in

reasonable answers.

1.3. Research Activities and Design Needs

In naval and offshore hydrodynamics research, theoretical developments maybe fall into three categories:

(i) sophisticated and complicated theories of more academic interest but with less practical applications,

(ii) simple engineering methods seemingly less scientific but readily accessible to practical engineers and designers, and

(iii) various degrees of simplified approaches having not only a theoretical basis but also of practical merit; this is achieved either by modifying complicated theories and/or from initiative development or experimental observation.

All these complementary approaches play their respective roles in promoting marine technology.

Investigations into rigorous theoretical models usually aim to gain better understanding of a phenomenon, to find new problems of interest, to check the relative influence or range of importance of factors neglected in a simpler method and to serve practical engineers with theoretical back-up. But a complicated approach is not necessarily more accurate than a simplified one because of the impossibility to perfectly match the realistic physical phenomenon, unimportance of ignored factors or the mutual error cancellation occurring in a simplified technique. As can be seen from the state of the art of the existing technology (§1.1), the contributions likely to be regarded as milestones or breakthroughs are unexceptionally simple, practical but creative. Eventually, for practical applications, the complexity of the theory, the accuracy of results and the cost

of use should be appropriate to its degree of importance or rating in a total design process. In other words, the ultimate version of our theoretical development must suit practical needs. To bridge the more sophisticated and academic theories and the more practicable and affordable techniques much demanded by industries, the key is simplification.

An ingenious concept of simplification may greatly reduce the time and effort from a research development to engineering applications as shown in Figure 1.2. If theoreticians would pay greater attention to tackle the problems of primary importance and with more physical sense, and engineering researchers could devote more efforts to creative work towards mathematical simplicity, numerical accuracy and high practicality, the difficulties existing in our field may be solved much faster.

1.4. Outline of the Thesis

In Chapter 2, the general potential solution problem for a marine structure advancing in waves is described and general formulations of the first-order motions and wave forces resulting from the linearised unsteady potential solutions are described.

In Chapter 3, a general form of the Green function representing a pulsating, translating source relating to the linearised general problem is given and reduced versions for various special cases are deduced systematically. By a transformation formula relevant two-dimensional forms can readily be derived.

In Chapter 4, a brief description of the integral equations corresponding to a singularity distribution is presented and a detailed discussion is focused on the Green function integral equation representing a mixed source-dipole distribution method. The difficulties due to irregular frequencies in applying the integral equations are discussed and two remedy techniques proposed. One is to predict the irregular frequencies more accurately and then to avoid numerical computations

around these frequency values. The other, to use modified Green functions free of irregular frequencies. Although a Green function integral equation has three forms depending whether the field point lies exterior to, on or interior to the body's wetted surface, the interior formulation has never been used to produce velocity potential solution for marine structures. In the final part of this Chapter, a numerical method and its theoretical basis are described, applying the interior integral equation effectively.

In Chapter 5, new results describing the mutual cancellation effect between the diffraction and radiation forces are reported. By an order analysis it is proved that all the three horizontal motions of a structure can be reasonably predicted by simply ignoring both the diffraction and radiation forces and leaving only the Froude-Krylov force as long as the body is elongated but with full sectional shape, and/or is of shallow draft feature.

Shallow draft structures are further investigated in Chapter 6. In terms of a perturbation procedure, new shallow draft theory formulations are derived. For the three horizontal motion modes, this analysis confirms the conclusion drawn in Chapter 5. As to the heave, roll and pitch modes, the new formulae retain the simplicity of the flat plate theory but enable a finite draft correction to be included.

With the aim of reducing the matrix size involved in the numerical solution of a three-dimensional hydrodynamic analysis, in Chapter 7 a hybrid three-dimensional strip method is proposed. Its feasibility in practical applications is further investigated by a series of studies involving three rectangular cylinders of different length to beam ratio.

In Chapter 8, the predictions of second-order mean drift forces are studied. At first, a numerical procedure based on the near field formulations of the mean drift forces and the horizontal plane method for the diffraction potential solution is described to determine exact theoretical values of the horizontal mean drift forces on multiple vertical cylinders. Then, it is further applied

to approximate those acting on offshore structures comprising of large multi-columns or -struts. Finally, examples are given for a semi-submersible and a tension leg platform.

Chapter 9 includes descriptions of two computer codes based on comprehensive application of the motion theories developed. The first method combines the three-dimensional diffraction theory and an estimation of the drag force, which is appropriate to analyse large offshore structures of more complicated configuration. The other, the two-dimensional strip formulation together with an estimation of the drag and lift forces, which is suitable to predict the seakeeping performance of multi-hulled vessels, such as SWATH ships. Example studies of a semi-submersible and a tension leg platform demonstrate how theoretical development can be successfully applied to the process of research and development or design of more complicated large offshore structures and special vessels.

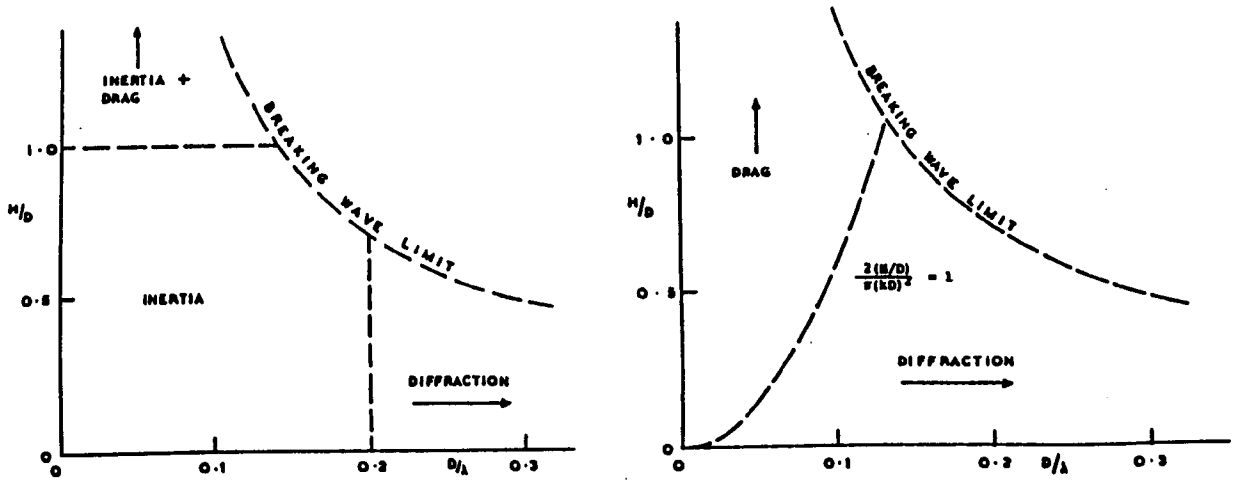

(a) First-order force (b) Mean second-order force

Figure 1.1. Force regime for a fixed vertical cylinder (Standing et al 1981)

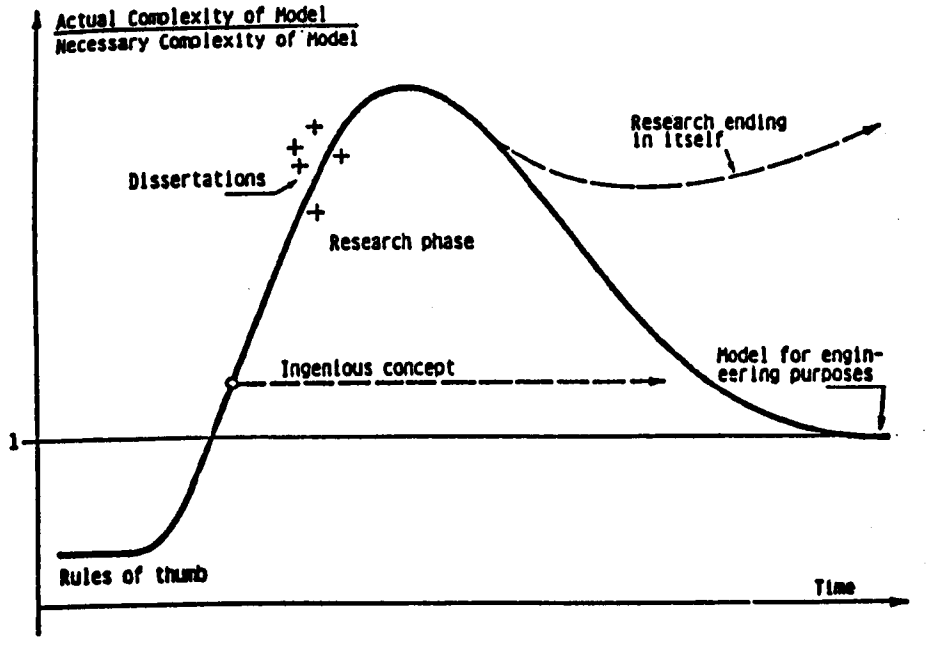

Figure 1.2. The research progress (quoted from "Some notes on engineering science with a view to future ship technology", by O. Krappinger, Hamburg).

2. GENERAL PROBLEM

As discussed in §1.1.1, to avoid any unnecessary complexity in solving the Navier-Stokes equation with the imposed rather complicated boundary conditions, Kelvin's principle of linear superposition of a potential flow and a vortex motion component can be used (Lighthill 1979, 1986). It requires only two independent analyses, i.e. a more sophisticated potential flow solution and a crude drag force estimate. Therefore, the major focus is now concentrated on the potential theory analysis of wave-body interaction problems.

2.1. The General Potential Solution Problem

The water flow is assumed incompressible, invicid and irrotational and the marine structure is of arbitrary geometry, floating in the free-surface. An uniqueness solution of the flow motion is also assumed since there exist no general uniqueness theorem as reviewed briefly in §1.2.2.

In the analysis four coordinate systems are chosen such that

$$\vec{r}_o = (x_o, y_o, z_o), \quad \textit{fixed in space};$$

$$\vec{r}' = (x', y', z'), \quad \textit{fixed in the body};$$

$$\vec{\bar{r}} = (\bar{x}, \bar{y}, \bar{z}) = (x_o - Ut, y_o - Vt, z_o)$$

steadily translating with velocity

$$\vec{W}_o = (U, V, 0) = (W_o \cos\alpha, W_o \sin\alpha, 0)$$

with $\bar{x}$ coincident with the body axis;

$$\vec{r} = (x, y, z) = (x_o - W_o t, y_o, z_o) = (\bar{x}\cos\alpha + \bar{y}\sin\alpha, -\bar{x}\sin\alpha + \bar{y}\cos\alpha, \bar{z})$$

similar to $\vec{\bar{r}}$ but with x axis coincident with the composite velocity $\vec{W}_o$.

The axes z_o, $\bar{z}$, z and z' (when no angular motion) are upwards and origins $\bar{O}$, O and O' are at the same location on the undisturbed free-surface, see Figure 2.1.

The flow velocity potential Φ satisfies the Laplace equation in the steadily moving reference frame Oxyz:

$$\nabla^2 \Phi(x, y, z; t) = 0 \quad \textit{in the fluid domain } D \tag{2.1.1}$$

The fluid pressure derived from the Bernoulli equation is

$$p = -\rho \left[D\Phi/Dt + gz + \frac{1}{2}(\nabla\Phi \cdot \nabla\Phi) \right] \tag{2.1.2}$$

with $D/Dt = \partial/\partial t + \nabla\Phi \cdot \nabla$.

On the free-surface p = 0 and the wave elevation $\zeta(x, y; t)$ is given by

$$z = \zeta(x, y; t) = -\frac{1}{g}\left[D\Phi/Dt + \frac{1}{2}(\nabla\Phi \cdot \nabla\Phi) \right]_{z=\zeta} \tag{2.1.3}$$

On the boundary interfaces the kinematic conditions are given by

$$(\vec{V}_s - \nabla\Phi) \cdot \vec{n} = 0 \quad \textit{on } S_w(x, y, z; t), \textit{ the body wetted surface} \tag{2.1.4}$$

$$\frac{D}{Dt}(\zeta - z) = 0 \quad \textit{on } z = \zeta(x, y; t) \tag{2.1.5}$$

where $\vec{V}_s$ is the local velocity on S_w and $\vec{n}$ is the unit normal pointing into the fluid.

In terms of the conditions represented by Equations (2.1.3) and (2.1.5) the free-surface condition is derived as

$$D^2\Phi/Dt^2 + 2\nabla\Phi \cdot D\Phi/Dt + \frac{1}{2}\nabla\Phi \cdot \nabla(\nabla\Phi \cdot \nabla\Phi) + g\partial\Phi/\partial z = 0 \quad \textit{on } z = \zeta(x, y; t) \tag{2.1.6}$$

By rearranging Equation (2.1.4), the body surface condition can be rewritten as

$$\partial\Phi/\partial n = \vec{n} \cdot (\nabla\Phi - \vec{W}_o) \quad \textit{on } S_w(x, y, z; t) \tag{2.1.7}$$

For simplicity, the seabed topography is taken as level and flat, i.e. the water is assumed of uniform depth, d, or deep ($d = \infty$). Thus, the seabed condition is now written as

$$\partial\Phi/\partial z = 0 \quad \textit{on } z = d \tag{2.1.8}$$

In addition, a radiation condition is required to guarantee an unique solution of this boundary value problem but its correct form is not known. In practice, as an approximation, use is

made of the Sommerfeld condition adopted in linear potential problems.

Application of such a nonlinear set of equations is rather difficult and may be limited to zero forward speed cases (e.g. Isaacson 1982), but more success has been achieved when a linearised set of equations is considered.

2.2. Linearisation of the Unsteady Wave Potential

At first the total wave potential is assumed to be the sum of the steady wave potential component Φ_s and the unsteady one Φ_u, i.e.

$$\Phi = \Phi_s + \Phi_u \tag{2.2.1}$$

To make the problem more tractable, a perturbation procedure can always be used under the assumption that the steady wave elevation and the body oscillatory motion are both small. Therefore, relative physical and geometrical quantities can be expressed in a series of expansion form with respect to a small parameter ε, chosen as the wave steepness say, e.g.

$$\Phi_u = \sum_{n=0}^{\infty} \Phi^{(n)}, \quad \zeta_u = \sum_{n=0}^{\infty} \zeta^{(n)}, \quad etc.$$

(see Wehausen and Laitone 1960). Hence, correct to order ε^3, the total potential is given by

$$\Phi = \Phi_s + \Phi^{(1)} + \Phi^{(2)} + O(\varepsilon^3) \tag{2.2.2}$$

The first order unsteady potential can be derived by the following conditions (Newman 1978):

(A) Laplace equation

$$\nabla^2 \Phi^{(1)} = 0 \quad \textit{in the fluid domain } D^{(1)} \tag{2.2.3}$$

(B) the free-surface condition

$$-(\Phi_t^{(1)} + \vec{W}\cdot\nabla\Phi^{(1)})[\frac{1}{2}\frac{\partial}{\partial z}(\vec{W}\cdot\nabla W^2) + g\Phi_{zz}]/(g + \vec{W}\cdot\frac{\partial}{\partial z}\vec{W}] + \Phi_{tt}^{(1)}$$

$$+2\vec{W}\cdot\nabla\Phi_t^{(1)}+\vec{W}\cdot\nabla(\vec{W}\cdot\nabla\Phi_t^{(1)})+\frac{1}{2}\nabla\Phi^{(1)}\cdot\nabla(W^2)+g\Phi_z^{(1)}=0 \quad on\ z=\zeta_s \tag{2.2.4}$$

(C) the body surface condition

$$\partial\Phi^{(1)}/\partial n=[\dot{\vec{x}}+(\vec{W}\cdot\nabla)\vec{x}-(\vec{x}\cdot\nabla)\vec{w}]\cdot\vec{n} \quad on\ S_w^{(1)} \tag{2.2.5}$$

(D) the seabed condition

$$\partial\Phi^{(1)}/\partial z=0 \quad on\ z=-d \tag{2.2.6}$$

and a radiation condition.

The total free-surface elevation is now of the form

$$\zeta=-\frac{1}{g}[\Phi_t^{(1)}+\frac{1}{2}(W^2-W_o^2)+\vec{W}\cdot\nabla\Phi^{(1)}]_{z=\zeta} \tag{2.2.7}$$

Here $\vec{x}$ is the body replacement vector in the form

$$\vec{x}=(x_1, x_2, x_3)+(x_4, x_5, x_6)\times(\vec{r}-\vec{r}_G) \tag{2.2.8}$$

where (x_1, x_2, x_3) and (x_4, x_5, x_6) denote the unsteady translation and rotation components of the body. The relative velocity vector is given by

$$\vec{W}=\nabla\Phi_s=\nabla(\phi_s-W_o x) \tag{2.2.9}$$

Here the steady wave potential includes the first-order unsteady wave effect and it satisfies the following equations:

(a) the Laplace equation

$$\nabla\phi_s=0 \quad in\ the\ fluid\ domain \tag{2.2.10}$$

(b) the free-surface condition

$$\frac{1}{2}\vec{W}\cdot\nabla(W^2)+g\phi_{sz}+\Phi_{tt}^{(1)}+2\vec{W}\cdot\nabla\Phi_t^{(1)}+\vec{W}\cdot\nabla(\vec{W}\cdot\nabla\Phi^{(1)})$$

$$+\frac{1}{2}\nabla\Phi^{(1)}\cdot\nabla(W^2)+g\Phi_z^{(1)}=0 \quad on\ z=\zeta \tag{2.2.11a}$$

or

$$\frac{1}{2}\vec{W}\cdot\nabla(W^2)+g\phi_{sz}=0 \quad on\ z=\zeta \tag{2.2.11b}$$

(c) the body surface condition

$$\vec{W}\cdot\vec{n} = 0 \quad or \quad \partial\phi_s/\partial n = W_o n_1 \quad on\ S_s,\ the\ body\ steady\text{-}state\ position \tag{2.2.12}$$

and the seabed condition and a radiation condition.

The steady free-surface elevation component is

$$\zeta_s = -\frac{1}{2g}\,(W^2 - W_o^2)_{z=\zeta_s} \tag{2.2.13}$$

The combination of Equations (2.2.7) and (2.2.13) results in the total wave elevation as given by

$$\zeta = \zeta_s - [(\Phi_I^{(1)} + \vec{W}\cdot\nabla\Phi^{(1)})/(g + \vec{W}\cdot\partial\vec{W}/\partial z)]_{z=\zeta_s} \tag{2.2.14}$$

This linearisation validates a further linear decomposition of the total first-order unsteady wave potential as

$$\Phi^{(1)} = \phi\ exp\,(-i\omega_e t) = (\phi_0 + \phi_7 + \sum_{j=1}^{6} X_{ja}\phi_j)\ exp\,(-i\omega_e t) \tag{2.2.15}$$

where ϕ_0 is the incident wave potential expressible in

$$\phi_0 = -\frac{ig\zeta_a}{\omega_0}\,Z(z)\ exp\,[ik(x\cos\beta + y\sin\beta)] \tag{2.2.16}$$

Here ω_o denotes the wave frequency, ζ_a the wave amplitude, β the wave incident angle ($\beta = 180^o$ indicating head seas), and

$$Z(z) = \begin{cases} exp\,(k_o z) & d = \infty \\ \cosh\, k(z+d)/cosh\ kd & d < \infty \end{cases} \tag{2.2.17}$$

The wave number k is determined by

$$\nu = \frac{\omega_o^2}{g} = \begin{cases} k & d = \infty \\ k\tanh kd & d < \infty \end{cases} \tag{2.2.18}$$

and the wave encounter frequency is defined as

$$\omega_e = \omega_o - kW_o\cos\beta \tag{2.2.19}$$

The diffraction potential ϕ_7 satisfies the body surface condition

$$\frac{\partial}{\partial n}(\phi_0 + \phi_7) = 0 \quad on\ S_w^{(1)} \tag{2.2.20}$$

The radiation potentials ϕ_j (j = 1, 2,..., 6) are due to bodily oscillatory motion of unit amplitude in the six degrees of freedom of the rigid body motions, i.e. surge, sway, heave, roll, pitch and yaw respectively. Each component satisfies the body surface condition

$$\partial\phi_j/\partial n = -i\omega_e n_j + W_o\, m_j \quad on\ S_w^{(1)} \tag{2.2.21}$$

where

$$(n_1, n_2, n_3) = \vec{n} \tag{2.2.22}$$

$$(n_4, n_5, n_6) = (\vec{r} - \vec{r}_G) \times \vec{n} \tag{2.2.23}$$

$$(m_1, m_2, m_3) = -(\vec{n} \cdot \nabla)\vec{W} \tag{2.2.24}$$

$$(m_4, m_5, m_6) = -(\vec{n} \cdot \nabla)[(\vec{r} - \vec{r}_G) \times \vec{W}] \tag{2.2.25}$$

and X_{ja} is the complex amplitude of the jth oscillatory mode as defined by

$$X_j = X_{ja}\, exp(-i\omega_e t) \quad j = 1, 2,..., 6 \tag{2.2.26}$$

Each of these linear potential components ϕ_j (j = 0, 1,..., 7) also satisfies the Laplace equation (2.2.3), the free-surface condition (2.2.4), the seabed condition (2.2.6) and a proper radiation condition.

Although a great step of simplification has been made to obtain the linearised unsteady wave potential problems as described, when coupled with a steady wave potential, these are still too difficult to be of practical solution and application. In practice, further simplifications are made to solve two special cases of great interest, i.e. a full three-dimensional body moving in low speed or undergoing current and a slender body advancing with considerable forward speed.

2.3. Low Speed Approach

The low speed assumption introduces an additional small parameter with respect to the speed either when the body is advancing or when there exist ocean current. By retaining terms up to $O(W_o)$ and ignoring all the terms containing $O(W_o^n)$, $n \geq 2$, the low speed boundary value problem can be expressed in the form

$$\nabla^2 \phi_j = 0, \quad j = 0, 1, \ldots, 8 \quad \textit{in the fluid domain} \tag{2.3.1}$$

$$(-\omega_e^2 \phi_j + g \partial \phi_j / \partial z) - 2i\omega_e \nabla \phi_s \cdot \nabla \phi_j + i\omega_e \partial^2 \phi_s / \partial z^2 \, \phi_j = 0 \quad j = 1, 2, \ldots, 8 \; \textit{on} \; z = \zeta \tag{2.3.2}$$

$$\begin{cases} \partial \phi_j / \partial n = -i\omega_e n_j + W_o m_j \quad j = 1, 2, \ldots, 6 \\ \partial \phi_8 / \partial n = \dfrac{\partial}{\partial n}(\phi_0 + \phi_7) = 0 \end{cases} \quad \textit{on the body surface} \tag{2.3.3}$$

$$\partial \phi_j / \partial z = 0 \quad j = 0, 1, \ldots, 8 \quad \textit{on the seabed} \tag{2.3.4}$$

and a radiation condition.

Here the approximate steady potential

$$\phi_s = \Phi_s + O(W_o^2)$$

is governed by the following conditions

$$\nabla^2 \phi_s = 0 \quad \textit{in the fluid domain} \tag{2.3.5}$$

$$g \, \partial \phi_s / \partial z + (-\omega_e^2 \, \phi + g \, \partial \phi / \partial z - 2i\omega_e \nabla \phi_s \cdot \nabla \phi) \, exp(-i\omega_e t) = 0 \quad \textit{on} \; z = \zeta \tag{2.3.6a}$$

or

$$\partial \phi_s / \partial z = 0 \quad \textit{on} \; z = \zeta_s = 0 \tag{2.3.6b}$$

$$\partial \phi_s / \partial n = W_o \, n_1 \quad \textit{on the body surface} \tag{2.3.7}$$

$$\partial \phi_s / \partial z = 0 \quad \textit{on the seabed} \tag{2.3.8}$$

and a radiation condition.

Noting that the steady wave elevation from Equation (2.2.13) is

$$\zeta_s = 0 + O(W_o^2) \tag{2.3.9}$$

the total wave elevation in Equation (2.2.14) takes the form

$$\zeta = -\frac{1}{g}\left[\Phi_t^{(1)} + \vec{W}\cdot\nabla\Phi^{(1)}\right]_{z=0} + O(W_o^2) \tag{2.3.10}$$

In terms of condition (2.3.2), condition (2.3.6a) can be rewritten as

$$g\,\partial\phi_s/\partial z - i\omega\,\partial^2\phi_s/\partial z^2\,\phi\,exp(-i\omega_e t) = 0 \quad on\ z = \zeta \tag{2.3.6c}$$

The steady wave potential can be easily solved for the rigid free-surface condition (2.3.6b) and for simple geometries analytical solutions are available (see Appendix 1). However, numerical solution of the radiation and diffraction potentials governed by Equations (2.3.1)-(2.3.4) are still very difficult because of the complexity of the free-surface and the radiation condition at infinity. Numerical and experimental investigations into a hemi-sphere have been conducted by Zhao and Faltinsen (1988) but further development of a numerical technique of reasonable accuracy and computational economy is required for applications of general body configurations.

2.4. Linearisation of Both the Steady and Unsteady Potentials

In order to decouple the steady wave potential effect on the unsteady wave potential solutions, further linearisation is necessary. Here, it is assumed that the geometry of a body is such that the steady wave potential ϕ_s and its derivatives are small and therefore, higher order terms and their cross products with the linearised unsteady potential components ϕ_j (j = 0, 1,..., 7) can be ignored. Thus the coupled conditions involving unsteady wave potentials in §2.2 reduce to fully linearised equations as are now described:

$$\nabla^2\phi_j = 0 \quad in\ the\ fluid\ domain \tag{2.4.1}$$

$$[(\partial/\partial t - W_o\,\partial/\partial x)^2 + g\,\partial/\partial z)]\,\phi_j = 0 \quad on\ z = 0 \tag{2.4.2}$$

$$\partial\phi_j/\partial n = \begin{cases} -i\omega\,n_j + W_o\,m_j & j = 1, 2,..., 6 \\ -\partial\phi_0/\partial n & j = 7 \end{cases} \quad on\ S_w \tag{2.4.3}$$

$$\partial\phi_j/\partial z = 0 \quad on\ the\ seabed \tag{2.4.4}$$

and the radiation condition

$$\lim_{R\to\infty} \sqrt{R}\,(\partial\phi_j/\partial R - ik\phi) = 0 \tag{2.4.5}$$

where the total unsteady wave potential is written as

$$\phi = \phi_0 + \phi_7 + \sum_{j=1}^{6} X_{ja}\phi_j \tag{2.4.6}$$

see Chang (1977) and Inglis and Price (1980). But here more general expressions are used to describe the composite velocity $\vec{W}$ resultant from both the forward speed and a current or a steady drift velocity (Figure 2.1).

It can be shown that the first-order steady wave potential satisfies the equations

$$\nabla^2\phi_s = 0 \quad \textit{in the fluid domain} \tag{2.4.7}$$

$$(W_o^2\,\partial^2/\partial x^2 + g\,\partial/\partial z)\phi_s = 0 \quad \textit{on } z = 0 \tag{2.4.8}$$

$$\partial\phi_s/\partial n = W_o\, n_1 \quad \textit{on } S_w \tag{2.4.9}$$

$$\partial\phi_s/\partial z = 0 \quad \textit{on the seabed} \tag{2.4.10}$$

$$\phi_s = \begin{cases} O(1/R) & x > 0 \\ O(1) & x < 0 \end{cases} \text{ for } \textit{as } R \to \infty \tag{2.4.11}$$

This linear steady wave potential problem is outside the scope of the present study and therefore no further discussion will be given.

Conditions (2.4.1)-(2.4.5) form the basic linear wave-structure interaction problem and further simplification can be introduced depending upon the problem under investigation. For example, if $W_o = 0$, i.e. $\omega_e = \omega_o$, these equation represent a linear interaction problem between waves and a stationary structure.

2.5. First-Order Motions and Wave Forces

By means of an appropriate numerical technique to solve the linear boundary value problem, Equations (2.4.1)-(2.4.5), the resultant velocity potential values are then used to calculate the wave elevation ζ, wave pressure p, wave force components F_r (r = 1, 2,..., 6), and hydrodynamic

coefficients (i.e. added mass A_{rj} and *damping* B_{rj}). It can be shown that these quantities are derived by the following formulae:

$$\zeta = \sum_{j=0}^{7} \zeta_j = \sum_{j=0}^{7} [-\frac{1}{g}(\partial/\partial t - W_o\, \partial/\partial x\,)\, \phi_j\, exp(-i\omega_e t)]_{z=0} \tag{2.5.1}$$

$$p_j = -\rho(\partial/\partial t - W_o\, \partial/\partial x)\phi_j exp(-i\omega_e t) \tag{2.5.2}$$

$$F_{0r} = -i\omega\rho \int_{S_w} \phi_0\, n_r\, ds \tag{2.5.3}$$

$$F_{7r} = -i\omega\rho \int_{S_w} (-i\omega_e - W_o\, \partial/\partial x\,)\phi_7\, n_r\, ds \tag{2.5.4}$$

$$F_{rj}^{H} = -i\omega\rho\, X_{ja} \int_{S_w} (-i\omega_e - W_o\, \partial/\partial x\,)\phi_j\, n_r\, ds \tag{2.5.5}$$

$$A_{rj} = \frac{\rho}{\omega} \int_{S_w} Im[(-i\omega_e - W_o\, \partial/\partial x\,)\phi_j\,]\, n_r\, ds \tag{2.5.6}$$

$$B_{rj} = -\rho \int_{S_w} Re[(-i\omega_e - W_o\, \partial/\partial x\,)\phi_j\,]\, n_r\, ds \tag{2.5.7}$$

where r, j = 1, 2,..., 6. The total wave exciting forces are the sum of the Froude-Krylov force F_{0r} and the diffraction force F_{7r} , that is,

$$F_r = F_{0r} + F_{7r} \tag{2.5.8}$$

The equation of motion describing the behaviour of the body in a regular sinusoidal wave may be expressed as

$$\sum_{j=1}^{6} [(M_{rj} + A_{rj})\, \ddot{X}_j + (B_{rj} + B_{vrj})\, \dot{X}_j + C_{rj}\, X_j] = (F_{0r} + F_{7r} + F_{vr})\, exp(-i\omega_e t) \tag{2.5.9}$$

where M_{rj} is the generalised mass, C_{rj} is the hydrostatic restoring coefficients and $-B_{vrj}\, \dot{X}_j$ and F_{vr} are respectively the drag damping force and the viscous exciting force due to viscosity, vorticity and eddy making, etc. A description of these two terms is given in §9. From all the information calculated, shearing forces and bending moments can also be determined (Salversen, Tuck

and Faltinsen 1970).

With all these regular wave loading and motion information on hand the irregular sea characteristics are readily estimated for a required wave spectrum and sea state (St. Denis and Pierson 1953, Price and Bishop 1974). Detailed applications are discussed in §9 for SWATH ships.

2.6. Second-Order Wave Forces

The second-order wave forces arise from the products of first-order quantities and the second-order wave potential $\Phi^{(2)}$ (see Equation (2.2.2)). According to Pinkster (1979) and Standing and Dacunha (1982) these may be expressed by the sum of six terms, namely,

$$F^{(2)} = F_I + F_{II} + F_{III} + F_{IV} + F_V + F_{VI} \tag{2.6.1}$$

These force components are known as the force term associated with the surface elevation, the quadratic pressure term arising from the Bernoulli's equation, the structure displacement term due to the effect of first-order motions, the contribution due to the rotation of the force vector, the second-order motions of the structural centre of buoyancy and waterplane area and the contribution from the second-order potential, respectively. The time average measures of these second-order forces have steady components known as the wave drift forces. Details of the approach are described in §8.

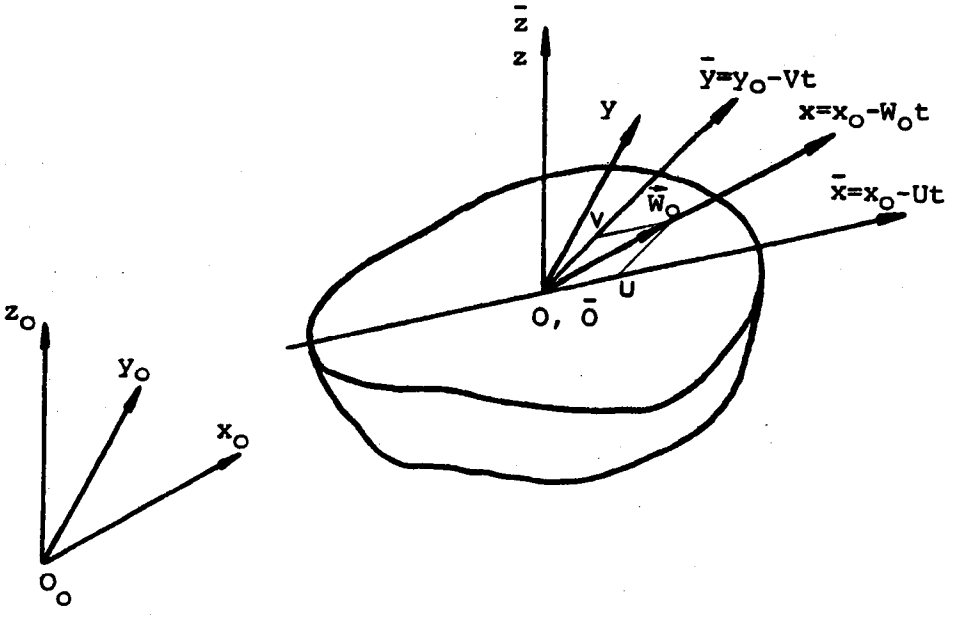

Figure 2.1. The coordinate systems.

3. FUNDAMENTAL SOLUTIONS

The disturbance created by a body in a flow field can be represented by singularity distributions on the body surface, including source, dipole, their mixture (Yeung 1982) or multipoles (Ursell 1949a, b). The Green function representing a pulsating, translating source related to the general problem of an oscillatory body moving in waves, i.e. Equations (2.4.1)-(2.4.5), can be derived from the following Poisson equation and associated boundary conditions:

$$\nabla^2 G(x, y, z; \xi, \eta, \zeta) = \delta(x-\xi)\,\delta(y-\eta)\,\delta(z-\zeta) \quad \textit{in the fluid domain } D \tag{3.0.1}$$

$$(-i\omega_e - W_o\,\partial/\partial x)^2 G + g\,\partial G/\partial z = 0 \quad \textit{on } z = 0 \tag{3.0.2a}$$

or

$$(-i\omega_e - U\,\partial/\partial \bar{x} - V\,\partial/\partial \bar{y})^2 G + g\,\partial G/\partial z = 0 \quad \textit{on } z = 0 \tag{3.0.2b}$$

$$\partial G/\partial z = 0 \quad \textit{on } z = -d \tag{3.0.3}$$

$$\lim_{R\to\infty} \sqrt{R}\,(\partial G/\partial R - ikG) = 0 \tag{3.0.4}$$

where δ is the Dirac delta function. To distinguish the Green function expression for various cases, it is now denoted by G(P, Q; $\vec{W}_o$, k, d) with two point P(x, y, z) and Q(ξ, η, ζ) , speed $\vec{W}_o$, wave number k and water depth d.

3.1. Three-Dimensional Source Potential (Finite Depth)

3.1.1. General solution

In the most general case governed by Equations (3.0.1)-(3.0.4), the source potential can be derived as:

$$G(P, Q; \vec{W}_o, k, d) = \frac{1}{r} + \frac{1}{r_2} + \frac{1}{\pi}\int_0^\infty d\mu \int_{-\pi}^{\pi} d\theta\, exp(-\mu d)\cosh\mu(z+d)\cosh\mu(\zeta+d)\,H(\mu,\theta)$$

(3.1.1)

with $r^2 = R^2 + (z-\zeta)^2$, $r_2^2 = R^2 + (z+\zeta+2d)^2$, $R^2 = (x-\xi)^2 + (y-\eta)^2$

$$H(\mu,\theta) = \frac{[g\mu + (\omega_e + W_o\,\mu\cos\theta)^2]\exp\left\{i\mu\,[(x-\xi)\cos\theta + (y-\eta)\sin\theta]\right\}}{\cos\mu d\,[g\mu\tanh\mu h - (\omega_e + W_o\,\mu\cos\theta)^2]}$$

or alternatively with $\vec{W}_o = (U,\ V,\ 0)$ in the $\bar{O}\,\overline{xyz}$ frame

$$H(\mu,\theta) = \frac{[g\mu + (\omega_e + U\mu\cos\theta + V\mu\sin\theta)^2]\exp\left\{i\mu\,[(\bar{x}-\bar{\xi})cos\theta + (\bar{y}-\bar{\eta})\sin\theta]\right\}}{\cos\mu d\,[g\mu\tanh\mu d - (\omega_e + U\mu\cos\theta + V\mu\sin\theta)^2]}$$

3.1.2. Zero speed case

If there exists neither a body forward speed nor wave current influence, i.e. $\vec{W}_o = 0$, the Green function reduces to (John 1950)

$$G(P,\ Q;\ 0,\ k,\ d) = 1/r + 1/r_2 + I_{1d} + i\,I_{2d} \tag{3.1.2a}$$

with

$$I_{1d} = 2\,PV\int_0^\infty d\mu\,\frac{\nu+\mu}{\mu\sinh\mu h - \nu\cosh\mu d}\,exp(-\mu d)\cosh\mu(z+d)\cosh\mu(\zeta+d)\,J_o(\mu R)$$

$$I_{2d} = 2\pi\,\frac{k^2-\nu^2}{(k^2-\nu^2)\,d+\nu}\cosh k(z+d)\cosh k(\zeta+d)\,J_o(kR)$$

or in a series form

$$G(P,\ Q;\ 0,\ k,\ d) = \frac{2\pi(\nu^2-k^2)}{(k^2-\nu^2)\,d+\nu}\cosh k(z+d)\cosh k(\zeta+d)[\,Y_o(kR) - i\,J_o(kR)]$$

$$+ 4\sum_{m=1}^{\infty}\frac{\mu_m^2+\nu^2}{(\mu_m^2+\nu^2)\,d-\nu}\cos\mu_m(z+d)\cos\mu_m(\zeta+d)\,K_o(\mu_m R) \tag{3.1.2b}$$

with μ_m being the mth positive root of equation

$$\mu_m \tan\mu_m d + \nu = 0$$

where J_m is the Bessel function of the first kind of mth order,

Y_m is the Bessel function of the second kind of mth order,

K_m is the modified Bessel function of the second kind of mth order.

Practical numerical procedures to evaluate G(P, Q; 0, k, d) can be found in Hogben and Standing (1974) and Faltinsen and Michelsen (1974). Pidcock (1985) presented an alternative form of expression (3.1.2b) useful for small R/d values whilst Endo (1987) proposed a Gauss-Laguerre quadrature method based on expression (3.1.2a).

An algorithm developed by Newman (1985) re-writes expression (3.1.2a) into

$$\mathrm{Re}\,[\,G(P,\,Q;\,0,\,k,\,d)] = \frac{1}{r} + \frac{1}{r_2} + \Big(\sum_{m=1}^{4} I_{1m} + \sum_{n=1}^{2} I_{on}\Big) \qquad (3.1.3)$$

with

$$I_{1m} = PV\int_0^{\infty} \frac{\mu+\nu}{\mu-\nu}\, exp(-\mu V_m)\, J_o(\mu R)\, d\mu \qquad V_m = \begin{cases} 2d - |z-\zeta| & m=1 \\ 2d + |z-\zeta| & m=2 \\ |z+\zeta| & m=3 \\ 4d - |z+\zeta| & m=4 \end{cases}$$

$$I_{on} = PV\int_0^{\infty} d\mu\, [\frac{1}{\mu\,\sinh\mu d - \nu\,\cosh\mu d} - \frac{2\,exp(-\mu d)}{\mu-\nu}]\,(\mu+\nu)\,\cosh\mu U_n\, exp(-\mu d)\, J_o(\mu R)\, d\mu$$

$$U_n = \begin{cases} |z-\zeta| & n=1 \\ 2d - |z-\zeta| & n=2 \end{cases}$$

Here terms denoted by I_{1m} can be more efficiently evaluated by the methods developed for the deep water Green function, which are to be described in §3.2. The integrand in I_{on} decays like $exp(-2\mu d)$ for *large* μ *values* and a numerical approximation can be implemented for its estimation.

3.1.3. Asymptotic forms ($k \to \infty$ *or* 0)

At high frequencies, i.e. k $\to \infty$, the asymptotic form of the Green function can be readily derived as

$$G(P, Q; 0, \infty, d) = 1/r + 1/r_1 + \sum_{n=1}^{\infty} [(-1)^n (1/r_{2n} + 1/r_{4n}) + (-1)^{n+1}(1/r_{1n} + 1/r_{3n})] \quad (3.1.4)$$

with

$$r_1 = \sqrt{R^2 + (z+\zeta)^2} \quad \text{and} \quad r_{mn} = \sqrt{R^2 + (-2nd - V_m)^2}$$

As the frequency tends to zero, i.e. k $\to$ 0, it can be shown that

$$G(P, Q; 0, 0, d) = 1/r + 1/r_1 + \sum_{n=1}^{\infty} \sum_{m=1}^{4} 1/r_{mn} \quad (3.1.5)$$

Expressions (3.1.4) and (3.1.5) can also be found in Garrison (1978).

3.1.4. Shallow draft structure ($z = \zeta = 0$)

If the draft of the body is small enough, say h $\to$ 0, expression (3.1.2) can be rewritten as (Wu and Price 1986a) :

$$G(x, y, 0; \xi, \eta, 0; 0, k, d) = \frac{2\pi(\nu^2 - k^2)}{(k^2 - \nu^2)\, d + \nu} \cosh^2 kd \, [\, Y_o(kR) - i\, J_o(kR)]$$

$$+ 4 \sum_{m=1}^{\infty} \frac{\mu_m^2 + \nu^2}{(\mu_m^2 + \nu^2)d - \nu} \cos^2 \mu_m d \; K_o(\mu_m R) \quad (3.1.6)$$

An alternative integral form can be deduced from Newman's expression (3.1.3) when setting z = ζ = 0.

3.1.5. Steady source potential ($k = 0$, $W_o \neq 0$)

For a steady moving source, i.e. k = 0 but $\vec{W}_o \neq \vec{0}$, the general Green function expression (3.1.1) takes a form given by Kostyukov (1959):

$$G(P,Q;\vec{W}_o,\,0,\,d) = 1/r + 1/r_2 + \frac{4}{\pi}\int_0^{\infty} d\theta\, PV\int_0^{\infty}\frac{A}{B}d\mu + 4\,\nu_o\int_{\theta_o}^{\pi/2}\frac{C}{D}d\theta \qquad (3.1.7)$$

where

$$A = exp(-\mu d)\,\cosh\mu(z+d)\,\cosh\mu(\zeta+d)\,cos[\mu(x-\xi)\cos\theta]\,cos[\mu(y-\eta)\sin\theta]\,(\mu\cos^2\theta+\nu_o) - \nu_o$$

$$B = \cosh\mu d\,(\mu\cos^2\theta - \nu_o\tanh\mu d)$$

$$C = cosh[k_o(z+d)]\,cosh[k_o(\zeta+d)]\,sin[k_o(x-\xi)cos\theta]\,cos[k_o(y-\eta)\sin\theta]$$

$$D = \cos^2\theta\cosh^2 k_o d - k_o d$$

$$\theta_o = \begin{cases} \cos^{-1}\sqrt{\nu_o d} & \nu_o d < 1 \\ 0 & \nu_o d \geq 1 \end{cases} \quad \text{for } \pi/2 \geq \theta_o \geq 0$$

where $\nu_o = g/W_o^2$ and k_o is the real positive root of

$$k_o - \nu_o\, sec^2\theta\tanh k_o d = 0$$

3.2. Three-Dimensional Source Potential (Infinite Depth)

Let the water depth in the finite depth Green function expression in 3.1 tend to infinity, i.e. $d \to \infty$, then formulae applicable to relative deep water can be readily derived.

3.2.1. General solution in deep water

In expression (3.1.1), let $d \to \infty$ and this results in the general deep water Green function in the following form (Havelock 1958, Wehausen and Laitone 1960):

$$G(P,\,Q;\vec{W}_o,\,k,\,\infty) = 1/r - 1/r_1 + \frac{2}{\pi}\int_0^{\infty} d\mu\int_0^{\pi} P(\mu,\,\theta)\,d\theta \qquad (3.2.1a)$$

$$P(\mu,\,\theta) = \frac{\mu\, exp[\mu(z+\zeta) + i\,\mu(x-\xi)\cos\theta]\, cos[\mu(y-\eta)\sin\theta]}{[\mu - (\omega_e + W_o\,\mu\cos\theta)^2/g\,]}$$

or alternatively, in the $\bar{O}\bar{x}\bar{y}\bar{z}$ frame as

$$P(\mu,\theta)=\frac{\mu\, exp[\mu(\bar{z}+\bar{\zeta})+i\,\mu(\bar{x}-\bar{\xi})\cos\theta]\, cos[\mu(\bar{y}-\bar{\eta})\sin\theta]}{\mu-(\omega_e+U\mu\cos\theta+V\mu\sin\theta)^2/g\ ]} \tag{3.2.1b}$$

where the integral is defined as

$$\int_0^{\infty} d\mu \int_0^{\pi} d\theta = \left(\int_0^{\gamma}\int_0^{\infty} + \int_{\gamma}^{\pi/2}\int_{L_1} + \int_{\pi/2}^{\pi}\int_{L_2}\right) d\mu\, d\theta \tag{3.2.1c}$$

and

$$\gamma=\begin{cases}0 & \tau<1/4\\ \cos^{-1}\left(\dfrac{1}{4\tau}\right) & \tau\geq 1/4\end{cases} \qquad (\tau=\omega W_o/g) \tag{3.2.1d}$$

The contours L_1 and L_2 are illustrated in Figure 3.1 with singularities at

$$\sqrt{gk_1},\ \sqrt{gk_3}=\omega\,[1-\sqrt{1-4\,\tau\cos\theta}\,]\,/\,(2\,\tau\cos\theta) \tag{3.2.1e}$$

$$\sqrt{gk_2},\ -\sqrt{gk_4}=\omega\,[1+\sqrt{1-4\,\tau\cos\theta}\,]\,/\,(2\,\tau\cos\theta)$$

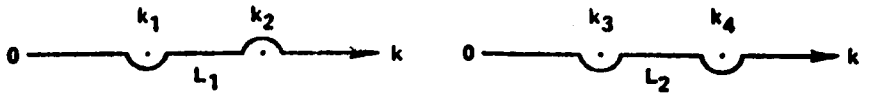

Figure 3.1. The contours L_1 and L_2 in Equation (3.2.1c).

Applications of this Green function form have been conducted by Chang (1977), Inglis and Price (1980) and Guevel and Bougis (1982). Its evaluation, however, is very computer time consuming. Therefore, it necessitates further development of more efficient algorithms. Moreover, the predictions derived by this most sophisticated theoretical approach so far available do not appear to provide much improvement over simple strip method results. Because of this, Inglis and Price (1979) suggested the use of a simplified forward speed correction, similar to that adopted in strip theories.

3.2.2. Zero speed case ($W_o = 0$)

In the absence of the speed, i.e. $\vec{W}_o = \vec{0}$, Equation (3.2.1a) reduces to a much simpler version:

$$G(P, Q; \vec{0}, \nu, \infty) = 1/r + 1/r_1 + I_1 + i\, 2\pi\nu\, exp\,[\nu(z+\zeta)]\, J_o(\nu R) \tag{3.2.2}$$

$$I_1 = 2\nu\, PV \int_0^\infty d\mu\, exp\,[\mu(z+\zeta)]\, J_o(\mu R) / (\mu - \nu) \tag{3.2.2a}$$

Kim (1963) re-wrote I_1 in a very useful finite integral form:

$$I_1 = -\nu\, exp\,[\nu(z+\zeta)] \left\{ \pi\,[Y_o(\nu R) + H_o(\nu R)] + 2 \int_0^{-\nu(z+\zeta)} \frac{e^s\, ds}{\sqrt{(\nu R)^2 + s^2}} \right\} \tag{3.2.2b}$$

Numerical evaluations of this finite integral form have been reported by Hearn (1977), Newman (1985) and Telste and Noblesse (1986). An efficient numerical approximation is also derived in the present work.

3.2.3. Asymptotic forms ($k \to \infty$ *or* 0)

At high frequencies, i.e. $k \to \infty$, both the non-zero and zero speed Green function expressions (3.2.1) and (3.2.2) reduce to the same simple form

$$G(P, Q; 0, \infty, \infty) = 1/r - 1/r_1 \tag{3.2.3}$$

In the low frequency limit $k \to 0$, the zero speed expression (3.2.2) becomes the double body formula:

$$G(P, Q; 0, 0, \infty) = 1/r + 1/r_1 \tag{3.2.4}$$

whilst the non-zero speed form (3.2.1) becomes the Kelvin source expression

$$G(P, Q; \vec{W}_o, 0, \infty) = 1/r - 1/r_1 - \frac{4\nu_o}{\pi} \int_0^{\pi/2} d\theta\, PV \int_0^\infty A(\mu, \theta)\, d\mu - 4\nu_o \int_0^{\pi/2} C(\theta)\, d\theta \tag{3.2.5}$$

$$A(\mu, \theta) = \frac{exp[\mu(z+\zeta)]\, cos[\mu(x-\xi)\cos\theta]\, cos[\mu(y-\eta)\sin\theta]}{(\mu\cos^2\theta - \nu)}$$

$$C(\theta) = exp[\nu(z+\zeta)\, sec^2\theta]\, sin[\nu_o(x-\xi)\, sec\theta]\, cos[\nu_o(y-\eta)\sin\theta\, sec^2\theta]\, sec^2\theta$$

with $\nu_o = g/W_o^2 = g/\sqrt{U^2+V^2}$.

3.2.4. Shallow draft structure ($z = \zeta = 0$)

For a marine structure of small draft, say $z \to 0$, $\zeta \to 0$, a zero forward speed and zero draft Green function formulation (Kim 1963, Wu and Price 1986a) can be derived as

$$G(x, y, 0; \xi, \eta, 0; 0, \nu, \infty) = 2/R - \pi\nu\,[\,Y_o(\nu R) + H_o(\nu R)\,] + i\,2\pi\nu\,J_o(\nu R) \qquad (3.2.6)$$

and $\partial G/\partial z = \nu G$, which is an important result, providing much simplification in the theoretical model.

3.3. Two-Dimensional Source Potential

In engineering practices, two-dimensional methods and solutions are much more popular than the three-dimensional ones. It can be shown that there exists a two-dimensional form corresponding to each Green function expression described in 3.1 and 3.2. These two-dimensional formulations can be derived either from a two-dimensional boundary value problem (Wehausen and Laitone 1960) or from the Fourier transformation of a three-dimensional Green function (Wu and Price 1986b). As suggested by Wu and Price (1986b) a two-dimensional Green function may be expressible by a transformation of the relative three-dimensional one as:

$$G_{2d}(p, q; \vec{W}_o, k, d) = -\frac{1}{2}\int_{-\infty}^{+\infty} G(0, y, z; \xi, \eta, \zeta; \vec{W}_o, k, d)\, exp[-i\,\xi\,(-k\cos\beta)]\, d\xi \qquad (3.3.1)$$

where $p(y, z) = P(0, y, z)$, $q(\eta, \zeta) = Q(\xi, \eta, \zeta)$, and β is the wave heading as defined previously.

3.3.1. General solution (finite water depth)

The insertion of the general three-dimensional Green function expression (3.1.1) into Equation (3.3.1) allows the general two-dimensional finite water depth Green function to be derived. It represents the behaviour of a two-dimensional translating, pulsating source in a incident wave of heading angle β. After completing the Fourier transformation, the two-dimensional Green function is given by

$$G_{2d}(p,\ q;\ \vec{W}_o,\ k,\ d) = -K_o(k\,|\cos\beta\,|R) - K_o(k\,|\cos\beta\,|R_2)$$

$$+ PV \int_{-\infty}^{+\infty} d\mu\, F_1(\mu,\ -k\cos\beta) + i\,\pi \sum_{m=1}^{2} F_2(\mu_m^*,\ -k\cos\beta) \qquad (3.3.2)$$

with $R_2 = \sqrt{(y-\eta)^2 + (z+\zeta+2d)^2}$, and

$$F_1(a,\ b) = \frac{exp(-cd)\ cosh[c(z+d)]\ cosh[c(\zeta+d)]\ [cg + (\omega_e + bU + aV)^2]\ exp[i\,a(y-\eta)]}{c\ \cosh cd\ [cg\ \tanh cd - (\omega_e + bU + aV)^2]}$$

$$F_2(a,\ b) = \frac{exp(-cd)\ cosh[c(z+d)]\ cosh[c(\zeta+d)]\ [cg + (\omega_e + bU + aV)^2]\ exp[i\,a(y-\eta)]}{ag\ [sinh\ cd + cd\ sech\ cd - 2\,V\,(\omega_e + bU + aV)\cosh cd\ ]}$$

where $c = \sqrt{a^2 + b^2}$, μ_m^* $(m = 1,\ 2)$ are the two roots of the following equation:

$$\sqrt{\mu^2 + (k\cos\beta)^2}\ \tanh\sqrt{\mu^2 + (k\cos\beta)^2}\,d] - (\omega_e - Uk\cos\beta + \mu V)^2 = 0 \qquad (3.3.3)$$

From this two-dimensional general formulation, various two-dimensional Green function formulae can directly be deduced for individual special cases.

3.3.2. Zero speed case ($W_o = 0$)

At a zero composite velocity, i.e. $\vec{W}_o = 0$, the following Green function form is obtainable, either reduced from Expression (3.3.2) or derived from a combination of Equation (3.3.1) and expression (3.1.2a) as

$$G_{2d}(p,\ q;\ 0,\ k,\ d) = -K_o(k\,|\cos\beta\,|R) - K_o(k\,|\cos\beta\,|R_2)$$

$$-2\,PV\int_{(k\cos\beta)^+}^{\infty} d\mu\, F_3(\mu, -k\cos\beta) - i\,2\pi F_4(\nu,-k\cos\beta) \qquad (3.3.4a)$$

$$F_3 = \frac{(\nu+\mu)\,exp(-\mu d)\,cosh[\mu(z+d)]\,cosh[\mu(\zeta+d)]}{\mu\sinh\mu d - k\cosh\mu d}\;\frac{cos[(y-\eta)\sqrt{\mu^2-(k\cos\beta)^2}\,]}{\sqrt{\mu^2-(k\cos\beta)^2}}$$

$$F_4 = \frac{(k^2-\nu^2)cosh[k(z+d)]\,cosh[k(\zeta+d)]}{(k^2-\nu^2)d+\nu}\begin{cases}\dfrac{cos[(y-\eta)\sqrt{k^2-(k\cos\beta)^2}\,]}{\sqrt{k^2-(k\cos\beta)^2}} & |cos\beta| \neq 1\\ 0 & |cos\beta| = 1\end{cases}$$

The combination of Equations (3.3.1) and (3.3.2b) results in an alternative expression given by

$$G_{2d}(p,\,q;\,0,\,k,\,d) = \frac{4\pi(\nu^2-k^2)}{(k^2-\nu^2)d+\nu}\,cosh[k(z+d)]\,cosh[k(\zeta+d)]\left\{\begin{array}{l}|y-\eta|\\ \dfrac{i\,exp(i\,|y-\eta|\sqrt{\nu^2-(k\cos\beta)^2}\,)}{\sqrt{k^2-(k\cos\beta)^2}}\end{array}\right\}$$

$$-2\sum_{m=1}^{\infty}\frac{\mu_m^2+\nu^2}{(\mu_m^2+\nu^2)d-\nu}\,cos[\mu_m(z+d)]\,cos[\mu_m(\zeta+d)]\,\frac{\pi\,exp(-|y-\eta|\sqrt{\mu_m^2+(k\cos\beta)^2}}{\mu_m^2+(k\cos\beta)^2}\quad\begin{array}{l}|\cos\beta|=1\\ |\cos\beta|\neq 1\end{array} \qquad (3.3.4b)$$

3.3.3. The case of zero speed and beam seas

For the case of zero speed and in beam sea waves (i.e. $\beta = \pi/2$), the relative Green function form can be readily derived from expressions (3.3.4a) or (3.3.4b). Its series expansion form reduced from expression (3.3.4b) is given by

$$G_{2d}(p,\,q;\,0,\,k,\,d) = \frac{1}{k}\,\frac{4\pi(\nu^2-k^2)}{(k^2-\nu^2)d+\nu}\,cosh[k(z+d)]\,cosh[k(\zeta+d)]\,[sin(k\,|y-\eta|) - i\,cos(k\,|y-\eta|)]$$

$$+4\sum_{m=1}^{\infty}\frac{\mu_m^2+\nu^2}{(\mu_m^2+\nu^2)d-\nu}\,cos[\mu_m(z+d)]\,cos[\mu_m(\zeta+d)]\,\frac{\pi\,exp(-\mu_m\,|y-\eta|)}{\mu_m} \qquad (3.3.5)$$

It should be noted that this form also represents a two-dimensional pulsating source in an otherwise calm water (Wehausen and Laitone 1960).

3.4. Two-Dimensional Source Potential in Deep Water

For two-dimensional deep water cases, not all the inclusive forms are described but those in practical use.

When allowing d $\rightarrow \infty$, expression (3.3.4a) reduces to

$$G_{2d}(p,\ q;\ 0,\ k,\ \infty) = -K_o(k\,|\cos\beta|R) - K_o(k\,|\cos\beta|R_2) + I_1 + i\,I_2 \tag{3.4.1}$$

$$I_1 = -2\,PV\int_0^{\infty} d\mu\ \frac{exp(-|z+\zeta|\sqrt{\mu^2+(k\cos\beta)^2})\,cos[\mu(y-\eta)}{\sqrt{\mu^2+(k\cos\beta)^2}-k} \qquad |cos\beta| \neq 1 \tag{3.4.1a}$$

$$I_2 = \begin{cases} \dfrac{-2\pi\,k\,exp(-k\,|z+\zeta|)\,cos[\mu(y-\eta)\sqrt{k^2-(k\cos\beta)^2}]}{\sqrt{k^2-(k\cos\beta)^2}} & |cos\beta| \neq 1 \\ 0 & |cos\beta| = 1 \end{cases}$$

This Green function form has been derived by Haskind (1953) and Wehausen and Laitone (1960) and an alternative series expression by Ursell (1975).

To gain high numerical efficiency, an alternative expression for I_1, expression (3.4.1a), can be derived from Equations (3.3.1) and (3.2.2b) in the form:

$$I_1 = 2k\,exp(-k\,|z+\zeta|)\left\{\frac{-\pi\,sin[|y-\eta|\sqrt{k^2-(k\cos\beta)^2}]}{\sqrt{k^2-(k\cos\beta)^2}} + \int_{-|z+\zeta|}^{+\infty} ds\ exp(-ks)\,K_o(k\,|\cos\beta|\sqrt{s^2+(y-\eta)^2}\right\} \tag{3.4.1b}$$

This alternative remains valid even as $|cos\beta| \rightarrow 1$, because

$$\lim_{|cos\beta|\rightarrow 1} \frac{sin(|y-\eta|\sqrt{k^2-(k\cos\beta)^2})}{\sqrt{k^2-(k\cos\beta)^2}} = |y-\eta|$$

3.4.1. Deep water pulsating source

In expression (3.4.1) let $\beta \rightarrow \pi/2$, the Green function representing a two-dimensional pulsating source in deep water is readily deduced as

$$G_{2d}(p,\ q;\ 0,\ k,\ \infty) = \frac{1}{2} \ln \frac{(y-\eta)^2 + (z-\zeta)^2}{(y-\eta)^2 + (z-\zeta)^2} + I_1 + i\, I_2 \tag{3.4.2}$$

$$I_1 = -PV \int_0^{\infty} d\mu\, exp(-\mu\,|z+\zeta\,|)\, \cos[\mu(y-\eta)] \,/\, (\mu - k)$$

$$I_2 = -\pi\, exp(-k\,|z+\zeta\,|)\, cos\,[k(y-\eta)]$$

This expression can be easily evaluated by the numerical procedure proposed by Frank (1967) and it seems to be the most popular one used in solving the two-dimensional wave-structure interaction problems.

3.4.2. Shallow draft source in deep water

When both the source and the field points reach the free-surface, i.e. $z,\ \zeta \rightarrow 0$, expression (3.4.2) further reduces to the two-dimensional shallow draft, deep water Green function given by

$$\begin{aligned} G_{2d}(p_o,\ q_o;\ 0,\ k,\ \infty) = {} & [\pi + 2\, Si\,(k\,|y-\eta\,|)]\, \sin(k\,|y-\eta\,|) \\ & + 2\, cos\,(k\,|y-\eta\,|)\, Ci\,(k\,|y-\eta\,|) - i\, 2\pi\, cos\,(k\,|y-\eta\,|) \end{aligned} \tag{3.4.3}$$

This expression has been derived by MacCamy(1961) and used by Wu and Price(1986d)in developing a new two-dimensional shallow draft theory.

4. INTEGRAL EQUATIONS

The singularity distribution is the technique most widely adopted to analyse wave-body interaction problems. In such an analysis, an integral equation representing a certain kind of singularity distribution is formulated to solve the unknown wave potentials induced by a marine structure. Accordingly, the hydrodynamic coefficients, wave forces and motion responses, together with generated wave patterns, can be predicted.

In this Chapter, a brief description of the integral equations is given. Further discussions are focused on their mathematical failure at irregular frequencies associated with floating body analyses. Then, modified formulations and methods are proposed to eliminate or remedy this theoretical difficulty. Finally, an interior integral equation approach is presented.

4.1. The Three-Dimensional Integral Equation

According to Brard (1972), the Green function integral equation associated with a mixed source-dipole distribution is given in the form:

$$\begin{Bmatrix}4\\2\\0\end{Bmatrix} \pi\,\phi(P) = \int_{S_w} [\phi(Q)\frac{\partial}{\partial n_Q}G(P,Q) - \frac{\partial\phi(Q)}{\partial n_Q}G(P,Q)]dS + \frac{1}{g}\int_{L_o} \Big\{ i2\omega\, W_o\phi(Q)\, G(P,Q)$$

$$+ W_o^2\,[\phi(Q)\frac{\partial}{\partial\xi}G(P,Q) - \frac{\partial\phi(Q)}{\partial\xi}\,G(P,Q)] \Big\} d\eta \quad \text{for } Q \in S_w,\ P \in \begin{cases} D & a \\ S_w & (4.1.1b) \\ \bar{D} & c \end{cases}$$

where D and $\bar{D}$ refer to the two fluid domains outside and inside the body surface S_w, respectively. L_o is the mean waterline of the body. The Green function G(P, Q) is given by G(P, Q; $\vec{W}_o$, k, d) in expression (3.1.1) for finite water depth or by G(P, Q; $\vec{W}_o$, k, ∞) in expression (3.2.1) for deep water.

This formulation can be rearranged into a more compact source distribution form with a source strength σ (Chang 1977):

$$2\pi\phi(P) = \int_{S_w} \sigma(Q)\, G(P, Q)\, dS + \frac{W_o^2}{g} \int_{L_w} \sigma(Q)\, G(P, Q)\, n_1\, d\eta \quad \text{for} P, Q \in S_w \qquad (4.1.2)$$

For a marine vehicle travelling at high speed or an intermediate speed vessel with a blunt bow, the additional line integral in the two equations above provides a significant contribution to the final solution. However, for a marine structure travelling at a low speed, i.e. $W_o = O(\varepsilon)$, or with a slenderness feature, i.e. $n_1 = O(\varepsilon)$, this line integral is a higher order small quantity and therefore, it may be ignored in some cases of practical application.

For stationary or fixed offshore structures and service vessels, a zero speed approach is often appropriate. As derived by John (1950), the zero speed Green function integral takes the form:

$$\begin{Bmatrix} 4 \\ 2 \\ 0 \end{Bmatrix} \pi\phi(P) = \int_{S_w} [\phi(Q) \frac{\partial}{\partial n_Q} G(P,Q) - \frac{\partial \phi(Q)}{\partial n_Q} G(P, Q)]\, dS \quad \text{for} Q \in S_w, P \in \begin{cases} D & a \\ S_w & (4.1.3b) \\ \bar{D} & c \end{cases}$$

where the Green function is given by the three-dimensional zero speed Green function G(P, Q; 0, k, d) in expression (3.1.2) for finite water depth, or by G(P, Q; 0, k, ∞) in expression (3.2.2) for deep water.

Correspondingly, the source distribution form (4.1.2) reduces to

$$2\pi\phi(P) = \int_{S_w} \sigma(Q)\, G(P, Q)\, dS \quad \text{for } P, Q \in S_w \qquad (4.1.4)$$

4.2. The Two-Dimensional Integral Equation

Two-dimensional versions of the integral equation can be derived directly by applying the Green's theorem in the same manner as the three-dimensional ones, or indirectly by a transformation procedure (Wu and Price 1986b). The equation equivalent to Equation (4.1.1) is

$$\begin{Bmatrix}2\\1\\0\end{Bmatrix}\pi\,\phi(p)=\int_{C_w}\left[-\phi(q)\,\frac{\partial}{\partial n_q}G(p,\,q)+\frac{\partial\phi(q)}{\partial n_q}G(p,\,q)\right]dl-\frac{V^2}{g}\sum^{m}\left[\phi(q)\,\frac{\partial G(p,\,q)}{\partial\eta}-G(p,\,q)\,\frac{\partial\phi(q)}{\partial\eta}\right.$$

$$\left.+\left(i\,2\omega_e\frac{W_o}{V}-i\,2k\,\frac{U}{V}\cos\beta\right)\phi(q)\,G(p,\,q)\right]_{\zeta=0}\quad\text{for } q\in C_w,\quad p\in\begin{cases}D & a\\ C_w & (4.2.1b)\\ \overline{D} & c\end{cases}$$

whilst the one equivalent to Equation (4.1.2) is

$$2\,\pi\,\phi(p)=\int_{C_w}\sigma(q)\,G(p,\,q)\,dl-\frac{V^2}{g}\sum^{m}\left[\sigma(q)\,G(p,\,q)\,n_2(q)\right]_{\zeta=0}\quad\text{for } p,\,q\in C_w\qquad(4.2.2)$$

In the cases of zero speed, the equation equivalent to Equation (4.1.3) is

$$\begin{Bmatrix}2\\1\\0\end{Bmatrix}\pi\,\phi(p)=\int_{C_w}\left[-\phi(q)\,\frac{\partial}{\partial n_q}G(p,\,q)+\frac{\partial\phi(q)}{\partial n_q}G(p,\,q)\right]dl\quad\text{for } q\in C_w,\,p\in\begin{cases}D & a\\ C_w & (4.2.3b)\\ \overline{D} & c\end{cases}$$

and that equivalent to Equation (4.1.4) takes the form:

$$2\,\pi\,\phi(p)=\int_{C_w}\sigma(q)\,G(p,\,q)\,dl\quad\text{for } p,\,q\in C_m\qquad(4.2.4)$$

where G(p, q) is a two-dimensional zero speed Green function given by G(p, q; 0, k, d) in expressions (3.3.4) and (3.4.5) for finite water depth, or expressions (3.4.1) and (3.4.2) for deep water.

4.3. Mathematical Failure at Irregular Frequencies

The Green function integral equations in §4.1-2 take the form of the Fredholm integral equation of the second kind which has no unique solution at an infinite number of discrete frequencies. It shows that the related set of discretised linear equation describing the problem is ill-conditioned over a finite frequency bandwidth (Newman 1983).

In his classical paper, John (1950) showed that, for a free-surface piercing body, the Green function integral equation admits non-trivial solution at the eigenfrequencies of the related inte-

rior fluid oscillation problem. These solutions satisfy the free-surface condition inside the body and are of zero value on the interior body boundary. In his two-dimensional computation, Frank (1967) identified that at an irregular frequency the matrix formulation becomes ill-conditioned. Yeung (1982) further pointed out that both the source and mixed source-dipole distribution methods have irregular frequencies at the same values since the kernel of one is the "transpose" of the other.

It may be concluded from reported investigations that whichever distribution method is adopted with a classical Green function expression in any numerical calculation associated with floating marine structures, it is difficult to hit the irregular frequencies precisely unless some proper remedy techniques are introduced.

For a marine structure piercing the free-surface in deep water, there exists, as always assumed, an exterior velocity potential solution $\phi(x, y, z)$ which satisfies the following conditions:

$$\nabla^2 = \left(\frac{\partial^2}{\partial x^2} + \frac{\partial^2}{\partial y^2} + \frac{\partial^2}{\partial z^2} \right) \phi = 0 \quad in\ D \tag{4.3.1a}$$

$$\nu \phi - \frac{\partial \phi}{\partial z} = 0 \quad on\ S_f \tag{4.3.1b}$$

$$\frac{\partial \phi}{\partial z} = 0, \quad on\ seabed \tag{4.3.1c}$$

$$\frac{\partial \phi}{\partial n} = v_n, \quad on\ S_w \tag{4.3.1d}$$

and a radiation condition

$$\lim_{R \to \infty} \sqrt{R} \left(\frac{\partial \phi}{\partial R} - i\, k\, \phi \right) = 0 \tag{4.3.1e}$$

To describe the corresponding interior problem, an interior velocity potential $\bar{\phi}$ may be constructed, which satisfies the equations:

$$\nabla^2 \bar{\phi} = 0 \quad in\ \bar{D} \tag{4.3.2a}$$

$$\nu \phi - \frac{\partial \bar{\phi}}{\partial z} = 0 \quad on \bar{S}_f \tag{4.3.2b}$$

and an imposed interior body boundary condition. Here S_f and $\bar{S}_f$ denote the exterior and the interior free-surface.

As previously discussed by John (1950), the determination of a solution to the exterior irregular frequency problem may be replaced by a solution to the equivalent interior eigenvalue problem derived from the following set of equations describing the interior boundary value problem, namely

$$\nabla^2 \bar{\phi} = 0 \quad in\ \bar{D} \tag{4.3.3a}$$

$$\nu \bar{\phi} - \frac{\partial \bar{\phi}}{\partial z} = 0 \quad on\ \bar{S}_f \tag{4.3.3b}$$

$$\bar{\phi} = 0 \qquad on\ S_w \tag{4.3.3c}$$

At an irregular frequency related to the solution of Equation (4.3.3), the Fredholm integral determinant of Equation (4.1.3b) or (4.1.4) (or, (4.2.3b) or (4.2.4) in two-dimensional cases) equals zero. According to the Fredholm integral equation theorem, Equation (4.1.3b) (or (4.2.3b)) is solvable but has no unique solution; whilst Equation (4.1.4) (or (4.2.4)) has no solution at all. In numerical computation practice, however, the determinant tends to a small value over a narrow band of frequency and the numerical formulation becomes ill-conditioned. Therefore, for both the mixed source-dipole and the source integral equations, only erroneous solutions can be obtained.

There may be two alternatives to solve the irregular frequency problem:

(1) To predict the irregular frequencies precisely and then simply ignore computations around these frequency values.

(2) To develop modified mathematical formulations free of irregular frequency effects.

4.4. Prediction of Irregular Frequencies

4.4.1. Analytical formulations

For some simple and regular body geometries, analytical expressions of $\bar{\phi}$ and the irregular frequencies corresponding to Equation (4.3.3) can be derived.

A rectangular section

For a two-dimensional rectangular section of beam B and draft h, a suitable form of $\bar{\phi}$ satisfying Equation (4.3.3) is given by

$$\bar{\phi}_m = \sin[\frac{m\pi}{B}(y - \frac{B}{2})] \sinh[k(z+h)] \quad \text{for } m = 1,2,3,\cdots \quad \begin{matrix} B/2 \geq y \geq -B/2 \\ 0 \geq z \geq -h \end{matrix} \tag{4.4.1a}$$

provided that

$$k = m\pi/B \tag{4.4.1b}$$

and there exists an irregular frequency with value

$$\omega_m = \sqrt{g\ k\ coth(kh)} \tag{4.4.1c}$$

A triangular section

For a triangular section of beam B and draft h = B/2 the solution satisfies Equation (4.3.3) can be obtained as

$$\bar{\phi} = \begin{cases} sinh(ky)\ sin(kz') - sin(ky)\ sinh(kz') & (antisymmetric) \\ cosh(ky)\ cos(kz') - cos(ky)\ cosh(kz') & (symmetric) \end{cases} \tag{4.4.2a}$$

where $z' \geq y \geq -z'$ and $h \geq z' \geq 0$ with $z' = z + h$.

Irregular frequencies occur at

$$\omega = \begin{cases} \sqrt{gk\ cotan\,(kh)} & (antisymmetric) \\ \sqrt{gk\ tan\,(kh)} & (symmetric) \end{cases} \tag{4.4.2b}$$

This formula can be further simplified to (Wu and Price 1986d):

$$\omega_m \simeq \begin{cases} \sqrt{g\,(m + 1/4)\,\pi/h} & (antisymmetric) \\ \sqrt{g\,(m - 1/4)\,\pi/h} & (symmetric) \end{cases} \quad \text{for } m = 1, 2,... \tag{4.4.2c}$$

Three-dimensional bodies

In three-dimensional cases, analytical solutions of irregular frequencies are available for a rectangular box (Inglis and Price 1981), a circular tank (Nojiri 1981), a sector of a circular tank and a horizontal triangular prism (Appendix 4.1). In addition, analytical expression can also be derived for an elliptical dock.

An elliptical dock

For a dock of elliptical waterplane area with the major and minor axes a and b ($c = \sqrt{a^2 + b^2}$) and draft h, $\bar{\phi}$ of Equation (4.4.3) is expressible by

$$\bar{\phi}_{pm} = \begin{cases} Ce_p(\xi, q_{pm})\, ce_p(\eta, q_{pm}) \sinh[k_{pm}(z + h)] & (p = 0,1,...) \\ Se_p(\xi, \bar{q}_{pm})\, se_p(\eta, \bar{q}_{pm}) \sinh[\bar{k}_{pm}(z + h)] & (p = 1,2,...) \end{cases} \tag{4.4.3a}$$

for $\xi_o \geq \xi$, $2\pi \geq \eta \geq 0$ and $0 \geq z \geq -h$.

Here $Ce_p(\,)$ and $Se_p(\,)$ are modified Mathieu function of the first kind (McLachlan 1951). (ξ, η) are the elliptical coordinates defined by

$$\begin{cases} x = c\ \cosh\xi \cos\eta \\ y = c\ \sinh\xi \sin\eta \end{cases}$$

The elliptical sectional contour is represented by $\xi = \xi_o = \frac{1}{2} \ln\frac{a+b}{a-b}$, and

$$q_{pm} = \frac{k_{pm}^2 c^2}{4}, \bar{q}_{pm} = \frac{\bar{k}_{pm}^2 c^2}{4}.$$

Irregular frequencies occur as q_{pm} and $\bar{q}_{pm}$ are positive roots satisfying

$$\begin{cases} Ce_p(\xi_o, q_{pm}) = 0 & (p = 0,1,...) \\ Se_p(\xi_o, \bar{q}_{pm}) = 0 & (p = 1,2,...) \end{cases} \tag{4.4.3b}$$

To find values of q_{pm} and $\bar{q}_{pm}$ necessitates solving a linear equation. For example, by solving

$$Ce_o(\xi_o, q_{0m}) = \frac{1}{\sqrt{2}} [1 - \frac{q}{2}\cosh 2\xi_o + q^2(\frac{\cosh 4\xi_o}{32} - \frac{1}{16}) - ...] = 0$$

to obtain

$$\begin{Bmatrix} q_{01} \\ q_{02} \end{Bmatrix} \approx (\cos 2\xi_o \pm \sqrt{\frac{3}{2}})/(\frac{\cosh 4\xi_o}{16} - \frac{1}{8})$$

4.4.2. Approximate formulations

As derived and described in §4.4.1, analytical predictions for the irregular frequency are quoted only for very simple geometries and not available for realistic marine structures of more complicated or of more irregular configuration. By using the known expressions of irregular frequencies for a rectangle or a rectangular box, Wu and Price (1986e) introduced an equivalent rectangle or rectangular box method to approximate the irregular frequencies occurring in the analysis of an arbitrary two- or three-dimensional body.

4.4.2a. The equivalent rectangle formulation

The equivalent rectangle formulation is based on an assumption that

the irregular frequencies in an arbitrary two-dimensional section are equal to those of an equivalent rectangle of an equal sectional area (A_s) with an equivalent beam (B_e) and draft (h_e).

The equivalent rectangle formula is given by

$$\omega_m = \sqrt{gk \coth(kh_e)}$$
$$k = \frac{m\pi}{B_e} \quad \text{for } m = 1,2,... \tag{4.4.4}$$

where ω_m is the mth irregular frequency and

$$B_e = (C_s)^{\alpha} B, \quad h_e = \frac{A_s}{B_e}$$

Here $C_s = A_s/Bh$ is the cross-sectional coefficient, B is the beam on the waterline and h is the draft measured from the midpoint of the beam. α is an empirical correction coefficient and the recommended value is $\alpha = (1 + \ln m)/8$.

Apparently, when a section tends to a rectangle, the above equivalent rectangle formula becomes the exact solution of a rectangle as given in Equation (4.4.1). It can also be found that the approximate predictions correlate the analytical results for a triangle from Equation (4.4.2). That is, the first three irregular frequencies ($\omega\sqrt{B/2g}$) are 1.53, 1,94 and 2.38 by approximation against 1.54, 1.98 and 2.34 by analytical solution.

The equivalent rectangle method has been incorporated in the developed two-dimensional hydrodynamic analysis computer package and experience gained through various practical applications to ships and offshore structures. To demonstrate this, Station 16 of a ship is taken as an example computation. The predicted approximate values of the first two irregular frequencies are 1.43 and 1.86. These precisely coincide with the irregular phenomena observed in numerical calculation of added mass and damping coefficients of the section appearing around frequencies 1.43 and 1.89, see Figure 4.4.1.

4.4.2b. The equivalent box formulation

Similar to the equivalent rectangle formulation for two-dimensional bodies (§4.4.2a), an equivalent box technique is also devised to approximate the irregular frequency values associated with the three-dimensional body analysis. It is dependent upon an equivalent box assumption:

in order to evaluate irregular frequencies, an arbitrary three-dimensional body may be represented by a rectangular box of 'equivalent' length, beam and draft with the same displacement volume as the original structure.

Based on the above assumption, the irregular frequencies of an arbitrarily shaped body may be expressed by an equivalent box formula:

$$\begin{aligned} \omega_{pm} &= \sqrt{gk\coth(kh_e)} \\ k &= \pi\sqrt{(\frac{p}{L_e})^2 + (\frac{m}{B_e})^2} \quad \text{for } p = 1,2,\ldots,\ m = 1,2,\ldots \end{aligned} \tag{4.4.2}$$

where L_e, B_e and h_e are the equivalent length, beam and draft.

Detailed formulation, validation and application of the equivalent box technique are given in Appendix 4.1.

4.5. Modified Green Function Method

Great efforts have been made to eliminate the irregular frequencies. Though various remedies are proposed (for details, see INTRODUCTION, Appendix 4.2), few have been widely accepted and efficiently applied in practical computation. Amongst all these proposed techniques, the modified Green function approach seems rather promising and is more relevant to the present work.

Theoretical approaches using the modified Green function originate in the solution of high frequency problems derived by Ursell (1953). And recently, Ursell (1981) further provided the

method with a rigorous theoretical basis, and proved that a modified Green function integral equation is free of irregular frequencies when a proper combination of the basic Green function and a sufficient large number of multipoles is used.

In a more practical way, Ogilvie and Shin (1978) proposed an efficient two-dimensional Green function form and showed that the method was capable of eliminating the first irregular frequency.

Because of practical importance in analysing SWATH ships, catamarans and offshore structures, this method is further extended in the present work to eliminate irregular frequencies associated not only with mono-hulls but also with twin- and multi-hulled bodies.

4.5.1. Outline of Ursell's theory

Ursell (1981) defined a modified two-dimensional Green function as

$$G^*(p,q) = G_o(p,q) + \sum_{m=0}^{M} a_m \Phi_m(p) \Phi_m(q) + \sum_{m=0}^{N} b_m \Psi_m(p) \Psi_m(q) \qquad (4.5.1a)$$

where $G_o(p,q)$ is the ordinary Green function, Equation (3.4.2). The multipoles Φ_m and Ψ_m are given by

$$\begin{aligned}
\Phi_o(p) &= \int_0^\infty \frac{e^{\mu z}\cos\mu y}{\mu - \nu} d\mu - i\,\pi \exp(\nu z + i\nu z) \\
\Psi_o(p) &= -\frac{\partial \Phi_o}{\partial y} = \int_0^\infty \frac{\mu\, e^{\mu z}\sin\mu z}{\mu - \nu} d\mu - \pi\nu \exp(\nu z + i\nu z) \\
\Phi_m(p) &= \frac{\cos 2m\theta}{r^{2m}} + \frac{\nu}{2m-1}\frac{\cos(2m-1)\theta}{r^{2m-1}} \quad (M = 1,2,\ldots) \\
\Psi_m(p) &= -\frac{\partial \Phi_m}{\partial y} = \frac{\sin(2m+1)\theta}{r^{2m+1}} + \frac{\nu}{2m}\frac{\sin 2m\theta}{r^{2m}} \quad (M = 1,2,\ldots)
\end{aligned} \qquad (4.5.1b)$$

with a_m and b_m chosen such that the imaginary parts of a_m and b_m are positive. If M and N are sufficiently large, Ursell proved that the two-dimensional Green function integral equations

(4.2.3b) and (4.2.4) are free of irregular frequency. A modified Green function form for finite water depth is also derived by Ursell (1981).

4.5.2. Modified three-dimensional Green function

Analogous to Ursell's two-dimensional theory outlined in §4.5.1, a possible modified three-dimensional Green function may be written as

$$G^*(P,Q) = G_o(P,Q) + \sum_{m=0}^{M} a_m \Phi_m(P)\Phi_m(Q) + \sum_{m=0}^{N} b_m \Psi_m(P)\Psi_m(Q) + \sum_{m=0}^{L} c_m \Theta_m(P)\Theta_m(Q) \quad (4.5.2a)$$

where $G_o(P,Q)$ is the ordinary three-dimensional Green function given by Equation (3.2.2).

The multipoles Φ_m, Ψ_m and Θ_m may have the forms:

(1) Wave source: $\Psi_o(P) = G_o(P,\bar{Q})$;

(2) X-direction dipole: $\Psi_o(P) = -\dfrac{\partial}{\partial x}\Phi_o$;

(3) Y-direction dipole: $\Theta_o(P) = -\dfrac{\partial}{\partial y}\Phi_o$;

(4) Symmetrical multipoles:

$$\Phi_m(P) = \frac{P_{2m}(\mu)}{r^{2m+1}} - \frac{\nu}{2m}\frac{P_{2m-1}(\mu)}{r^{2m}} \quad (M = 1,2,\ldots);$$

(5) Anti-symmetrical multipoles:

$$\begin{Bmatrix}\Psi_m(P)\\ \Theta_m(P)\end{Bmatrix} = \begin{Bmatrix}x-a\\ y-b\end{Bmatrix}\frac{-1}{r^{2m+2}}\left\{\frac{\nu}{2m}\left[(2m)P_{2m-1}(\mu) + \frac{z-c}{r}P'_{2m-1}(\mu)\right] - \frac{2m+1}{r}P_{2m}(\mu) - \frac{z-c}{r^2}P'_{2m}(\mu)\right\}$$

where $\bar{Q}(a, b, c) = \bar{Q}(a, b, 0) \in \bar{D}$ is a point on the interior free-surface. P_n is the Legendre function. M, N and L are chosen sufficiently large and the imaginary parts of a_m, b_m and c_m are positive. $r = \sqrt{(x-a)^2 + (y-b)^2 + (z-c)^2}$ and $\mu = (z-c)/r$.

An equivalent expression for finite water depth is possible if the multipoles take the forms given by Thorne (1953).

4.5.3. A multiple Green function

Two-dimensional hydrodynamic computation programs are the routine tools used in sea-keeping (or further, structural) analysis of ships and a wide range of offshore structures such as semi-submersibles. In particular, a recent development in both naval research and commercial use is focused on SWATH ships and catamarans (§9.3). Development of a more sophisticated two-dimensional method free of mathematical failures for twin- and multi-hulled marine structures becomes an urgent task.

4.5.3a. Formulation

By extending Ogilvie and Shin's asymmetric Green function form (1978), a procedure has been proposed to derive a multiple Green function expression (Appendix 4.2). The new formula is given by

$$G^*(p,\ q, \bar{p}_1, \bar{p}_2, \ldots, \bar{p}_N) = G_o(p,q) + \sum_{j=1}^{N} \tilde{G}(p,\ q,\ \bar{p}_j) \qquad (4.5.3a)$$

where $G_o(p,q)$ is again the basic two-dimensional Green function, whilst $\tilde{G}(p,\ q,\ \bar{p}_j)$ is the additional Green function written as

$$\tilde{G}(p,\ q,\ \bar{p}_j) = exp(\nu\zeta - i\,\nu|\eta - \bar{y}_j|)\left\{C_{j1}\, sgn(\eta - \bar{y}_j)\,\frac{\partial G_o}{\partial \eta}\Big|_{\zeta=0}^{\eta=\bar{y}_j} + C_{j2}\frac{\partial G_o}{\partial \zeta}\Big|_{\zeta=0}^{\eta=\bar{y}_j}\right\} \qquad (4.5.3b)$$

The integer N relates to the multi-hull body with N separate free-surface piercing hulls. $\bar{p}_j(\bar{y}_j,\ 0)$ is located on the interior free-surface of the jth sub-hull. That is, for a mono-hull, N = 1; for a twin-hull (or two mono-hull system), N = 2; and for a four-hulled body (or four monohull sys-

tem), N = 4; and so on.

Details of the theory, derivation and reasoning are given in Appendix 4.2.

4.5.3b Examples

Around an irregular frequency, the mathematical formulation of the Green function integral equation becomes ill-conditioned and erroneous solutions are obtained. In particular, abrupt changes with unrealistic values are found in the resultant added mass, damping coefficients and wave exciting forces (Appendix 4.1).

In addition to the application of the multiple Green function in effectively eliminating irregular frequency effects in the analysis of a rectangular section shown in Appendix 4.2, another three examples, i.e. a circular, a triangular and a caisson section, are presented in Figures 4.5.1-3 respectively. In these mono-hull examples, again, abrupt variations associated with irregular frequencies in sway, heave and roll added mass and damping coefficients are removed by the present method. These confirm the validity of the present technique in solving the irregular frequency problem associated with mono-hull sections.

Moreover, the present formula is also capable of removing irregular frequency effects from the analysis of twin-hulls (or two body systems). Two examples are already displyed in Appendix 4.2 for a twin rectangular section, and a two-hull section consisting of a rectangle and a triangle. Here, a set of computational data is shown in Figures 4.5.4a, b, for a twin rectangular hull at 15^o of heel angle. It can be seen from Figure 4.5.4a that, by an ordinary Green function method, abrupt changes appear in the resultant added mass and damping coefficients with unrealistic negative damping values. When the multiple Green function formulation is used, however, the abrupt variations with negative damping values disappear, whilst the rapid changes due to resonant waves between the two sub-hulls remain. According to Wu and Price's formulae (1986f) of

resonant waves for various marine structures, the first wave resonance occur at around $\omega^2 B/2g = \pi/2 = 1.57$, exactly matching the remaining rapid changes in the calculated added mass and damping coefficients in Figure 4.5.4b.

The final examination involves the floating four circular structure shown in Figures 4.5.5a, b and c. This consists of four circular cylinders of radius a = 1.0m, with a central line distance between adjacent cylinders of 3.0m. The results derived using the basic Green function are shown in Figure 4.5.5a, whilst those produced by the present multiple Green function technique are given in Figure 4.5.5b. In Figure 4.5.5a, a mathematical failure occurs in the ordinary method analysis at frequency $\omega^2 B/2g = 1.87$, but this is eliminated by the present modified mathematical model. In Figure 4.5.5c, the results of both methods are presented together. This shows that the predictions derived by the two theories agree very well except in the vicinity of the irregular frequency.

From these studies and several more practical applications carried out though not described here, it may be concluded that:

(1) The present method calculation coincides with the original integral equation method results at the frequencies below the first irregular frequency.

(2) The multiple Green function method removes irregular frequencies from the calculations associated with mono-, twin-, and multi-hulled ship or offshore structure sections.

In short, the proposed multiple Green function method is efficient and effective.

4.6. The Interior Integral Equation Solution

In analysing hydrodynamic characteristics of ships and offshore structures by a singularity

distribution technique, without exception, the surface integral equation, i.e. Equation (4.1.3b) or (4.2.3b) (or the related source distribution form, Equation (4.1.4) or (4.2.4)) is used to obtain the wave velocity potential (or source strength) solution. Subsequently, the velocity potential at any exterior location can be determined by the exterior integral equation, e.g. Equation (4.1.3a) or (4.2.3a), from the solution obtained over the body surface.

In the present work, the feasibility of applying the interior integral equation, i.e. (4.1.3c) or (4.2.3c), to solve the boundary value problem representing the wave-structure interaction is examined. The theoretical explanation and numerical techniques for the interior integral equation are given in Appendix 4.3.

In Appendix 4.3, two major conclusions are drawn:

(1) The resultant matrix equation of the interior integral equation retains the diagonal dominant feature to the same level as the surface integral one, if all the interior field points are arranged close to the body's wetted surface.

(2) If all the interior field points are located on an artificial interior surface nearly parallel and sufficiently close to the body surface, the interior integral equation method results in hydrodynamic data correlating well with those derived from the surface integral approach.

Two examples are illustrated in Appendix 4.3 including a ship section and a rectangular section. The first example indicates that the interior formulation works and possesses the same irregular frequency problem as the surface integral equation. And the second shows that the modified Green function proposed in §4.5.3 eliminates the irregular frequency effects associated with an interior method as it does in the surface integral technique.

A range of numerical experiments have been conducted to examine the applicability of the proposed method. Of these, three more examples are discussed here.

A triangular section

A triangular section of beam B and draft h = B/2 is taken in a series of computational study. The interior field points are chosen such that they form an interior triangle of scale reduction factor C_s. These interior geometric data are produced automatically in the calculation. When $C_s = 1.0$, these field points are on the true body surface and the interior integral equation becomes identical with the surface integral one.

Numerical studies range from $C_s = 0.5$ to 1.0 and the calculated data are shown in Figures 4.6.1a-d with each compared with the surface integral equation results denoted by $C_s = 1.0$.

Figures 4.6.1a-c show computed sway, heave and roll added mass and damping coefficients by the interior integral technique for $C_s = 0.99$, 0.9 and 0.8 respectively in comparison with the surface integral method data, i.e. $C_s = 1.0$. These demonstrate that except for the abrupt variations due to the irregular frequencies, good agreements are observed.

In Figure 4.6.1d, the interior integral method data for $C_s = 0.65$, 0.60, 0.55 and 0.5 are presented against the surface data indicated by $C_s = 1.0$. The comparison clearly shows that when the interior surface is chosen too small, the interior integral formulation produces hydrodynamic data greatly deviating from those derived by the surface integral method.

Similar observations can be found from investigations into various sectional geometries. Therefore, it is suggested that the interior surface, where the interior points are located, be chosen sufficiently close to the real body surface.

A rectangular box

For a rectangular box of length B, beam B and draft h = B/2, computations are carried out using both the interior and the surface integral equation methods with $C_s = 0.965$ and 1.0, respectively. As can be seen from Figure 4.6.2, the calculated sway and heave added mass coefficients are again in reasonable agreement.

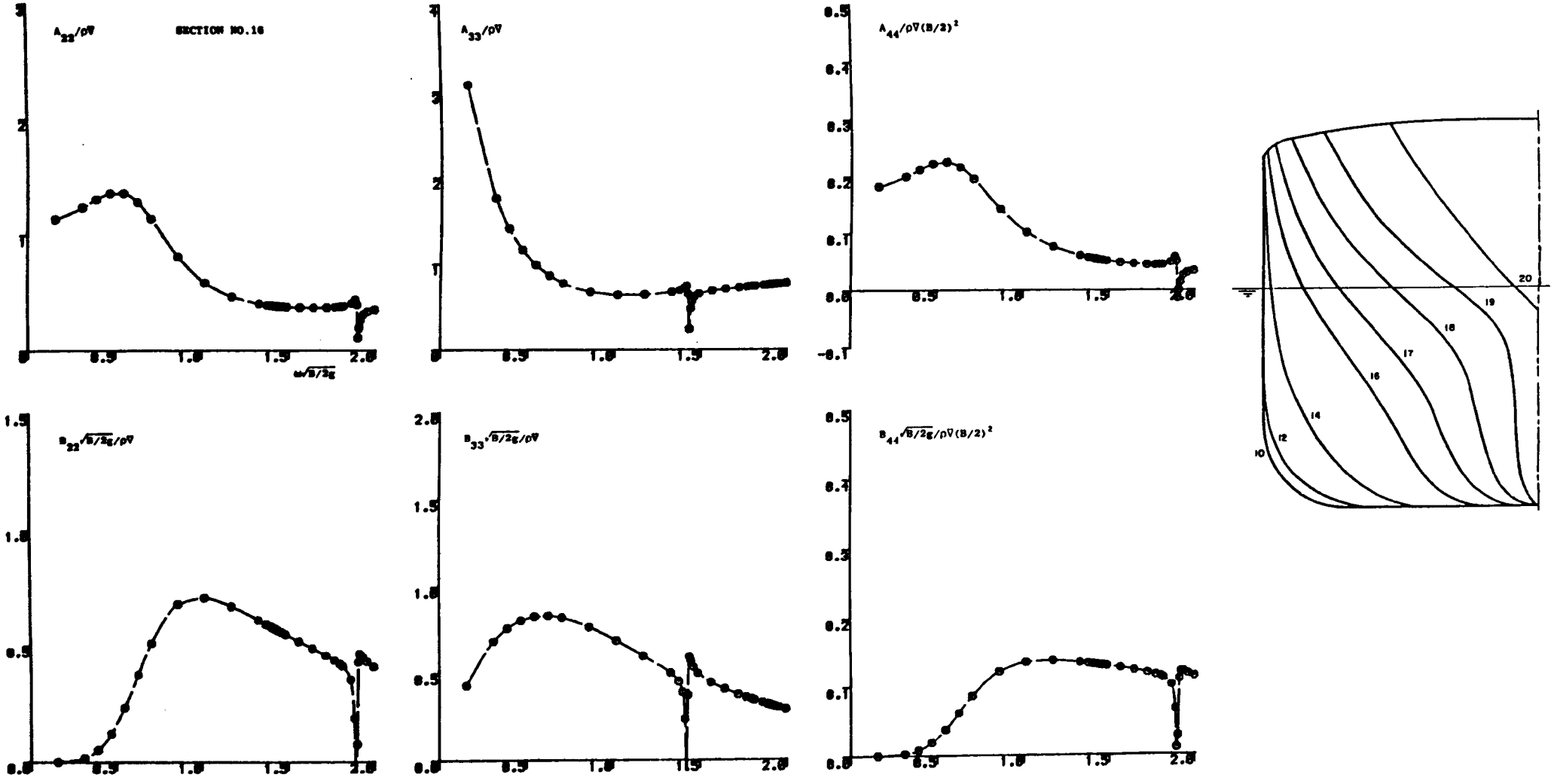

Figure 4.4.1. Irregular frequency phenomena in calculated added mass and damping coefficients for a ship section (No. 16).

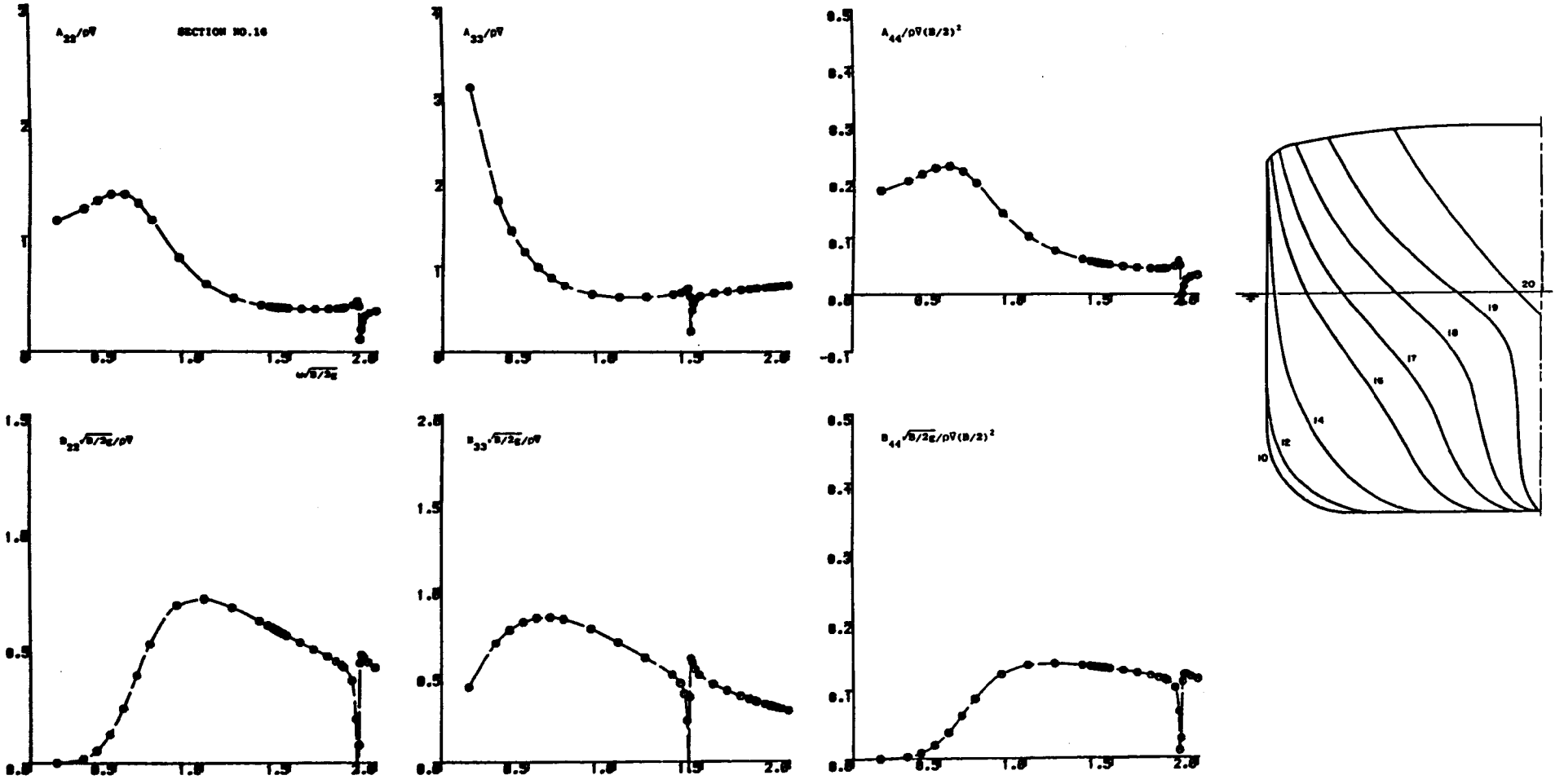

Figure 4.4.1. Irregular frequency phenomena in calculated added mass and damping coefficients for a ship section (No. 16).

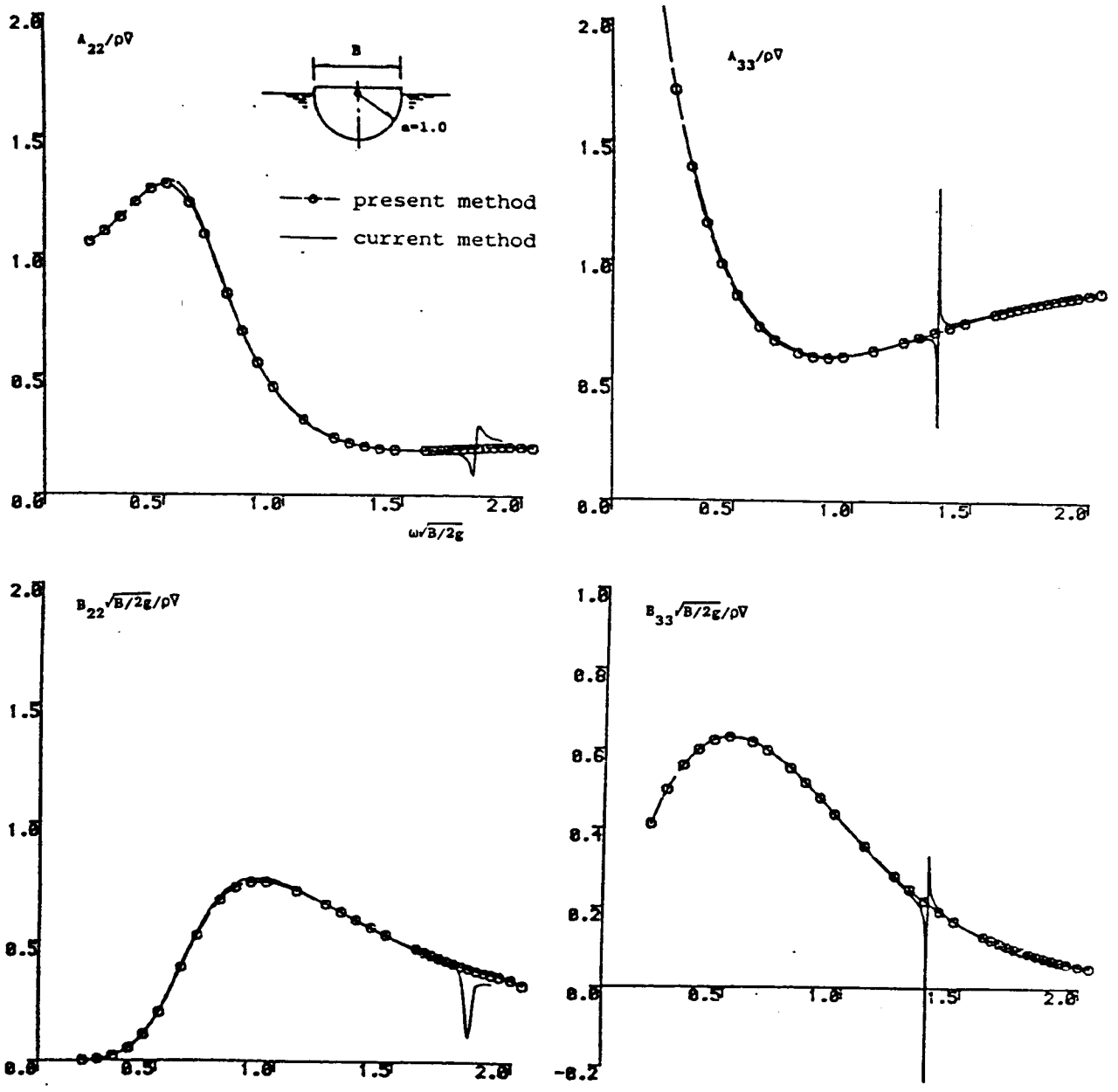

Figure 4.5.1. Sway and heave added mass and damping coefficients of a circular section calculated by the ordinary and the present multiple Green function method.

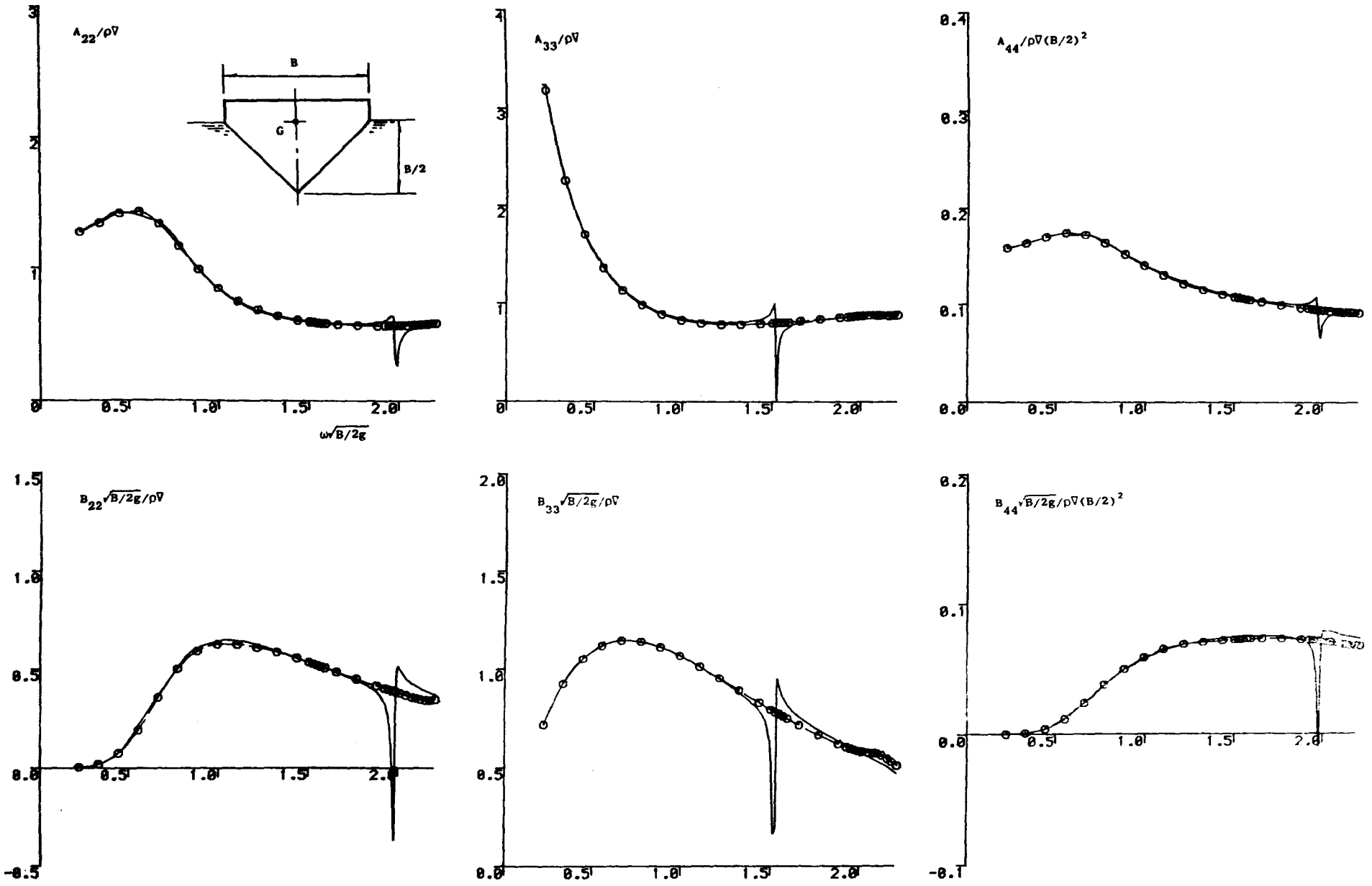

Figure 4.5.2. Hydrodynamic coefficients of a triangular section calculated by the ordinary Green function technique (solid lines) and the present multiple Green function method (circular points).

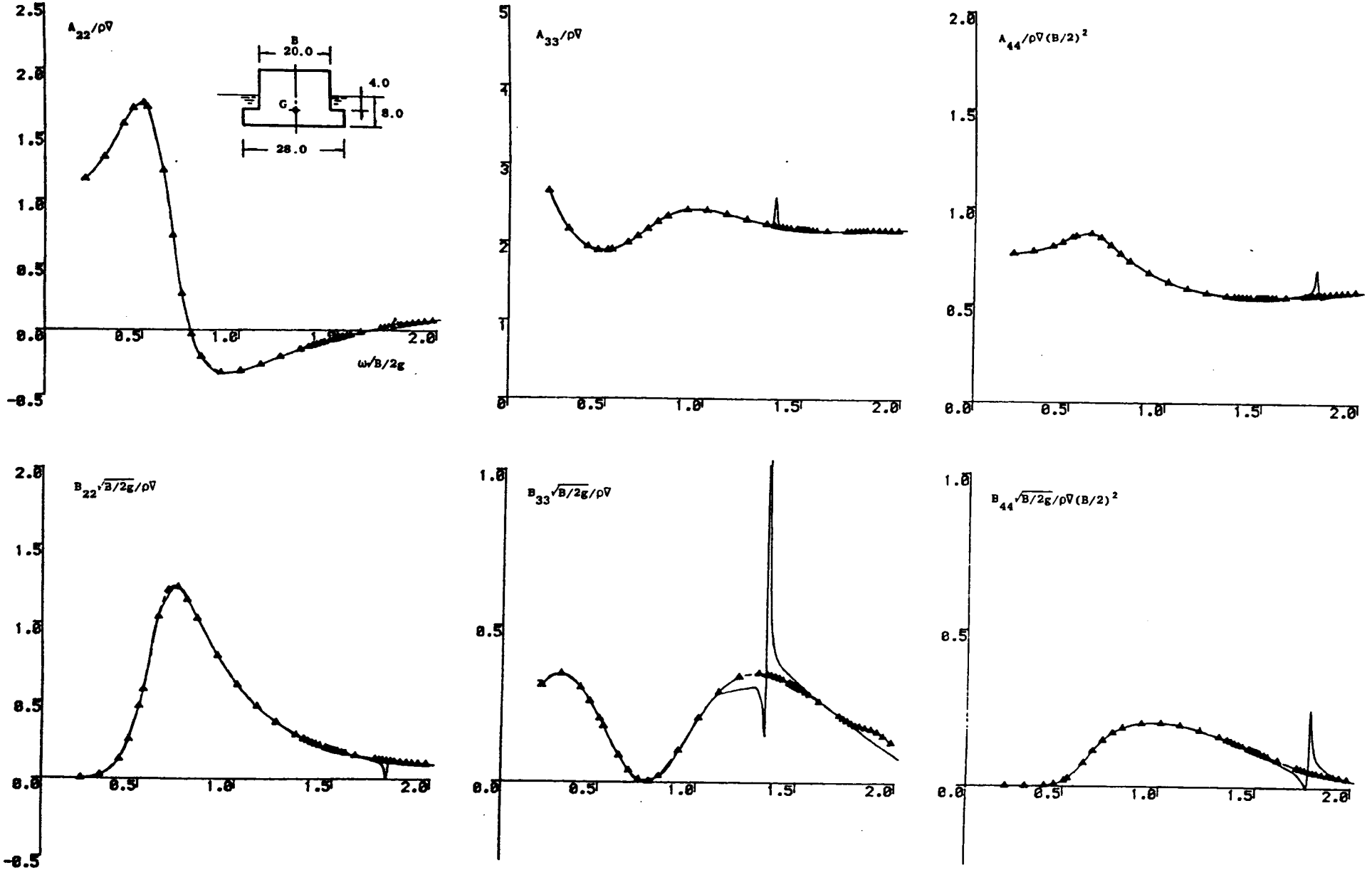

Figure 4.5.3. Hydrodynamic coefficients of a caisson section calculated by the ordinary Green function technique (solid lines) and the present multiple Green function method (triangular points).

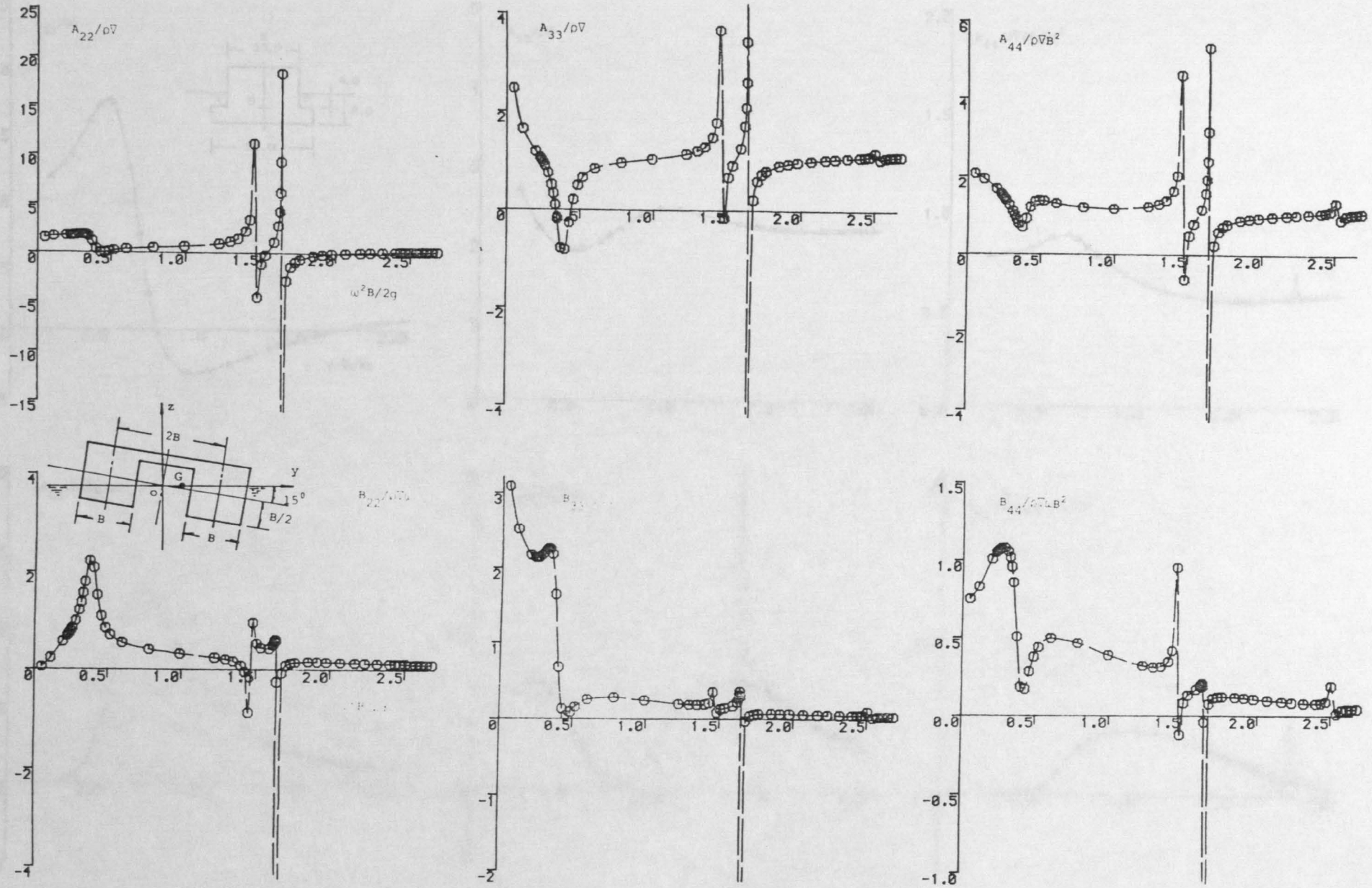

Figure 4.5.4a. Hydrodynamic coefficients of a twin rectangular hull at 15° of heel angle calculated by the ordinary Green function method.

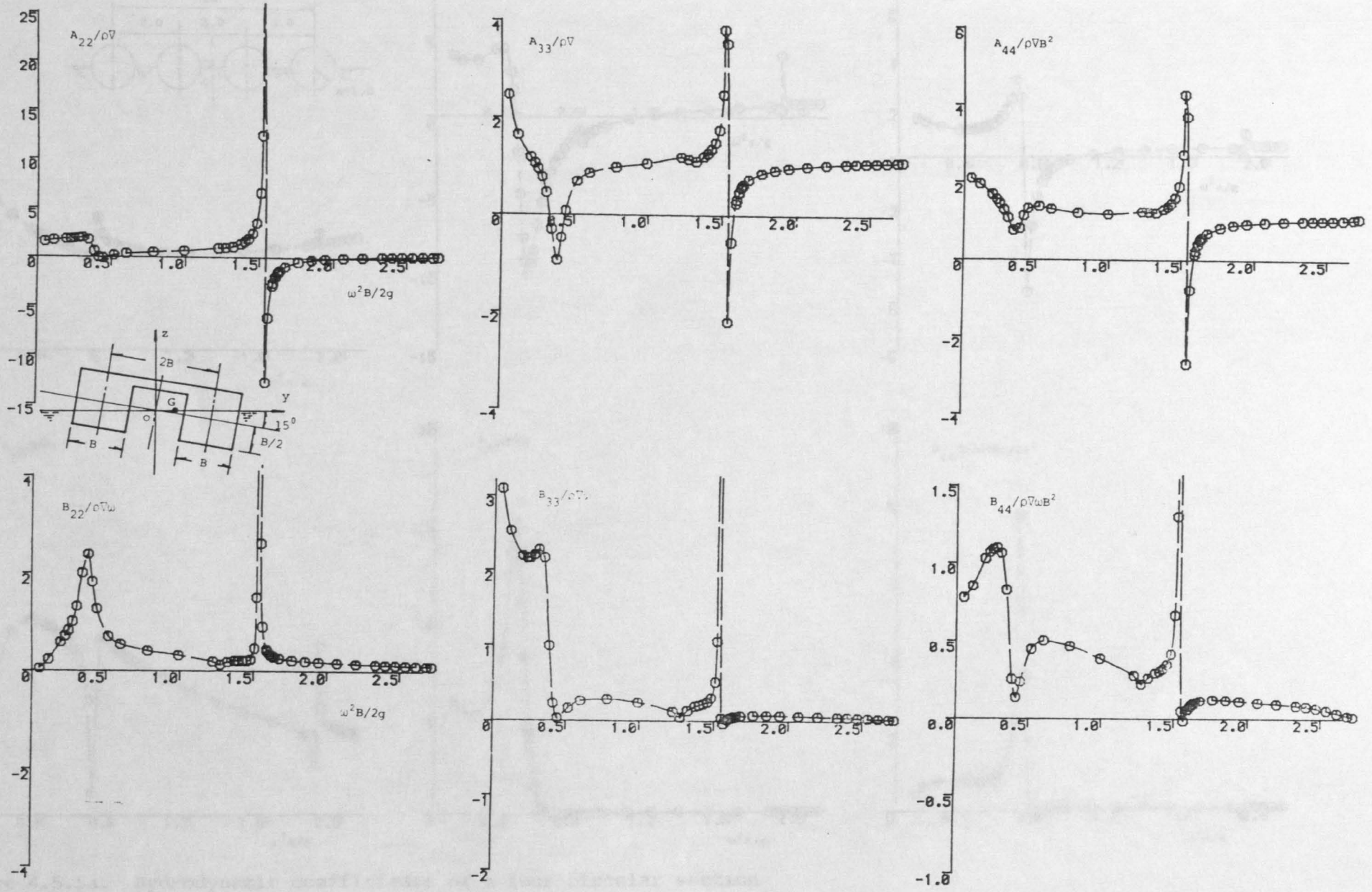

Figure 4.5.4b. Hydrodynamic coefficients of a twin rectangular hull at 15° of heel angle calculated by the present multiple Green function method.

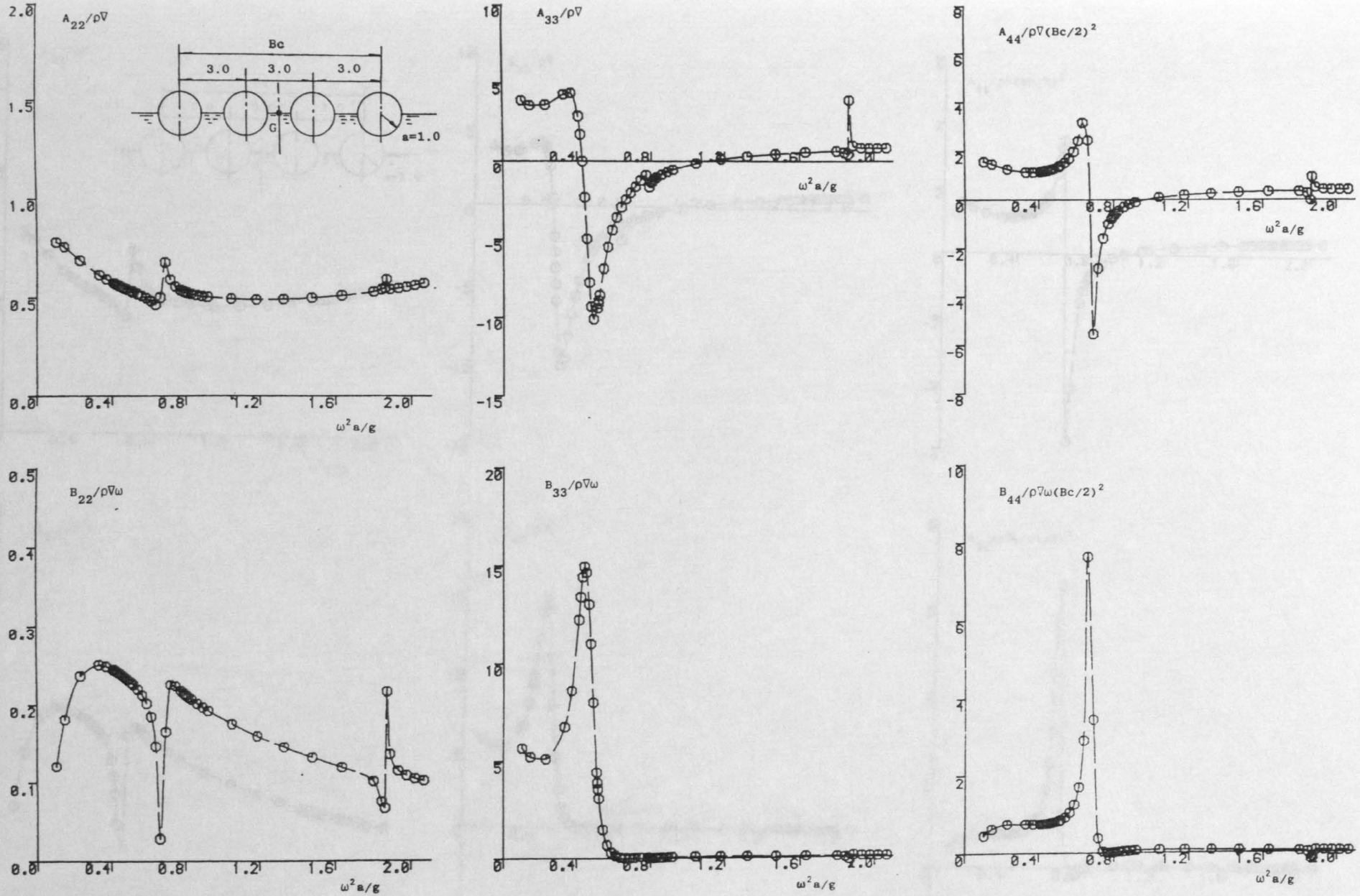

Figure 4.5.5a. Hydrodynamic coefficients of a four circular section calculated by the ordinary Green function method.

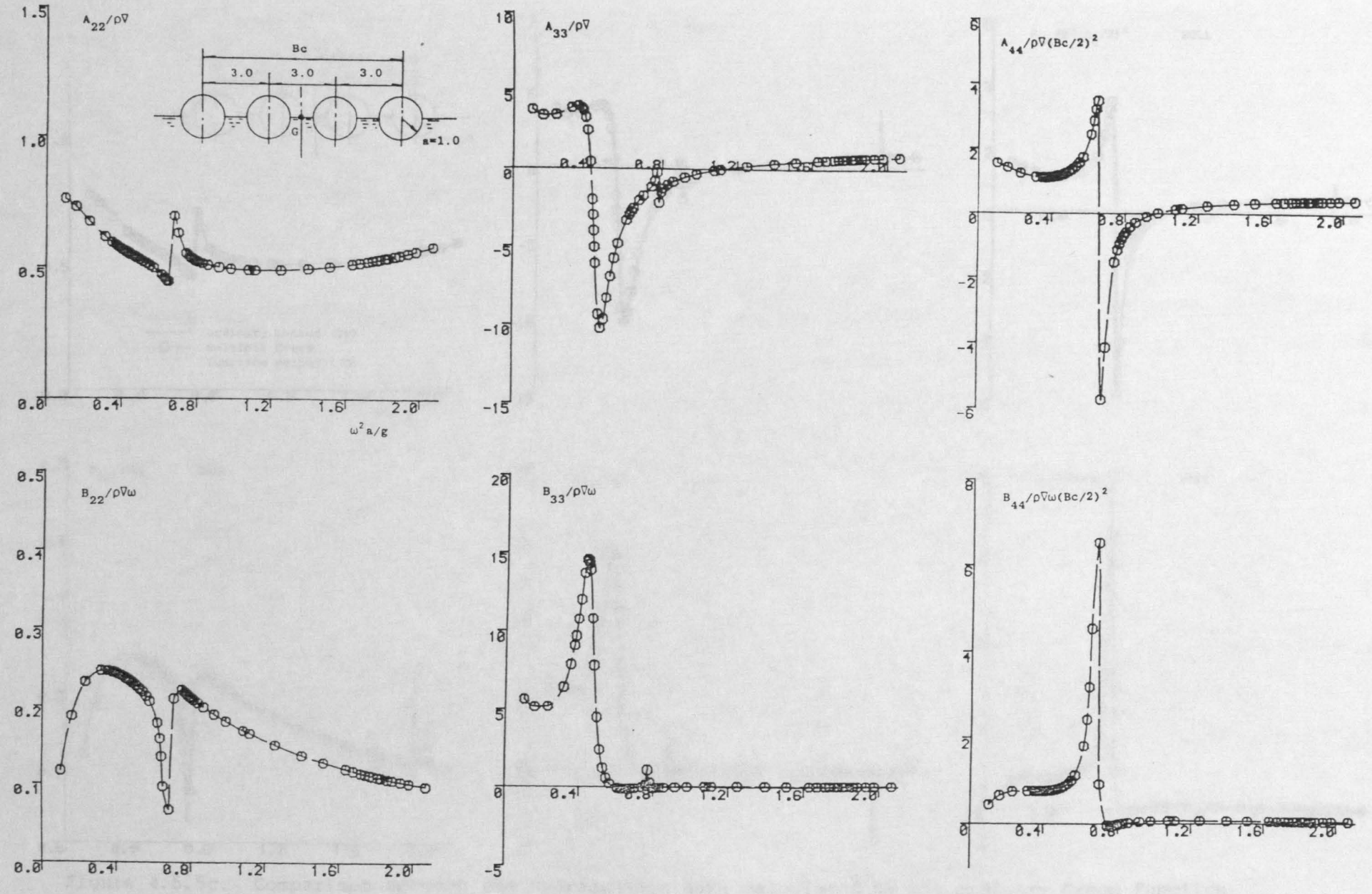

Figure 4.5.5b. Hydrodynamic coefficients of a four circular section calculated by the multiple Green function method.

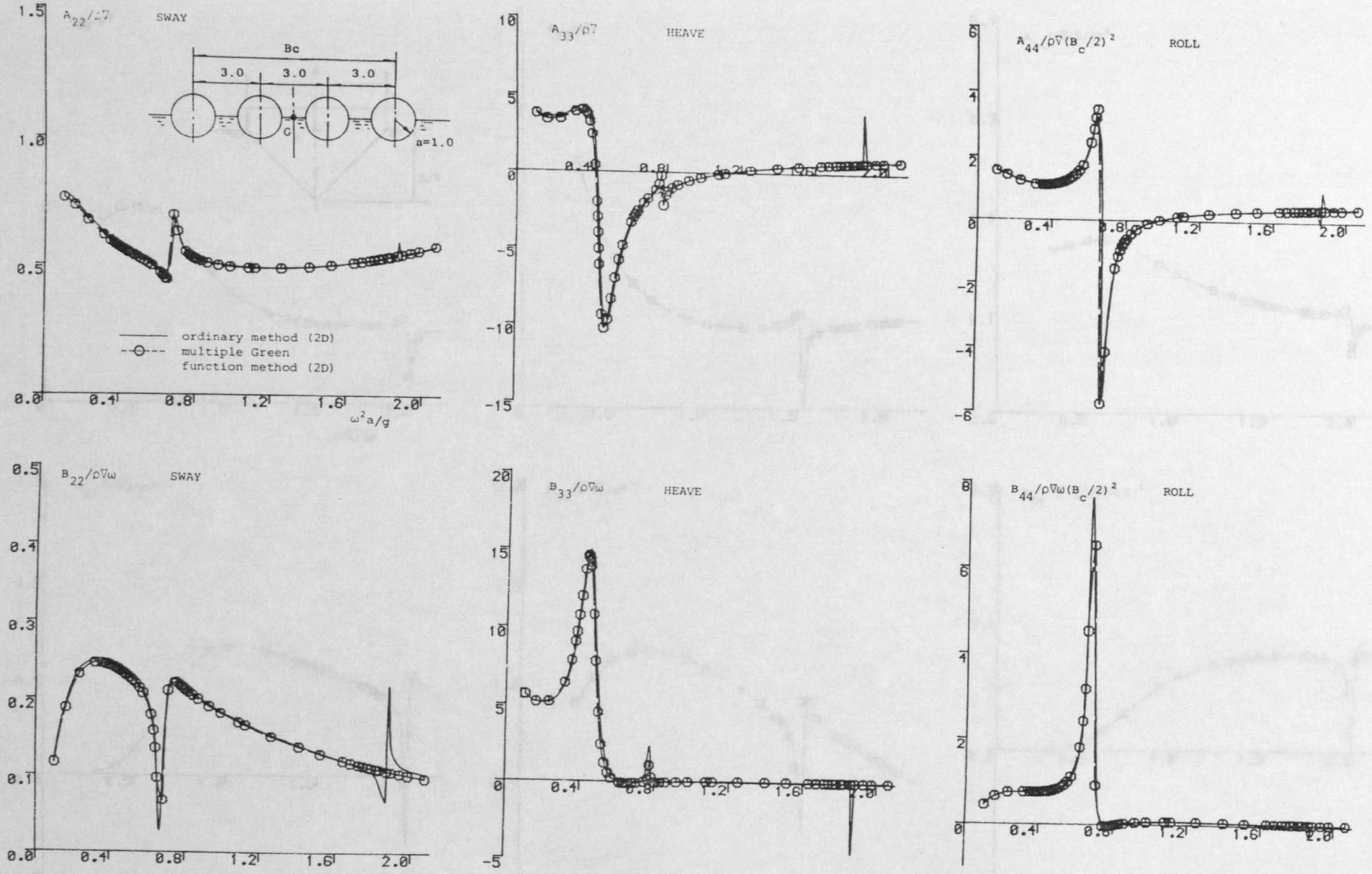

Figure 4.5.5c. Comparison between the hydrodynamic data calculated by the ordinary Green function technique and the present multiple Green function method.

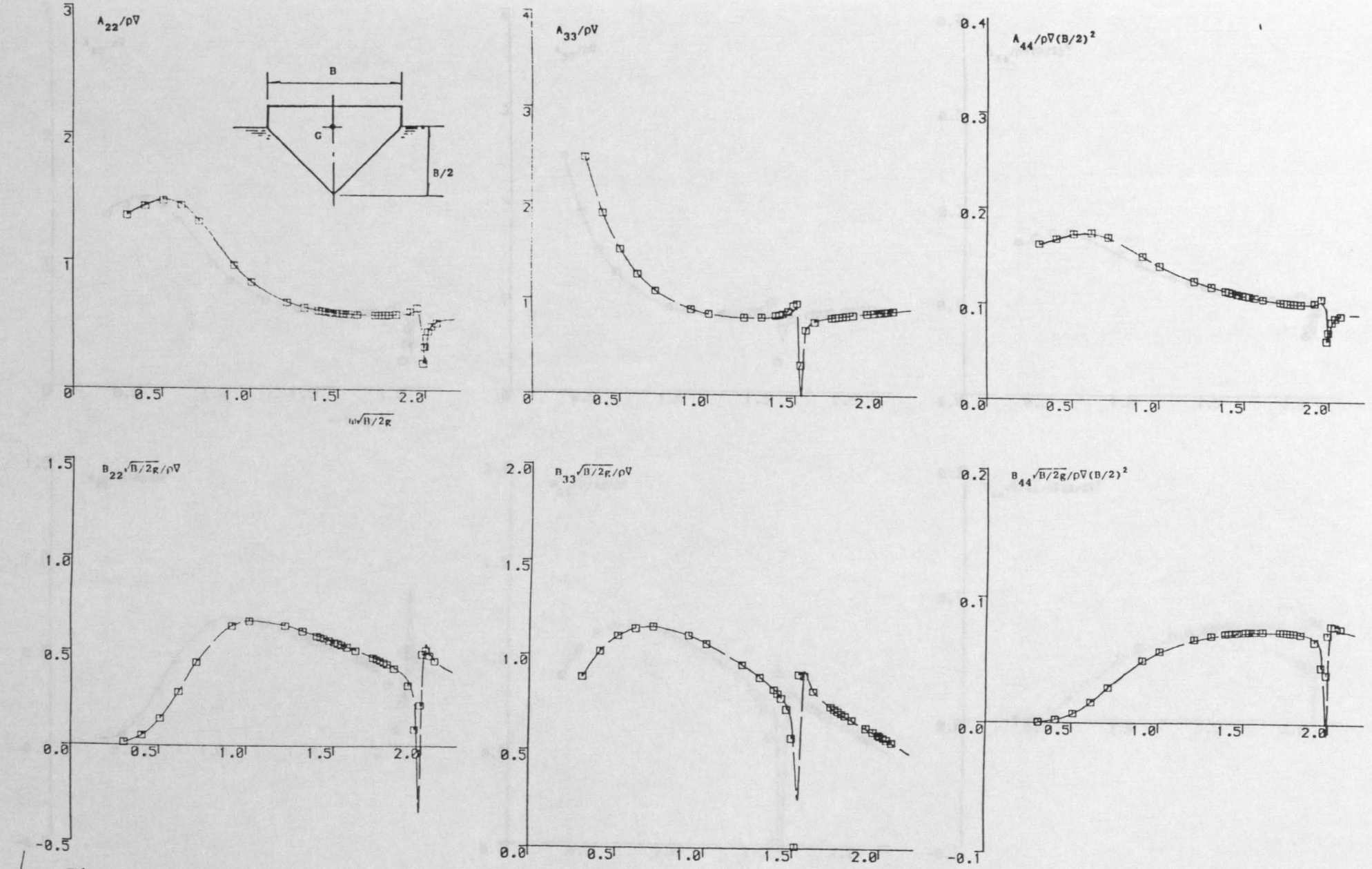

Figure 4.6.1a. Hydrodynamic coefficients of a triangular section calculated by the surface (square points) and the interior integral equation formulation (dash lines, for C_s=0.99).

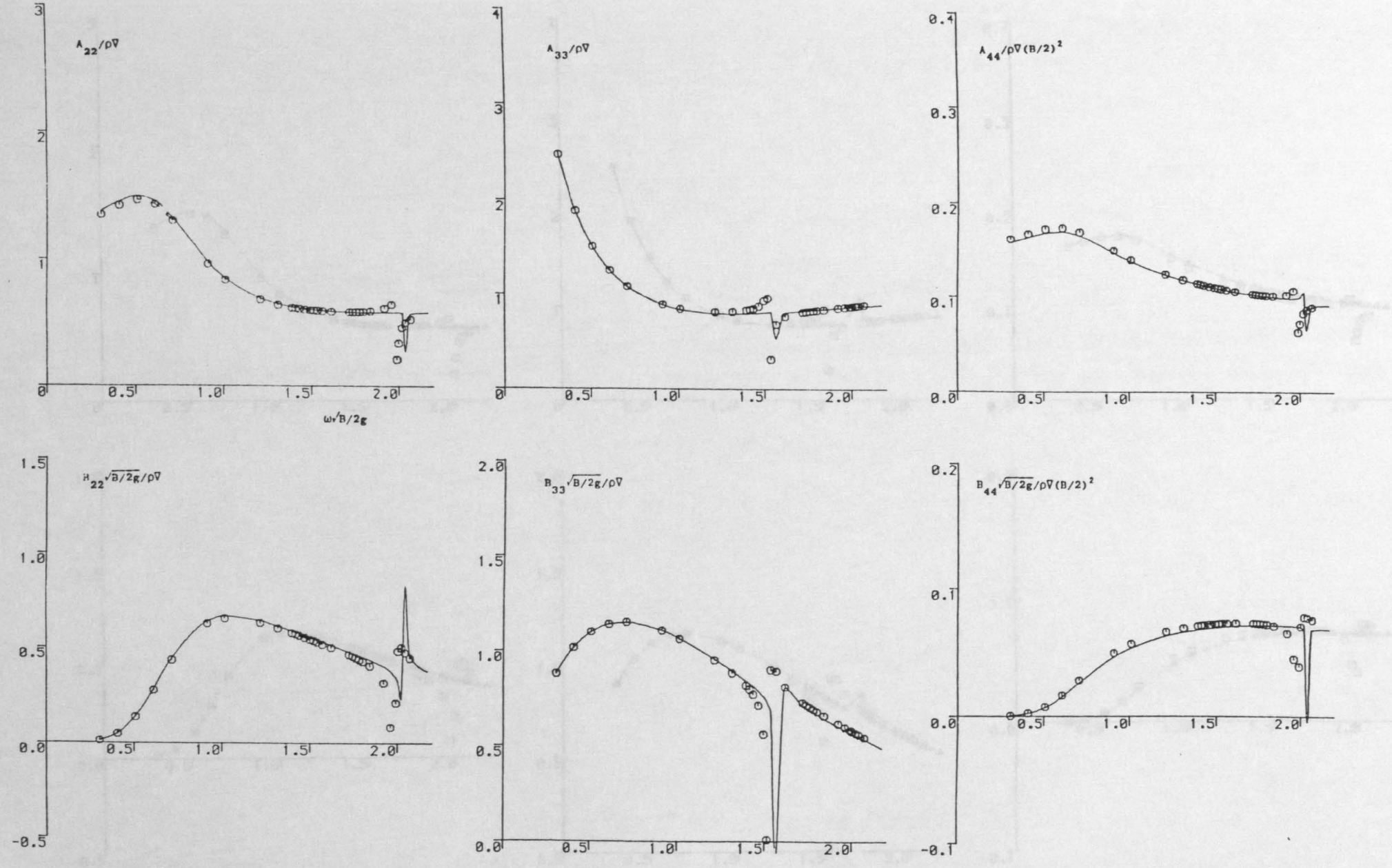

Figure 4.6.1b. Hydrodynamic coefficients of a triangular section calculated by the surface (circular points) and the interior integral equation formulation (solid lines, for C_S=0.9).

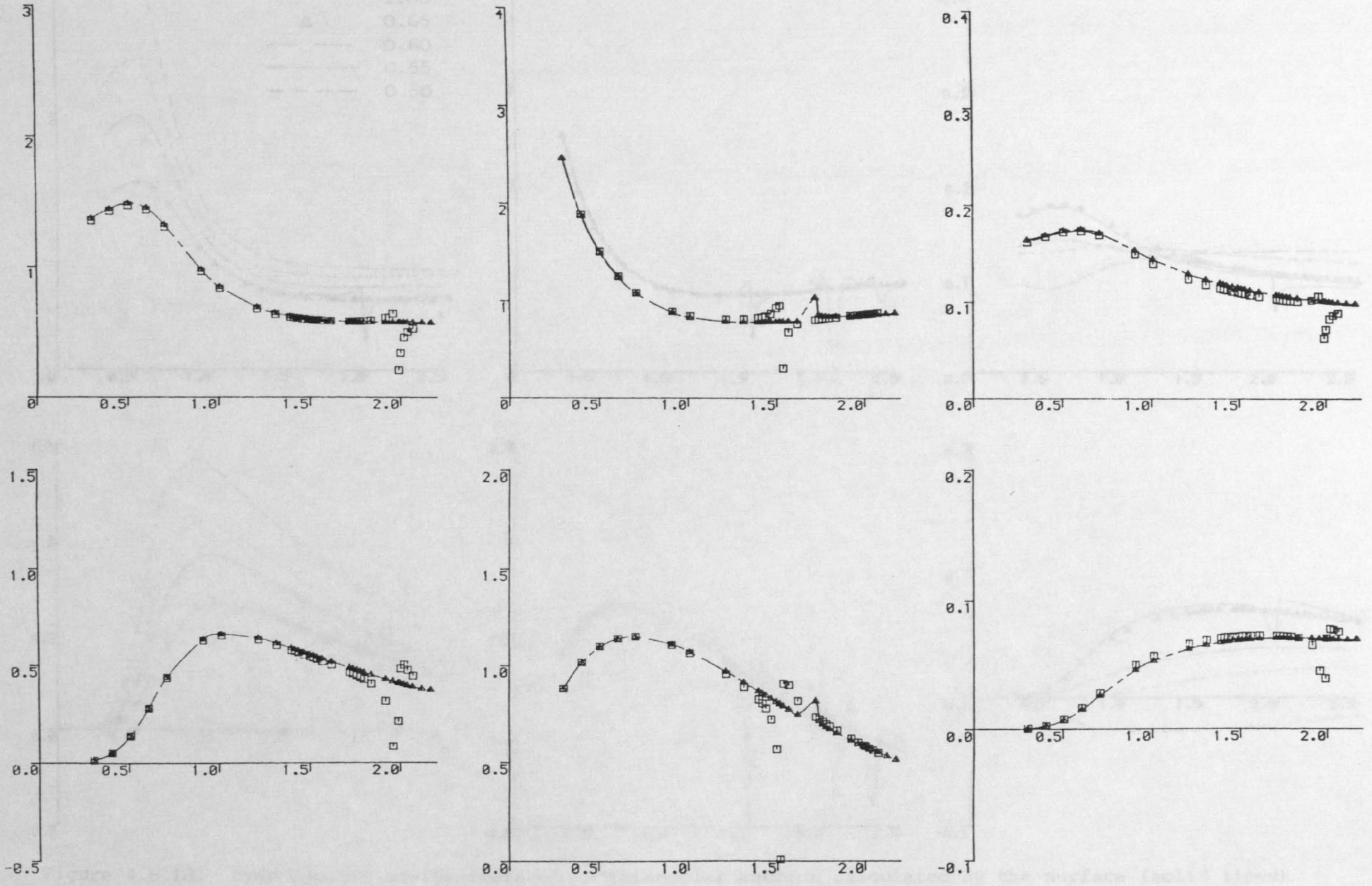

Figure 4.6.1c. Hydrodynamic coefficients of a triangular section calculated by the surface(square points) and the interior integral equation formulation (triangular points and dash lines, for C_s=0.8).

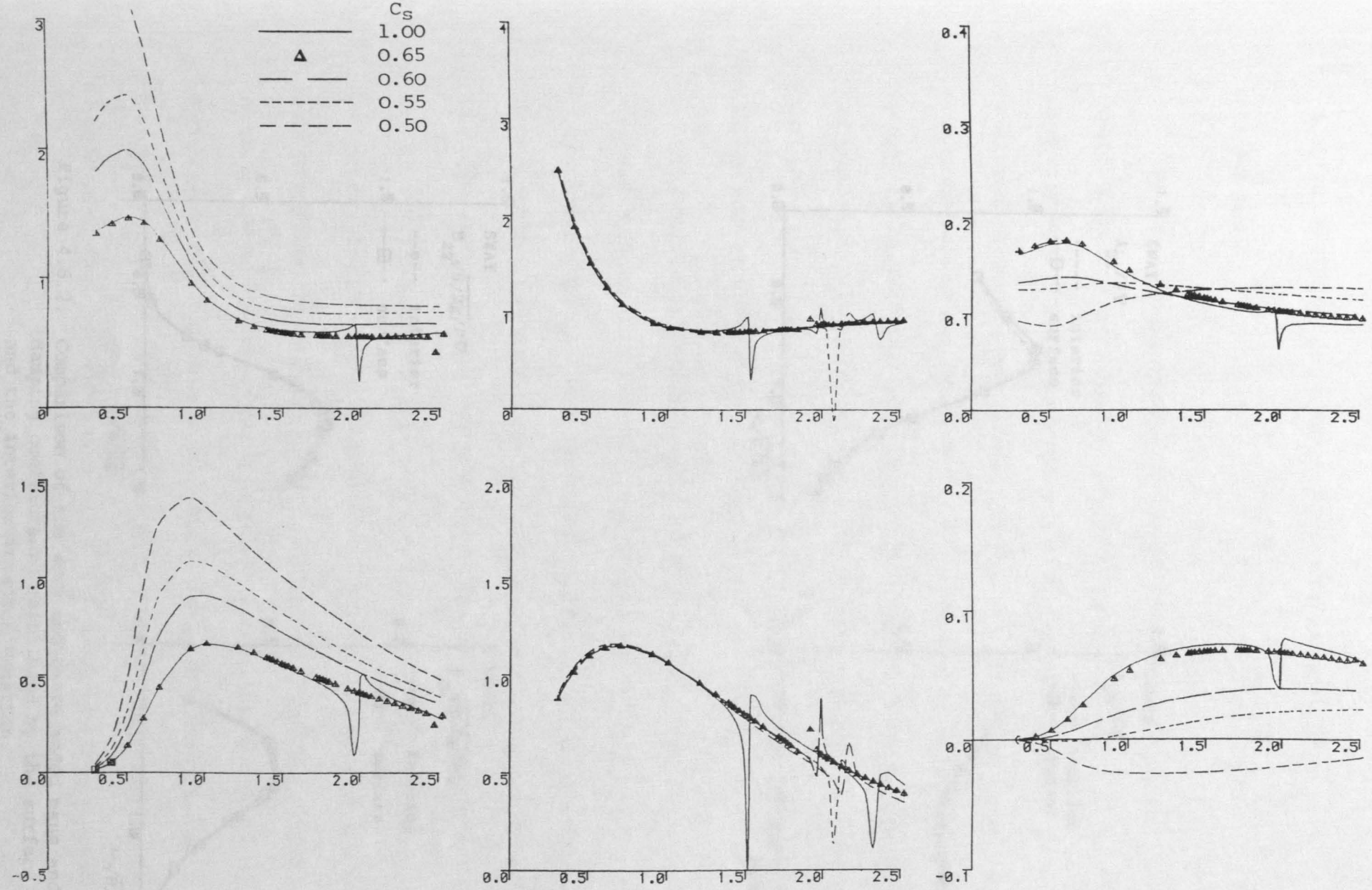

Figure 4.6.1d. Hydrodynamic coefficients of a triangular section calculated by the surface (solid lines) and the interior integral equation formulation (for C_S=0.5-0.65).

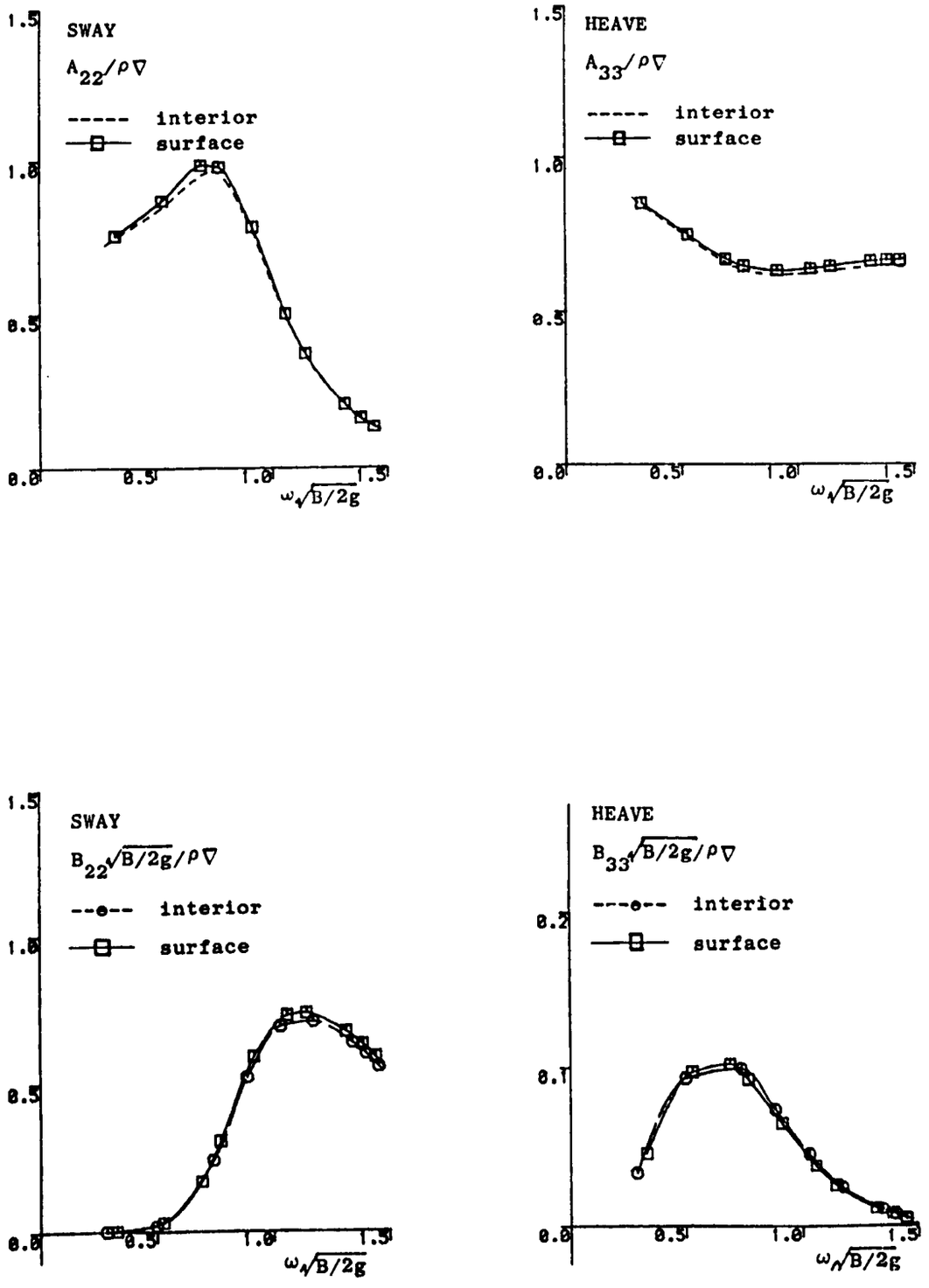

Figure 4.6.2. Comparison of the sway and heave added mass and damping coefficients calculated by the surface and the interior integral equation.

5. SOLUTION APPROXIMATION TO HORIZONTAL PLANE MOTIONS

5.1. Introduction

Due to the sophisticated theories developed by theoreticians and with the help of modern computers, more and more complicated mathematical formulations and related computer packages are used nowadays for the predictions of wave loads and motion responses of offshore structures and unconventional vessels. Such rapid advances bring great advantages but they may also conceal dangers, since some researchers and analysts rely too much on mathematics and forget, partly or wholely, the physical 'feel' of the problem under investigation. With a little insight into the physical nature of the phenomenon, some confused theoretical predictions puzzling theoretical researchers might be clearly explained and some so-called rigorous approaches appear superfluous and can therefore be substituted by much simpler ones.

As discussed in §1.2, two important organised international investigations into the numerical evaluation of motions and wave forces of a semi-submersible (Takagi et al 1985) and a TLP (Eatock Taylor and Jefferys 1986) showed that although significant discrepancies were observed in the predictions of vertical plane modes, i.e. heave, roll and pitch, numerical results for the horizontal plane modes including surge, sway and yaw displayed good mutual agreement.

The reported discrepancies in the vertical plane modes indicate a large scattering of the predicted data of radiation and diffraction wave forces. This should occur not only in the vertical plane but also in the horizontal plane since both are solved by an identical mathematical process. Hence, the achieved reasonable correlation in the horizontal plane motions can only arise because of the negligible contributions from the total of the radiation and diffraction forces compared with the Froude-Krylov forces. Previously, Wu and Price(1986a) realised this possibility and intuitively set up an assumption that both the radiation and diffraction forces in the horizontal plane

modes can be ignored for certain types of marine structures. Based on this hypothesis, very reasonable approximations for the horizontal plane motions of shallow draft structures are obtained though originally no full theoretical proof was given.

This Chapter provides a theoretical basis and physical reasoning of the phenomenon occurring in the horizontal modes of motion of long bodies of full sectional shape or shallow draft structures. This is of significance since the main floaters of many large offshore structures and service vessels likely fall into these two groups of geometries. On the basis of order estimates, approximate solutions to the horizontal plane motions of these structures can be derived and are further verified by comparison with experimental data or more sophisticated theoretical results. These solutions are applicable in the preliminary design stages of vessels. Details of this theoretical study are described in Appendix 5 and here only the major points and conclusions are outlined.

5.2. Brief Description of the Work

The marine structures under consideration are restricted to full shaped bodies of slender and/or shallow draft geometric feature. A full shaped body is one having a full midsection form and a large vertical prismatic coefficient. Namely, $C_m = A_m/(Bh)$ is nearly unity and $C_{vp} = \nabla/(A_w\, h)$ tends to 1.0. Here A_m and A_w are the midship section and the waterplane area. B is the beam. h is the draft. ∇ represents the body displacement volume.

Within Appendix 5, §3 deals with floating slender bodies, §4 treats submerged slender structures, §5 includes a discussion of two-dimensional shallow draft bodies and §6 involves full three-dimensional shallow draft structures.

5.2.1. Slender bodies (§3-4, Appendix 5)

A slender body is characterised by a slenderness parameter $\varepsilon = B/L$, $h/L = O(\varepsilon)$ and $n_1 = O(\varepsilon)$ as listed in Table 1 of Appendix 5. Corresponding to wave length $L/\lambda = O(1)$, estimated orders of various force components are listed in Tables 2 and 3 (Appendix 5). From the order analysis, the following conclusion can be drawn:

(1) In the surge motion, the radiation and diffraction forces (F_1^H andF_1^7) are higher order small quantities compared to the Froude-Krylov force (F_1^0), which therefore dominates the surge response.

(2) In the sway and yaw modes, the radiation and diffraction forces (F_j^H and F_j^7 for j = 2, 6) are of the same order in magnitude to the Froude-Krylov forces ($F_j^0, j = 2, 6$) but their combinations, i.e. $F_j^B = F_j^7 + F_j^H$, j = 2, 6, are of $O(\varepsilon)$ smaller than the latter. Therefore, in the sway and yaw response predictions, by ignoring the former two contributions (i.e. F_j^B) leads to an error of $O(\varepsilon)$ only.

5.2.2. Three-Dimensional Shallow Draft Bodies (§6, Appendix 5)

The shallow draft feature of a body is denoted by the small parameter $\varepsilon = h/B$ and also $h/L = O(\varepsilon)$. Orders of geometric dimensions are displayed in Table 7 (Appendix 5). Based on wave length $L/\lambda = O(1)$, the derived orders of individual force components are given in Table 8 of the Appendix. Resultant order estimates show clearly that for all the three horizontal motions the radiation and diffraction forces are of order ε^2 and are respectively $O(\varepsilon)$ higher than the relative Froude-Krylov forces of $O(\varepsilon)$. Hence, to the first order approximation, the surge, sway and yaw responses can be rationally predicted by inclusion merely of the Froude-Krylov force contributions.

5.2.3. Two-Dimensional Shallow Draft Bodies (§5, Appendix 5)

A combination of the slenderness and shallow draft features of the vessel makes the main body dimensions of orders $h/B = O(\varepsilon)$, $B/L = \varepsilon$ and $h/L = O(\varepsilon^2)$, see Tables 4, 5 of Appendix 5. With assumed wave length $L/\lambda = O(1)$, the orders of magnitudes of various forces on such a body can be estimated as displayed in Table 6 of the Appendix. Now the sum of the radiation and diffraction forces for each horizontal plane mode is a $O(\varepsilon^2)$ higher small quantity than the Froude-Krylov force. Thus more accurate horizontal motion predictions can be expected, correct to $O(\varepsilon^2)$, by neglecting both the radiation and diffraction force contributions in the case of a slender shallow draft body.

These discussions lead to a conclusion that as a marine structure possesses slenderness and shallow draft, the surge, sway and yaw motions can be reasonably approximated by considering only the Froude-Krylov forces, and the error in the motion predictions are generally $O(\varepsilon)$ or $O(\varepsilon^2)$.

According to this approximation theory, analytical formulae describing the surge, sway and yaw responses are derived for marine structures of simple geometry i.e. rectangular barges, circular or elliptical docks and triangular jack-up rig platform, etc.

Besides the theoretical proof, numerical data provided by the present theory for horizontal motions of rectangular barges, a circular dock and a triangular platform are illustrated together with other available data. These show satisfactory correlation with existing experimental results and data derived from full three-dimensional analyses not only in long wave lengths as initially imposed in the theory but also in shorter waves (§7, Appendix 5).

5.3. Practical Importance

The following points of practical importance may be deduced from this investigation:

(1) This work validates the negligibility of the radiation and diffraction forces in surge motion predictions of slender and/or shallow draft bodies.

(2) This analysis reveals the mutual cancellation phenomenon between the radiation and diffraction force components in sway and yaw modes of a long marine structure of full shaped sectional geometry.

(3) The above two findings provide an explanation to the observed good agreement of horizontal motion data from the different sources included in the international investigations as discussed in §5.1, despite the severe deviations existing in the vertical plane motions.

(4) An approximation theory for the horizontal motions is established similar to the Froude-Krylov hypothesis (§1.1.4) and is proved correct to $O(\varepsilon)$ for slender or shallow draft bodies, or to $O(\varepsilon^2)$ for slender shallow draft structures.

(5) High computational economy and prediction accuracy comparable to much more complicated approaches may make this approximation theory of more practical use in preliminary design stages.

6. A NEW SHALLOW DRAFT THEORY

6.1. Introduction

Because a large group of offshore structures and service vessels can be classified as shallow draft bodies, theories to tackle this type of marine structure have been proposed. As discussed in the introductory part and illustrated in Figure 1 of Appendix 6, the original development work was done by MacCamy (1961) and Kim (1963), and extended by Maeda (1981), to deal with flat plates only. The weakness of the idealised model in application is obvious, since the real shallow draft structures are of finite draft rather than of zero value, and they experience six modes of motion (as far as rigid body is concerned) rather than only the three vertical plane motions.

To achieve further improvement on the shallow draft theory, Wu and Price (1986a, d) suggested a self-consistent shallow draft method capable of predicting the six degrees of motion as well as including the effect of finite draft. Their assumptions can be summarised as follows:

(1) In determining the surge, sway and yaw motions, both the radiation and diffraction forces can be ignored.

(2) The finite draft effect on the wave exciting forces in heave, roll and pitch is taken into account by a factor of $exp(-kh)$, where k denotes the wave number and h draft of the body.

This more or less heuristic theory in both the two- and three-dimensional versions has been successfully applied to various realistic marine structures, including barges, docks, offshore platforms and a semi-submersible in transit (Appendix 6). This effective approach, however, has not been fully theoretically justified.

In the discussion of §5 and Appendix 5, it was concluded that for a shallow draft body the errors introduced in surge, sway and yaw motion predictions are of higher order small quantities due to the neglect of both the radiation and diffraction forces. This goes the same way to justify

the first assumption as stated above.

To complement the work presented in Appendix 6, a perturbation procedure is adopted, which enables the present theory to be formulated more rigorously. To avoid tedious mathematical derivation, which is of less interest to naval architects and offshore engineers, mathematical descriptions are given only where thought necessary.

6.2. Special Case: a Flat Plate

Consider an idealised flat plate, i.e. a structure of zero draft (h = 0) and of flat surface S_w coincident with its waterplane area or projective area on the free surface, S_o. There exist the results that

$$\frac{\partial G}{\partial n} = -\frac{\partial G}{\partial z} = k\,G(P,Q) \quad on\ S_o\ (z=0)$$

$$\lim_{\substack{z\to 0\\ \zeta\to 0}} \left[4\pi - \int_{\Delta S_Q} \frac{\partial}{\partial n_Q}\left(\frac{1}{r}+\frac{1}{r_1}\right)dS\right] = 4\pi$$

Hence, the integral equation (4.1.3b) reduces to

$$4\pi\,\phi_j(P_o) + k\int_{S_o}\phi_j(Q_o)\,G(P_o,Q_o)\,dS = -\int_{S_o} V_{nj}(Q_o)\,G(P_o,Q_o)\,dS \quad P_o,Q_o \in S_o \qquad (6.2.1)$$

$$V_{nj} = \begin{cases} -i\omega n_j & j = 1,2,\ldots,6 \\ -\partial\phi_o/\partial n & j = 7 \end{cases}$$

Here the Green function $G(P_o,Q_o)$ is given by the shallow draft Green function (3.2.6) for deep water or (3.1.6) for finite water depth. Apparently, over the flat surface, $n_j = 0$ for j = 1, 2, 6 and therefore potential solutions for these three horizontal modes are all zero.

The integral equation (6.2.1) with the Green function expression (3.2.6) forms the deep water flat plate theory of Kim (1963), whilst with expression (3.1.6) represents the flat plate theory of Maeda (1981) for finite water depth. The following discussion shows how the finite

draft can be included in the mathematical model and approximations given for the three horizontal motions.

6.3. Shallow Draft Perturbation

For a three-dimensional shallow draft body of length L, beam B and draft h, the shallow draft characteristic is given by a parameter $\varepsilon = kh \ll 1$, and

$$h/L = O(\varepsilon),\ h/B = O(\varepsilon),\ h/\lambda = O(\varepsilon),$$

$$n_1 = O(\varepsilon),\ n_2 = O(\varepsilon),\ n_3 = O(1).$$

The mean wetted surface S_w is assumed expressible by

$$z = \varepsilon S(x, y) \le 0 \tag{6.3.1}$$

and its projected area on the mean free-surface is denoted by S_o.

The velocity potential solution satisfying the boundary value problem (4.3.1) is assumed expandable with respect to order ε, i.e. the same as the other physical and geometrical quantities. That is

$$\phi_j(x,y,z;\varepsilon) = \sum_{n=0}^{\infty} \phi_j^{(n)}(x,y,z)\,\varepsilon^n \quad \text{for } P(x,y,z) \in D \tag{6.3.2a}$$

On the body surface S_w, a Taylor series expansion gives

$$\phi_j(x,y,z) = \phi_j(x,y,\varepsilon S(x,y)) = \sum_{n=0}^{\infty}\sum_{m=0}^{\infty} \frac{1}{m!} \frac{\partial^m \phi_j^{(n)}(x,y,0)}{\partial z^m} [S(x,y)]^m\, \varepsilon^{n+m} \tag{6.3.2b}$$

$$\frac{\partial \phi_o(x,y,z)}{\partial n} = \sum_{n=0}^{\infty} [\frac{\partial \phi_o(x,y,0)}{\partial n}]^{(n)}\, \varepsilon^n = \sum_{n=0}^{\infty} \frac{k^{n+1}\,[S(x,y)]^n}{n!\,A} B_o(x,y)\,\varepsilon^n \tag{6.3.2c}$$

$$n_j = \sum_{n=0}^{\infty} n_j^{(n)}(x,y,0)\,\varepsilon^n \tag{6.3.2d}$$

and so on. Here $A = \sqrt{1 + \varepsilon^2[(\frac{\partial S}{\partial x})^2 + (\frac{\partial S}{\partial y})^2]}$, and for deep water

$$B_o(x,y) = -\frac{ig\zeta_a}{\omega}\exp[ik(x\cos\beta + y\sin\beta)]\,[-1 + i\varepsilon(\frac{\partial S}{\partial x}\cos\beta + \frac{\partial S}{\partial y}\sin\beta)].$$

The resultant perturbation potential $\phi_j^{(n)}(x,y,z)$ (n = 0, 1,...) satisfies the equations

$$\nabla^2 \phi_j^{(n)}(x,y,z) = 0 \qquad in\ D \qquad a$$

$$(\frac{\partial}{\partial z} - k)\,\phi_j^{(n)}(x,y,z) = 0 \qquad on\ z = 0\ (off\ the\ body) \qquad (6.3.3b)$$

$$\frac{\partial}{\partial z}\phi_j^{(n)}(x,y,z) = 0 \qquad on\ the\ seabed \qquad c$$

$$-\frac{\partial}{\partial z}\phi_j^{(n)}(x,y,0) = V_j^{(n)}(x,y,0) + \begin{cases} -i\omega\, n_j^{(n)}\, A \\ -[\dfrac{\partial \phi_o(x,y,0)}{\partial n}]^{(n)}\, A \end{cases} \quad on\ z = 0\ (on\ the\ body) \quad (6.3.3d)$$

$$\lim_{R\to\infty} \sqrt{R}\,[\frac{\partial}{\partial R}\phi_j^{(n)}(x,y,z) - i\,k\,\phi_j^{(n)}(x,y,z)] = 0 \qquad (6.3.3e)$$

with

$$V_j^{(0)}(x,y,0) = 0$$

$$V_j^{(1)}(x,y,0) = -(\frac{\partial S}{\partial x}\frac{\partial}{\partial x} + \frac{\partial S}{\partial y}\frac{\partial}{\partial y})\,\phi_j^{(0)}(x,y,0) + S(x,y)\,\frac{\partial^2}{\partial z^2}\phi_j^{(0)}(x,y,0)$$

$$V_j^{(n)}(x,y,0) = -[\frac{\partial \phi_j(x,y,0)}{\partial n}]^{(n)} - \frac{\partial}{\partial z}\phi_j^{(n)}(x,y,0)$$

$$(n_1^{(0)}, n_2^{(0)}, n_3^{(0)}) = (0, 0, -1)/A$$

$$(n_1^{(1)}, n_2^{(1)}, n_3^{(1)}) = (\frac{\partial S}{\partial x}, \frac{\partial S}{\partial y}, 0)/A$$

$$(n_1^{(i)}, n_2^{(i)}, n_3^{(i)}) = 0 \quad \text{for } i \geq 2$$

$$(n_4^{(0)}, n_5^{(0)}, n_6^{(0)}) = (-(y - y_G), x - x_G, 0)/A$$

$$(n_4^{(1)}, n_5^{(1)}, n_6^{(1)}) = (z_G\frac{\partial S}{\partial y}, -z_G\frac{\partial S}{\partial x}, (x - x_G)\frac{\partial S}{\partial y} - (y - y_G)\frac{\partial S}{\partial x})/A$$

$$(n_4^{(2)}, n_5^{(2)}, n_6^{(2)}) = (-S\,\frac{\partial S}{\partial y}, S\,\frac{\partial S}{\partial x}, 0)/A$$

$$(n_4^{(i)}, n_5^{(i)}, n_6^{(i)}) = (0, 0, 0) \qquad \text{for } i \geq 3$$

Equations (6.3.3) define a set of perturbed linear potential problems and therefore, each individual order of the velocity potential $\phi_j^{(n)}$ (n = 0, 1,...) may be solved by the integral equation below:

$$4\pi\,\phi_j^{(n)}(P_o) + k\int_{S_o}\phi_j^{(n)}(Q_o)\,G(P_o,Q_o)\,dS = -\int_{S_o} -\frac{\partial}{\partial\zeta}\phi_j^{(n)}(Q_o)\,G(P_o,Q_o)\,dS \quad P_o,\,Q_o \in S_o \tag{6.3.4}$$

6.4. First approximation

To a first approximation, only $\phi_j^{(0)}$ needs to be solved. That is,

$$4\pi\,\phi_j^{(0)}(P_o) + k\int_{S_o}\phi_j^{(0)}(Q_o)\,G(P_o,Q_o)\,dS = -\int_{S_o} -\frac{\partial}{\partial\zeta}\phi_j^{(0)}(Q_o)\,G(P_o,Q_o)\,dS \quad P_o,\,Q_o \in S_o \tag{6.4.1}$$

This is identical with the flat plate theory of §6.2.

From the perturbed normal components of the body given by Equation (6.3.3), it shows that

$$\frac{\partial}{\partial z}\phi_j^{(0)}(x,y,0) \equiv 0 \quad \text{for } j = 1,\,2,\,6$$

resulting in

$$\phi_j^{(0)}(x,y,0) \equiv 0 \quad \text{for } j = 1,\,2,\,6$$

Consequently, the zero order radiation forces are equal to zero for the surge, sway and yaw modes. According to the Haskind relationship, the zero order for the diffraction forces for these three horizontal modes should also have zero values. Since the zero order component of the incident potential ϕ_o is non-zero, the relevant Froude-Krylov forces, as well as the inertia forces, become dominant in the predictions of the surge, sway and yaw motion responses. The resultant orders of magnitudes of the various forces are exactly the same as those listed in Table 8 of Appendix 5.

Therefore, from the perturbation procedure based on the shallow draft of a three-dimensional body, it can also be concluded:

In surge, sway and yaw motion predictions, when both the radiation and diffraction forces are ignored, errors of order ε *are introduced into the mathematical model.*

This proves assumption one adopted by Wu and Price (§6.1).

6.5. Solutions of Order ε

In addition to the first approximation formulation given by Equation (6.4.1) the integral equation with respect to $O(\varepsilon)$ may be written as follows:

$$4\pi \phi_j^{(1)}(P_o) + k \int_{S_o} \phi_j^{(1)}(Q_o)\, G(P_o,Q_o)\, dS = -\int_{S_o} I_{nj}\, G(P_o,Q_o)\, dS \quad P_o, Q_o \in S_o \tag{6.5.1}$$

with

$$I_{nj} = \begin{cases} -i\omega \dfrac{\partial S}{\partial x} & \text{for } j = 1 \\ -i\omega \dfrac{\partial S}{\partial y} & \text{for } j = 2 \\ -i\omega[(x-x_G)\dfrac{\partial S}{\partial y} - (y-y_G)\dfrac{\partial S}{\partial x}] & \text{for } j = 6 \\ V_j^{(1)}(x,y,0) & \text{for } j = 3 \\ V_j^{(1)}(x,y,0) - i\,\omega\,(z_G)\dfrac{\partial S}{\partial y} & \text{for } j = 4 \\ V_j^{(1)}(x,y,0) - i\,\omega\,(-z_G)\dfrac{\partial S}{\partial x} & \text{for } j = 5 \\ V_j^{(1)}(x,y,0) - [\dfrac{\partial \phi_o(x,y,0)}{\partial n}]^{(1)} A & \text{for } j = 7 \end{cases}$$

Adding these order ε solutions to the zero order ones of Equation (6.4.1), all the radiation and diffraction potentials can be derived with error of $O(\varepsilon^2)$, i.e.

$$\phi_j^* = \phi_j^{(0)}(x,y,0) + \varepsilon\, \phi_j^{(1)}(x,y,0) + O(\varepsilon^2) \quad \text{for } j = 1, 2, ..., 7 \tag{6.5.2}$$

6.6. Finite Draft Correction

It can be seen that, for a three-dimensional shallow draft structure, Equation (6.5.2) together with integral equations (6.4.1) and (6.5.1) can be used to achieve motion and force predictions up to error $O(\varepsilon^2)$.

From a practical point of view, however, it is not convenient to solve Equation (6.5.1) related to order ε. Instead, a rational finite draft correction can be derived at least for a shallow draft body of a large flat bottom area. At first, only the diffraction potential is treated. In Equation (6.5.1) for $j = 7$, a simplification can be introduced by ignoring the first term $V_j^{(1)}$ on the right hand of I_{nj} (j = 7), i.e. assuming

$$I_{n7} \simeq -[\frac{\partial}{\partial n}\phi_o(x,y,0)]^{(1)}A.$$

Under this assumption, the combined diffraction potential of Equation (6.5.2) is now dependent upon a combined body boundary condition given as:

$$\nu_{n7}^* \simeq -(1-kh)[\frac{\partial}{\partial n}\phi_o(x,y,0)]^{(0)} \simeq -exp(-kh)[\frac{\partial}{\partial n}\phi_o(x,y,0)]^{(0)} = -\frac{\partial}{\partial n}\phi_o|_{z=-h} \qquad (6.6.1)$$

The combined potential is now solvable by the combination of integral equations (6.4.1) and (6.5.1). That is,

$$4\pi\,\phi_7^*(P_o) + k\int_{S_o}\phi_7^*(Q_0)\,G(P_o,Q_o)\,dS = -\int_{S_o}\nu_{n7}^*\,G(P_o,Q_o)\,dS \quad P_o, Q_o \in S_o \qquad (6.6.2)$$

This confirms the second assumption by Wu and Price as stated in §6.1 and used in Appendix 6.

The rationality of the proposed draft correction can also be verified by the form of the inner region solution which is explained as follows.

In *the inner region close to the body surface,* there exist:

$$\frac{\partial}{\partial x} = O(\varepsilon), \quad \frac{\partial}{\partial y} = O(\varepsilon), \text{ and } \frac{\partial}{\partial z} = O(1)$$

and therefore, the Laplace equation governing the diffraction potential in the inner region may be approximated by

$$\frac{\partial^2}{\partial z^2}\phi_7(x,y,z) \simeq 0 \tag{6.6.3}$$

This sheds light on the possible solution in the near field. An approximation solution satisfying Equation (6.6.3) and the free surface condition (6.3.3) in the inner region may be written in the form:

$$\phi_7(x,y,z) \simeq (1 + kz)\,\phi_7^{(0)}(x,y,0) \tag{6.6.4}$$

where $\phi_7^{(0)}(x,y,0)$ is the first approximation solution from the integral equation (6.4.1).

For a shallow draft structure of large flat bottom surface (other than curved one) of draft h, the diffraction solution on the flat bottom surface may be constructed as

$$\phi_7(x,y,z) = exp(-kh)\,\phi_7^{(0)}(x,y,0) + O(\varepsilon^2) \tag{6.6.5}$$

This derived formula is identical to expression (6.6.1). Therefore, from the point of view of the inner region solution, integral equation (6.6.2) together with the body boundary condition (6.6.1) represents a suitable approximation to the diffraction problem of a three-dimensional shallow draft structure.

6.7. Practical Procedure

In §6.6, a simple small draft correction is derived for the diffraction potential solution. However, the draft correction factor becomes more complicated as far as radiation potentials are concerned. Instead of finding directly a correction term, use can be made of the energy relationship between the wave exciting force and the related damping coefficient. From the energy rela-

tionship (see Newman 1978), there exists

$$B_{jj} = \frac{k}{8\pi\rho g\, V_g} \int_0^{2\pi} |F_j(\beta)|^2 \, d\theta \tag{6.7.1}$$

where $V_g = \omega/2k$ in deep water and β is the heading angle of the incident wave as defined previously.

From §6.6 it can be seen that

$$\phi_7^* = exp(-kh)\, \phi_7^{(0)}(x,y,0) \tag{6.7.2}$$

and the resultant wave exciting force

$$F_j^* = exp(-kh)\, F_j^{(0)} \quad \text{for } j = 3, 4, 5 \tag{6.7.3}$$

Substitute Equation (6.7.3) into Equation (6.7.1) it is resulted that

$$B_{jj}^* = exp(-2kh)\, B_{jj}^{(0)} \quad \text{for } j = 3, 4, 5 \tag{6.7.4}$$

That is, the finite draft correction to the damping coefficients of heave, roll and pitch take the form of exp(-2kh). In other words, when the shallow draft correction is considered, the heave, roll and pitch damping values equal those from the zero draft solution (6.4.1) (or (6.2.1)) multiplied by a factor exp(-2kh).

When the damping coefficient becomes known, the relative added mass can be calculated from the Kramer-Kronig relation:

$$A_{jk} - A_{jk}(\infty) = \frac{2}{\pi} PV \int_0^{\infty} \frac{B_{jk}(\mu) - B_{jk}(\infty)}{\mu^2 - \omega^2} d\mu \tag{6.7.5}$$

The above derivations complete the shallow draft solution with draft correction. But the last formula is not applicable because it needs the damping data over a very wide range of frequency. Therefore, it introduces excessive demands on computational effort and this offsets the major gain due to the shallow draft approximation. In the computer code of the present shallow draft theory, the added mass coefficients are simply set equal to those from the zero draft formulation. This is

accurate for the heave motion and may be acceptable for roll and pitch modes. Further reasoning will be presented in §6.8.

6.8. Two-Dimensional Shallow Draft Body

For an elongated shallow draft body, as discussed in §5 of Appendix 5, its main dimensions can be characterised in orders of magnitude by (Table 4, Appendix 5)

$$kh = \bar{\varepsilon} = \varepsilon^2,\ kB = O(\varepsilon),\ kL = O(1),$$

$$n_1 = O(\varepsilon^2),\ n_2 = O(\varepsilon),\ n_3 = O(1), \text{ and } S_w = O(\varepsilon).$$

The mean wetted surface S_w is assumed of the form

$$z = \varepsilon^2 S(x,y)$$

The perturbation procedure is rather similar to those described in §6.2-7. Similar conclusions and the same finite draft correction factors are derived. Therefore, no theoretical derivations will be performed or included here for the two-dimensional shallow draft structure.

6.8.1. Major conclusions

(1) **Surge, sway and yaw motions:** Based on the perturbation analysis, order estimates given in Table 6, Appendix 5, are confirmed. Hence, in surge, sway and yaw motion predictions, ignoring both the radiation and diffraction forces leads to a small error of order ε^2.

(2) **Shallow draft correction:** In deep water, with the finite draft correction the diffraction forces in heave, roll and pitch are those for the related zero draft line times a factor exp(-kh), but multiplied by exp(-2kh) when wave damping coefficients are concerned. Similarly, a draft correction factor of $\frac{\sinh[k(d-h)]}{\cosh(kd)}$ may be appropriate when the sea is of finite water

depth of order $kd = O(1)$.

(3) **Zero draft formula:** The integral equation for a zero draft line (MacCamy 1961) can be written as

$$2\pi\phi_j(p_o) - k\int_{C_o} \phi_j(q_o)\, G(p_o,q_o)\, dl = \int_{C_o} v_{nj}\, G(p_o,q_o)\, dl \qquad \text{for} p_o,\, q_o \in C_o \text{ on } z = 0 \tag{6.8.1}$$

$$v_{nj} = \begin{cases} -i\omega n_j & j = 3, 4 \\ -\dfrac{\partial \phi_o(q_o)}{\partial n} & j = 7 \end{cases}$$

where the two-dimensional shallow draft Green function is given by Equation (3.4.3) in deep water or Equation (31) (Wu 1986) in finite water depth. Calculated radiation and diffraction forces, based on the radiation and diffraction potential solutions from the above zero draft integral equation, are corrected by draft factors as stated in (2).

(4) **The principle of similarity:** Since any two flat lines lying on the free-surface are geometrically similar, stored non-dimensional hydrodynamic data for a unit straight line on the free-surface can be used for any flat line of arbitrary length. By multiplying with the draft correction factor, the standard data set is capable of producing hydrodynamic coefficients for any two-dimensional section of a shallow draft feature. This finding may be called *the principle of similarity of a two-dimensional shallow draft section.* In graphic presentation, such a set of standard non-dimensional data for a flat line is given in Figure 6.8.1.

6.8.2. Comparison of three rectangular sections

Numerical formulation and treatment have been described in Appendix 6 for the three-dimensional shallow draft body and these are much simpler for two-dimensional cases. In the present study, using both the ordinary and shallow draft methods, three rectangular sections are investigated, involving three different draft values, i.e. h/B = 0, 1/20, and 1/10.

For the zero draft case, the two-dimensional shallow draft program based on Equation (6.8.1) is used, whilst for the two non-zero draft cases, calculations are based on the two-dimensional formulation (4.2.3b). Resultant heave and roll exciting forces and phases, added mass and damping coefficients are given in Figures 6.8.2-3.

In Figure 6.8.2, the wave exciting forces for heave and roll modes are also estimated by the values for the zero draft line times the shallow draft correction factor exp(-kh), as suggested by the present shallow draft theory. Such estimates appear in reasonable agreement with the force data derived from the ordinary two-dimensional approach.

For the heave and roll damping coefficients, as shown in Figure 6.8.3, the resultant data from the zero draft values multiplied by the draft correction factor exp(-2kh) seem to give reasonable approximations. As far as heave added mass is concerned, the change in the small draft value has very little impact on their predictions and therefore no draft correction may be needed for the prediction of the heave added mass coefficients by the shallow draft theory. But deviations are observed for the roll added mass coefficients among these three small draft structures. This is because the side wall, which is ignored in the shallow draft theory, has an influence on the roll added mass (but obviously much less influence on the heave). Nevertheless, example computations for various shallow draft structures have shown that even for the roll motion, predictions by the present shallow draft method correlate well with experimental data and results from more complicated theories.

6.9. Example Studies

Various numerical applications of the present shallow draft theory to realistic offshore structures and service vessels have been conducted and very promising results have been achieved so

far. These include:

(1) A rectangular jack-up rig in transit (Figures 4 and 5, Appendix 6);

(2) A triangular platform (Figures 10-12, Appendix 6);

(3) Rectangular barge models (2.4x0.8x0.105m and 3.0x0.75x0.015m respectively) (Figures 6-8, Appendix 6);

(4) A circular dock (Figure 9, Appendix 6); and

(5) A semi-submersible in transit (Figures 13-14, Appendix 6).

Detailed discussions can be found in §7 of Appendix 6 and will not be repeated here.

In addition to these three-dimensional example calculations, applications of the present two-dimensional shallow draft version are now described. These involve a long drydock and a rectangular barge.

A drydock

The configuration of a drydock in marine operation is shown in Figure 6.9.1a and its under-water portion is illustrated in Figure 6.9.1b. The major dimensions of the dock are such that:

$L/B = 4.8$, $B/h = 20$, $L/B_1 = 1.9$, $L/B_2 = 1.4$ and $L/l = 7.6$.

The centre of gravity is at G(-3.3h, 0, 0.8h) and the radii of gyration are $K_{xx} = 0.43B$ and $K_{yy} = 0.33L$.

By means of the two-dimensional shallow draft theory, calculations for this drydock were performed at wave heading angles $\beta = 0, 45, 90, 135$ and 180 degrees for wave lengths within the range $0.35 \leq \lambda/L \leq 3.0$.

Predicted heave, roll and pitch motion amplitudes are given in Figures 6.9.1c-e. These again were found to have the same degree of correlation with measured model testing data.

A rectangular barge

A rectangular barge model of length L = 3.0m, beam B = 0.75m and draft h = 0.0159m has been used by Nojiri (1981) and both the experimental and theoretical data are available. Since L/B = 4.0, the two-dimensional shallow draft theory of §6.8 can be applied to derive the motion response data.

According to conclusion (1) of §6.8.1, the surge, sway and yaw motions can be reasonably approximated when both the radiation and diffraction forces are neglected. Moreover, the barge is of rectangular shape and the analytical formulae, i.e. Equations (36) and (37), derived in Appendix 5 are applicable. The predicted surge, sway and yaw responses are presented in Figures 6.9.2a, b and f. As can be clearly seen, good agreement exists between the present predictions and those reported by Nojiri.

In the computation of the heave, roll and pitch motions, the zero draft formulation is used together with the finite draft correction factor exp(-kh). The integral equation is solved over a straight line of length B = 0.75m. The very simple and well defined shape of the integral domain enables a much smaller number of discrete elements to be used to describe the contour. In fact, only half of the line contour is required in the calculation, which is further subdivided into 5 line elements of equal length. Figures 6.9.2c-e includes illustrations of the computed heave responses in beam and head seas, the roll response in beam and bow seas and the pitch response in head seas.

All the information displayed in Figure 6.9.2 further confirms the validity and acceptance of the present shallow draft approach, providing results with an accuracy similar to those derived from more elaborate ordinary three-dimensional theories, but at a fraction of the computing effort.

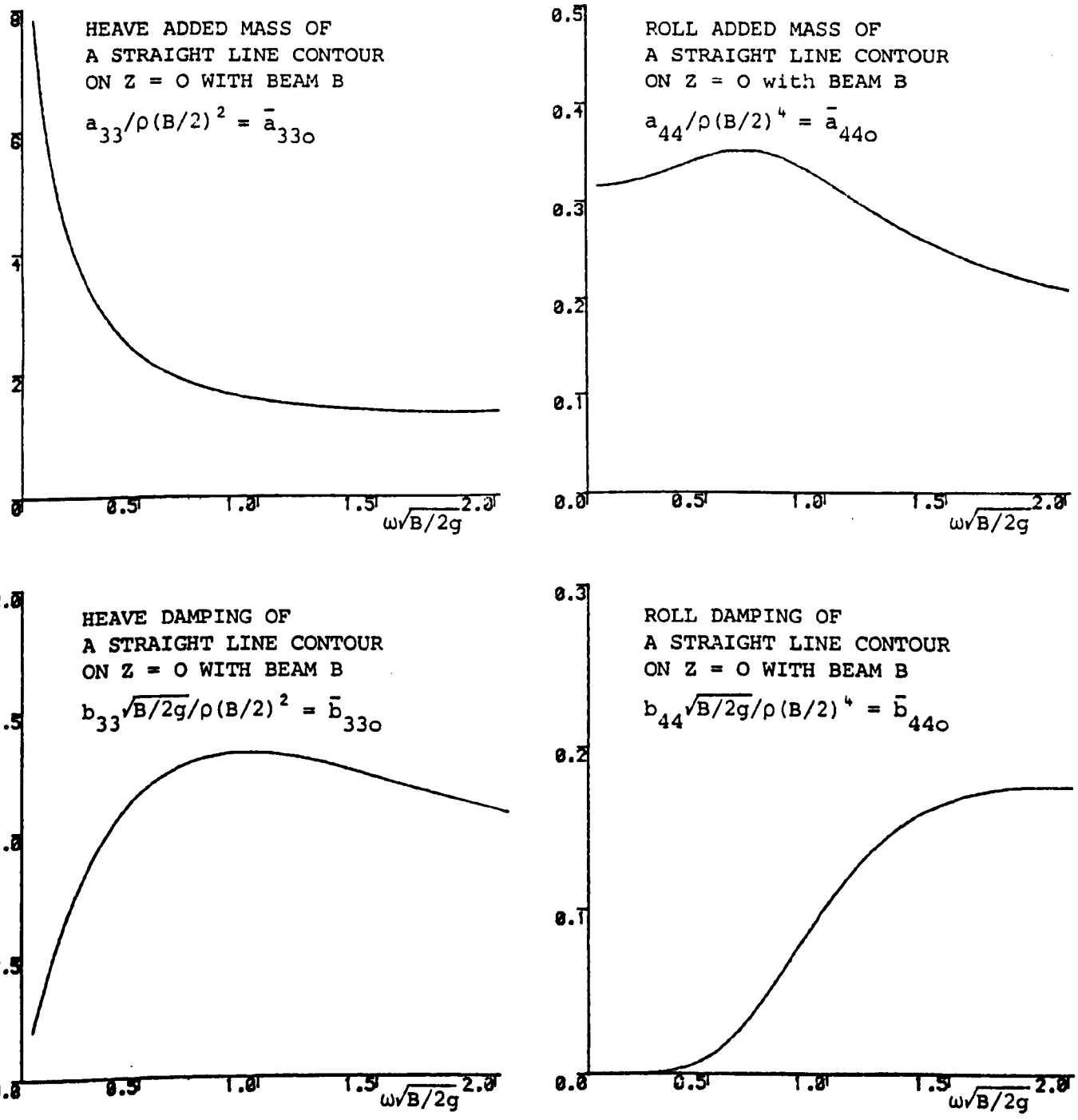

Figure 6.8.1. Non-dimensional heave and roll added mass and damping coefficients of a straight line contour on z = O with beam B.

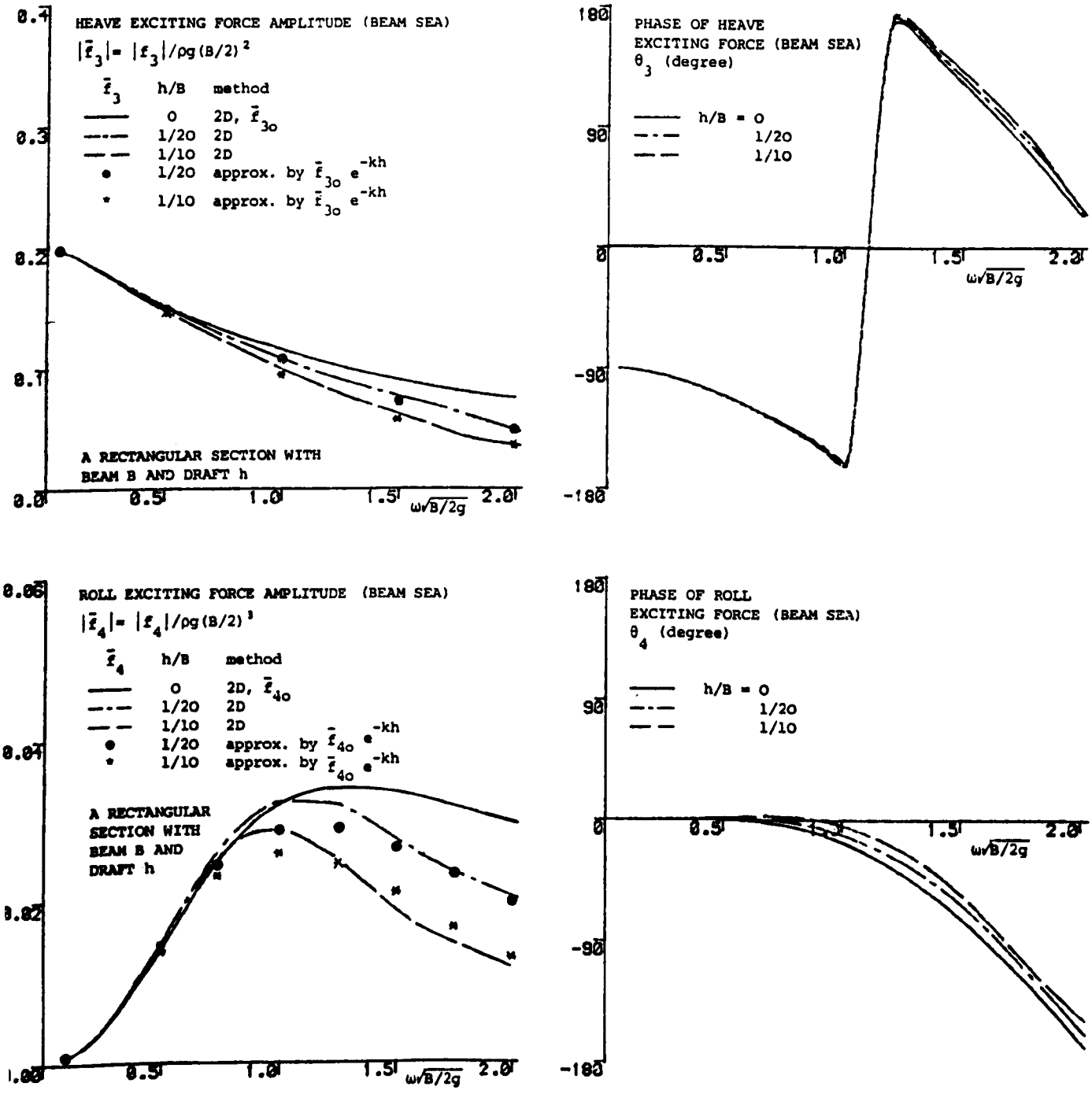

Figure 6.8.2. Heave and roll exciting forces on a rectangular section of beam B and draft h predicted by the ordinary method and the present shallow draft approximation with a draft correction e^{-kh}.

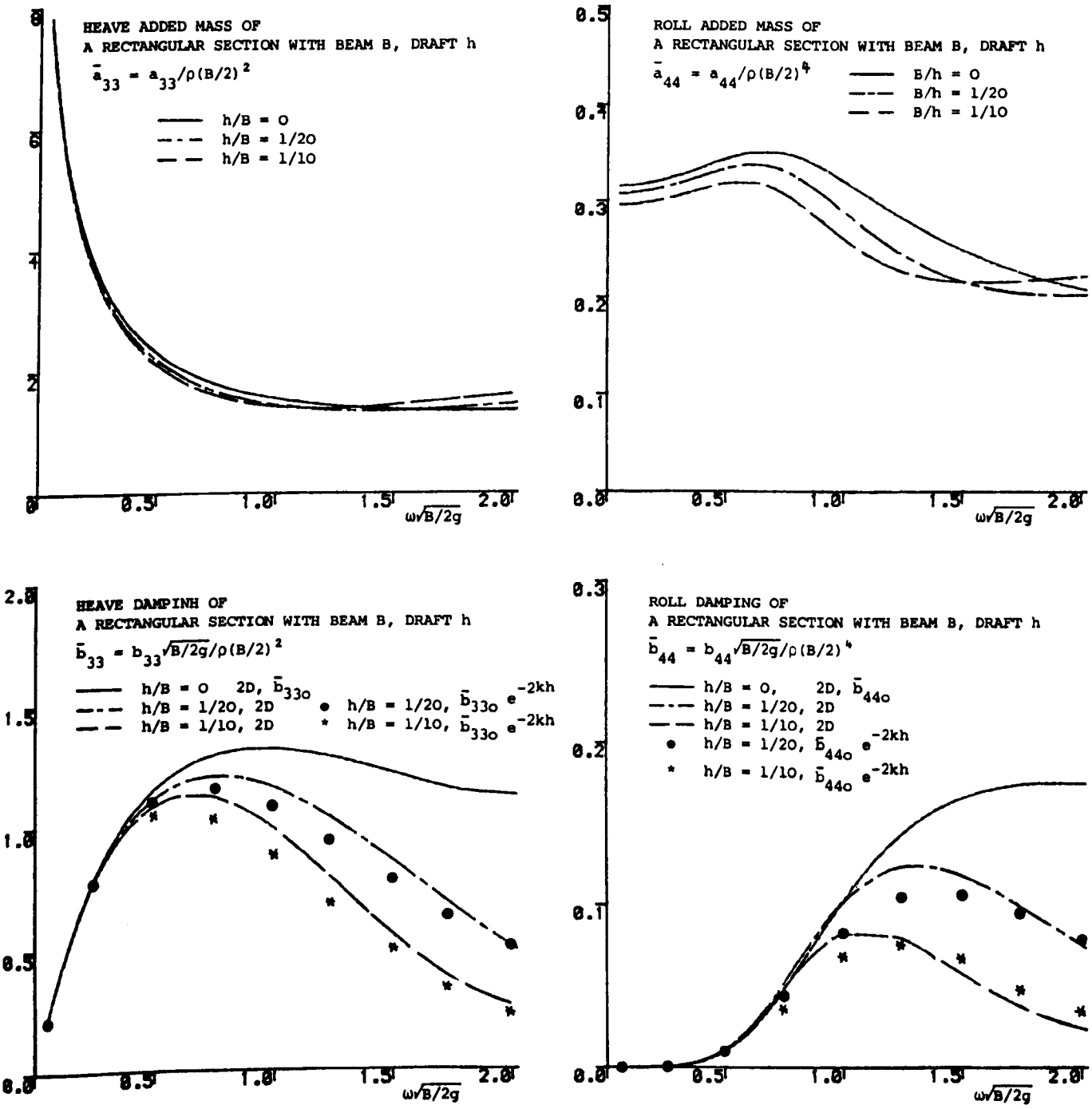

Figure 6.8.3. Comparison of heave and roll added mass and damping coefficients of a rectangular section of beam B and draft h predicted by the ordinary method and the present shallow draft approximation with a draft correction.

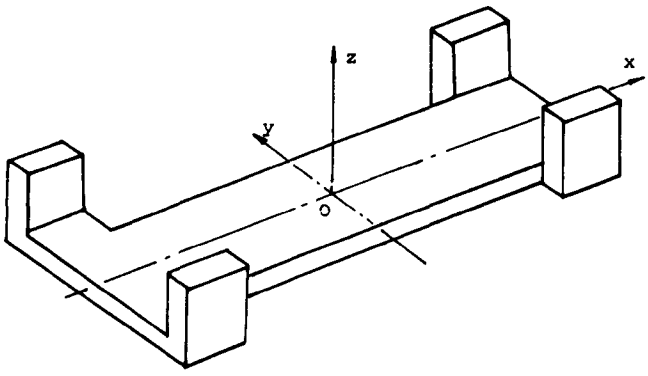

Figure 6.9.1a.
Configuration of a drydock.

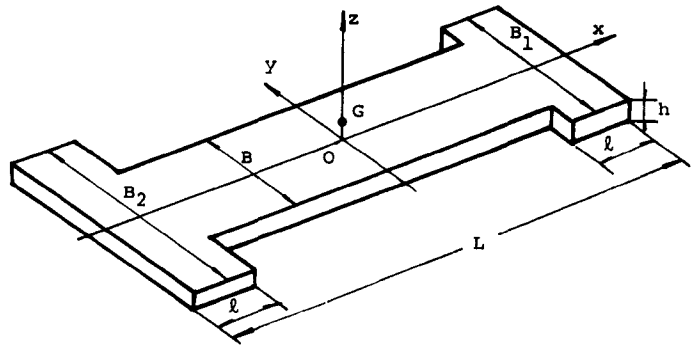

Figure 6.9.1b.
Underwater portion of the drydock.

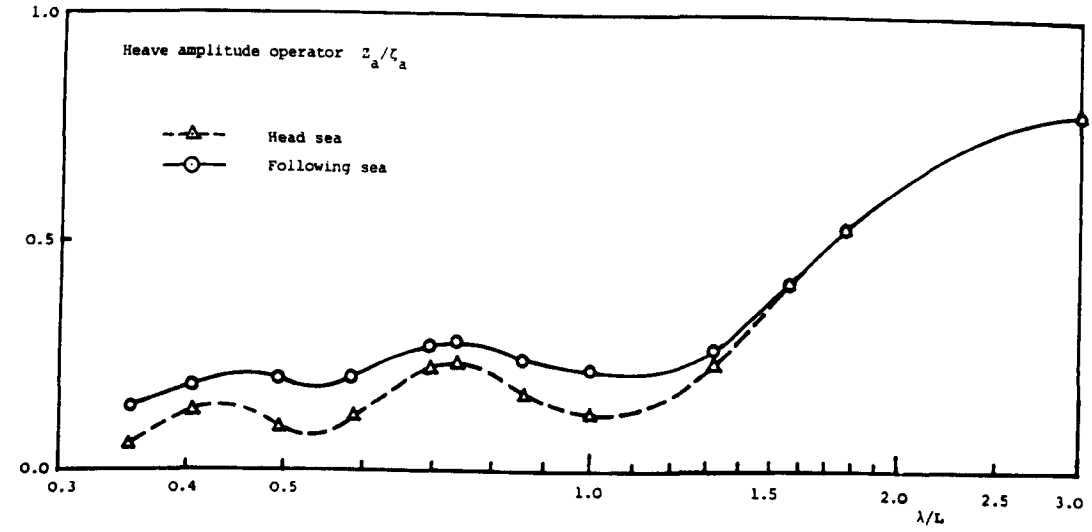

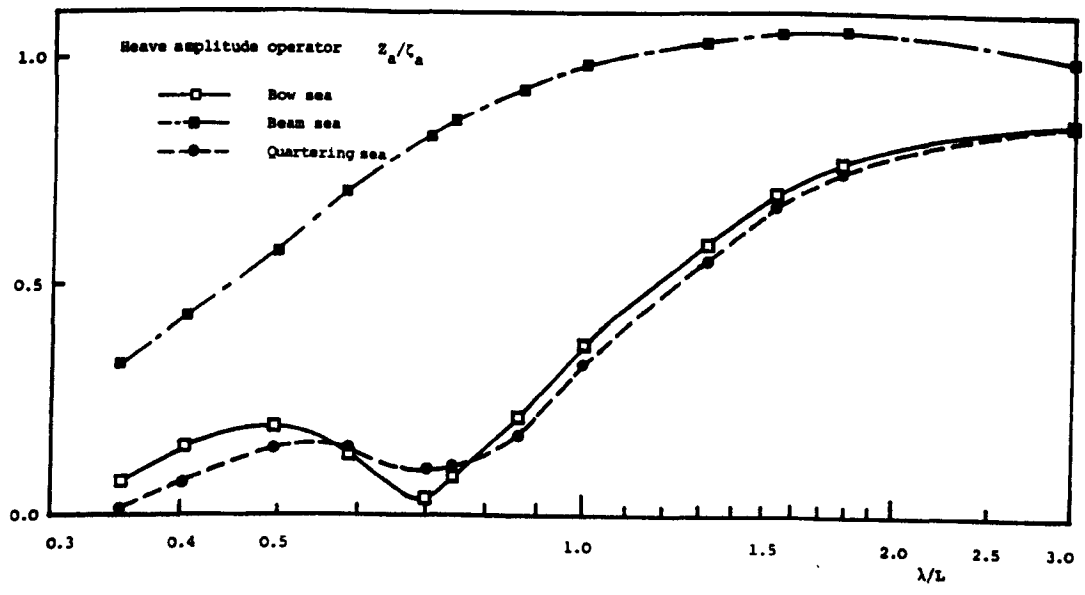

Figure 6.9.1c. Heave amplitude operator of the drydock in head, bow, beam, quartering and following seas predicted by the present shallow draft method.

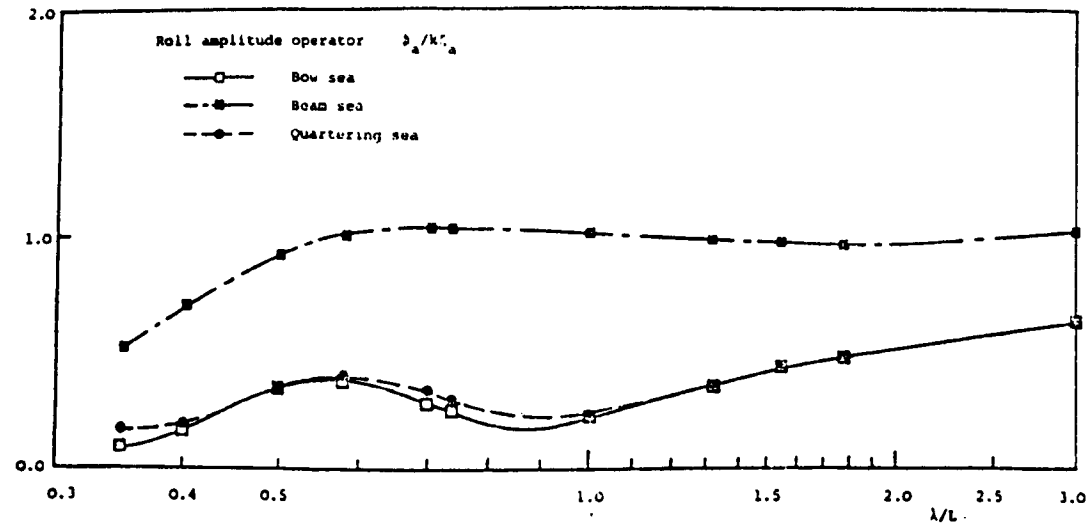

Figure 6.9.1d. Roll amplitude operator of the drydock in bow, beam and quartering seas by the present shallow draft method.

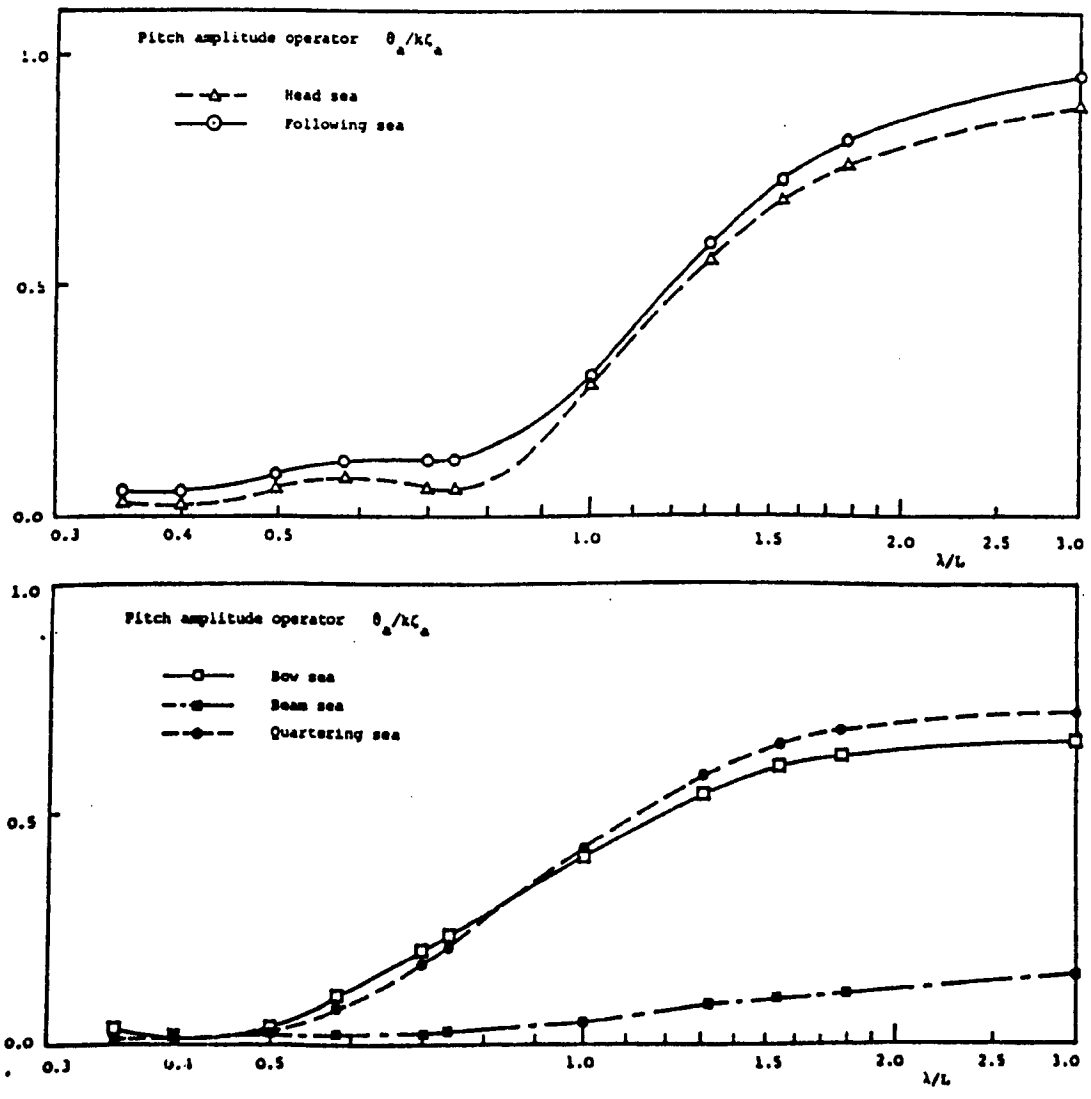

Figure 6.9.1e. Pitch amplitude operator of the drydock in head, bow, beam, quartering and following seas predicted by the present shallow draft method.

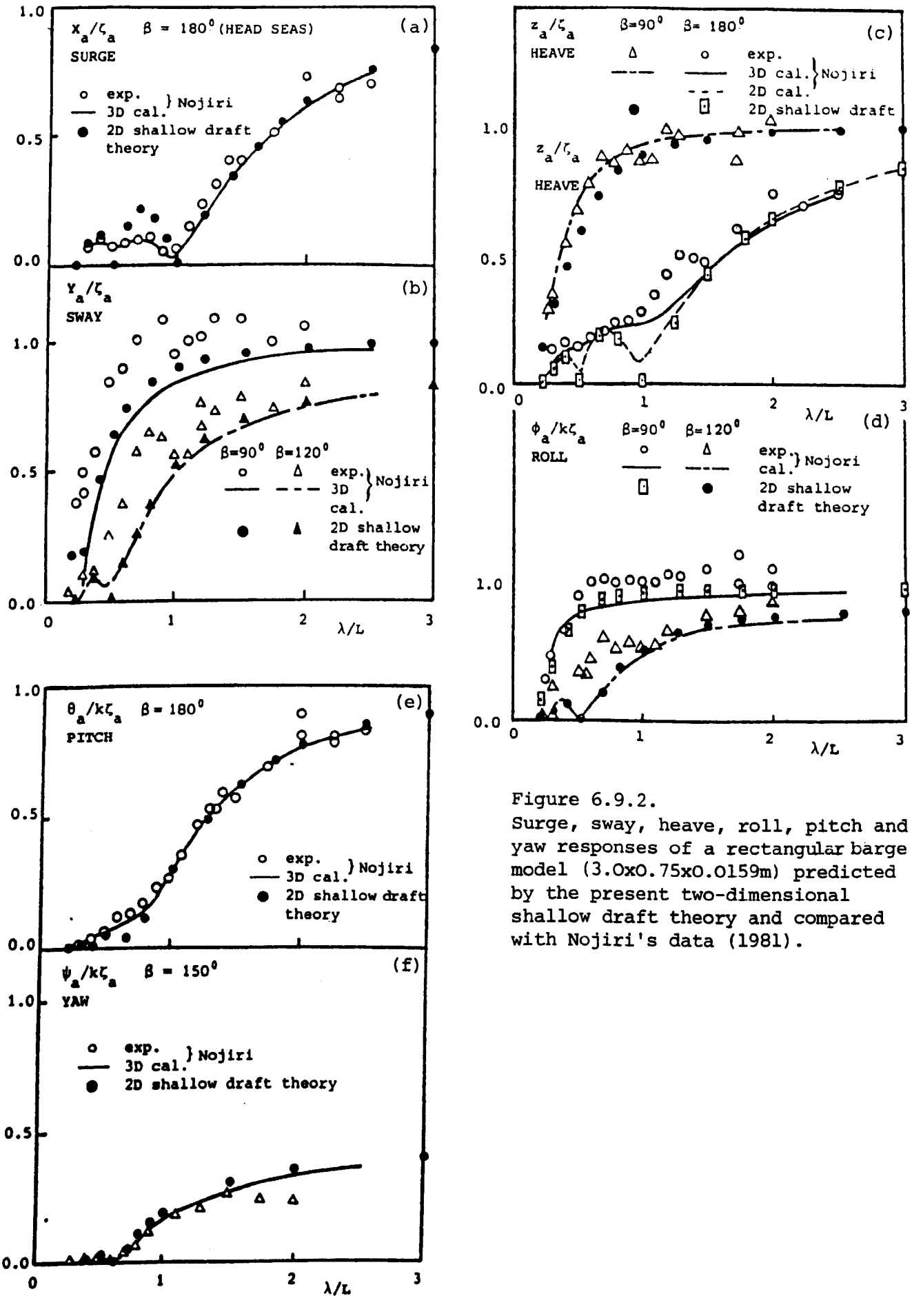

Figure 6.9.2.
Surge, sway, heave, roll, pitch and yaw responses of a rectangular barge model (3.0x0.75x0.0159m) predicted by the present two-dimensional shallow draft theory and compared with Nojiri's data (1981).

7. A HYBRID THREE-DIMENSIONAL STRIP METHOD

7.1. Introduction

The development of three-dimensional wave-structure interaction analyses commenced forty years ago or more. Namely, the theoretical establishment of the method in the late 1940s and early 50s (e.g. John 1950); the early stage applications to simple geometries (e.g. Kim 1963, 1965); the development of basic numerical concepts in the 1960s (Hess and Smith 1964); detailed numerical procedures and applications to arbitrary body geometries in the 1970s (Garrison et al 1970, Garrison 1978). The 1980s saw great improvements in the numerical evaluation of the Green function (e.g. Telsle and Noblesse 1986).

Before a three-dimensional model can be used in a design process, the remaining major problem to be overcome is the difficulty in deriving solutions since this can require an enormous amount of CPU time to solve the matrix equations involving large matrices. In particular, when the structural configuration of the body is complicated, for example, with shape variations around the bow and the stern or possessing joints at an angle, the time factor appears to be a real big obstacle to its applications to design analysis and synthesis.

The computing effort required in the analysis depends mainly on the size of the matrix to solve the unknown wave potentials. Suppose N panels are necessary to describe the whole wetted surface of the body. If the ratio of the time needed to generate a matrix coefficient to that required in an inversion process is "a", the total computing efforts may be roughly estimated by (Yeung 1981)

$$T_{3D} = N^2 (N + 3\,a)$$

In a simplified two-dimensional strip method, if a structure is divided into n_s sections and

the average number of elements at each section is denoted by n, the computing efforts needed for this approach is

$$T_{2D} = n_s\, n^2\, (n + 3\, a)$$

In terms of these estimate formulae, relative computational efficiency can be examined. For instance, a mono-hull marine structure analysed by a two-dimensional strip method with 20 discretised sections and an average of 18 elements on each section, requires a total computational effort of $T_{2D} = 20\times18^2\ (18 + 3a)$. Whilst in a three-dimensional computation of 280 (20x14) panels, it needs $T_{3D} = 280^2\ (280 + 3a)$. These estimates result in $\frac{T_{3D}}{T_{2D}} \approx 188$ provided that the ratio "a" is relatively small owing to the development of more efficient techniques in evaluation of the Green function. Although by use of symmetry properties the size of matrix can be reduced, the comparative order holds.

This comparison gives a simple explanation why two-dimensional strip theories are still the routine tools used by practical engineers when three-dimensional techniques are so well established.

The strip method has, however, its own theoretical and practical weaknesses. For example:

(1) The infinitely long length assumption may lead to accumulative error of longitudinal wave loading such as bending moments and shearing forces;

(2) Ignoring ends effect results in no information for the surge mode and also difficulties in the head sea diffraction problem when suitable modified formulations may be required.

(3) It is not applicable to marine structures of small length to beam ratio.

To update the routine two-dimensional strip method and to popularise the application of the more sophisticated three-dimensional theory, new concept based approaches should be developed to gain both the accuracy of the three-dimensional model and the efficiency of the two-

dimensional simplification.

It is most desirable if a theoretical approach possesses the accuracy of a three-dimensional theory and the efficiency of a two-dimensional strip method. To reach this target, the geometric property of the structure under consideration is of most significance. Many large ships, offshore service vessels and the main floaters of offshore platforms have a long parallel midbody portion, and their cross-sectional geometries change slowly over the whole length of the body except at the bow and the stern, where large curvature or abrupt changes occur in bodily shape. The slowly varying sectional geometry implies less variation of the wave potentials over the main body portion, whilst the sharply shaped bow and stern indicate rapid changes of these quantities.

Logically, a rational new approach should utilise the midbody portion geometric feature and account for the three-dimensional details of the bow and stern regions. To realise this, the concept of a three-dimensional strip method has been proposed by Wu (1985) to analyse surge forces and motions of three-dimensional barges. This idea was further extended by Wu and Price (1986c) to include other motion modes. In this chapter, details of the three-dimensional strip technique is described.

7.2. Mathematical Model

7.2.1. Geometric parameters

Figure 7.2.1 illustrates the form of a typical structure under discussion. It has a long parallel midbody S_m, between coordinates $x_s \leq x \leq x_b$, a bow and a stern area S_b and S_s respectively, each of large curvature. These three portions make up the whole wetted surface of the body $S_w (= S_m + S_b + S_s)$.

It is assumed that

$$n_1 = \begin{cases} \varepsilon \ll 1 & on\ S_m \\ O(1) & on\ S_b,\ S_s \end{cases} \qquad n_j = O(1)\ \ on\ S_m\ \ \text{for } j = 2,\ 3 \tag{7.2.1}$$

In addition, all the major dimensions of the body, i.e. the length, beam and draft, are assumed of O(1), too.

7.2.2. The potential distribution

Over the slowly varying midbody portion, the velocity potential distribution is assumed separable in the form:

$$\phi_j(x,y,z) = \psi_j(y,z)\,\chi_j(x) \quad \text{for } x_s \le x \le x_b \tag{7.2.2a}$$

with $\chi(x)$ expressible in a polynomial expansion form:

$$\chi_j(x) = \sum_{m=1}^{\infty} c_{jm}\, x^{m-1} \simeq \sum_{m=1}^{M} c_{jm}\, x^{m-1} \tag{7.2.2b}$$

where $c_{jm}(m = 1,2,...M)$ denote unknown coefficients dependent on the midbody geometry and the form of the hull's extremities. M is an integer number.

7.2.3. The integral equation

Substituting Equation (7.2.2a) into the integral equation (4.1.3b) yields the following three-dimensional strip formulation (correct to order ε):

$$\begin{aligned} 2\pi\,\phi_j(P) - \int_{S_b+S_s} \phi_j(Q)\,\frac{\partial}{\partial n_Q} G(P,Q)\,dS - \int_{C_m} \psi_j(q)\,\frac{\partial}{\partial n_q}\, G_{32}(P,q)\,dl \\ = -\int_{S_b+S_s} v_{nj}(Q)\,G(P,Q)\,dS - \int_{C_m} v_{nj}(q)\,\xi^{-i}\,G^*_{32}(P,q)\,dl \end{aligned} \tag{7.2.3}$$

with

$$\begin{matrix} G_{32}(P,q) \\ G^{*}_{32}(P,q) \end{matrix} = \int_{x_a}^{x_b} \chi(\xi)\, G(P,Q) \begin{Bmatrix} 1 \\ \xi^i \end{Bmatrix} d\xi = \sum_{m=0}^{M} c_{jm} \int_{x_a}^{x_b} G(P,Q) \begin{Bmatrix} \xi^m \\ \xi^{m+i} \end{Bmatrix} d\xi$$

where i = 0 for j = 1-4, and i = 1 for j = 5, 6. C_m is a characteristic sectional contour of S_m.

7.3. Numerical Formulation

To solve the three-dimensional strip method equation (7.2.3), numerical techniques are required to deal with its discretised version and to evaluate the transformed Green function.

Suppose M coefficients are needed in expression (7.2.2b), M sections in the midbody S_m are necessary to solve all the unknowns. Provided that these chosen sections are located at $x = x_m$ (m = 1, 2,... ,M), there exists the relationship

$$\begin{bmatrix} c_{j1} \\ c_{j2} \\ \cdots \\ c_{jm} \end{bmatrix} \psi(y,z) = \tilde{T} \begin{bmatrix} \phi_j(x_1,y,z) \\ \phi_j(x_2,y,z) \\ \cdots \\ \phi_j(x_M,y,z) \end{bmatrix} \qquad with\ \tilde{T} = [t_{mk}]_{MxM} = \begin{bmatrix} 1\ x_1\ x_1^2\ \cdots\ x_1^M \\ 1\ x_2\ x_2^2\ \cdots\ x_2^M \\ \cdots \\ 1\ x_M\ x_M^2\ \cdots\ x_M^M \end{bmatrix}^{-1} \tag{7.3.1}$$

and this indicates

$$\phi_j(x,y,z) = \sum_{m=1}^{M} c_{jm}\, x^{m-1}\ \psi(y,z) = \sum_{m=1}^{M} \sum_{k=1}^{M} t_{mk}\, \phi_j(x_k,y,z)\, x^{m-1} \tag{7.3.2}$$

Therefore, the discretised version of the three-dimensional strip integral equation takes the form:

$$\begin{aligned} 2\pi\, \phi_j(P) - \int_{C_m} \sum_{k=1}^{M} \sum_{m=1}^{M} t_{mk}\, \phi_j(\xi_k,\eta,\zeta)\, \frac{\partial}{\partial n_q} G_m(P,q)\, dl - \int_{S_b+S_s} \phi_j(Q) \frac{\partial}{\partial n_Q} G(P,Q)\, dS \\ = -\int_{C_m} \sum_{k=1}^{M} \sum_{m=1}^{M} t_{mk}\, v_{nj}(\xi_k,\eta,\zeta)\, \xi^{-i}\, G_{m+i}(P,q)\, dl - \int_{S_b+S_s} v_{nj}(Q)\, G(P,Q)\, dS \end{aligned} \tag{7.3.3}$$

where i = 0 for j = 1-4 and i = 1 for j = 5, 6, and

$$G_m(P,q) = \int_{x_s}^{x_b} \xi^m \, G(P,Q)\, d\xi \tag{7.3.3a}$$

Here the Green function G(P,Q) is defined by Equation (3.2.2) and efficient approximations, in partly or fully polynomial expansion forms, are available (e.g. Newman 1985). Therefore, no numerical problems exist in the evaluation of G_m of expression (7.3.3a). The following formulations are given to show how the singularity is treated in the numerical calculation of G_m.

Integration of 1/r

$$\int_{x_1}^{x_2} \frac{dx}{r} = \begin{cases} \ln \dfrac{x_2 - \xi + R_2}{x_1 - \xi + R_1} & R \neq 0 \\ \ln \dfrac{-x_1 + \xi}{x_2 - \xi} + 2\alpha\sqrt{\pi} & R = 0,\ x_1 < \xi < x_2 \\ -\ln \dfrac{\xi - x_2}{\xi - x_1} & R = 0,\ \xi > x_2, x_1 \\ \ln \dfrac{x_2 - \xi}{x_1 - \xi} & R = 0,\ \xi < x_1, x_2 \end{cases} \tag{7.3.4a}$$

$$\int_{x_1}^{x_2} \frac{x\, dx}{r} = R_2 - R_1 + \xi \int_{x_1}^{x_2} \frac{dx}{r} \tag{7.3.4b}$$

...

Here $R_k = r\,|_{x=x_k}$. $\alpha = 0.9945$ and the term of $2\alpha\sqrt{\pi}$ is derived by integration of 1/r over a square panel.

Integration of derivatives of 1/r

$$\int_{x_1}^{x_2} \frac{dx}{r^3} = \frac{1}{R}\left(\frac{x_2 - \xi}{R_2} - \frac{x_1 - \xi}{R_1}\right) \quad R \neq 0 \tag{7.3.5a}$$

$$\int_{x_1}^{x_2} \frac{x\, dx}{r^3} = -\frac{1}{R_2} + \frac{1}{R_1} + \xi \int_{x_1}^{x_2} \frac{dx}{r^3} \tag{7.3.5b}$$

$$\int_{x_1}^{x_2} \frac{\partial(1/r)}{\partial n}\, dx = \begin{cases} -[(y-\eta)\, n_2 + (z-\zeta)\, n_3] \int_{x_1}^{x_2} \frac{dx}{r^3} & R \neq 0 \\ -2\pi/\Delta l & R = 0,\ x_1 < \xi < x_2 \\ 0 & R = 0,\ \xi < x_1 \text{ or } \xi > x_2 \end{cases} \tag{7.3.5c}$$

$$\int_{x_1}^{x_2} \frac{\partial(1/r)}{\partial n}\, x\, dx = -[(y-\eta)\, n_2 + (z-\zeta)\, n_3] \int_{x_1}^{x_2} \frac{x\, dx}{r^3} \tag{7.3.5d}$$

and so on. Here Δl is the elemental length on the contour C_m.

Provided that M = 3 or 4 is appropriate, the above formulation is rather simple and involves unknown wave potentials on the bow, the stern and 3 or 4 selected representative cross-sections.

7.4. Numerical Examples

7.4.1. A submerged pontoon

For a submerged pontoon of length L = 117m, beam B = 45m, draft h = 15m and submergence H = 15m, two discretisations are used. In the three-dimensional calculation (i.e. Equation (4.1.3b)), the pontoon surface in divided into 88 panels in total, whilst in the hybrid three-dimensional strip approach (Equation (7.3.3)), only 16 panels are used for the flat bow and stern and three representative sections in the midbody portion. The calculated heave and roll hydrodynamic coefficients are illustrated in Figure 7.4.1. It can be seen that the latter calculation correlate well with the experimental evidence of Ohkawa (1980) and are also in good agreement with the conventional three-dimensional calculation data.

7.4.2. Three rectangular cylinders

The second example study involves a series of floating rectangular cylinders of beam B = 40m, draft h = 20m and varying length L = 120, 80 and 40m. Three theoretical methods are used, including the ordinary two- and three-dimensional methods, based on Equation (4.2.3b) and (4.1.3b), and the present hybrid formulation (7.3.3).

In the three-dimensional computation, the mean wetted surface area is discretised into 136, 80 and 48 panels, respectively for the three cylinders of different length. When the two-dimensional theory is adopted, each cross-sectional contour is divided into 16 elements. For the present method calculation, the bow and the stern are each represented by 8 panels only, and the midbody by three selected sections.

Figures 7.4.2 illustrates the computed surge added mass and damping coefficients. Apparently, the two-dimensional method fails to produce the surge data. However, the present hybrid method results demonstrate its capability and accuracy in the prediction of the surge related information.

For sway, heave and roll motions (Figures 7.4.3-5), deviation exists between the data from the two- and the three-dimensional computations, and becomes wider when the body's length to beam ratio decreases. Again, the present method results are shown in reasonable agreement with those from the three-dimensional calculation.

This series of study clearly demonstrate that the proposed three-dimensional strip method can achieve a similar degree of accuracy to the ordinary three-dimensional technique.

7.5. Concluding Remarks

(1) The slowly varying longitudinal geometry of the midbody of a marine structure implies a slow variation of the wave potentials along the midbody length. This geometric property can be used to simplify the solution formulation.

(2) A three-dimensional strip method is derived based on an assumption that the wave potential on the parallel midbody has a separable longitudinal distribution function, i.e. Equation (7.2.2).

(3) Consequently, the body wetted surface is represented by three-dimensional panels over the bow and the stern areas but by a number of sections over the parallel midbody, which are further divided into two-dimensional elements. This reduces the large matrix size as required in the three-dimensional calculation into a hybrid three-dimensional strip formula of much smaller size.

(4) Because of the inclusion of the details of the bow and stern regions in the computation, the present method is capable of generating surge motion related data, which, however, cannot be produced by a two-dimensional strip theory.

(5) Example studies correlate well with experimental data and the full three-dimensional results and show that the hybrid method works even when the length to beam ratio is equal to unity. This can be a major merit over the conventional two-dimensional strip theories.

(6) From computational practice, it is found that three or four sections (i.e. M = 3 or 4 in Equation(7.3.3)) are sufficient to produce data of reasonable accuracy. When the wave length becomes much shorter than the body length, it is necessary to increase the section number.

(7) Numerical studies covered only structures of long parallel midbody without any sectional geometric change. Further investigation should be directed to deal with a body with a small midbody variation.

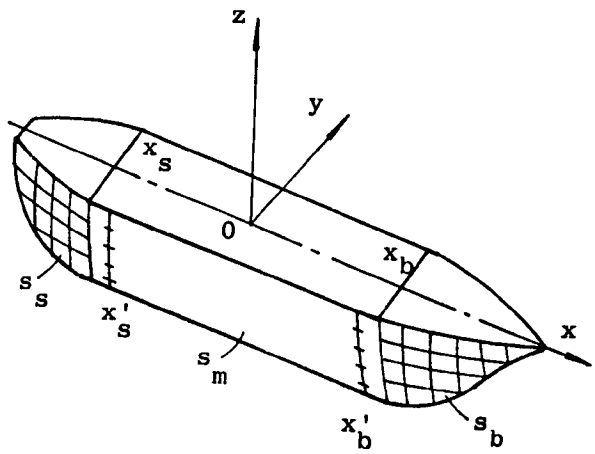

Figure 7.2.1.
A marine structure with a long parallel midbody S_m and a bow and a stern area (S_b and S_s) with large curvature.

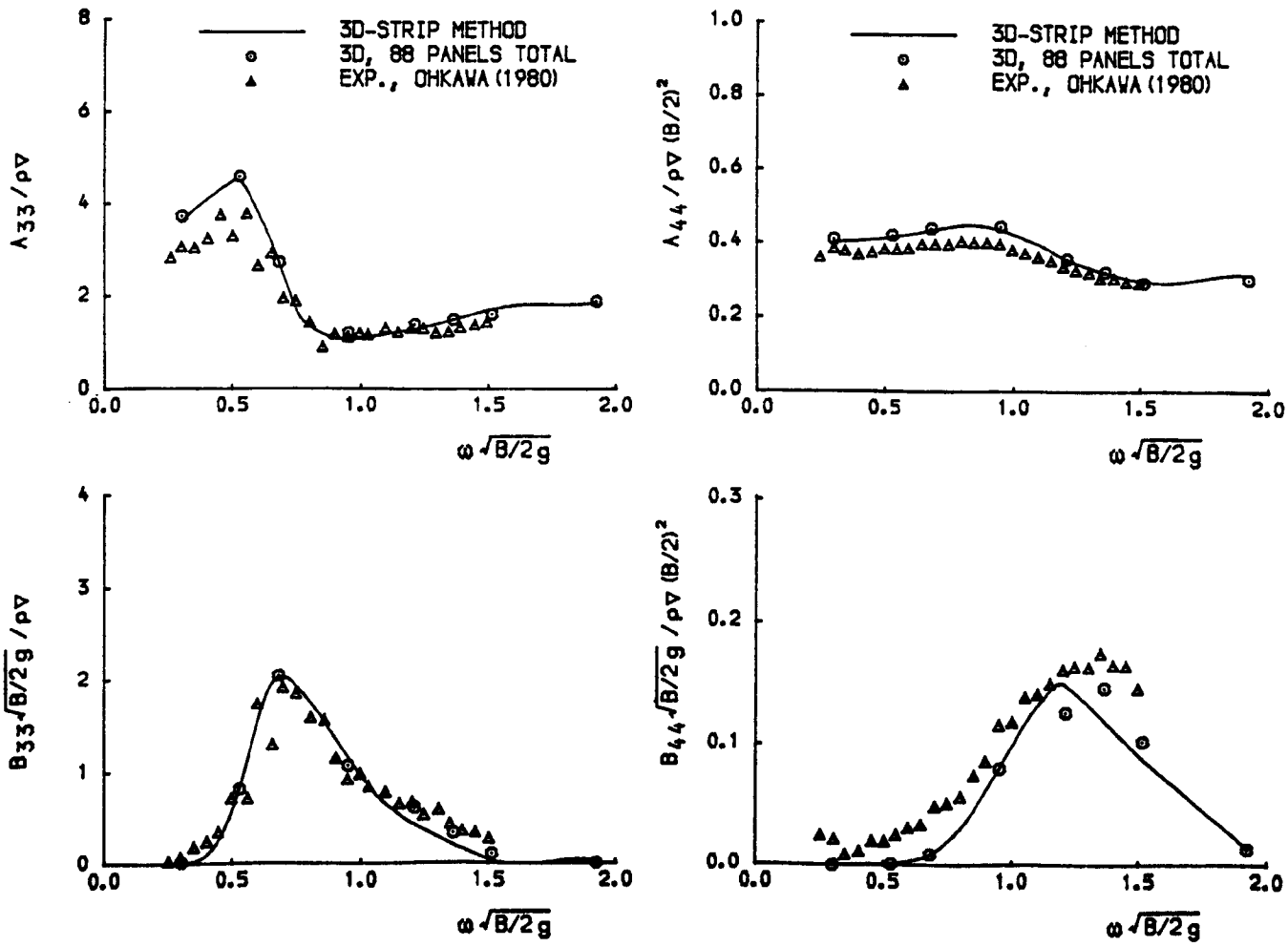

Figure 7.4.1. Heave and roll added mass and damping coefficients for a submerged pontoon (117x45x15m).

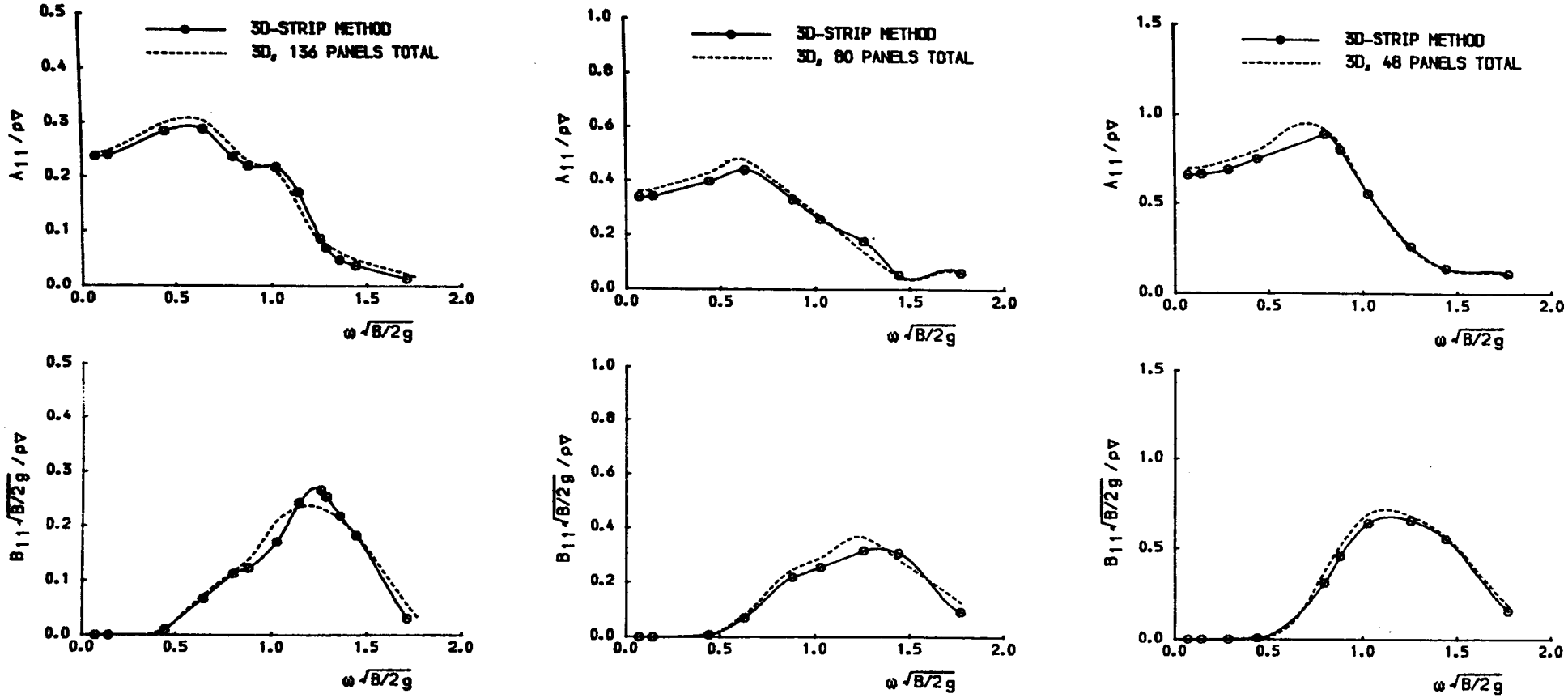

(a) Surging added mass and damping for a rectangular cylinder 120x40x20.

(b) Surging added mass and damping for a rectangular cylinder 80x40x20.

(c) Surging added mass and damping for a rectangular cylinder 40x40x20.

Figure 7.4.2. Surge added mass and damping coefficients for three rectangular cylinders of beam 40m, draft 20m and varying lengths 120, 80 and 40m respectively.

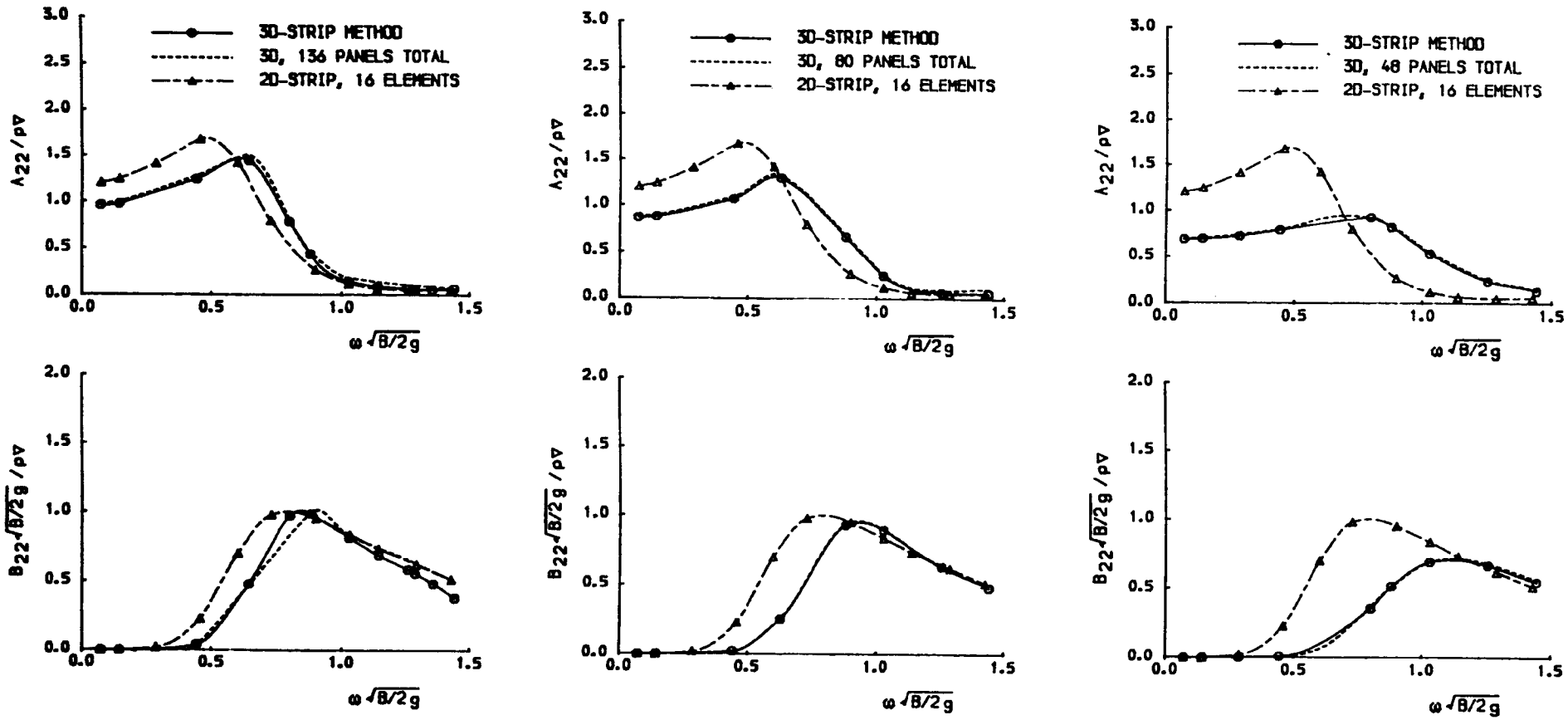

(a) Swaying added mass and damping for a rectangular cylinder 120x40x20.

(b) Swaying added mass and damping for a rectangular cylinder 80x40x20.

(c) Swaying added mass and damping for a rectangular cylinder 40x40x20.

Figure 7.4.3. Sway added mass and damping coefficients for three rectangular cylinders of beam 40m, draft 20m and varying lengths 120, 80 and 40m respectively.

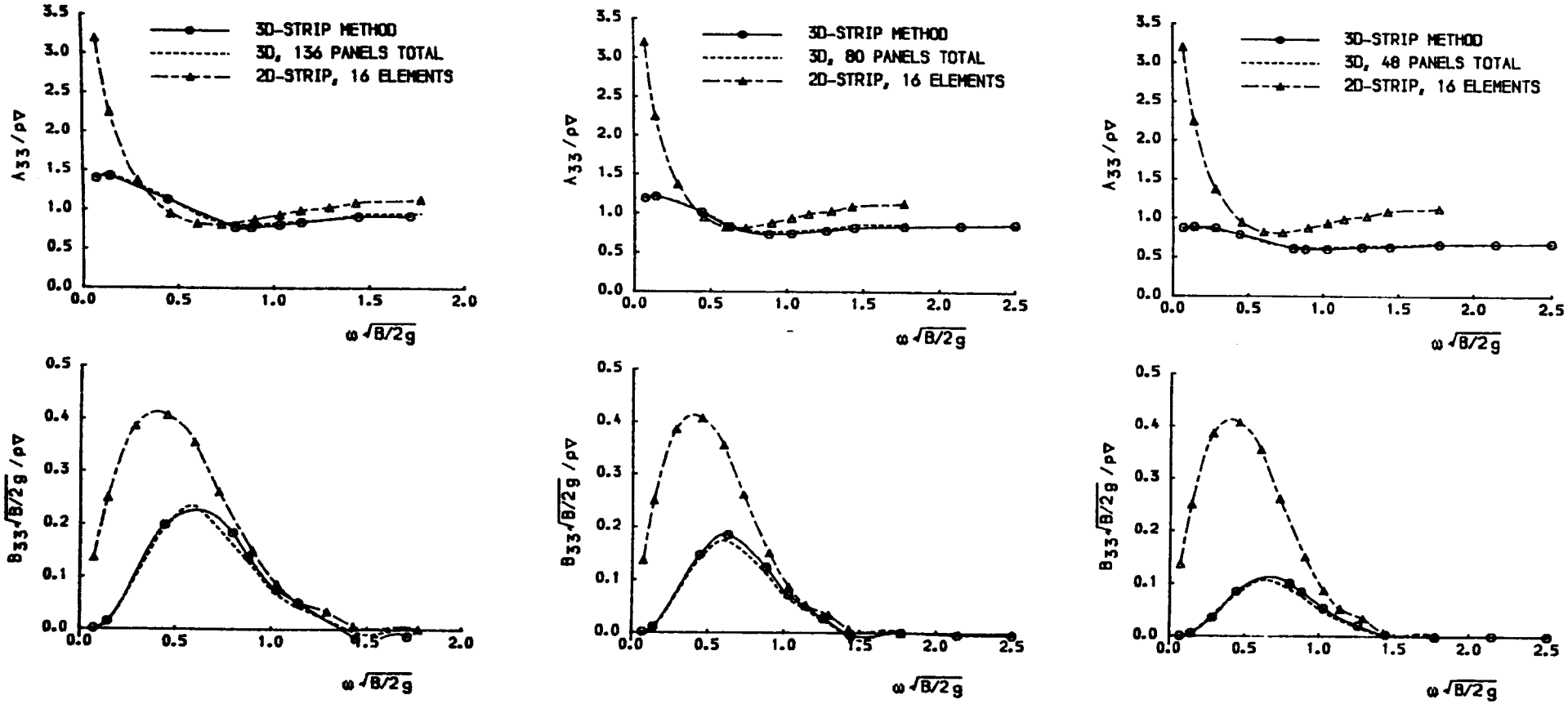

(a) Heaving added mass and damping for a rectangular cylinder 120x40x20.

(b) Heaving added mass and damping for a rectangular cylinder 80x40x20.

(c) Heaving added mass and damping for a rectangular cylinder 40x40x20.

Figure 7.4.4. Heave added mass and damping coefficients for three rectangular cylinders of beam 40m, draft 20m and varying lengths 120, 80 and 40m respectively.

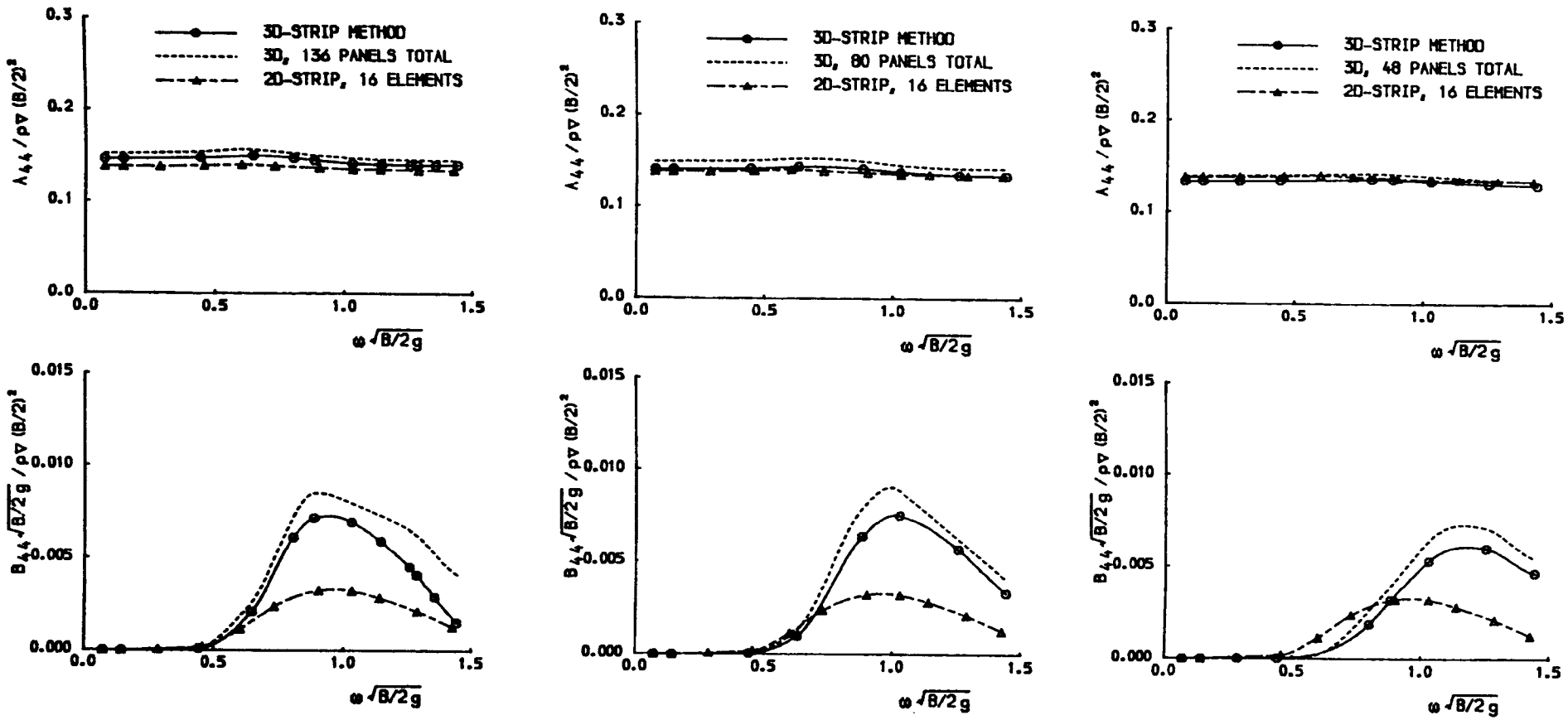

(a) Rolling added mass and damping for a rectangular cylinder 120x40x20.

(b) Rolling added mass and damping for a rectangular cylinder 80x40x20.

(c) Rolling added mass and damping for a rectangular cylinder 40x40x20.

Figure 7.4.5. Roll added mass and damping coefficients for three rectangular cylinders of beam 40m, draft 20m and varying lengths 120, 80 and 40m respectively.

8. WAVE DRIFT FORCES ON OFFSHORE STRUCTURES

8.1. Introduction

In recent years, the calculations of the second-order wave drift forces have attracted much attention. This is because of their importance in estimating the performance of moored ships and offshore structures in offshore operation. A general review of the second-order wave forces and motions has been given in §1.1.5.

The evaluation of the second-order wave drift forces is associated with the practical requirements of offshore operations. As far as large and complicated offshore structures are concerned, the conventional methods based on a three-dimensional diffraction solution may be too time consuming to be of practical use in a preliminary design. Therefore, an engineering estimating technique rather than a complicated rigorous mathematical proof is sometimes required.

In particular, according to organised international investigations into a semi-submersible and a TLP, hydrodynamic prediction data from various sources displayed vast scattering even for the first-order radiation and diffraction forces. Since the second-order calculation is dependent on the first-order solutions, logically, one can not expect good correlations among the second-order predictions by these different methods, programs or organisations. If a general good agreement is found in calculated second-order force data, this lucky success can only be attributed to either

(1) some first-order terms are of no significance; or

(2) the mutual error cancellation effect.

These two are quite often the reasons why, in the field of naval architecture and offshore engineering, a much simplified method works or performs even better than a much more sophisticated theory.

It is not an illogical consideration to ignore these terms of much less significance and/or of mutual cancellation effect in order to concentrate on contributions of greater importance and to develop simpler techniques of higher efficiency and with acceptable accuracy.

In this chapter, the "horizontal plane method" of Hwang and Tuck (1970) is used to evaluate the first order wave potentials on vertical cylinders of arbitrary geometry. Together with the near field approach of Pinkster (1979) the second-order mean drift forces are calculated. Then, this exact theoretical solution method is extended to approximate the horizontal mean drift forces on offshore structures composed of multiple vertical columns and submerged horizontal pontoons. Finally, this approximate method is used for predictions of the horizontal mean drift forces and moments on a semi-submersible and a TLP.

8.2. General Formulation

It has been shown by Pinkster (1979) and Standing et al (1981, 1982) that the second-order mean drift forces can be expressed in the form:

$$\bar{F}^{(2)} = (\bar{F}_1^{(2)}, \bar{F}_2^{(2)}, \bar{F}_3^{(2)}) = \sum_{m=I}^{VI} \bar{F}_m \qquad (8.2.1)$$

where the bar indicates the time average, i.e. the mean value. The six components are:

$$
\begin{aligned}
\bar{F}_I &= -\frac{1}{2}\rho g \int_{L_o} \underline{\zeta}_r^2 \vec{n}' dl \\
\bar{F}_{II} &= \frac{1}{2}\rho \int_{S_w} |\nabla \underline{\phi}|^2 \vec{n}\, dS \\
\bar{F}_{III} &= -\rho \int_{S_w} [\nabla \underline{\phi}_t \cdot \vec{\underline{\eta}}] \vec{n}\, dS \\
\bar{F}_{IV} &= \underline{R}\,\vec{\underline{F}} \\
\bar{F}_V &= \vec{W}_1 \\
\bar{F}_{VI} &= -\rho \int_{S_w} \underline{\phi}_t^{(2)} \vec{n}\, dS
\end{aligned}
\qquad (8.2.2)
$$

These are respectively (I) the force term associated with the surface elevation, (II) the quadratic pressure term arising from Bernoulli's equation, (III) the structure displacement term due to the effects of first order motions, (IV) the contribution due to the rotation of the force vector, (V) the effect of the second-order motions of the structure's centre of buoyancy and waterplane area (Standing et al 1981, Ogilvie 1983), and (VI) the contribution from the second-order potential $\phi^{(2)}$.

Here L_o is the mean water line, A_w is the mean waterplane area and

$$
\vec{n}' = \vec{n}/\sqrt{n_1^2 + n_2^2}
$$

$$
\vec{\underline{\eta}} = (\underline{X}_1, \underline{X}_2, \underline{X}_3) + ((\underline{X}_4, \underline{X}_5, \underline{X}_6) \times (\vec{r} - \vec{r}_G))
$$

$$
\underline{R} = \begin{bmatrix} 0 & -\underline{X}_6 & \underline{X}_5 \\ \underline{X}_6 & 0 & -\underline{X}_4 \\ -\underline{X}_5 & \underline{X}_4 & 0 \end{bmatrix}
$$

The relative wave surface elevation is given by

$$
\underline{\zeta}_r = \underline{\zeta} - \underline{X}_3 - \underline{X}_4 (y - y_G) + \underline{X}_5 (x - x_G)
$$

with the first-order wave elevation

$$
\underline{\zeta} = -\frac{1}{g}\underline{\phi}_t
$$

Here ϕ is the first-order wave potential. In the above equations, the underlying subscript - denotes

a real number.

Since the complex values are much more convenient to manipulate in the diffraction solution, the real values in the above equations can be re-expressed as a complex number using the identities:

$$
\begin{aligned}
&Re(A)\,Re(B) = \frac{1}{2} Re(AB) + \frac{1}{2} Re(AB^*) \\
&[Re(A)]^2 = \frac{1}{2} |A|^2 + \frac{1}{2} Re(A^2) \\
&\overline{Re(A)\,Re(B)} = \frac{1}{2} Re(AB^*) \\
&\overline{[Re(A)]^2} = \frac{1}{2} |A|^2
\end{aligned}
$$

where A, B are complex numbers and A^* and B^* are their conjugates.

In complex variable notation the above mean drift force components may be written as

$$
\begin{aligned}
\bar{F}_I &= -\frac{1}{4} \rho g \int_{L_w} |\zeta_r|^2 \vec{n}\, dl \\
\bar{F}_{II} &= \frac{1}{4} \rho \int_{S_w} |\nabla \phi|^2 \vec{n}\, dS \\
\bar{F}_{III} &= \frac{1}{2} \rho \int_{S_w} [\vec{\eta}^* \cdot \nabla \phi_t] \vec{n}\, dS \\
\bar{F}_{IV} &= \frac{1}{2} R^* \vec{F} \\
\bar{F}_V &= -\frac{1}{4} \rho g z_G A_w (|X_4|^2 + |X_5|^2)(0, 0, 1) \\
\bar{F}_{VI} &= \bar{P} A_w (0, 0, 1)
\end{aligned}
\qquad (8.2.3)
$$

where $\bar{P}$ is the mean set-down pressure in the undisturbed incident wave as given by Standing et al (1981).

8.3. Mean Drift Forces on Vertical Rigid Cylinders

For a system of multiple vertical cylinders of arbitrary cross-sectional contour C_w, extending from the seabed of depth d and piercing the free-surface, as illustrated in Figure 8.3.1, the horizontal mean drift forces have only two components, i.e.

$$\bar{F}^{(2)} = \bar{F}_I + \bar{F}_{II} \tag{8.3.1}$$

and the total first-order potential ϕ is the sum of the incident wave potential and the diffraction potential, i.e.

$$\phi = \phi_o + \phi_7 \tag{8.3.2}$$

8.3.1. First-order diffraction solution

A horizontal plane method can be used to evaluate the diffraction (also the radiation) wave potentials associated with the vertical cylinders excited by regular waves. This method was first developed by Hwang and Tuck (1970) in the study of harbour resonances and it has also been applied by Isaacson (1978) for the determination of the wave loads on offshore cylinders. In their formulation the source distribution technique was applied whilst here a mixed source-dipole distribution is used, but the general procedure is rather similar.

In the case of finite water depth, the incident wave potential expression (2.2.16) may be rewritten as

$$\phi_o = Z(z)\,\psi_o \quad with \psi_o = -\frac{ig\zeta_a}{\omega}\, exp\,[ik(x\cos\beta + y\sin\beta)] \tag{8.3.3}$$

$$Z(z) = \begin{cases} \cosh k(z+d)/\cosh kd & d < \infty \\ exp\,(kz) & d = \infty \end{cases}$$

The relative diffraction potential amplitude is expressible by

$$\phi_7 = Z(z)\,\psi_7 \tag{8.3.4}$$

From expression (8.3.4), the Laplace equation valid over the whole fluid domain transforms into the Helmholtz equation over any horizontal plane, i.e.

$$\frac{\partial^2 \psi_7}{\partial x^2} + \frac{\partial^2 \psi_7}{\partial y^2} + k^2 \psi_7 = 0 \tag{8.3.5}$$

and the corresponding Green function, satisfy the radiation condition, is given by

$$G_H(p,q) = i\,\pi H_o^{(1)}(kR) = -\pi\,[Y_o(kR) - i\,J_o(kR)] \tag{8.3.6}$$

with p(x,y) being the field point and $q(\xi,\eta)$ on the contour C_w.

The integral equation in a mixed source-dipole distribution form can be written in the form:

$$2\pi\psi_7(p) - \int_{C_w} \psi_7(q) \frac{\partial}{\partial n_q} G_H(p,q)\,dl = \int_{C_w} G_H(p,q) \frac{\partial}{\partial n_q} \psi_o(q)\,dl \quad p,\ q \in C_w \tag{8.3.7}$$

This provides a means of solving for ψ_7. Subsequently from Equation (8.3.4), the first order wave diffraction amplitude can be determined.

In solving the relevant discretised linear equations of Equation (8.3.7), the elemental integrals over each discrete line element Δl are estimated by following approximations:

$$\begin{aligned} I &= \int_{\Delta l} G\,dl \simeq -2 \int_{\Delta l} ln\,(kR) + [i\,\pi H_o^{(1)}(kR) + 2\,ln\,(kR)]\,\Delta l \\ I_n &= \int_{\Delta l} \frac{\partial G}{\partial n}\,dl \simeq -2 \int_{\Delta l} \frac{\partial}{\partial n} ln\,(kR)\,dl + \frac{\partial}{\partial n}[i\,\pi H_o^{(1)}(kR) + 2\,ln\,(kR)]\,\Delta l \end{aligned} \tag{8.3.8}$$

where the remaining integrals on the right hand are calculated analytically for $R \geq 2\,\Delta l$ and otherwise approximately. The Bessel functions involved can be efficiently evaluated by polynomial approximations (Abramowitz and Stegun 1972)

8.3.2. Mean drift forces

When the diffraction potential is known, the wave elevation and wave particle velocity on the body surface can be readily determined from the relationships:

$$\zeta_r|_{z=0} = \zeta|_{z=0} = \frac{i\omega}{g}(\psi_o + \psi_7)_{z=0} \tag{8.3.9}$$

$$|\nabla\phi|^2 = |\frac{\partial}{\partial\tau}(\phi_o + \phi_7)|^2 + |\frac{\partial}{\partial z}(\phi_o + \phi_7)|^2 \quad on\ S_w \tag{8.3.10}$$

where τ is the local tangent coordinate to the cross-sectional contour C_w.

From expressions (8.3.9) and (8.3.10), the horizontal mean drift forces on vertical cylinders (single pile or multiple columns) of arbitrary sectional geometry can be evaluated by Equations (8.2.3) and (8.3.1).

8.3.3. An example

To verify the described numerical procedures developed, a vertical cylinder is used in an example study. It has radius $a = 1.5m$, extends from the seabed (at depth d = 5m) and pierces the free-surface.

To apply the horizontal plane method described above, the circular cross-sectional contour of the cylinder is discretised separately by 16, 24 and 36 segments in order to test for numerical convergence. It is found that only small deviations occur between these three sets of data. Therefore, the mean drift force displayed in Figure 8.3.2 is calculated from a 16 segment model. The present numerical results agree well with other quoted sources (e.g. Standing et al 1981).

8.4. Approximation for Offshore Structures

To develop a simplified method to estimate the horizontal mean drift forces for offshore structures consisting of multiple vertical columns and horizontal pontoons, the following assumptions (based on physical reasoning and intuition) are made:

(1) The first order motion responses are comparatively small and their contribution to the second-order mean drift forces can be ignored.

(2) The interactions between the vertical columns and the horizontal pontoons are negligible.

(3) The contribution to the horizontal mean drift forces from horizontal members can be ignored.

The first assumption is true at frequencies of high or intermediate values because of the small waterplane area of the structure under consideration. Although at low frequencies the first order motion responses may have large values, the mean drift forces become rather small and may have little importance.

As far as this column-pontoon type of offshore structures is concerned, the first-order fluid forces, as discussed in §1.1.3,aremost likely out of the diffraction dominant regime and possibly fall into the inertia dominant one. In this case, either estimate method based on empirical inertia and drag coefficients or a diffraction theory can be used for prediction of the first-order forces, and the latter is not necessarily superior to the former. Moreover, the regime of the mean second-order forces is less clear. Therefore, the second assumption may be somewhat of a compromise between the two alternative methods mentioned.

The third assumption is based on existing theoretical proof and numerical evidence. In fact, it has been shown by Ogilvie (1963) that for a deeply (actually it is not necessarily very deep) submerged horizontal circular cylinder the mean horizontal drift force is zero.

In accordance with assumption (1), the mean horizontal drift forces are independent of the first-order motions, in other words, just like a fixed body as described in §8.3, they rely on only two force components, i.e. $\bar{F}_I$ and $\bar{F}_{II}$ as given by Equation (8.3.1).

Furthermore, by assumptions (2) and (3), these forces are solely dependent on the first-order potential solution for the multiple columns only. That is,

$$\bar{F}^{(2)} = -\frac{1}{4}\rho g \int_{L_w} |\zeta_r|^2 \vec{n}\, dl + \frac{1}{4}\rho \int_{S_c} |\nabla\phi|^2 \vec{n}\, dS \tag{8.4.1}$$

where S_c denotes the mean wetted surface area of the columns of the offshore structure.

When the cross-sectional geometry of the column is circular, exact or approximate analytical solutions for diffraction potentials are available, for example, by Masumoto (1982). The analytical formulation, however, is not applicable to columns of cross-sectional geometry other than circular ones.

To further simplify the problem solution, the approximation proposed by MacCamy and Fuchs (1954) for a single circular cylinder may be used, which suggests that horizontal wave forces on a circular cylinder of draft, h, less than the water depth, d, is the same as if the cylinder extended to the bottom. Based on this assumption, all the quantities required for evaluating expression (8.4.1) take the values from a system of multiple cylinders of the same cross-sectional geometry as the multi-columns of an offshore structure. Therefore, the exact theoretical and numerical procedures for solving the wave potential problem around multiple vertical cylinders of arbitrary sectional geometry, as described in §8.3, are exploitable.

On this basis, the horizontal mean drift force on an offshore structure of multiple columns is given by

$$\bar{F}^{(2)} = -\frac{1}{4}\rho g \int_{L_w} |\zeta_r|^2 \vec{n}\, dl + \frac{1}{4}\rho \int_{-h}^{0} dz \int_{C_w} |\nabla\phi|^2 \vec{n}\, dl \tag{8.4.2}$$

where ζ_r and ϕ are solved from Equation (8.3.7) for multiple cylinders extending to the seabed.

8.5. Numerical Examples

To verify the proposed approximation technique for multi-column offshore structures, and to provide a measure of the strength or weakness of the approximation adopted, the horizontal

mean drift forces associated with a semi-submersible and a TLP are determined and the results are compared with experimental and theoretical data where available.

8.5.1. A semi-submersible

A six-column semi-submersible platform is used for an example study since experimental and theoretical data have been presented by Pinkster (1979).

The lay-out of the semi-submersible and its main particulars are displayed in Figure 8.5.1. The length, width and draft are 100m, 76m and 20m respectively and its displacement volume is 35925 m^3. The diameter of the vertical columns is 12.6m. The pontoons are of rectangular shape of dimensions 100x16x8m and at submergence of 12m.

With the present approximation, the diffraction potential is obtained by solving Equation (8.3.7), in which the water line L_o is chosen for the sectional contour C_w, and the mean horizontal drift forces are determined by Equation (8.4.2). In the numerical calculation, the cross-sectional contour of each column is divided into 16 elements and this makes a total number of 96 segments. Because of its two planes of symmetry, the actual panel number involved in the numerical computation is rather small. The computations cover 3 wave headings, including the head, bow quartering and beam seas; 32 wave frequencies ranging from $\omega\sqrt{\nabla^{1/3}/g}$ = 0.35 to 2.60; the mean longitudinal and transverse (i.e. surge and sway) drift forces and mean yaw drift moment.

The resultant mean drift force predictions are given in Figures 8.5.2-6. In these figures, the solid circular points indicate the present approximation method data whilst the hollow circular points are the experimental data of Pinkster (1979). Pinkster's computational predictions are also shown by solid lines, which were calculated by a three-dimensional near field method over the whole wetted surface of the semi-submersible. A comparison amongst these data shows that for the semi-submersible under investigation, the present approximation method results are in

reasonable agreement with the model test measurements, and at least of the same degree of accuracy as the data derived from the much more complicated three-dimensional analysis.

8.5.2. A tension leg platform

The TLP illustrated in Figure 8.5.7a has been used in an experimental investigation by Tan and Boom (1981). It is constructed with four vertical columns of diameter 16.87m and length 24.5m. The four horizontal rectangular pontoons are of cross-section 7.5x10.5m and the structure is of total draft 35m floating in deep water.

In terms of the present method (§8.4), the evaluation of the horizontal mean drift force is determined from only a horizontal cross-sectional contour consisting of four circles as shown in Figure 8.5.7b.

In the numerical calculation each circular contour is discretised into 16 segments, such that the contour of the four circles is described by a total of 64 equal elements. However, only 16 segments on the same column is necessary in the computation owing to its geometric symmetry about two planes. After solving ϕ_7 by the numerical procedure presented in §8.3, the horizontal mean wave drift forces are further calculated from Equation (8.4.2) with draft $h = 24.5m$.

Computations are carried out for wave periods from 5 to 24 seconds and for wave headings $\beta = 0$, 22.5, 45 degrees. The resultant mean surge drift forces are given in Figures 8.5.8-10, respectively for wave heading 0, 22.5 and 45 degrees. Those for sway at a wave heading of 22.5 degrees are displayed in Figure 8.5.11. The calculated mean yaw drift moments are shown in Figure 8.5.12. In Figures 8.5.8-12, all the alphabetic points denote the numerical data from different sources following the notation adopted by Eatock Taylor and Jeffreys (1986), and the circular, triangular and square points indicate the experimental data by Tan and Boom (1981). It can be seen that, in general, the results derived from the present simplified approach display the

characteristics of the other data. It can be noted in Figure 8.5.12 that the model testing data for the mean yaw drift moment display significant scattering at the same wave period most likely due to other non-linear effects such as viscosity.

8.6. Concluding Remarks

A horizontal plane method was used to evaluate the mean drift forces on vertical cylinders (single or multiple) of arbitrary sectional geometry and extending to the seabed.

The proposed method was further extended to approximate the horizontal mean drift forces on multi-column offshore structures. Although assumptions are introduced into the mathematical model to simplify the numerical procedures, example studies of a semi-submersible and a TLP appear to show promise.

Although only offshore structures of circular column sections are presented in the example studies, the present method is capable of predicting mean wave drift forces on a multi-column offshore structure of column section other than a circle.

One of the advantages of adopting this approximation is the great saving in computing time and this may enable the proposed technique to be of more practical use at the preliminary design stages.

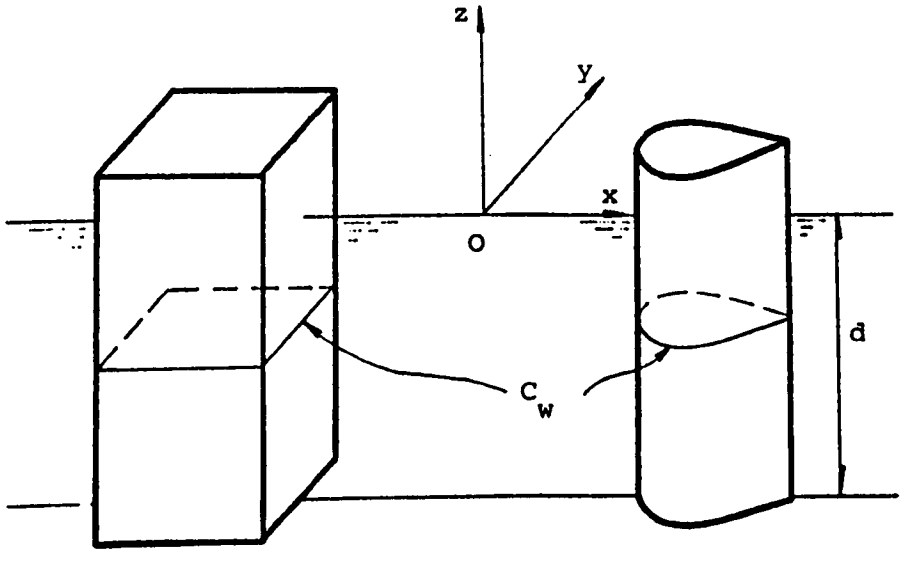

Figure 8.3.1. Vertical cylinders of arbitrary geometry.

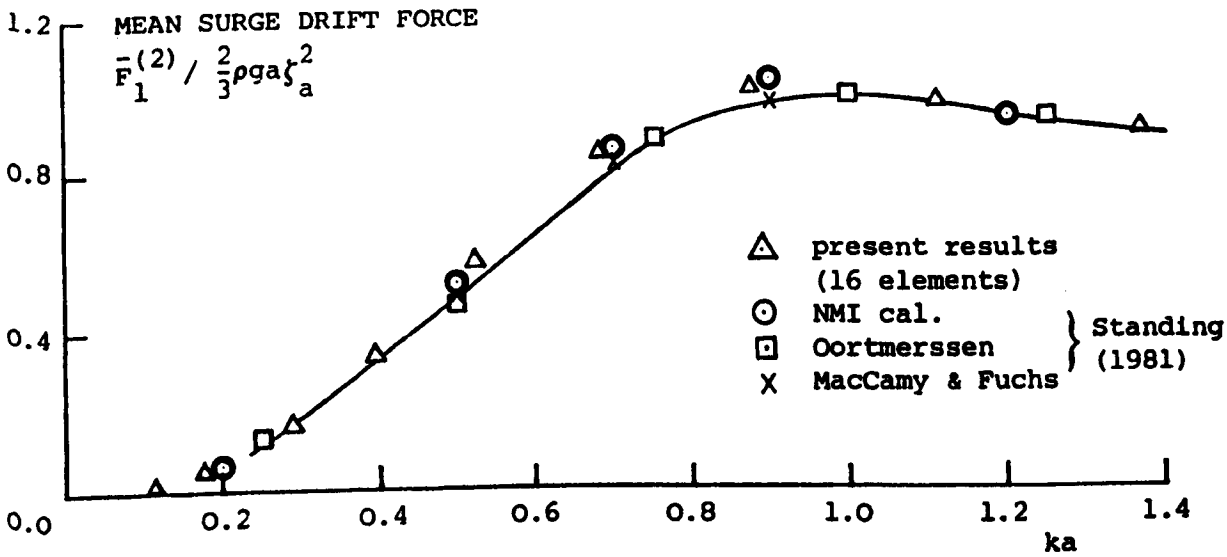

Figure 8.3.2. Mean surge drift force on a vertical circular cylinder of radius a = 1.5m in shallow water of depth d = 5m.

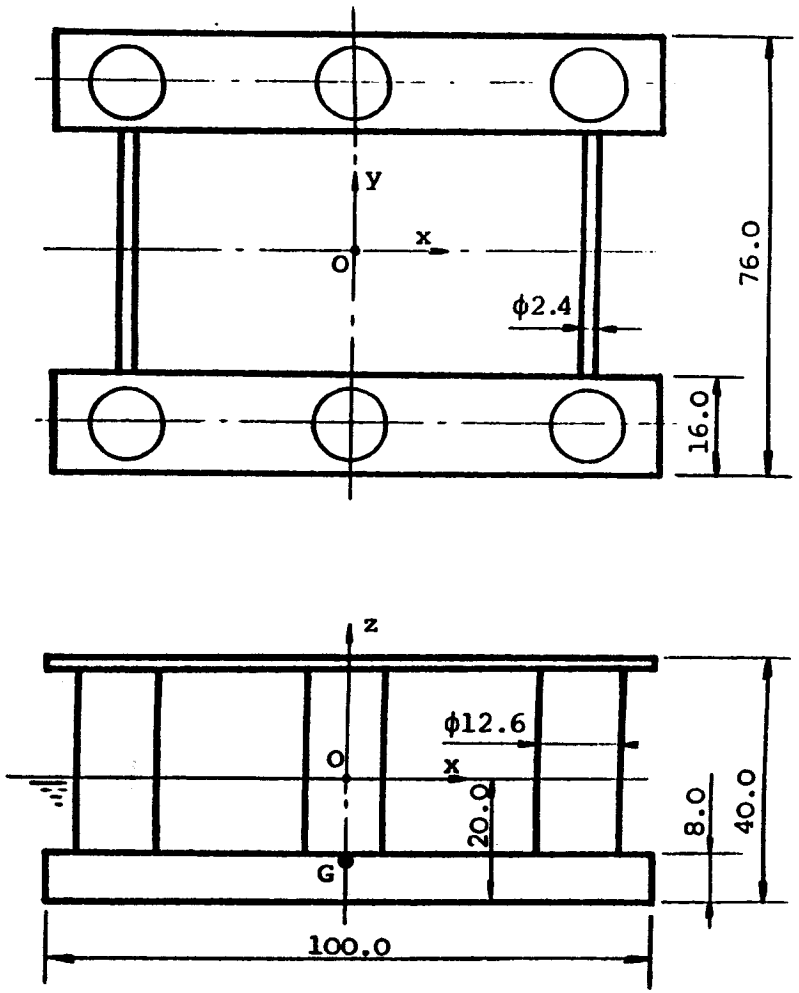

Figure 8.5.1. Main dimensions of the semi-submersible.

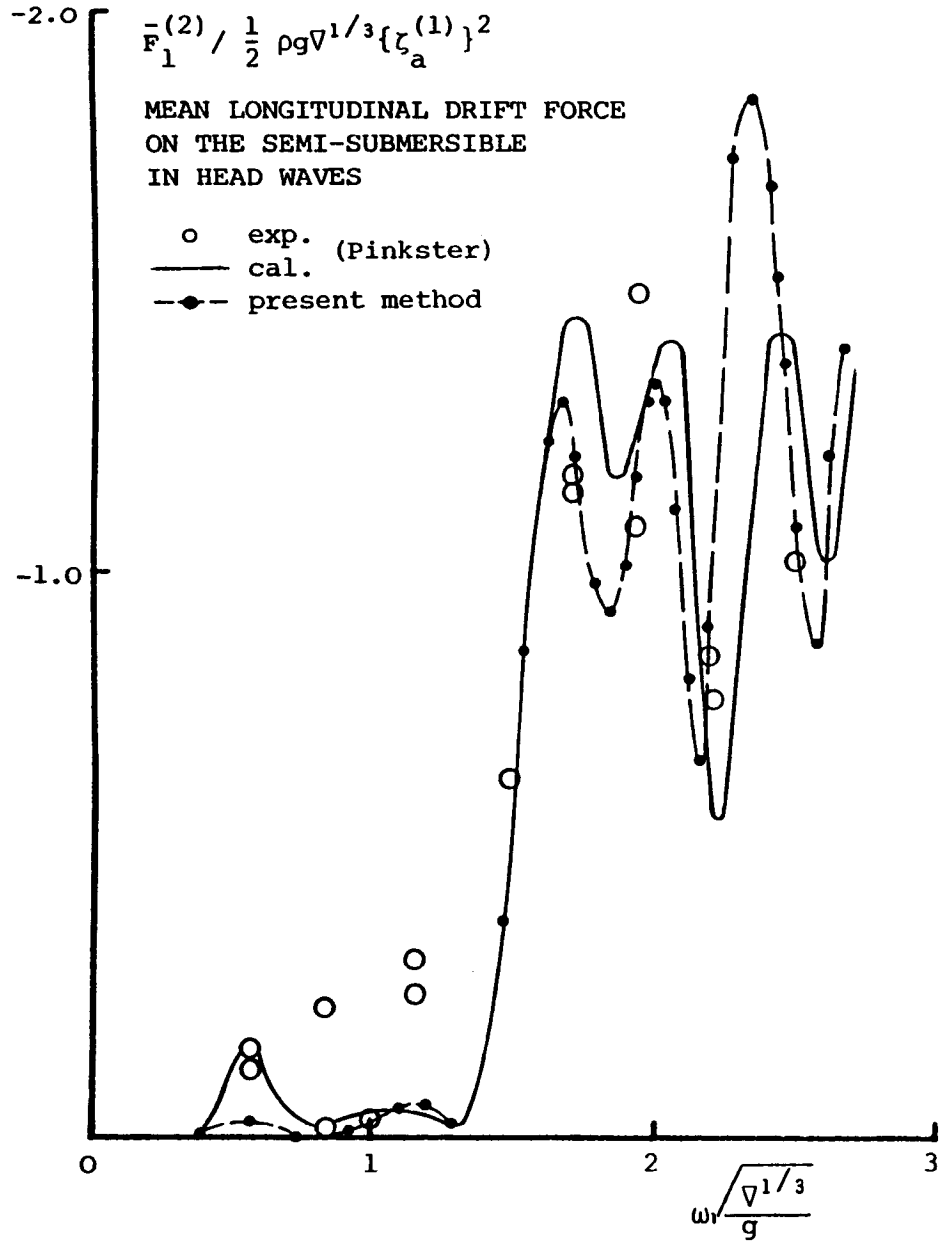

Figure 8.5.2. Mean longitudinal drift force on the semi-submersible in head waves.

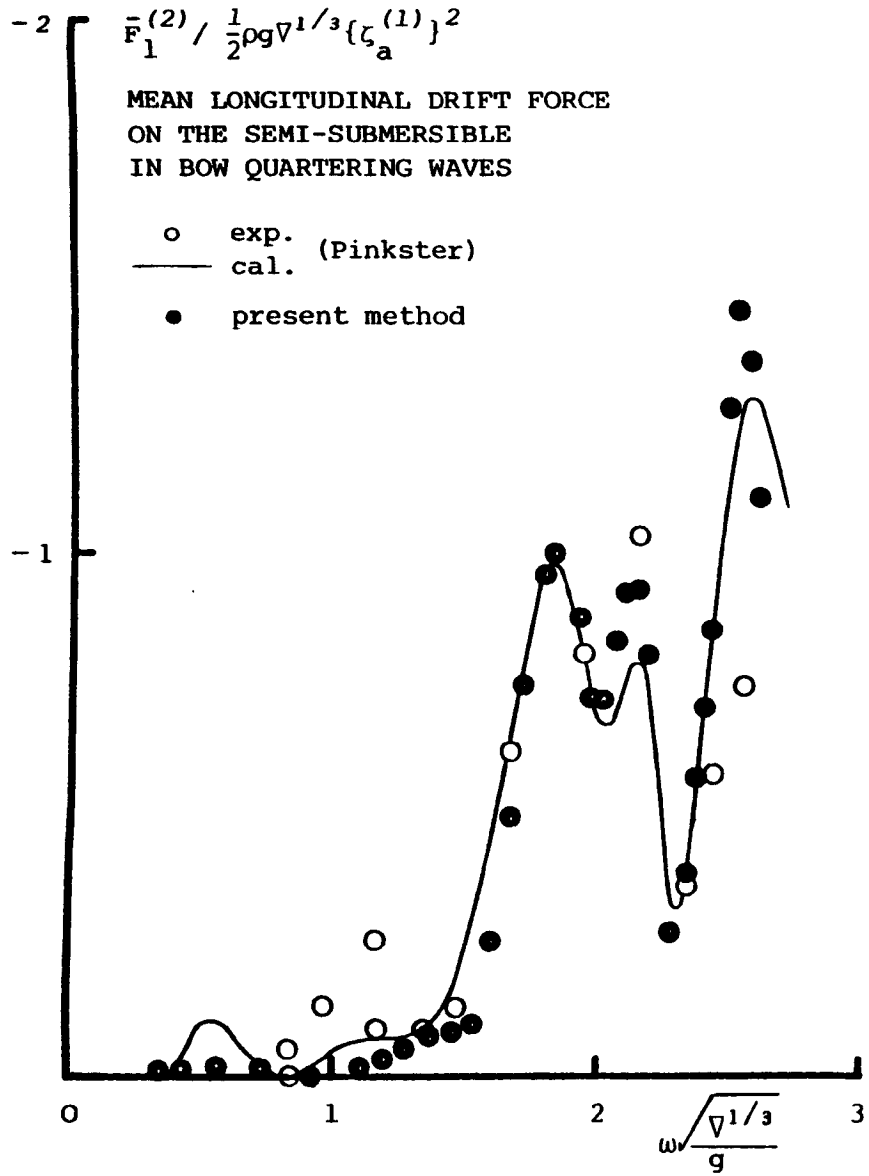

Figure 8.5.3. Mean longitudinal drift force on the semi-submersible in bow quartering seas.

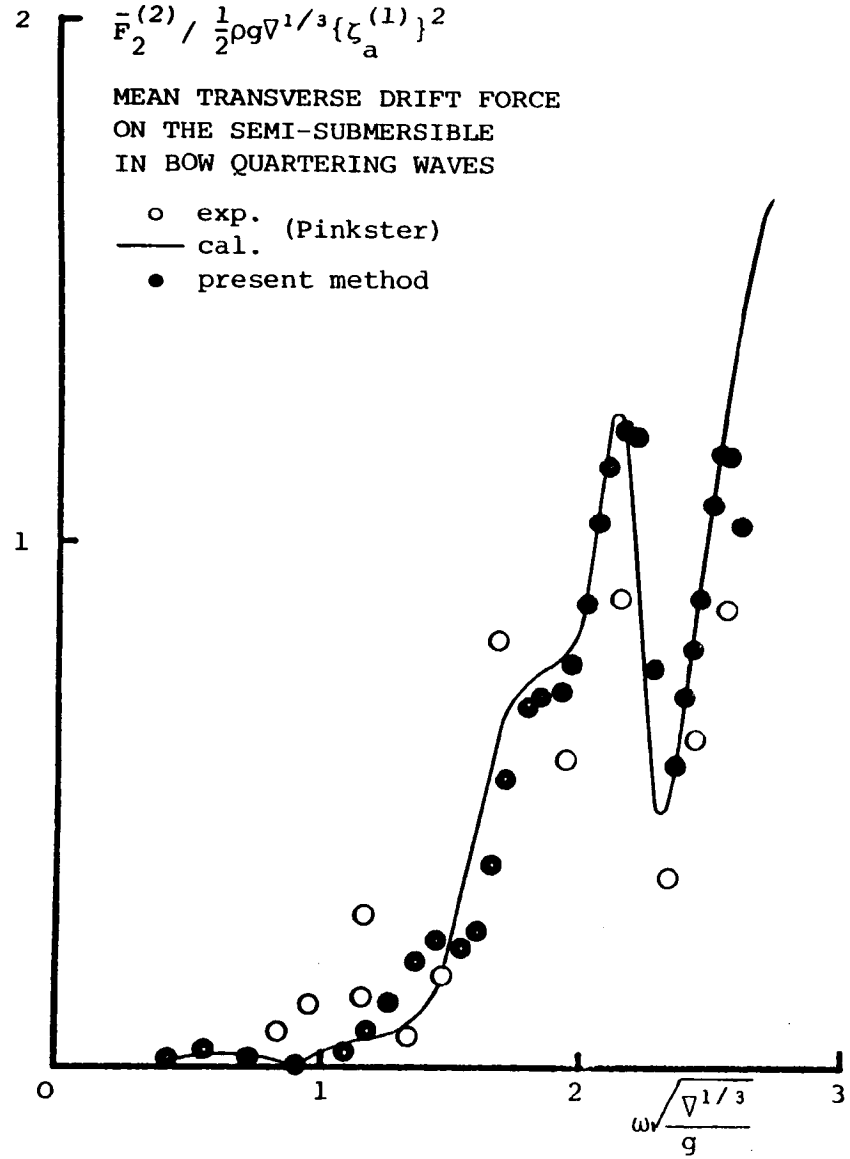

Figire 8.5.4. Mean transverse drift force on the semi-submersible in bow quartering seas.

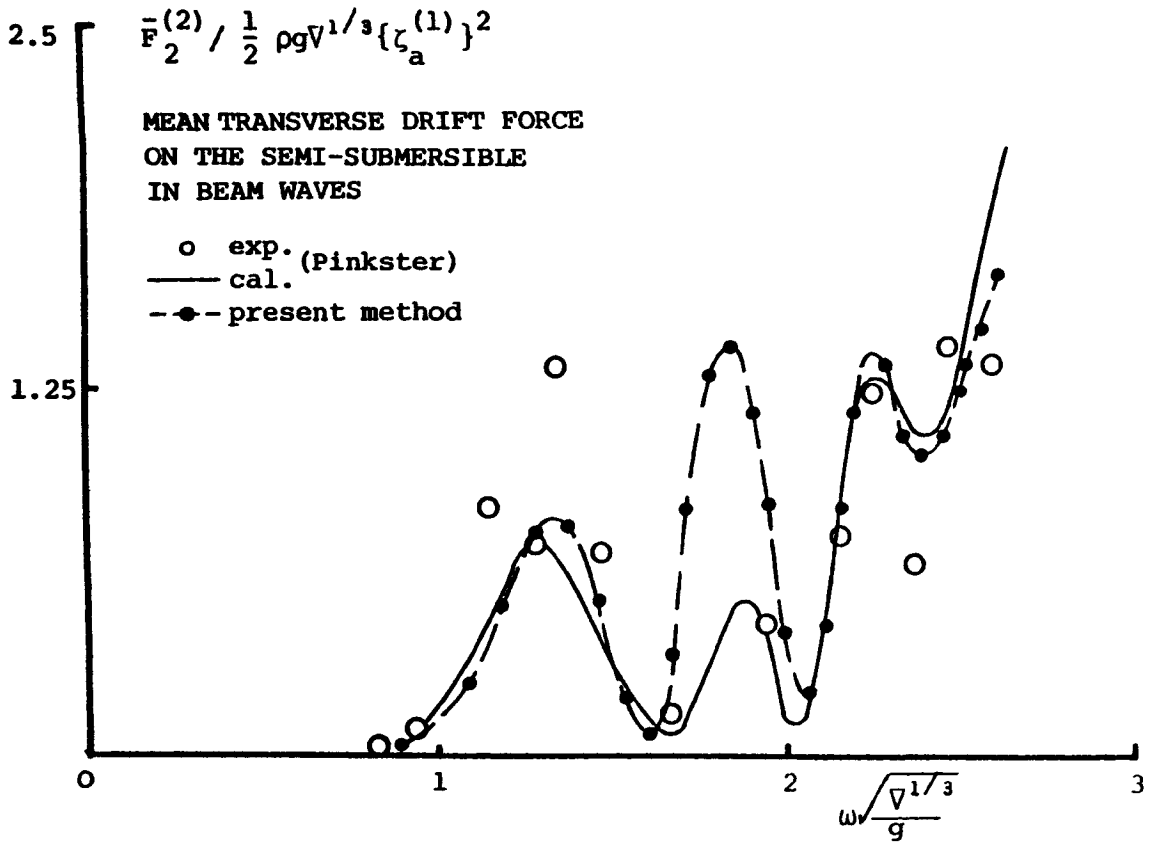

Figure 8.5.5. Mean transverse drift force on the semi-submersible in beam waves.

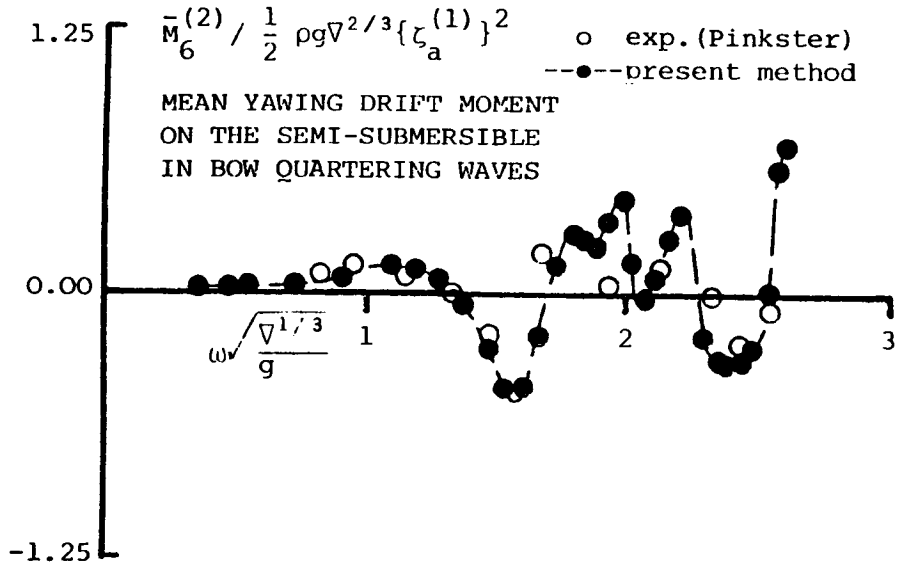

Figure 8.5.6. Mean yaw drift drift moment (Pinkster 1979) on the semi-submersible in bow quartering seas.

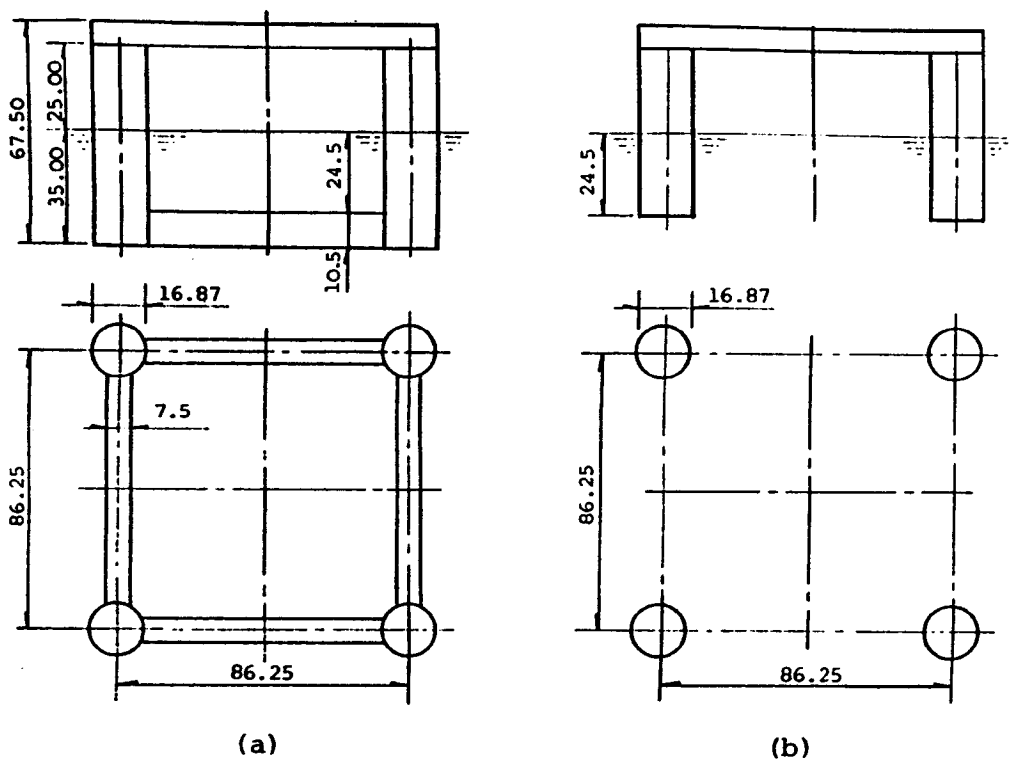

Figure 8.5.7. (a) A TLP model (Tan and de Boom 1981).
(b) The simplified model for the present method.

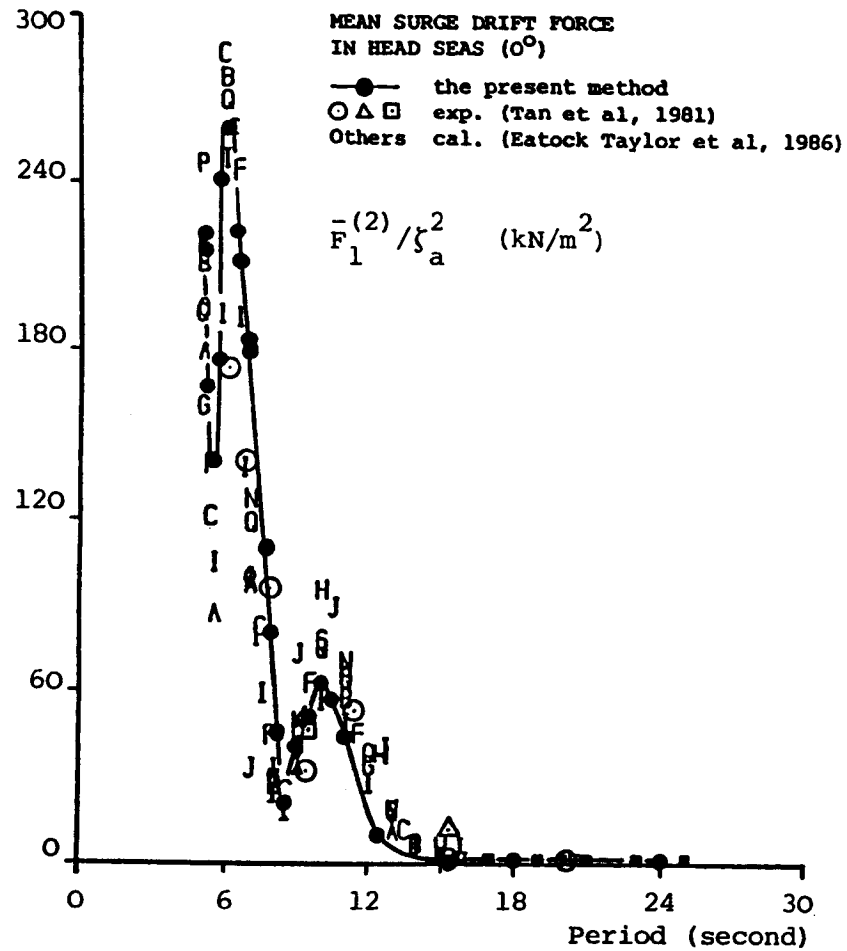

Figure 8.5.8. Mean surge drift force on the TLP in head seas.

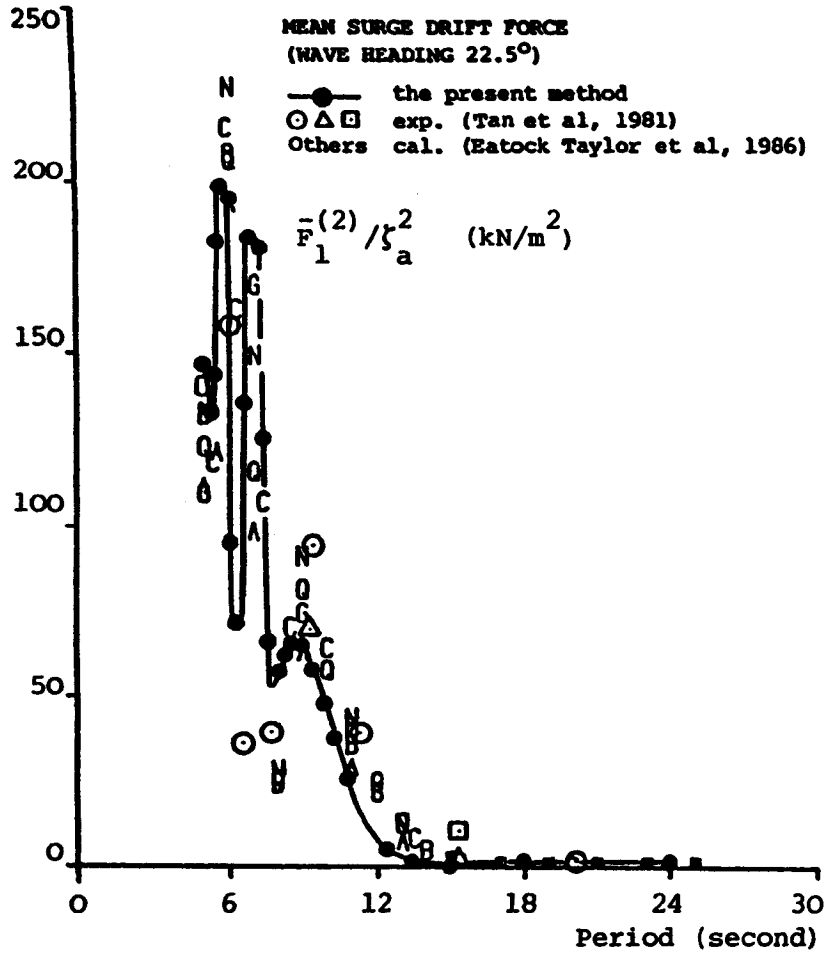

Figure 8.5.9. Mean surge drift force on the TLP at wave heading angle 22.5°.

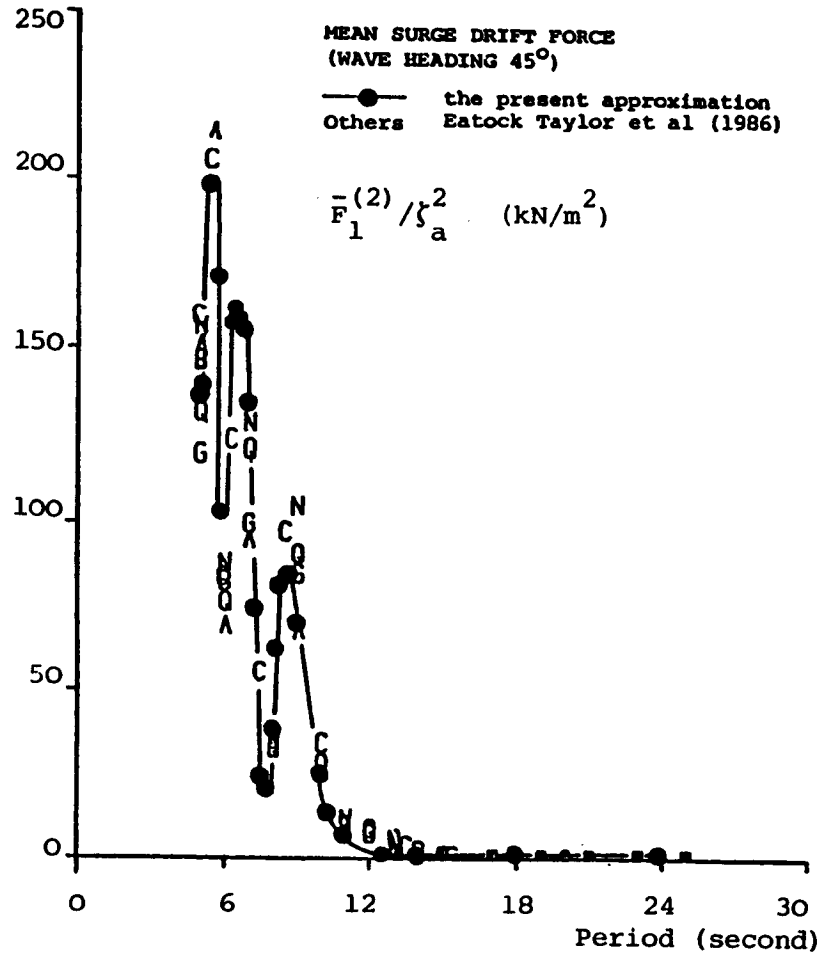

Figure 8.5.10. Mean surge drift force on the TLP at wave heading angle 45°.

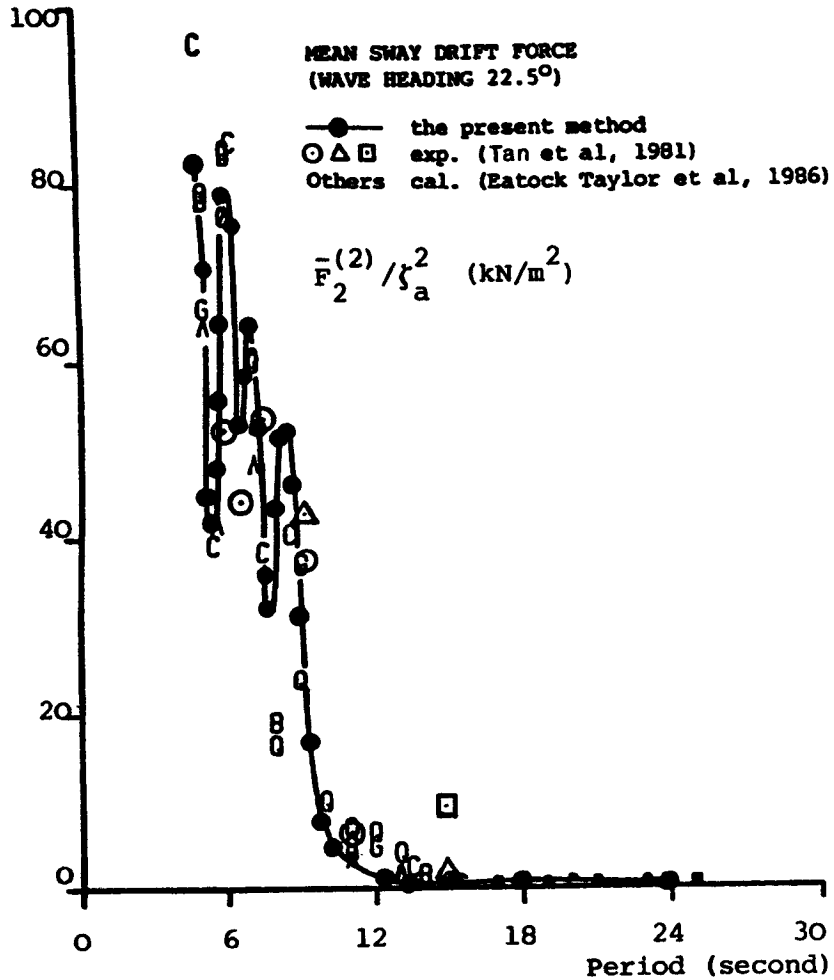

Figure 8.5.11. Mean sway drift force on the TLP at wave heading angle 22.5°.

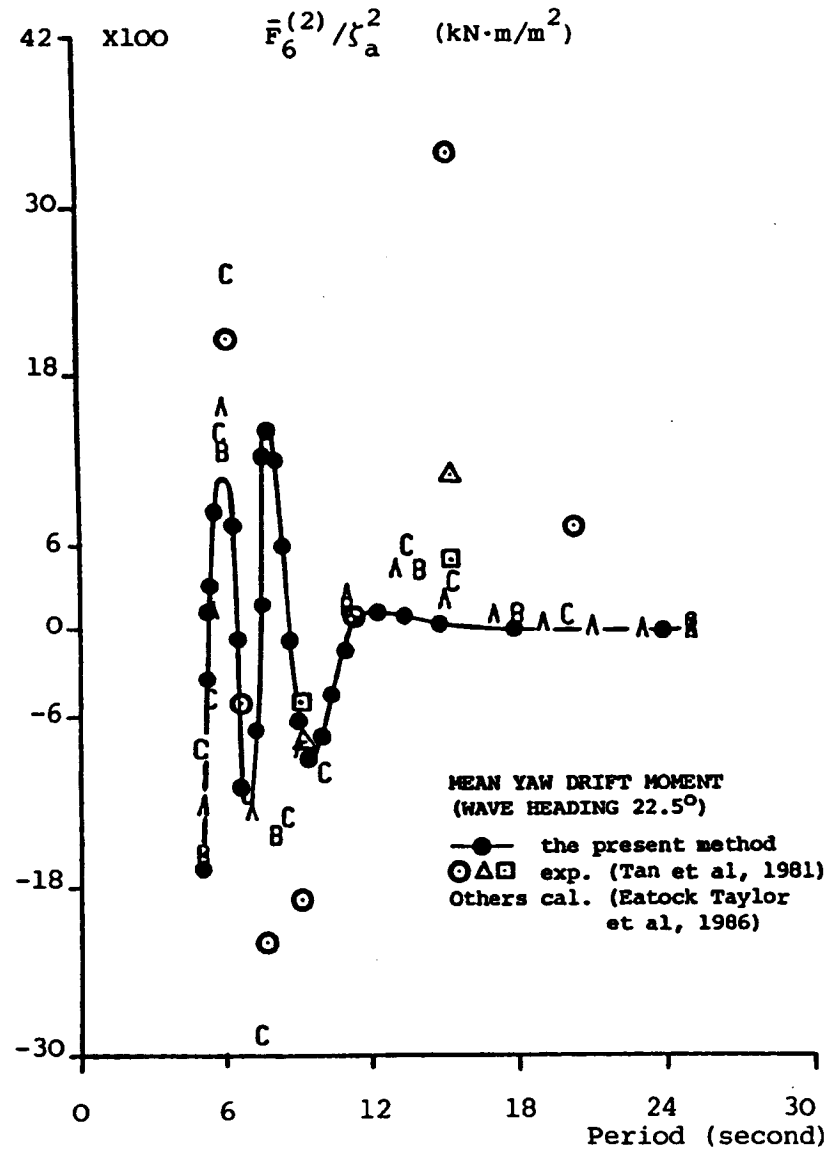

Figure 8.5.12. Mean yaw drift moment on the TLP at wave heading angle 22.5°.

9. SEAKEEPING ANALYSIS WITH VISCOUS EFFECT

9.1. Introduction

With the continuous development of maritime and offshore activities, there now exists a wide variety of floating structures with configurations of far greater complexity than is found in ordinary mono-hull ships. Among those designed and built, many novel structural features have been introduced, such as various semi-submersible and tension leg platforms (TLPs) in offshore operation and the small waterplane area twin-hull (SWATH) vessels for both civil and naval applications.

Being different from framed structures such as fixed jackets and conventional ships of one large floating hull, these large offshore structures and special vessels under discussion are composed of, in general, multiple submerged floaters (e.g. pontoons or lower hulls) as well as multiple vertical members (e.g. columns or struts) piercing the free-surface. Their relative smaller waterplane area results in much longer resonant motion periods such that better seakeeping performances can be achieved.

Due to the interaction between the surrounding fluid and the multiple sub-members of such a structure, multiple natural frequencies (Wu and Price 1986c) may occur in the vessel's motion, apart from the conventional resonant frequency designated at a small frequency value. It has been found that for these large marine structures viscosity plays an important role in determining motion responses at the vicinity of these natural frequencies but has little significance beyond these resonant frequency bands (Lee 1976, Wu and Price 1986c).

Corresponding to Kelvin's principle of fluid motion separation (§1.1.1) a rough estimate of the viscous drag forces can be added, as a correction, into the potential forces predicted by either

two- or three-dimensional diffraction theory analyses. A brief review of the drag forces has been given in §1.1.7.

As examples of comprehensive application of the hydrodynamic formulations, motion theories and numerical techniques described in the previous chapters, the seakeeping performances of two groups of structures are investigated. One is a multi-column or -strut stabilised large offshore structure without forward speed; and the other, a multi-hulled special vessel with forward speed.

9.2. Large Offshore Structures

In this study, focus is concentrated on large offshore structures of submerged massive floater(s) and multiple large columns or large struts. For motion predictions of this group of offshore structures, a method combining the three-dimensional diffraction theory and a drag force estimation is described. As an example, the motion characteristics of a derrick barge semi-submersible are investigated using the combination method developed.

9.2.1. Viscous effect

In order to estimate the viscous damping and the viscous exciting forces resulted from the drag forces on the structure, the method devised requires the structure wetted surface to be sub-divided into three typical sets of strips along the Ox, Oy and Oz axes. Suitable representative points on the strip contour are selected for the viscous force estimation. The elemental components of the viscous force due to drag acting on an elemental wetted surface area ΔS may be expressed by the approximate expressions (Sarpkaya and Isaacson 1981, Wu and Price 1986c):

$$(\Delta F_{D1},\ \Delta F_{D2},\ \Delta F_{D3}) = \frac{1}{2}\,\rho\, C_D\, |V_r|\, (\dot{X}_r \Delta S_1,\ \dot{Y}_r \Delta S_2,\ \dot{Z}_r \Delta S_3) \tag{9.2.1}$$

and when summed up over the total wetted surface result in the total drag forces in the form:

$$F_{Dj} = \sum \Delta F_{Dj} \qquad j = 1, 2, 3 \tag{9.2.2a}$$

The corresponding components of the moments of the drag forces may be simply given as

$$\begin{aligned} F_{D4} &= -\sum (z - z_G)\, \Delta F_{D2} + \sum (y - y_G)\, \Delta F_{D3} \\ F_{D5} &= -\sum (x - x_G)\, \Delta F_{D3} + \sum (z - z_G)\, \Delta F_{D1} \\ F_{D6} &= -\sum (y - y_G)\, \Delta F_{D1} + \sum (x - x_G)\, \Delta F_{D2} \end{aligned} \tag{9.2.2b}$$

where C_D is the drag coefficient which is dependent on the Keulegan-Carpenter number (Kc) and the Reynolds number (Rn). These may be chosen from experimental data or the recommended values tabulated for typical geometries (Sarpkaya and Isaacson 1981). ΔS_j is the projected area of a strip element in the jth direction. $\sum$ denotes a summation over the whole wetted surface of the body. $\dot{X}_r$, $\dot{Y}_r$ and $\dot{Z}_r$ are relative velocity components (along the Ox, Oy and Oz axes) of the overall relative velocity V_r between the water particle and the body motions. These are defined by

$$\begin{aligned} \dot{X}_r &= W_1 - \dot{X}_1 - (z - z_G)\, \dot{X}_5 + (y - y_G)\, \dot{X}_6 \\ \dot{Y}_r &= W_2 - \dot{X}_2 - (x - x_G)\, \dot{X}_6 + (z - z_G)\, \dot{X}_4 \\ \dot{Z}_r &= W_3 - \dot{X}_3 - (y - y_G)\, \dot{X}_4 + (x - x_G)\, \dot{X}_5 \end{aligned} \tag{9.2.3}$$

where $W_j = W_{oj}\, exp(-i\omega t)$ with $(W_{o1},\ W_{o2}, W_{o3}) = (\frac{\partial}{\partial x},\ \frac{\partial}{\partial y},\ \frac{\partial}{\partial z})\, \phi_o$, and $X_j = X_{ja}\, exp(-i\omega t)$ denotes the jth mode of motion.

After applying an equivalent linearisation procedure, it follows that

$$\begin{aligned} \Delta F_{D1} &= -\frac{4}{3\pi}\, \rho\, C_D\, \Delta_{S1}\, V_{ro}\, [\dot{X}_1 + (z - z_G)\, \dot{X}_5 - (y - y_G)\, \dot{X}_6 - W_1] \\ \Delta F_{D2} &= -\frac{4}{3\pi}\, \rho\, C_D\, \Delta_{S2}\, V_{ro}\, [\dot{X}_2 + (x - x_G)\, \dot{X}_6 - (z - z_G)\, \dot{X}_4 - W_2] \\ \Delta F_{D3} &= -\frac{4}{3\pi}\, \rho\, C_D\, \Delta_{S3}\, V_{ro}\, [\dot{X}_3 + (y - y_G)\, \dot{X}_4 - (x - x_G)\, \dot{X}_5 - W_3] \end{aligned} \tag{9.2.4}$$

where V_{ro} is written as

$$V_{ro} = \omega \sqrt{\sum_{j=1}^{3} (X_{mj})^2} \tag{9.2.4a}$$

and X_{mj} is defined by

$$\begin{aligned} X_{m1} &= |X_{1a} + (z - z_G) X_{5a} - (y - y_G) X_{6a} + W_{o1}/i\omega| \\ X_{m2} &= |X_{2a} + (x - x_G) X_{6a} - (z - z_G) X_{4a} + W_{o2}/i\omega| \\ X_{m3} &= |X_{3a} + (y - y_G) X_{4a} - (x - x_G) X_{5a} + W_{o3}/i\omega| \end{aligned} \tag{9.2.4b}$$

From such expressions, the viscous force may be separated into contributions associated with viscous damping and viscous exciting force terms. That is

$$F_{Di} = -\sum_{j=1}^{6} B_{vij} \dot{X}_j + F_{vi} \qquad i = 1, 2, ..., 6 \tag{9.2.5}$$

where the components of the viscous exciting forces are given by

$$\begin{aligned} F_{vi} &= \sum a_i V_{ro} W_i \qquad i = 1, 2, 3 \\ F_{v4} &= \sum (y - y_G) a_3 V_{ro} W_3 - \sum (z - z_G) a_2 V_{ro} W_2 \\ F_{v5} &= \sum (z - z_G) a_1 V_{ro} W_1 - \sum (x - x_G) a_3 V_{ro} W_3 \\ F_{v6} &= \sum (x - x_G) a_2 V_{ro} W_2 - \sum (y - y_G) a_1 V_{ro} W_1 \end{aligned} \tag{9.2.6}$$

with $(a_1, a_2, a_3) = -\frac{4}{3\pi} \rho C_D (\Delta S_1, \Delta S_2, \Delta S_3)$.

The determination of these viscous terms requires information on the motion response amplitudes (i.e. X_{ja}) and therefore the viscous effect can only be estimated simultaneously with the motion solution of Equation (2.5.9) by an iterative procedure.

9.2.2. General configuration

The semi-submersible consists of a huge barge-like submerged floater and six large struts as shown in Figure 9.2.1. The floater is of dimensions 144x43.5x10.5m and at 12m beneath the calm water surface, making a total draft of 23.5m. The major sizes for the mid-struts are 45x16.2m and for the end-struts, 15x16.2m. The displacement volume is 91,196 m^3 and the

coordinates of the centre of gravity are G(0.3, 0.0, -8.36). The gyradii for roll, pitch and yaw motions are 23.6, 41.0 and 40.35m, respectively. These main dimensions indicate that a three-dimensional diffraction theory is necessary for the hydrodynamic analysis. In particular, since a layer of partially truncated water region is surrounded by the structural members, resonant waves excited by the body motion make the wave-structure interaction problem much more complicated.

9.2.3. Numerical computation

Taking advantage of the port and starboard symmetry, only a half of the body's wetted surface is needed. This is discretised into 193 panels for the three-dimensional analysis. A quarter of the body surface is illustrated in Figure 9.2.2.

By the three-dimensional Green function method analysis based on Equations (4.1.3b) and (3.2.2), the three-dimensional hydrodynamic coefficients, including surge, sway, heave, roll, pitch and yaw added mass and damping, are calculated and illustrated in Figure 9.2.3.

In Figure 9.2.3, superposed on the heave and pitch added mass curves are the condition lines defined by

$$A_{jj} = C_{jj}/\omega^2 - M_{jj} \tag{9.2.7}$$

As used in naval architecture, the intersecting points of the condition line and the added mass curve represent the resonant frequencies. It can be seen that there exist three heave resonant frequencies at $\omega =$ 0.222, 0.393 and 0.52 rad/sec, two possible pitch natural frequencies at $\omega =$ 0.246 and 0.54 rad/sec but only one roll natural frequency at $\omega = 0.221$ rad/sec. The first resonant frequencies predicted precisely coincide with the measured data, i.e. 0.224 rad/sec for the heave, 0.247 rad/sec for the pitch and 0.227 for the roll mode (de Boom 1978). Besides these designed first natural frequencies of small values, extra resonances in the heave and pitch motions can

therefore be expected.

Using these computed three-dimensional hydrodynamic coefficients and wave exciting forces together with viscous effects, the predicted surge, sway, heave, roll and yaw responses are displayed in Figure 9.2.4. These theoretical predictions are shown in good correlation with existing experimental results (de Boom 1978) but generally these model testing data are not available for illustration. Fortunately, a set of data for the pitch motions in quartering seas have been released by MSC (1985), which provide some measure of the accuracy of the present theoretical predictions. As shown in Figure 9.2.5, the present calculation results are in very good agreement with the measured data of the pitch motion. Particularly, an additional pitch peak response occur around $\omega = 0.57$ rad/sec, which confirms the finding of the multiple resonances. A small frequency shift from the predicted second pitch natural frequency at 0.54 rad/sec is most likely due to the existence of damping.

For heave motions (Figure 9.2.4), besides the first heave natural frequency predicted at 0.222 rad/sec, peak heave responses appear around the third natural frequency but there is no indication of the second one. The reason for this is clearly evident from these figures since at the predicted second heave natural frequency (0.393 rad/sec) the damping coefficient is nearly a maximum value and this influence suppresses the appearance in the second peak response of the heave motion.

In Figure 9.2.4, two-dimensional calculation results are also presented. However, these are shown to be unsatisfactory; in particular, they fail to predict the multiple resonances occurring and associated with the wave-structure interaction. As can be seen from Figure 9.2.6, from the added mass curve derived by a two-dimensional analysis no additional heave natural frequencies can be found apart from the first one round about 0.222 rad/sec.

To understand the influence of the viscous effect, a comparison was made between heave motion data predicted with and without viscosity. These results are given in Figure 9.2.7 for the heave motions at wave heading angles 180, 225 and 270 degrees. It shows that the viscous effects have an important contributory influence in the vicinity of the natural frequencies of the body motion even for offshore structures with sizable sub-members.

9.2.4. Concluding Remarks

From this example study, the following conclusions are drawn:

(1) For a structure with multiple large sub-members, there can exist multiple natural frequencies in a motion mode and these can induce extra peak motion responses.

(2) For this kind of large marine structure, viscosity is of importance when determining the magnitudes of the body responses near natural frequencies.

(3) A combination of the three-dimensional hydrodynamic analysis and an estimation of the drag forces provides a useful tool for motion predictions of large offshore structures with more complicated configuration.

(4) For this particular example, the two-dimensional analysis seems inadequate to provide reasonable information for design purposes.

9.3. Multi-Hulled Special Vessels

This group of ships include SWATH ships, catamarans, tri-hull crafts and so on. In the present study, however, attention is focused on SWATH ships only.

9.3.1. SWATH ships

The revival of active research and development on SWATH ships started in the later 1980s associated with the design and construction of SWATH T-AGOS (Covich 1986), though initial theoretical and experimental studies were carried out in the mid 1970s (Lee 1976). Recently, the development of fast commercial SWATH prototypes of considerable displacement has caused much excitement worldwide.

From the geometric configuration, a SWATH ship is characterised by its twin-hulls of small waterplane area and a top deck of large operation area. The small waterplane area results in long natural periods of heave, pitch and, in particular, roll motions. These natural motion frequencies are designed to be far away from the energy concentration frequencies of the sea wave spectrum such that serious resonant motions can be effectively avoided. In addition, the added viscous damping due to the submerged lower hulls can reduce, to a great extent, the peak motion responses if resonances occur in these motion modes. Therefore, SWATH ships possess higher seakeeping qualities, especially, small vertical motion and acceleration amplitudes. The increased operability together with the large open deck area makes the SWATH ship very attractive for leisure, transportation, engineering and naval purposes.

9.3.2. Theoretical bases

To analyse the seakeeping performance of a SWATH ship advancing in water waves, great efforts have been made to improve the prediction theories (Lee 1976, McCreight 1987). In the present work, a computer program has been developed based on a comprehensive application of existing theories and new achievements:

(1) A two-dimensional strip theory is applied which is based on a forward speed correction (Salvesen, Tuck and Faltinsen 1970).

(2) A mixed source-dipole distribution method is used to obtain two-dimensional wave potential solutions, which is based on Equations (4.2.3b) and (3.4.2).

(3) At higher frequencies, the modified Green function form as described in §4.5.3 can be used.

(4) The estimation formulae for the viscous forces (Lee 1976, McCreight 1987) and calculation procedure over the body surface are similar to those described in §9.2.1 with minor modifications:

i) the relative velocity component $\dot{X}_r$ includes the forward speed U,

ii) the encounter frequency of expression (2.2.19) is used; and

iii) the drag coefficient C_D is treated as Kc number dependent;

(5) The lift force in the heave mode and the lift moment in the pitch mode due to the control fins are estimated by the following formulations:

$$\begin{aligned} \Delta F_{3L} &= \frac{1}{2} \rho A_p C_{L\alpha} U^2 \alpha_a \\ F_{3L} &= \sum \Delta F_{3L} \\ F_{5L} &= -\sum (x - x_G) \Delta F_{3L} \end{aligned} \tag{9.3.1}$$

where $\alpha_a = W_3/U - X_5$ with W_3 defined by Equation (9.2.3). Formulations for the lift coefficient $C_{L\alpha}$ with corrections can be found in Dallinga, Graham and Huijsmans (1988). A_p is the fin area. The summation is carried out for all the four fins involved.

(6) All the rigid body motion modes, except surge, are predicted. The surge motion responses, however, may be predicted by an approximation based on the Froude-Krylov hypothesis (§5.2.1) but this requires further experimental verifications.

9.3.3. Example studies

The general arrangement of the SWATH model is illustrated in Figure 9.3.1. The hydrodynamic behaviour of this vessel has been thoroughly studied by model tests and theoretical analyses by ARE (Haslar) (Blackman 1989). The picture of the model under test in the towing tank of Haslar is shown in Figure 9.3.2 (by courtesy of Blackman 1989).

The SWATH ship is composed of two parallel lower hulls, mainly of elliptical cross-sections, and two long struts, extending from the bow to the stern area and supporting the upper deck structure.

According to the scaling factor of 1:20.55, the main particulars of the relative SWATH ship are given in Table 9.3.1. That is, the two lower hulls are of overall length 61.75m and maximum sectional dimensions 6.72x4.45m (elliptical), with a separation distance 18.37m between their central lines. The two long struts are 50.459m long and 2.44m wide. The total displacement volume is 2167 m^3.

The present theoretical computations cover 4 speed conditions (i.e. U = 0, 5, 10 and 14 knots), 5 wave headings (β = 0, 60, 90, 120 and 180 degrees) and wave lengths ranging from λ/L = 0.407 to 5.086. The matrix of the computational analysis is given in Table 9.3.2.

The heave, roll and pitch motion, relative motion and vertical acceleration amplitudes are predicted by the method described in §9.3.2. These are compared with experimental data released by ARE (Haslar 1989) after the calculations were performed.

Figures 9.3.3-6 display the heave, pitch and relative bow motion amplitudes in head seas at forward speed 0, 5, 10 and 14 knots respectively. Good agreement between the experimental data (circular points) and the present theoretical predictions (solid lines) can be observed within this speed range. In particular, the predicted relative bow motion with respect to the wave surface appears rather promising and this parameter is of primary importance when determining slamming on the under deck of the SWATH ship.

In Figures 9.3.7a-c, calculated roll responses at heading angles 60, 90 and 120 degrees are presented. These correlate well with the model test data. The heave and pitch response predictions in beam seas are shown in Figure 9.3.8 and those related to stern seas given in Figure 9.3.9. Again, these computational results agree favourably with experimental results. This limited data set gives some indication of the validation of the present method over the conditions examined.

The acceleration parameter is the most important measure to define the suitability of the vessel for human activity and equipment operation. Figure 9.3.10a shows the predicted bow vertical acceleration amplitudes at speed of 10 knots in head seas, whilst Figure 9.3.10b displays the stern vertical acceleration amplitudes at the same speed but in stern seas. The present prediction method seems to provide reasonable data for this important parameter.

To complement the above study, some theoretical predictions for two other SWATH ships under design consideration are presented here. Figure 9.3.11 shows the surge motion amplitudes of a 1000 ton SWATH ship predicted by the simple method based on the Froude-Krylov hypothesis. Regrettably, no model tests are available to verify this simplification.

Corresponding to irregular waves of sea state 6 defined by the ITTC wave spectrum (Figure 9.3.12), the calculated significant heave, pitch, vertical acceleration amplitudes and the subjective motion magnitude (Price and Bishop 1974, Lloyd and Andrew 1977) are given in Figure 9.3.13 for two similar SWATH vessels of different displacements, i.e. 1000 and 2000 tons respectively. As expected and comfirmed by these findings, the larger vessels exhibited the better seakeeping performance.

9.3.4. Concluding remarks

From the comparative studies of the present method predictions and model test data, it may be concluded that the proposed method to analyse the seakeeping of a SWATH vessel can pro-

duce reliable theoretical predictions in the speed range up to Fn = 0.294 (equivalent to the speed of 14 knots in the example study). Further verification is necessary for forward speed far beyond this limit.

Because of the efficient two-dimensional formulations adopted, the present computer code is applicable in the design process of SWATH ships.

Since the recent worldwide interest is in developing fast SWATH prototypes travelling with forward speed greater than Fn = 1.0, significant modifications to the present method may be required to meet this new challenge.

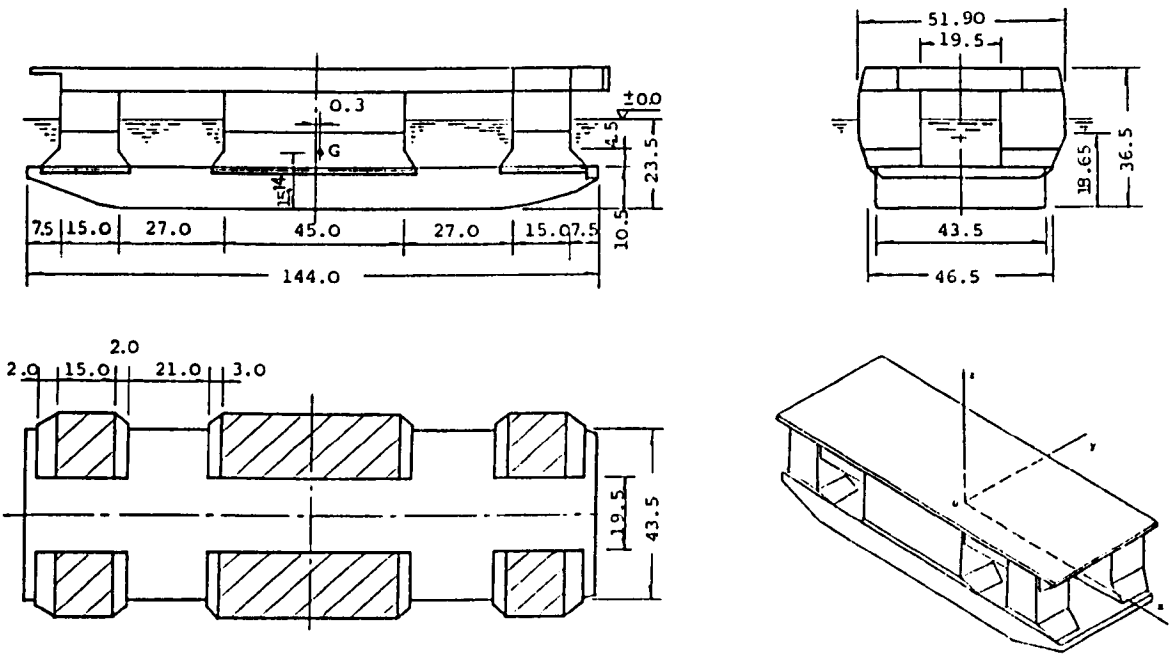

Figure 9.2.1. General arrangements of the derrick barge semi-submersible.

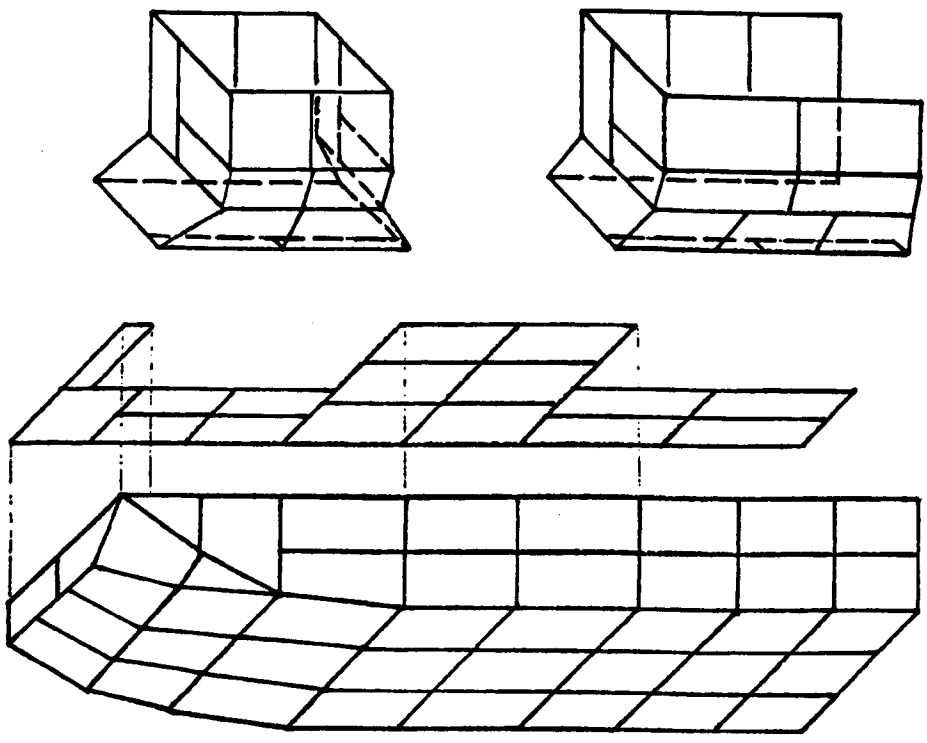

Figure 9.2.2. Surface panel arrangement of a quarter of the wetted surface of the semi-submersible.

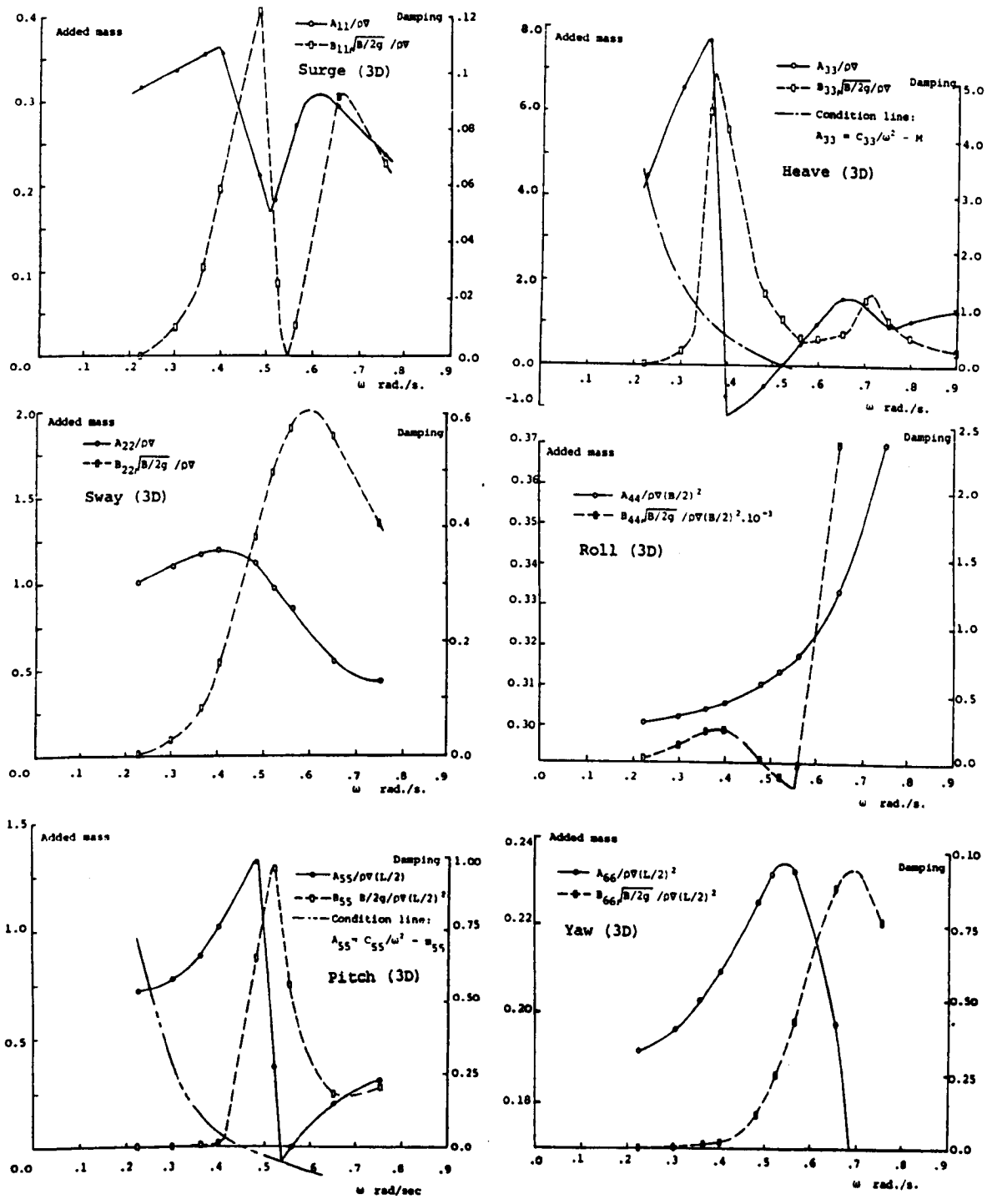

Figure 9.2.3. Three-dimensional added mass and damping coefficients of the semi-submersible.

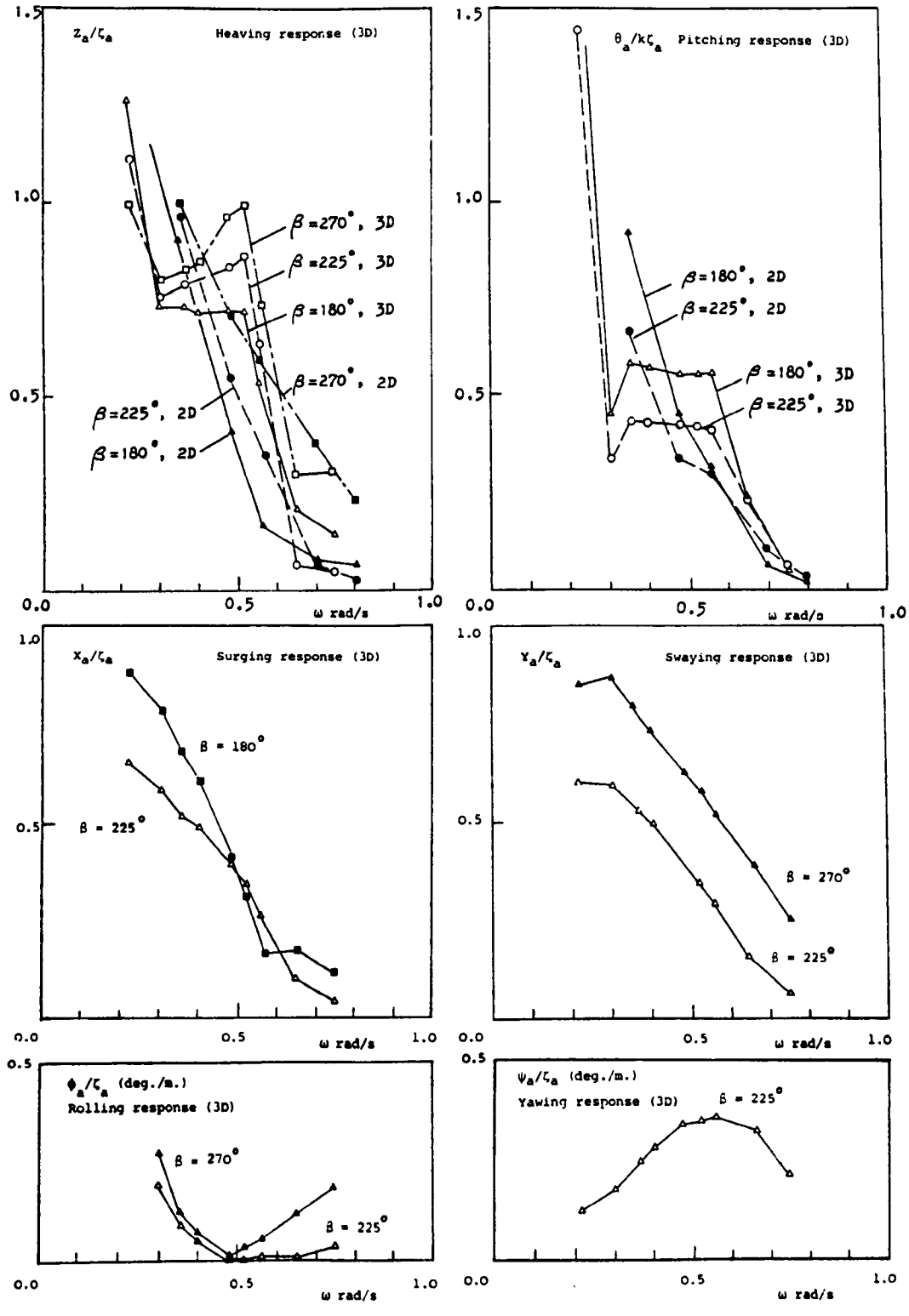

Figure 9.2.4. Motion responses of the semi-submersible predicted by the three-dimensional method with viscous damping.

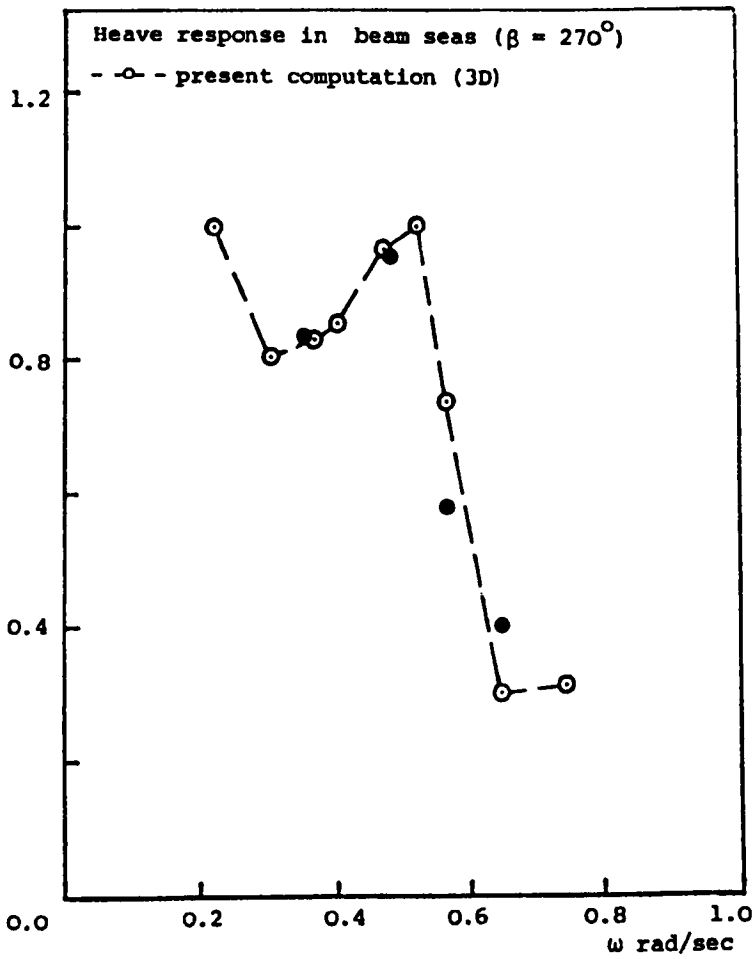

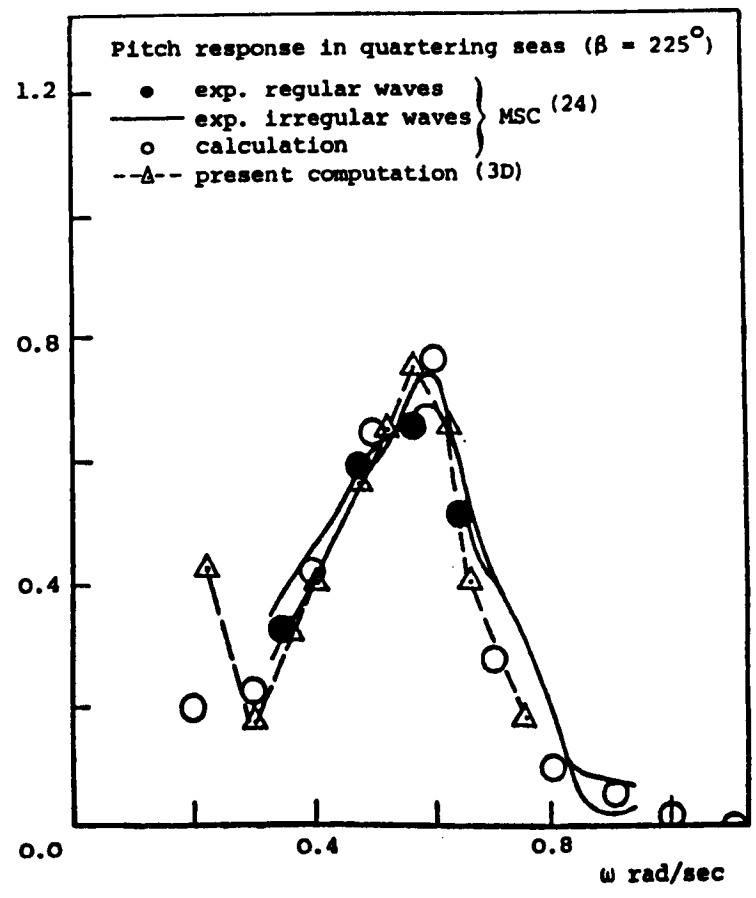

Figure 9.2.5. Comparison of the present motion predictions with experimental data.

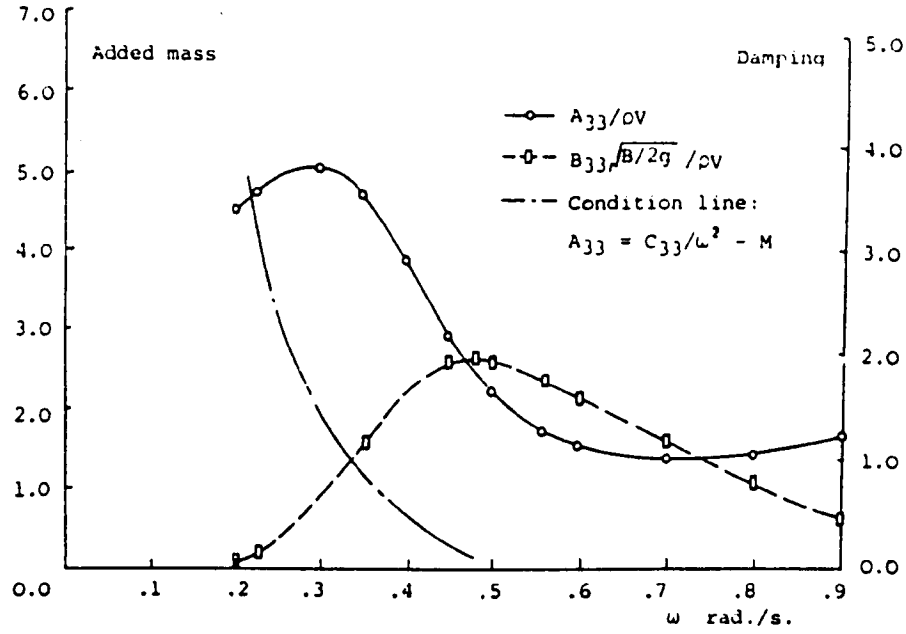

Figure 9.2.6. Calculated two-dimensional heave added mass and damping coefficients of the semi-submersible.

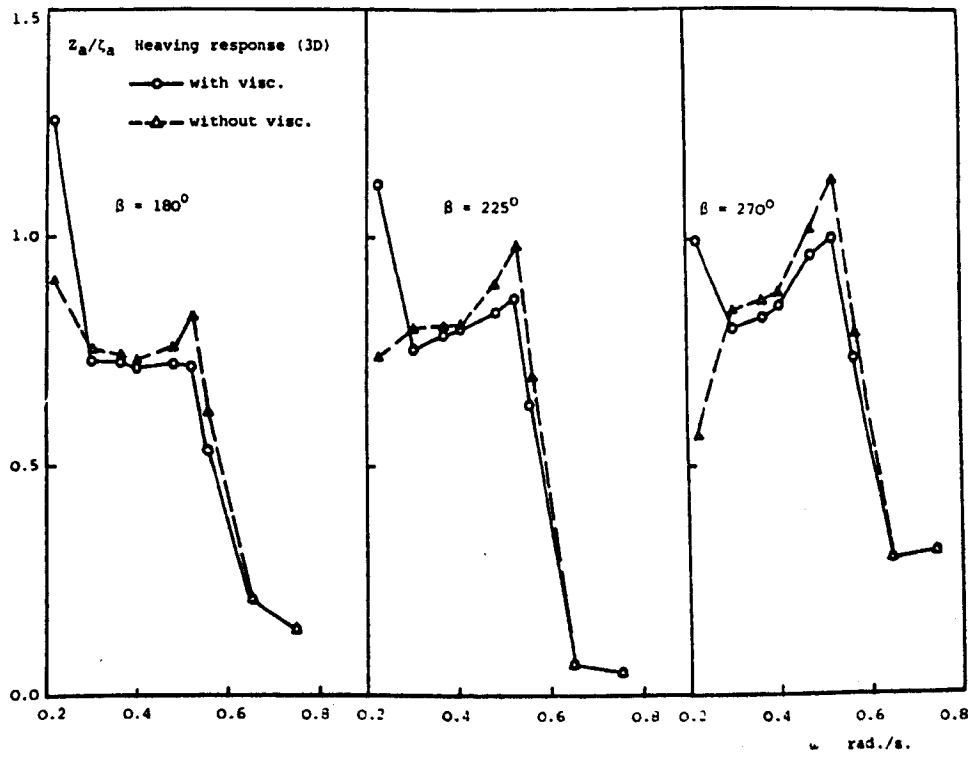

Figure 9.2.7. Viscous effect on heave motion predictions of the semi-submersible.

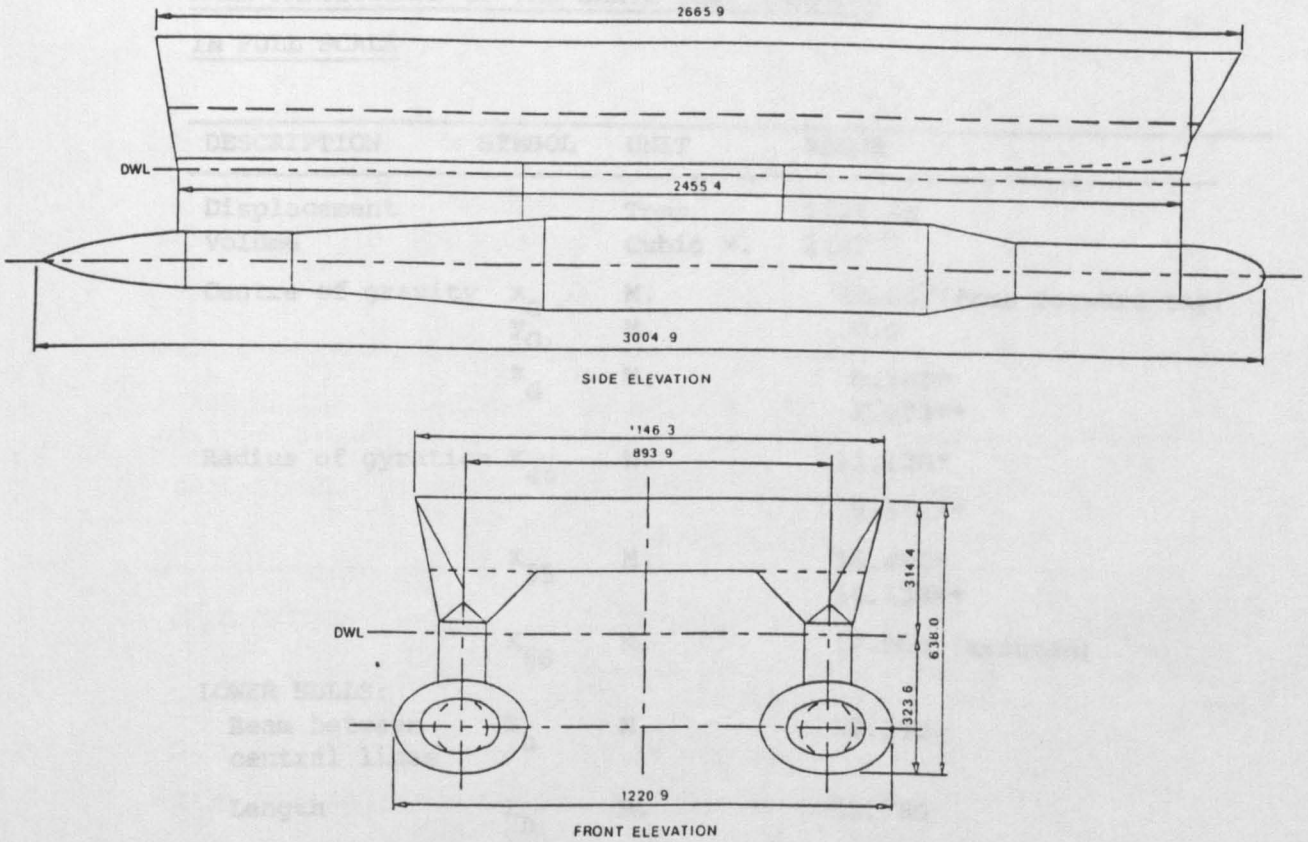

Figure 9.3.1. General configuration of the SWATH model (ARE, Haslar).

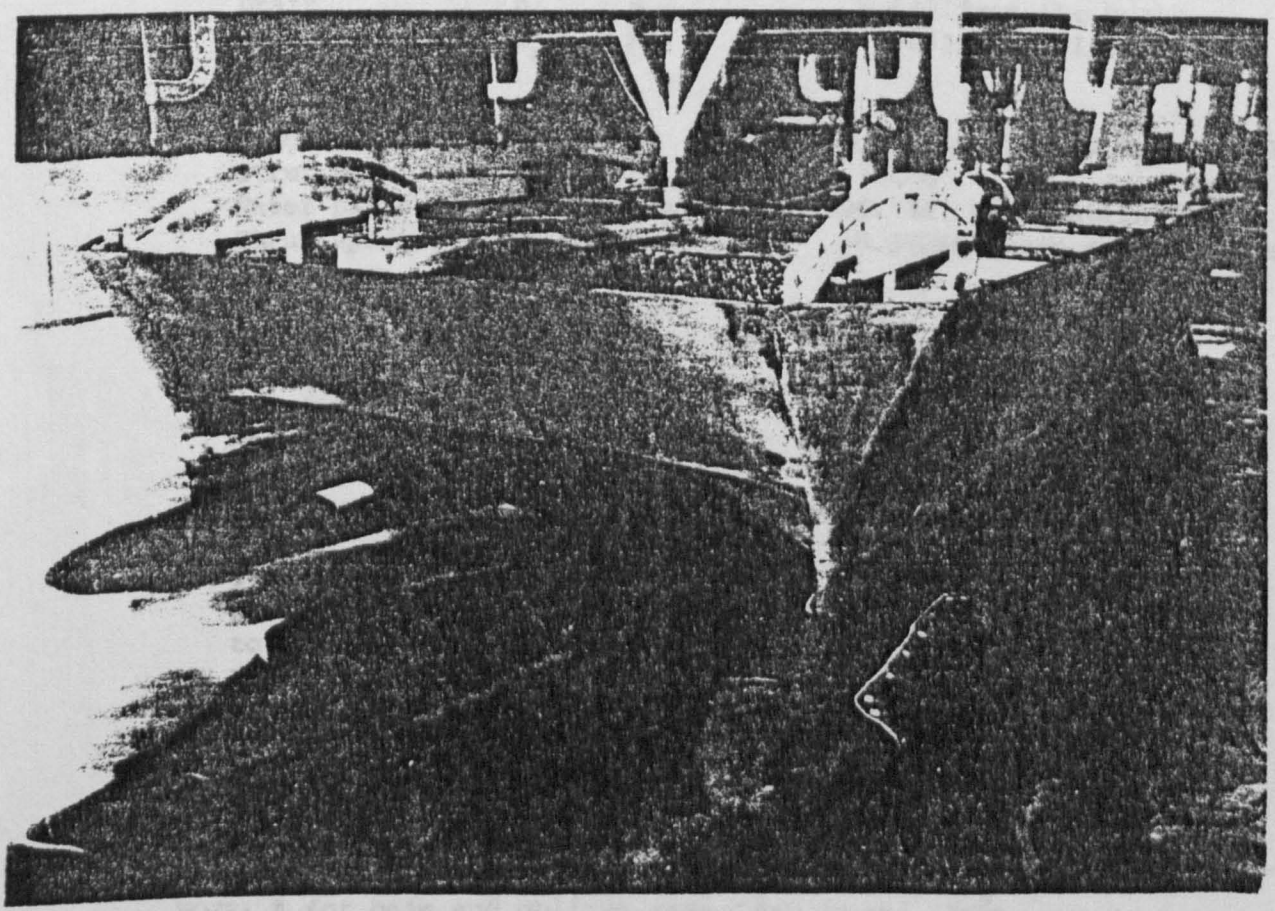

Figure 9.3.2. The SWATH model under test in the towing tank (by courtesy of Blackman, ARE Haslar, 1989).

Table 9.3.1.

MAIN PARTICULARS OF THE SWATH SHIP (HASLAR)

IN FULL SCALE

DESCRIPTION	SYMBOL	UNIT	VALUE
Displacement		Tons	2221.65
Volume		Cubic M.	2167
Centre of gravity	x_G	M.	28.667(from forward tip)
	y_G	M.	0.0
	z_G	M.	0.789*
			1.673**
Radius of gyration	K_{44}	M.	11.138*
			9.576**
	K_{55}	M.	16.461*
			14.138**
	K_{66}	M.	17.500 (assumed)
LOWER HULLS:			
Beam between central lines	B_h	M.	18.370
Length	L_h	M.	61.750
Max. diameter (elliptical)			4.449(height)
			6.720(width)
Draft	h	M.	6.649(from the keel)
	h_c	M.	4.425(from hull axis)
STRUTS:			
Length	L_s	M.	50.459(x=-26.042 to x=24.417)
Strut beam	b_s	M.	2.440
Water plane area	A_w	Square M.	196.940(two struts in total)
Strut spacing	B_s	M.	18.370(between central lines)
FORWARD FINS:			
Distance from nose to CL stock		M.	8.647
Dihedral angle		Degree	0.0
Chord		M.	3.699(root chord)
			1.670(tip chord)
Span		M.	3.479
AFT FINS:			
Distance from nose to CL stock		M.	50.477
Dihedral angle		Degree	20.0
Chord		M.	4.899(root)
			2.359(tip chord)
Span		M.	5.351

NOTE: * for beam and oblique seas (90, 60 and 120°).
** for head and following seas (180 and 0°).
*** the fin section is given by the standard NACA 0015 basic form.

Table 9.3.2.

MATRIX OF COMPUTATIONAL ANALYSIS OF THE SWATH SHIP (HASLAR)

WAVE HEADING	degrees	0, 60, 90, 120, 180
SHIP SPEED	knots	0 (for all the wave headings) 5, 10 and 14 (for headings 0° and 180°)
WAVE HEIGHT	metres	1.234 (for headings 60°, 90° and 120°) $\frac{1}{75}$ wave length (for headings 0° and 180°)
WAVE LENGTH/C.L. BEAM		1.118 - 13.427
WAVE LENGTH/STRUT LENGTH		0.407 - 4.888 ($U = 0$) 0.815 - 5.086 ($U \neq 0$)
INFORMATION REQUIRED		HEAVE RESPONSE ROLL RESPONSE PITCH RESPONSE RELATIVE BOW MOTION RELATIVE STERN MOTION BOW VERTICAL ACCELERATION STERN VERTICAL ACCELERATION

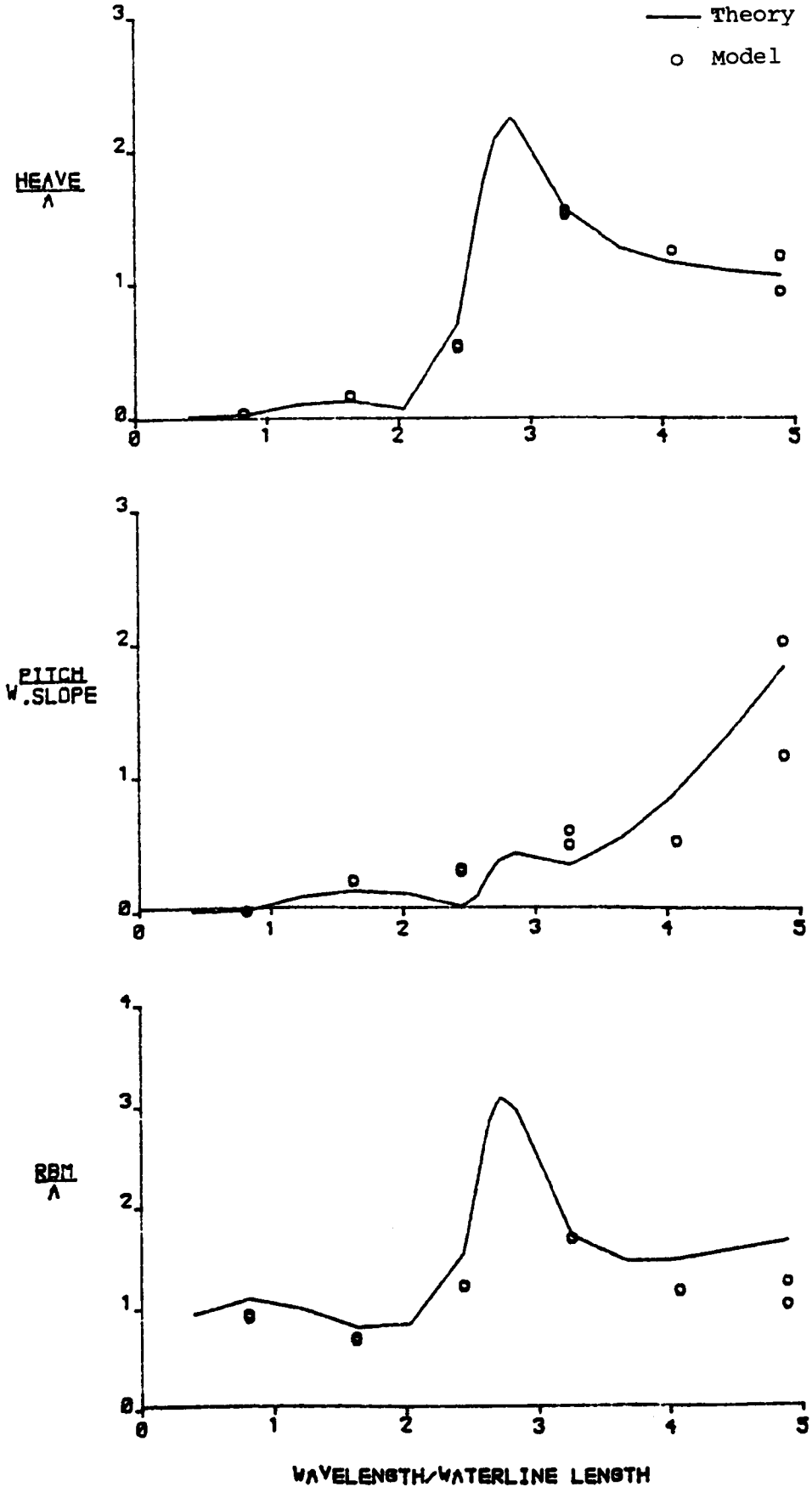

Figure 9.3.3. Comparison of heave, pitch and relative bow motion amplitudes of the SWATH ship at zero knots in head seas.

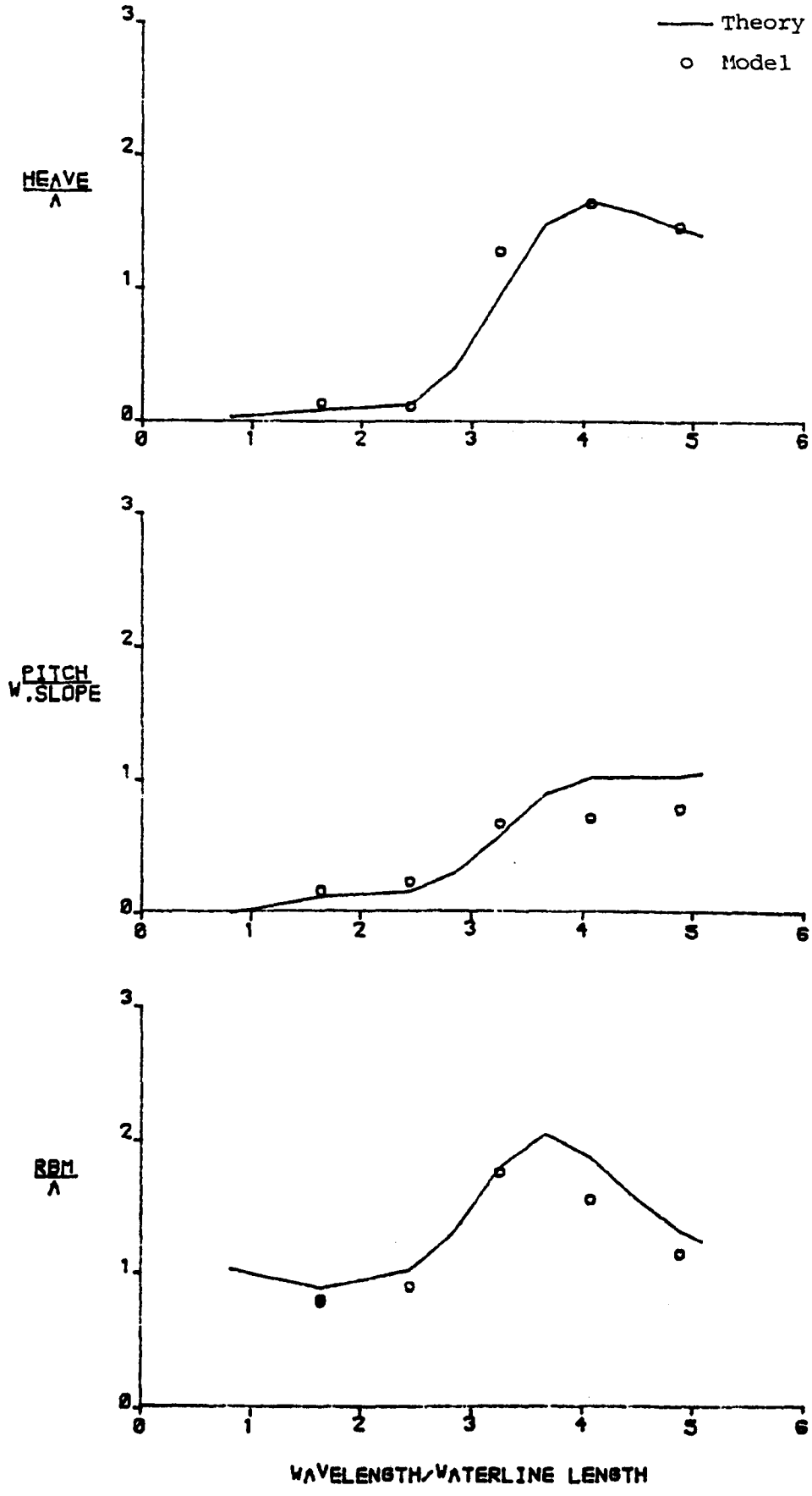

Figure 9.3.4. Comparison of heave, pitch and relative bow motion amplitudes of the SWATH ship at 5 knots in head seas.

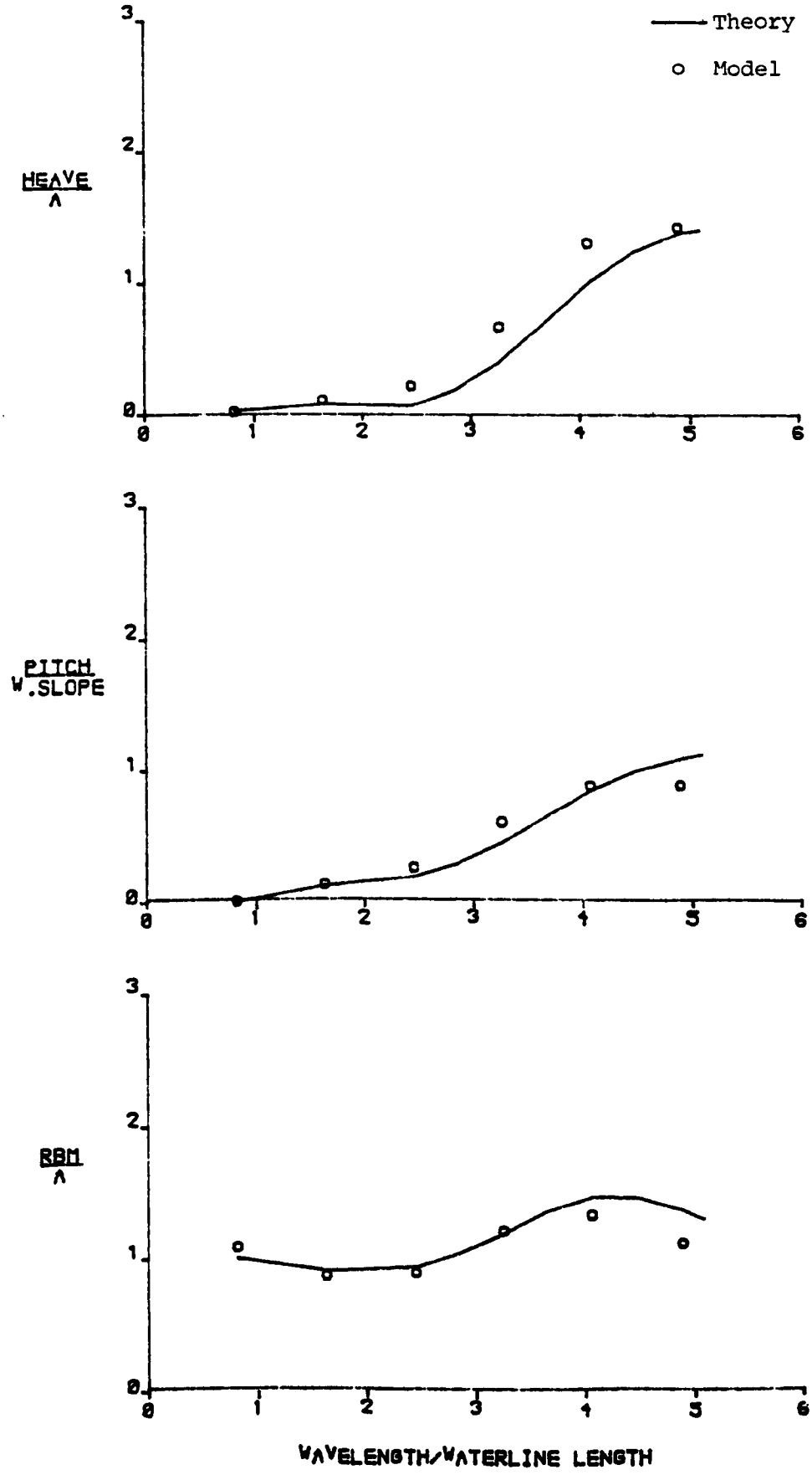

Figure 9.3.5. Comparison of heave, pitch and relative bow motion amplitudes of the SWATH ship at 10 knots in head seas.

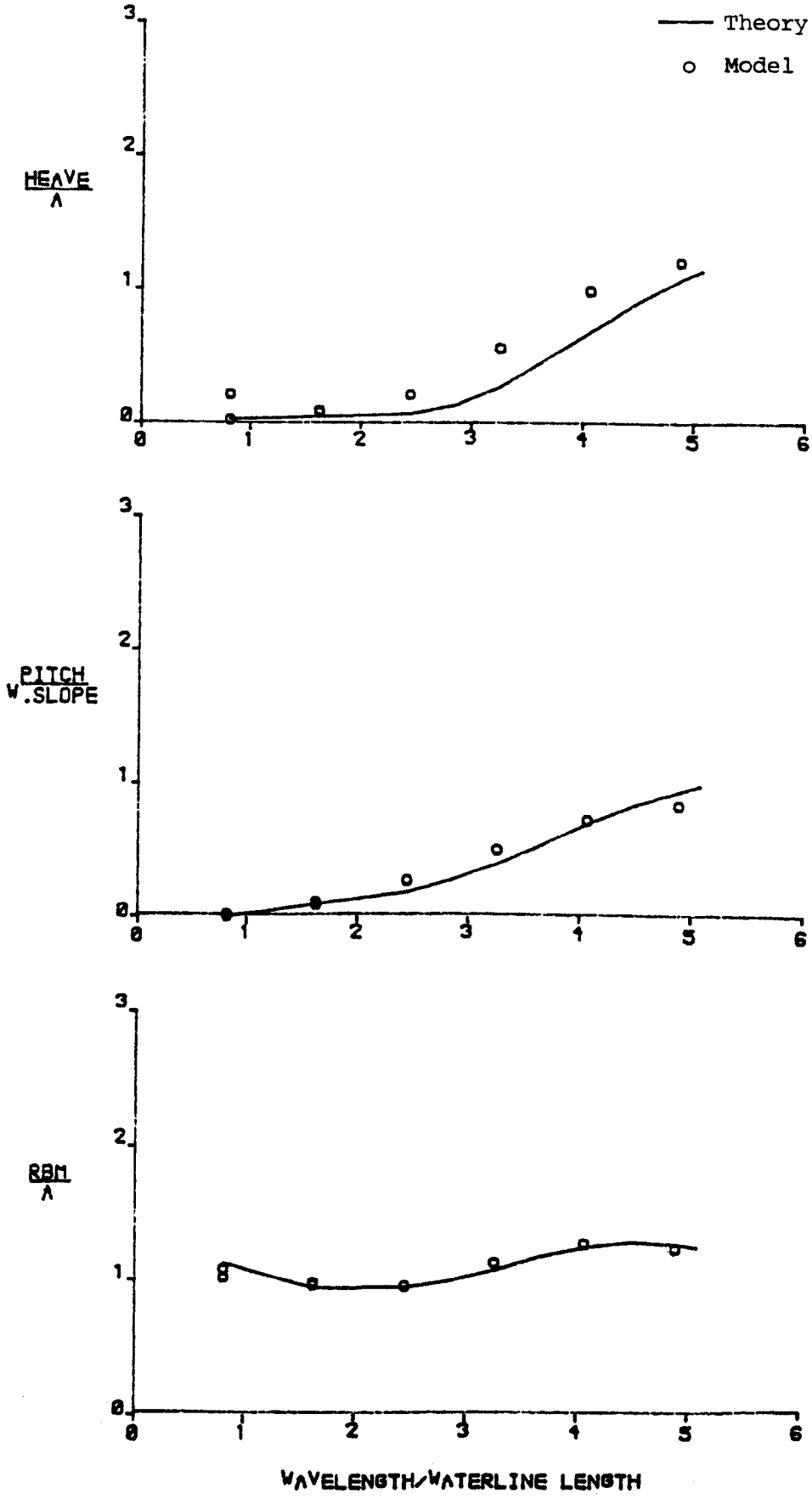

Figure 9.3.6. Comparison of heave, pitch and relative bow motion amplitudes of the SWATH ship at 14 knots in head seas.

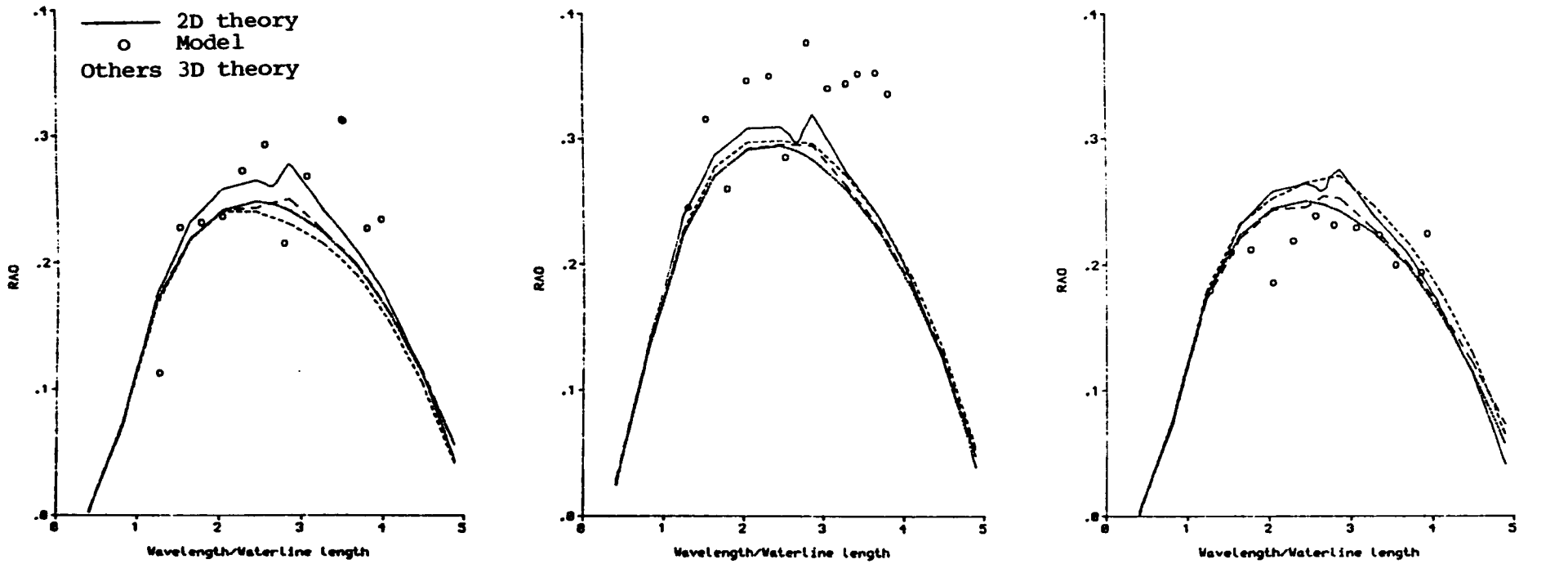

Figure 9.3.7. Roll motion amplitudes of the SWATH ship.

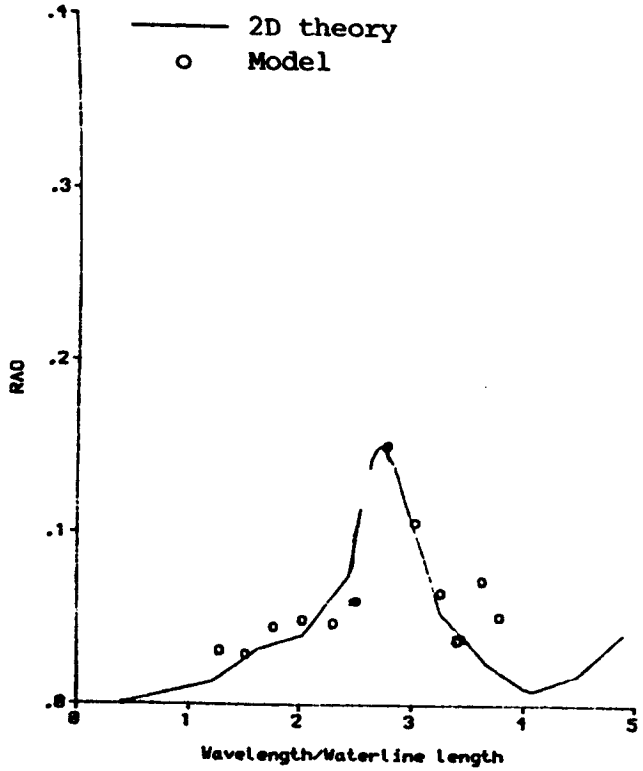

(a) COMPARISON OF PITCH RAOs

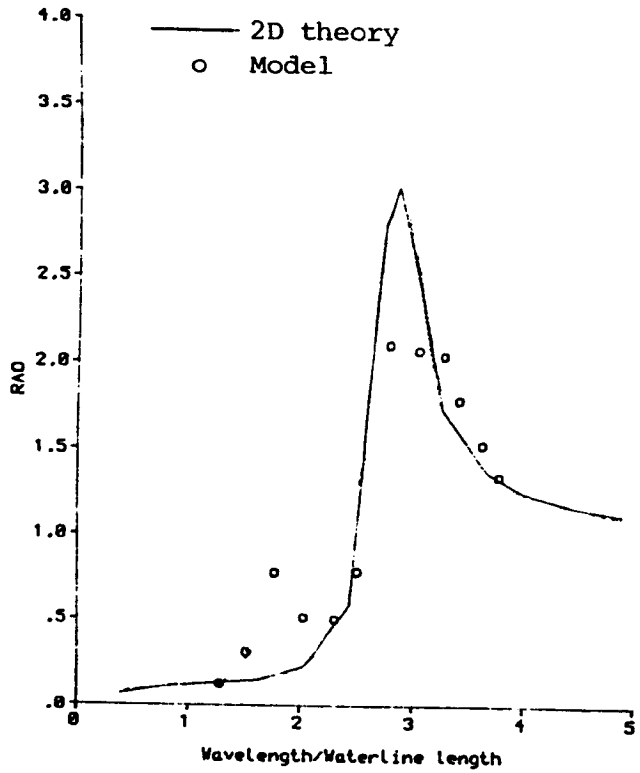

(b) COMPARISON OF HEAVE RAOs

Figure 9.3.8. Comparison of pitch and heave motion amplitudes of the SWATH ship at zero knots at zero knots in beam seas.

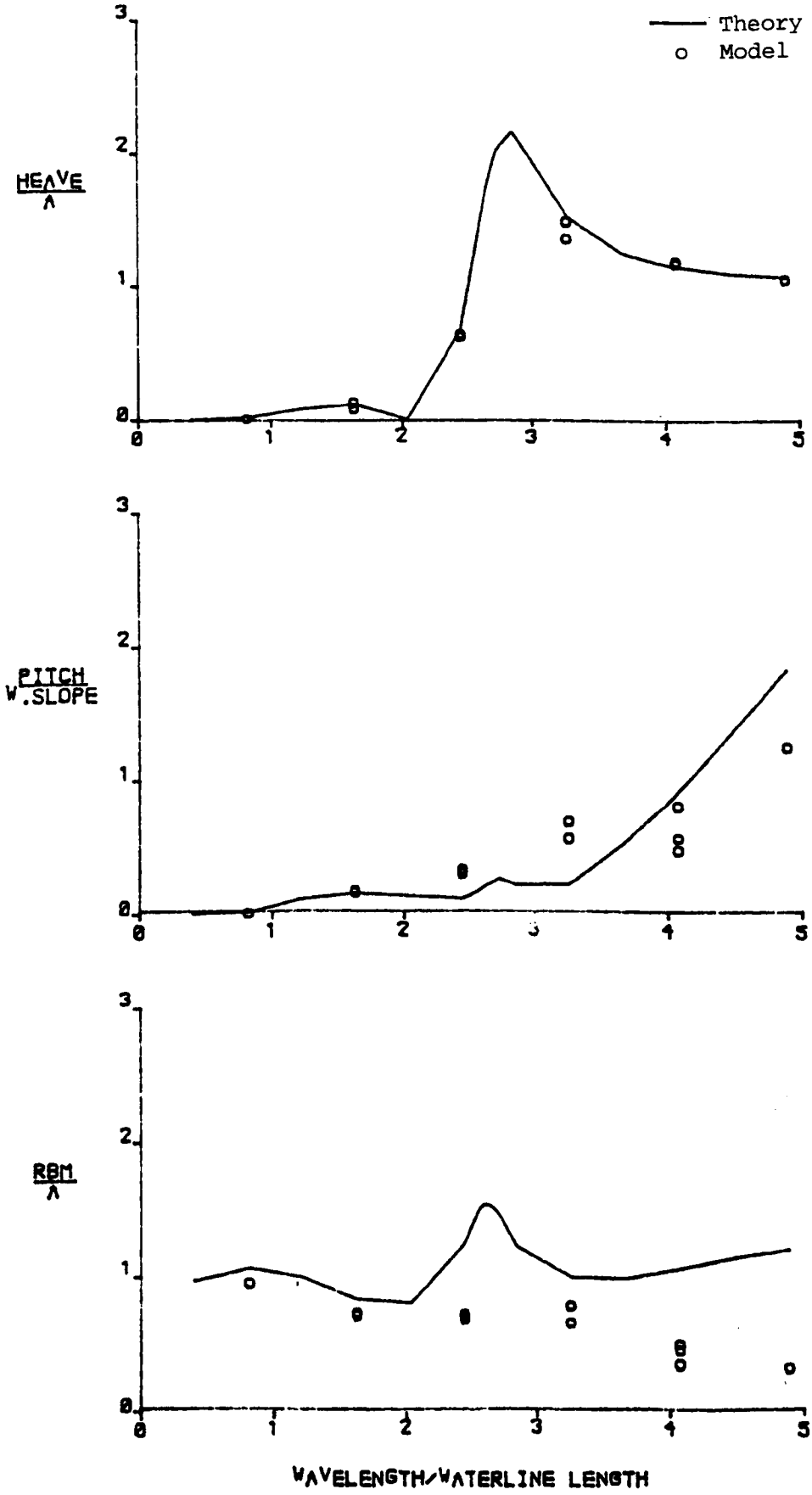

Figure 9.3.9. Comparison of heave, pitch and relative bow motion amplitudes of the SWATH ship at zero knots in stern seas.

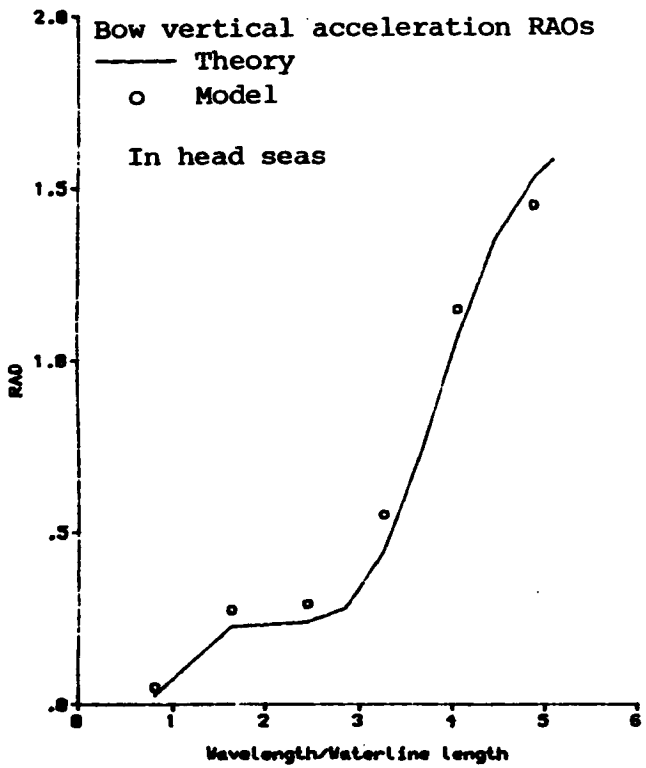

(a)

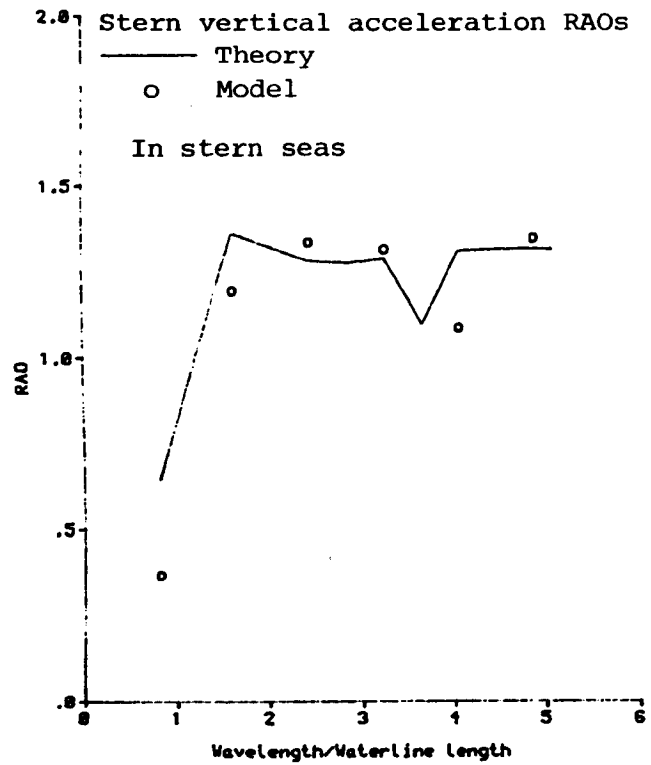

(b)

Figure 9.3.10. Comaprison of bow and stern vertical acceleration amplitudes of the SWATH ship at 10 knots.

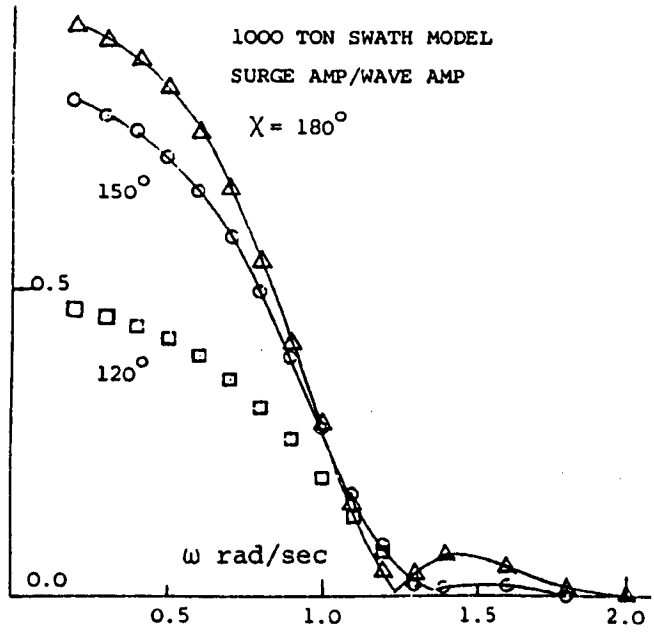

Figure 9.3.11. Surge motion amplitude of a 1000 ton SWATH ship.

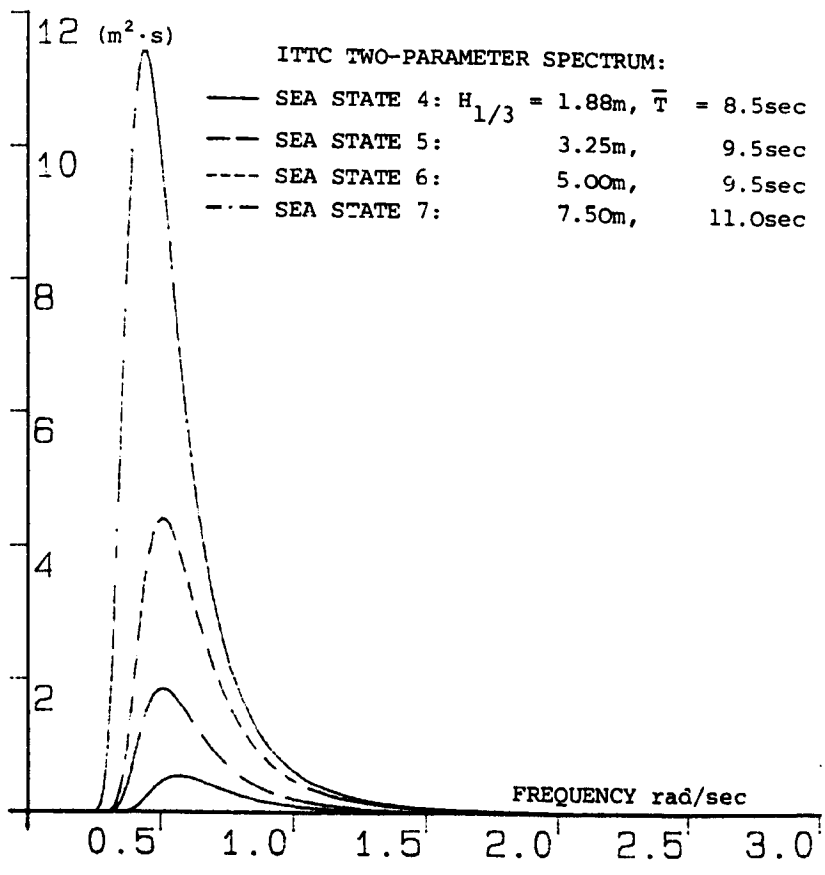

Figure 9.3.12. ITTC wave spectrum.

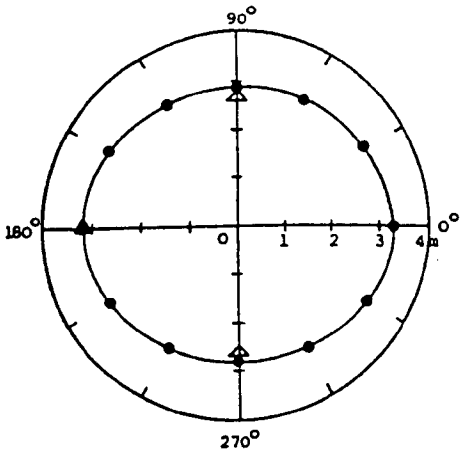

(a) SIGNIFICANT HEAVE AMPLITUDE OF TWO SWATH MODELS IN SEA STATE 6 ($H_{1/3}$ = 5m, $\bar{T}$ = 9.5sec).
—●— 2000 TON MODEL, Δ 1000 TON MODEL.

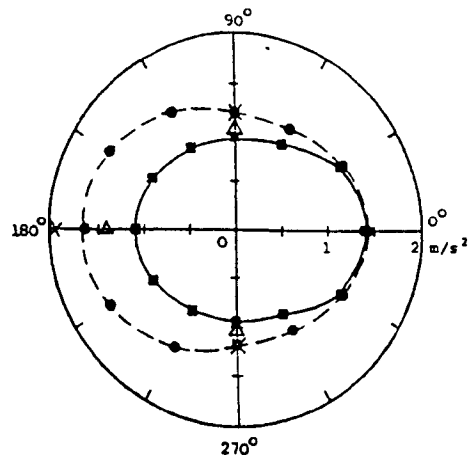

(b) SIGNIFICANT VERTICAL ACCELERATION OF TWO SWATH MODELS IN SEA STATE 6 ($H_{1/3}$ = 5m, $\bar{T}$ = 9.5sec).
—■— bow, - -●- - stern } 2000 TON MODEL, Δ bow, X stern } 1000 TON MODEL

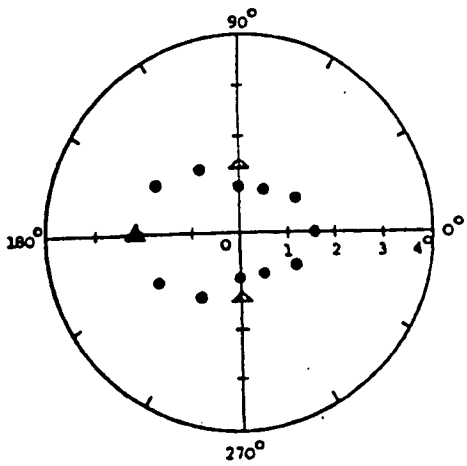

(c) SIGNIFICANT PITCH AMPLITUDE OF TWO SWATH MODELS IN SEA STATE 6 ($H_{1/3}$ = 5m, $\bar{T}$ = 9.5sec).
● 2000 TON MODEL, Δ 1000 TON MODEL.

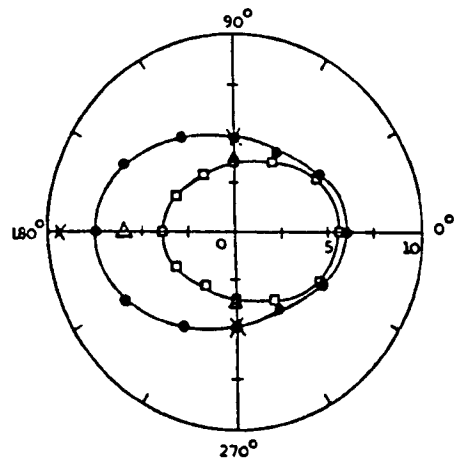

(d) SUBJECTIVE MOTION MAGNITUDE OF TWO SWATH MODELS IN SEA STATE 6 ($H_{1/3}$ = 5m, $\bar{T}$ = 9.5sec).
—□— bow, —●— stern } 2000 TON MODEL, Δ bow, X stern } 1000 TON MODEL.

Figure 9.3.13. Significant heave, pitch, vertical acceleration and subject motion amplitudes of two SWATH models in sea state 6.

10. CONCLUSIONS AND FURTHER DISCUSSIONS

From these investigations the following conclusion can be drawn:

(1) As far as large offshore structures and special vessels are concerned, the simple treatment to decompose the total fluid force into two separate components due to the potential flow and the viscous flow effect respectively is proven adequate.

The fluid viscosity seems to have significant effects on the peak motion amplitudes around the resonant frequencies of these large marine structures, but may be negligible outside these frequency regions.

As demonstrated by two industrial applications to a semi-submersible and a SWATH ship, a combination method of the diffraction theory for the wave potential solution and the Morrison damping formulation for the viscous force component can provide predictions of reasonable accuracy.

(2) Within the diffraction force dominant regime the linear wave-structure interaction problem can be solved by the Green function integral equation. In addition to its conventional surface integral form, an interior integral equation technique is developed and in terms of the numerical procedures proposed the same degree of numerical accuracy can be achieved.

(3) To avoid the mathematical failure of the integral equation at irregular frequencies, approximation formulae are proposed to predict the irregular frequency values for arbitrary three- and two-dimensional floating bodies. The formulations satisfy the exact solution of a rectangular box in three-dimensional cases and a rectangle section for two-dimensional bodies. Furthermore, these provide accurate predictions of irregular frequencies for well defined body geometries (analytical formulae can be derived) as well as realistic body shapes for offshore structures and ships. These proposed formulae have been accepted by marine

industries (e.g. Dawkins 1989).

(4) A modified Green function in a multiple Green function form is derived, which effectively eliminates irregular frequencies for mono-, twin- and multi-hulled sections.

(5) A new shallow draft theory is presented based on improvements over the existing flat ship approaches. It improves previous zero-draft theories by inclusion of all the six degrees of motion (rather than the vertical plane motions) and by introduction of a finite draft correction. Hence, the present theory is applicable to realistic shallow draft structures of small but finite draft and capable of more accurate predictions of motion responses. This conclusion is supported by vast example applications to various shallow draft structures.

In particular, according to the similarity principle revealed in the study, hydrodynamic properties of any two-dimensional shallow draft section is exclusively determined by the same data for a line section of unit length. Therefore, no further computations are required.

Since a large group of offshore service vessels and transportation barges, etc., are of shallow draft feature, the present shallow draft theory can be of more practical use.

(6) To significantly reduce the computing time involved in the solution of a large size matrix associated with a complicated three-dimensional wave-structure interaction and meanwhile to retain end effects of the body, the three-dimensional strip formulation derived reduces the large size matrix associated with the solution of a complicated three-dimensional wave-structure interaction and therefore can greatly reduce the computer time required. Meanwhile, because it retains the details of the body ends the proposed method can provide hydrodynamic information of three-dimensional feature. The method works well even for relative small length to width ratio.

This study does confirm that the wave potentials vary slowly around the length of a body of small sectional variation. This property should be exploited in further efforts to reduce

the computer time with the diffraction theory analyses.

Further work should be done to prove its applicability in practical analysis of marine structures.

(7) The three horizontal motion modes (i.e. surge, sway and yaw) of an elongated body of full cross-sectional shape or a structure with a shallow draft feature can be determined by considering only the Froude-Krylov forces. A mutual cancellation effect is found between the radiation and diffraction force components in the modes of sway and yaw. Therefore, this work provides a further extension of the conventional Froude-Krylov hypothesis.

(8) The exact solution based on the horizontal plane method for vertical cylinders of arbitrary sectional geometry may be used to approximate the horizontal mean drift forces on a multi-column offshore structure, such as a TLP or a semi-submersible.

(9) Although the outlined improvements, modifications and developments are restricted in the thesis to forces and motions for rigid bodies, in principle, these are also applicable to flexible structures. To achieve this one needs only replacing the rigid body boundary conditions imposed in the solution problem by flexible body boundary conditions for each flexible mode shape under consideration. Some work has been done and will be reported elsewhere.

(10) Because of the complicated flow phenomenon associated with the interaction between water waves and marine structures of peculiar configuration, a more sophisticated theory is not necessarily more accurate practically. As long as principal aspects in a physical phenomenon are properly treated, a simplified method works.

(11) As far as the hydrodynamic theories in motional and structural analysis are concerned, the gap between the academic theoretical development and the daily tools in industrial design is rather wide and deep. To meet the challenge in future marine and offshore activities, creative approaches are needed to produce more practicable and affordable techniques with

strong theoretical back-up.

ACKNOWLEDGEMENTS

I am grateful to Professor W.G. Price for his advice, encouragement and support during my work as a research fellow in the Department of Mechanical Engineering, Brunel University.

The research fellowship funded by SERC (through the MTD Ltd), MoD and BPP Ltd and the Royal Society/BP Awards are also gratefully acknowledged.

REFERENCES

AARSENES, J.V., Faltinsen, O.M. and Pettersen, B., 1985, "Application of a vortex tracking method to current force on ships", Proc. Symp. Separated Flow Around Marine Structures, Trondheim.

ABRAMOWITZ, M. and Stegun, I.A., 1972, Handbook of Mathematical Functions, Dover Pub., New York.

AIRY, G.B., 1845, "Tides and waves", Encyc. Metrop., Art. 192, pp. 241-396.

ANGWIN, J., "Results of a joint semi-submersible/submersible wave drift force project", RINA Int. Symp. Develop. Deeper Waters, London, Paper No. 12.

ARE (Haslar), 1989, private communications (see Wu, X.J. and Price, W.G., 1989, "Seakeeping performance of the SWATH model - comparison between theoretical predictions and model tests", Report, BPP Ltd (May 1989)).

ARNOLD, D.N. and Wendland, W.L., 1983, "On the asymptotic convergence of collocation methods", Math. Compu., Vol. 41, pp. 349-381.

BECK, R.F. and Troesch, A.W., 1980, "Wave diffraction effect in head seas", J. Int. Ship. Prog., Vol. , pp. 306-315.

BERHAULT, Ch, 1978, "Comparison of the main numerical methods in water wave diffraction and radiation", Inst. Francais du Petrole, Paris.

BEUKELMAN, W., Huijsmans, R.H.M. and Keuning, P.T., "Calculation methods of hydrodynamic coefficients of ships in shallow water", J. Int. Ship. Prog., Vol. 31, No. 360.

BISHOP, R.E.D. and Price, W.G., 1979, "Hydroelasticity of Ships", Cambridge

BLACKMAN, C.D., 1989, "SWATH - a novel hull form for improved seakeeping", Proc. Int. Conf. Defence Oceanology, Brighton. Univ. Press.

BOOM, W.C. de, 1978, "Model tests on the semi-submersible derrick barge,

BORRESEN, R. and Faltinsen, O.M., 1984, "Ship motions in shallow water by unified theory", Proc. 15th Symp. Naval Hydrodynamics, Hamburg.

BOWERS, E.C., 1976, "Long period oscillations of moored ships subject to short wave seas", Trans. RINA, Vol. 118, pp. 181-191.

BRANDSMA, F.J. and Hermans, A.J., 1985, "A quasi-linear free surface condition in slow ship theory", Schiffstechnik.

BRARD, R., 1972, "The representation of a given ship form by singularity distributions when the boundary condition on the free surface is linearised", J. Ship Res., Vol. 16, pp. 79-92.

BREIT, S.R. and Sclavounos, P., 1986, "Wave interaction between adjacent bodies", J. Fluid Mech., Vol. 165, pp. 273-296.

BUREAU VERITAS, 1975, Rules and Regulations for the Construction and Classification of Offshore Platforms, Paris.

CHANG, M.S., 1977, "Computations of three-dimensional ship motions with forward speed", Proc. 2nd Int. Conf. Num. Ship Hydrodynamics, Berkeley, pp. 124-135.

COLTON, D. and Kress, R., 1983, Integral Equation Methods in Scattering Theory, John Wiley & Sons.

COVICH, P.M., 1986, "SWATH T-AGOS, a producible design", Proc. AIAA 8th Adv. Marine Sys. Conf., San Diego.

DALLINGA, R.P., Graham, R. and Huijsmans, R.H.M., 1988, "Development of design tools for the prediction of SWATH motions", Proc. 17th Symp. Naval Hydrodynamics, The Hague.

DAWKINS, R.A., 1989, "NSMB co-operative sea loads W.G, user's manual for the HPCFEM suite of programs", Lloyd's Register Report TPDD No. 88/7.

DEAN, R.G., 1970, "Relative validities of water wave theories", J. Waterways, ASCE, Vol. 96, WW1, pp. 105-119.

DELVES, L.M. and Walsh, J. (editors), 1974, Numerical Solution of Integral Equations, Clarendon Press, Oxford.

DOWNIE, M.J., Bearman, P.W. and Graham, J.M.R., 1984, "Prediction of the roll damping of bodies including the effects of vortex shedding", NMI Report No. 188.

EATOCK TAYLOR, R. and Zietsman, J., 1982, "Hydrodynamic loading on multi-component bodies", BOSS '82, MIT, pp. 424-443.

Eatock Taylor, R. and Jefferys, E.R., 1986, "Variability of hydrodynamic load predictions for a tension leg platform", J. Ocean Eng., Vol. 13, No. 5, pp. 449-490.

Eatock Taylor, R. and Hung, S.M., 1987, "Second-order diffraction forces on a vertical cylinder in regular waves", J. Appl. Ocean Res.

EGGERS, K., 1981, "Non-Kelvin dispersive waves around non-slender ships", Schiffstechnik, Bd. 8.

ENDO, H., 1983, "Numerical evaluation of principal value integral by Gauss-Laguerre Quadrature", AIAA J., Vol. 21, No. 1, pp. 150-151.

Endo, H., 1987, "Shallow-water effect on the motions of three-dimensional bodies in waves", J. Ship Res., Vol. 31, No. 1, pp. 34-40.

EUVRARD, D., Jami, A., Lenoir, M. and Martin, D., 1981, "Recent progress towards an optimal coupling between finite elements and singularity distribution procedures", Proc. 3rd Int. Conf. Num. Ship Hydrodynamics, Paris, pp. 193-208.

FALTINSEN, O.M. and Michelsen , F.C., 1974, "Motions of large structures in waves at zero Froude number", Proc. Int. Symp. Dynamics Mar. Vehi. & Struct.in Waves, London, pp. 91-106.

Faltinsen, O.M., 1977, "Numerical solutions of transient nonlinear free-surface motion outside or inside moving bodies", Proc. 2nd Int. Conf. Num. Ship Hydrodynamics, Berkeley, pp. 347-357.

Faltinsen, O.M. and Loken, A.E., 1978, "Drift forces and slowly varying horizontal forces on ship in waves", Proc. Symp. Appl. Math., Delft, pp. 22-41.

Faltinsen, O.M. and Loken, A.E., 1979, "Slow drift oscillations of a ship in irregular waves", DNV Publication No. 108.

FRANK, W., 1967, "Oscillation of cylinders in or below the free surface of deep fluid", NSRDC Report 2375, Washington DC.

FROUDE, W., 1861, "On the rolling of ships", Trans. INA, Vol. 2, pp. 180-229.

Froude, R.E., 1896, "The non-uniform rolling of ships", Trans. INA, Vol. 37, pp. 293.

GARRISON, C.J., Rao, V.S. and Snider, R.H., 1970, "Wave interaction with large submerged objects", Proc. Offshore Tech. Conf., Paper OTC 1278.

Garrison, C.J., 1978, "Hydrodynamic loading of large offshore structures: three-dimensional source distribution methods", Chapter 3, Numerical Methods in Offshore Engineering, Editors: O.C. Zienkiewicz et al, John Wiley & Sons, pp. 87-140.

GREKAS, A., 1981, "Contribution a l'etude theorique et experimentale des efforts du second ordre et du comportement dynamique d'une structure marine sollicitee par une houle reguliere et un courant", These de Docteur Ingenieur (Ecole Nationale Superieure de Mecanique).

GRIM, O., 1963, "Surge motion and broaching tendencies in a severe irregular sea", Deutsche Hydrographischen Zeitschrift, Vol. 16, pp. 201.

GUEVEL, P. and Bougis, J., 1982, "Ship-motions with forward speed in infinite depth", J. Int. Ship. Prog., Vol. 29, pp. 103-111.

HARAGUCHI, T. and Ohmatsu, S., 1983, "On the improved solution of the oscillation problem on non-wall sided floating bodies and a new method for eliminating the irregular frequencies", Trans. West-Japan Soc. Nav. Archi., pp. 9-23.

HASKIND, M.D., 1957, "The exciting forces and wetting of ships in waves", NSRDC Translation No. 307 (1962).

HAVELOCK, T.H., 1940a, "The pressure of water waves upon a fixed obstacle", Proc. Royal Soc., London, Ser. A, Vol. 963, pp. 175-190.

Havelock, T.H., 1940b, "Waves produced by the rolling of a ship", Phil. Mag., Vol. 29, Ser. 7, pp. 407.

HEARN, G.E., 1977, "Alternative methods of evaluating Green's function in three-dimensional ship-wave problems", J. Ship Res., Vol. 21, No. 2, pp. 89-93.

Hearn, G.E., Tong, K.C. and Lau, S.M., 1987, "Sensitivity of wave drift damping coefficient predictions to the hydrodynamic analysis models used in the added resistance gradient method," 6th OMAE Conf., Houston.

HERTJORD, K. and Nielsen, F.G., 1986, "Non-linear wave forces on a fixed vertical cylinder due to the sum frequency of waves in irregular seas", J. Appl. Ocean Res., Vol. 8.

HESS, J.L. and Smith, A.M.O., 1964, "Calculation of nonlifting potential flow about arbitrary three-dimensional bodies", J. Ship Res., Vol. 8, pp. 22-44.

Hess, J.L., 1973, "High order numerical solution of the integral equation for the two-dimensional Neumann problem", Computer Methods in Appl. Mech. & Eng., Vol. 2, pp. 1-5.

Hess, J.L., 1980, "Review of integral-equation techniques for solving potential flow problems with complicated boundaries", 2nd Int. Symp. Innovative Numer. Analy. in Appl. Eng. Sci., pp. 131-143.

HOGBEN, N., Miller, B.L. and Searle, J.W and Ward, G., 1977, "Estimation of fluid loading on offshore structures", Inst. Civil Eng., Part 2, Vol. 63, pp. 515-562.

Hogben, N. and Standing, R.G., 1974, "Wave loads on large bodies", proc. Int. Symp. Dynamics Mar. Vehi. & Struct.in Waves, London, pp. 258-277.

HOOFT, J.P., 1971, "Mathematical method of determining hydrodynamically induced forces on a semi-submersible", SNAME, New York.

HSU, F.H. and Blenkarn, K.A., 1970, "Analysis of peak mooring force caused by slow vessel drift oscillation in random seas", Proc. Offshore Tech. Conf., OTC Paper No. 1159.

HWANG, L.S. and Tuck, E.O., 1970, "On the oscillation of harbours of arbitrary shape", J. Fluid Mech., Vol. 42, pp. 447-464.

HUIJSMANS, R.H.M. and Hermans, A.J., 1985, "A fast algorithm for computation of 3-D ship motions at moderate forward speed", 4th Int Conf. Num. Ship Hydrodynamics, Washington DC.

Huijsmans, R.H.M., 1986, "Wave drift forces in current", 16th Symp. Naval Hydrodynamics.

IKEDA, Y. and Tanaka, N., 1983, "On viscous drag of oscillating bluff bodies", Sci. & Methodol. Seminar Ship Hydrodynamics, Varna, Bulgaria.

INGLIS, R. and Price, W.G., 1979, "Motions of a ship in shallow water", Trans. RINA, Paper No. W10.

Inglis, R. and Price, W.G., 1980, "Calculation of the velocity potential of a translating pulsating source", Trans. RINA, Paper W2, pp. 1-13.

Inglis, R. and Price, W.G., 1981, "Irregular frequencies in three dimensional source distribution techniques", J. Int. Ship. Prog., Vol. 28, pp. 57-62.

Inglis, R. and Price, W.G., 1982a,b, "A three-dimensional ship motion theory", Trans. RINA, Vol. 124.

ISAACSON, M., 1978, "Vertical cylinders of arbitrary section in waves", J. Waterway, ASCE, Vol. 104, pp. 309-323.

Isaacson, M., 1982, "Nonlinear-wave effects on fixed and floating bodies", J. Fluid Mech., Vol. 120, pp. 267-281.

ITTC (Int. Towing Tank Conf.), 18th Conf. Report, 1987.

JOHN, F., 1949, "On the motion of floating bodies I", Comm. Pure & Appl. Math., Vol. 2, pp. 13.

John, F., 1950, "On the motion of floating bodies II", Comm. Pure & Appl. Math., Vol. 3, pp. 45-101.

KAGEMOTO, H. and Yue, D.K.P., 1986, "Interactions among multiple three-dimensional bodies in water waves: an exact algebraic method", J. Fluid Mech., Vol. 166, pp. 189-209.

KEIL, A.W., 1961, "The response of ships to underwater explosions", Paper presented at the Annual Meeting, SNAME (Nov. 1961).

KIM, W.D., 1963, "On the forced oscillations of shallow draft ships", J. Ship Res., Vol. 7, pp. 7-18.

Kim, W.D., 1965, "On the harmonic oscillations of a rigid body on a free surface", J. Fluid Mech., Vol. 21, pp. 427-451.

Kim, W.D., 1965, "On a free-floating ship in waves", J. Ship Res., pp. 182-200.

KOCHIN, N.E., 1939, "The two-dimensional problem of steady oscillations of bodies under the free-surface of a heavy incompressible fluid", Translated in SNAME Tech. Res. Bull., No. 1-9, 1952.

KORVIN-KROUKOVSKY, B.V., 1955, "Investigation on ship motions in regular waves", Trans. SNAME, Vol. 63, pp. 386-435.

KOSTYUKOV, A.A., 1968, Theory of Ship Waves and Wave Resistance, Translation, Eff. Comm. Inc., Iowa.

KRYLOV, A.N., 1896a, "A new theory of pitching of ships on waves, and of the stresses produced by this motion", Trans. INA. Vol. 37, pp. 326.

Krylov, A.N., 1896b, "A general theory of the oscillations of a ship on waves", Trans. INA, Vol. 40, pp. 184.

KYOZUKA, Y., 1982, "Experimental study on second-order forces acting on a cylindrical body in waves", Proc. 14th Symp. Naval Hydrodynamics, Michigan.

LEE, C.M., 1970, "Second-order theory for nonsinusoidal oscillations of a cylinder in a free surface", Proc. 8th Symp. Naval Hydrodynamics, Pasadena.

Lee, C.M., 1976, "Theoretical prediction of motion of small waterplane-area, twin-hull (SWATH) ships in waves", NSRDC Report 76-0046.

LEONARD, A., 1980, "Vortex methods for flow simulation", J. Computational Physics, Vol. 37, pp. 289-335.

LIGHTHILL, J., 1979, "Waves and hydrodynamic loading", BOSS '79, London, Vol. 1, pp. 1-40.

Lighthill, J., 1986, "Fundamentals concerning wave loading on offshore structures", J. Fluid Mech., Vol. 173, pp. 667-681.

LIN, W.M., Newman, J.N. and Yue, D.K., 1984, "Nonlinear forced motions of floating bodies", Proc. 15th Symp. Naval Hydrodynamics.

LIU, Y.Z., 1988, "Calculations of nonlinear wave-body hydrodynamic interaction", (private communication).

LOKEN, A.E., 1986, "Three-dimensional second order hydrodynamic effects on ocean structures in waves", Dr. ing Thesis, Norwegian Inst. Tech., Trondheim.

LLOYD, A.R.J.M. and Andrew, R.N., 1977, "Criteria for ship speed in rough weather", Proc. 18th ATTC, Annapolis.

LONGUET-HIGGINS, M.S., 1952, "On the statistical distribution of the heights of sea waves", J. Mar. Research, Vol. 11, pp. 245-266.

Longuet-Higgins, M.S. and Cokelet, E.D., 1976, "The deformation of steep surface waves on water I. A numerica method of computation", Proc. Royal Soc. London A., Vol. 350, pp. 1-26.

MAEDA, H., 1981, "On the hydrodynamic forces for shallow draft ships in shallow water", Nav. Archi & Ocean Eng. (Japan), Vol. 19, pp. 54-67.

MASUMOTO, A. et al, 1982, "Wave forces on multiple floating bodies", J. Appl. Ocean Res., Vol. 4, No. 1, pp. 2-8.

MATHIESEN, J., 1988, "Analysis of experiments and a functional model for ship rolling", PhD thesis, Brunel Univ.

MATHIESEN, M., 1984, "Current-depth refraction of directional wave spectra", Proc. Symp. Description and Modellong of Directional Seas, Tech. Univ. Denmark, Paper No. C6.

MAcCAMY, R.C. and Fuchs, R.A., 1954, "Wave forces on piles: a diffraction theory", Tech. Memo. No. 69, Beach Erosion Branch, Corps of Engineers.

MacCamy, R.C., 1961, "On the heaving motion of cylinders of shallow draft", J. Ship Res., Vol. 5, No. 3, pp. 34-43.

MARUO, H., 1960, "The drift of a body floating in waves", J. Ship Res., Vol. 4, No. 3, pp. 1-10.

MATSUI, T., 1986, "Analysis of slowly varying wave drift forces on compliant structures", 5th OMAE Conf., Tokyo, Vol. 1, pp. 289-296.

McCREIGHT, KK., 1987, "Assessing the seaworthiness of SWATH ships", Trans. ASME, Vol. 95, pp. 189-214.

McIVER, P. and Evans, D.V., 1984, "Approximation of wave forces on cylinder arrays", J, Appl. Ocean Res., Vol. 6, No. 2, pp. 101-107.

McLACHLAN, N.W., 1947, Theory and Application of Mathieu Function, Clarendon Press, Oxford.

MEI, C.C., 1978, "Numerical methods in water-wave diffraction and radiation", Ann. Rev. Fluid Mech., pp.393-416.

MIAO, G.P. and Liu, Y.Z., 1986, "A theoretical study on the second-order wave forces for two-dimensional bodies", 5th OMAE Conf., Tokyo, Vol. 1, pp. 330-336.

MILNE-THOMSON, L.M., 1968, Theoretical hydrodynamics , MaCmillan & Co, London.

MIYATA, H. and Nishimura, S., 1985, "Finite-difference simulation of nonlinear ship waves", J. Fluid Mech., Vol. 157, pp. 327-357.

MOLIN, B., 1979, "Second -order diffraction loads upon three-dimensional bodies", J. Appl. Ocean Res., Vol. 1, No. 4, pp. 197-202.

Molin, B. and Marion, A., 1986, "Second -order loads and motions for floating bodies in regular waves", 5th OMAE Conf., Tokyo, Vol. 1, pp. 353-360.

MORISON, J.R., O'Brien, M.P., Johnson, J.W. and Schaaf, S.A., 1950, "The force exerted by surface waves on piles", Trans. Amer. Inst. Metall. Eng., Petrol. Branch, Vol. 189, pp. 149-154.

MONACELLA, V.J., 1966, "The disturbance due to a slender ship oscillating in waves in a fluid of finite depth", J. Ship Res., Vol. 10, No. 4, pp. 242-252.

MSC (Marine Structure Consultants bv, Netherlands), 1985, Topics, Vol. 3, December Issue.

MULLER, V., 1985, "Theoretical and experimental determination of the vortex field during rolling of frame sections with bilge keel", Schiffstechnik, Vol. 24, No. 2.

NASS, A., 1986, "On the statistical analysis of slow-drift forces and motions of floating offshore structures", 5th OMAE Conf., Tokyo, Vol. 1, pp. 317-329.

NEWMAN, J.N., 1965, "The exciting forces on a moving body in waves", J. Ship Res., Vol. 9, pp. 190-199.

Newman, J.N., 1974, "Second order, slowly varying forces in irregular waves", Proc. Int. Symp. Dynamics Mar. Vehi. & Struct.in Waves, London, pp. 193-197.

Newman, J.N., 1967, "The drift force and moment on ships in waves", J. Ship Res., Vol. 11, pp. 51-60.

Newman, J.N., 1978, "The theory of ship motions", Advances Appl. Mech., Vol. 18, pp. 221-283.

Newman, J.N. and Sclavounos, P., 1980, "The unified theory of ship motions", Proc. 13th Symp. Naval Hydrodynamics, Tokyo, 373-397.

Newman, J.N., 1983, "Three-dimensional wave interactions with ships and platforms", Int. Workshop on Ship and Platform Motions, Berkeley, pp. 418-442.

Newman, J.N., 1985, "Algorithms for the free surface Green function", J. Eng. Math., Vol. 19, pp. 57-67.

NOBLESSE, F., 1982, "The Green function in the theory of radiation and diffraction of regular water waves by a body", J. Eng. Math., Vol. 16, pp. 137-169.

NOJIRI, N.A., 1981, "A study of hydrodynamic pressure and wave loads on three-dimensional floating bodies", IHI Eng. Rev. (Japan), Vol. 14, No. 2, pp. 6-20.

ODABASI, A.Y. and Hearn, G.E., 1978, "Sea keeping theories: what is the choice?", Trans. North East Coast Inst. Eng. & Shipbuilders, Vol. 94, pp. 53-84.

O'DEA, J.F. and Jones, H.D., 1983, "Absolute and relative motion measurements on a model of a high-speed containership", Proc. 20th ATTC, Hoboken.

OGILVIE, T.F., 1963, "First- and second-order forces on cylinder submerged under a free surface", J. Fluid Mech., Vol. 16, pp. 451-472.

Ogilvie, T.F. and Tuck, E.O., 1969, "A rational strip theory of ship motions - part I", Report No. 013, Dept Nav. Archi., Univ. Michigan.

Ogilvie, T.F. and Beck, R.F., 1973, "Transfer functions for predicting ship motions: a review of the theory", Proc. Symp. on Seakeeping, SNAME & Webb Inst. Nav. Archi.

Ogilvie, T.F., 1974, "Fundamental assumptions in ship-motion theory", Proc. Int. Symp. Dynamics Mar. Vehi. & Struct.in Waves, London, pp. 143-153.

Ogilvie, T.F. and Shin, Y.S., 1978, "Integral-equation solutions for time-dependent free-surface problems", J. Soc. Nav. Archi. Japan, Vol. 143, pp. 86-96.

Ogilvie, T.F., 1983, "Second order hydrodynamic effects on ocean platforms", Int. Workshop on Ship and Platform Motions, Berkeley, pp. 205-265.

OHKUSU, M., 1973, "Wave action on groups of vertical cylinders", J. Soc. Nav. Arch . Japan, Vol. 11, pp. 37.

Ohkusu, M., 1974, "Hydrodynamic forces on multiple cylinders in waves", Proc. Int. Symp. Dynamics Mar. Vehi. & Struct.in Waves, London, pp. 107-112.

OKAWA, Y., 1980, "On the hydrodynamic forces acting on submerged hexahedrons", Report Ship Res. Inst. (Japan), Vol. 17, No. 2, pp. 133-149 (in Japanese).

OMAE 1986, Earthquake Engineering, 5th OMAE Conf., Tokyo, Vol. 1, pp. 641-705.

OMER, G.C. and Hall, H.H., 1949, "The scattering of a tsunami by a cylindrical island", J. Seismolog. Soc., Amer., Vol. 39, No. 4, pp. 257-260.

OORTMERSSEN, G., 1976, "The motions of a ship in shallow water", J. Ocean Eng., Vol. 3, pp. 221-255.

Oortmerssen, G., 1979, "Hydrodynamic interaction between two structures, floating in waves", BOSS '79, London, pp. 339-356.

PAPANIKOLAOU, A., 1984, "On calculations of non-linear hydrodynamic effects on ship stations", Schiffstechnik, Vol. 31.

PAULLING, J.R., 1981, "The sensitivity of predicted loads and responses of floating platforms to computational methods", Proc. Integrity of Offshore Structures, pp. 50-69.

PEREGRINE, D.H. and Jonsson, I.G., 1983, "Interaction of waves and currents", Report No. 83-6, U.S. Army, Corps of Engineers, Coastal Eng. Res. Centre.

PETERS, A.S. and Stoker, J.J., 1957, "The motion of a ship as a floating rigid body in a seaway", Comm. Pure & Appl. Math., Vol. 10, pp. 399-490.

PIDCOCK, M.K., 1985, "The calculation of Green's functions in three dimensional hydrodynamic gravity wave problems", Int. J. Num. Method in Fluids, Vol. 5, pp. 891-909.

PINKSTER, J.A., 1979, "Mean and low frequency wave drifting forces on floating structures", J. Ocean Eng., Vol. 6, pp. 593-615.

Pinkster, J.A. and Boom, W.C. de, 1983, "Motion and tether force prediction for a deep water tension leg platform", Proc. Offshore Tech. Conf., OTC Paper No. 4487.

PORTER, W.R., 1960, "Pressure distributions, added mass and damping coefficients for cylinders oscillating in a free surface", Series No. 82, Issue No. 16, Inst. Eng. Res., Univ. California.

POTASH, R.L., 1971, "Second-order theory of oscillating cylinders", J. Ship Res., Vol. 15, No. 4, pp. 295-324.

PRICE, W.G. and Bishop, R.E.D., 1974, Probabilistic Theory of Ship Dynamics, Chapman & Hall.

QIU, D.H. and Wang, Y.X., 1986, "The nonlinear wave force on large cylinder", 5th OMAE Conf., Tokyo, Vol. 1, pp. 212-217.

REMERY, G.F.M. and Hermans, A.J., 1971, "The slow drift oscillations of a moored object in random seas", Proc. Offshore Tech. Conf., OTC Paper No. 1500.

RICE, S.O., 1944, 1945, "Mathematical analysis of random noise", Bell System Tech. J., Vol. 23, pp 282-332 (1944); Vol. 24, pp. 46-156 (1945).

ROFF, A.I., 1972, "Program SCORES - ship structural response in waves", Ship Structure Committee Report SSC-230, US Coast Guard.

SARPKAYA, T. and Isaacson, M., 1981, Mechanics of Wave Forces on Offshore Structures, Van Nostrand.

SAKAI, T., Hirosue, F. and Iwagaki, Y., 1986, "Wave directional spectra change due to underwater topography and current", 5th OMAE Conf., pp. 59-65.

SALVESEN, N., Tuck, E.O. and Faltinsen, O., 1970, "Ship motions and sea loads", Trans. SNAME, Vol. 78, pp. 250-287.

SCLAVOUNOS, P., 1984, "The unified slender-body theory: ship motion in waves", Proc. 15th Symp. Naval Hydrodynamics, Hamburg, pp. 177-192.

SIMON, M.J. and Ursell, F., 1984, "Uniqueness in linearized two-dimensional water-wave problems", J. Fluid Mech., Vol. 148, pp. 137-154.

SMITH, S.N., 1983, "Design and hydrodynamic performance of a small semi-submersible (SWATH) research vessel", Trans. RINA, Vol. 125, pp. 69-91.

SODING, H., 1976, "Second-order forces on oscillating cylinders in waves", Schiffstechnik, Vol. 23, pp. 205-209.

ST. DENIS, M. and Pierson, W.J., 1953, "On the motion of ships in confused seas", Trans. SNAME, Vol. 61, p. 280-332.

STANDING, R.G., 1981, "Wave loading on offshore structures: a review", NMI Report 102.

Standing, R.G., Dacunha, N.M.C. and Matten, R.B., 1981, "Mean wave drift forces: theory and experiment" NMI Report No. 124.

Standing, R.G. and Dacunha, N.M.C., 1982, "Slowly-varying and mean second-order wave forces on ships and offshore structures", NMI Report 147.

STANSBY, P. and Isaacson, M. (editors), 1986, Report, Int. Workshop on Recent Development in Offshore Hydrodynamics, Univ. Manchester.

STOKES, G.G., 1851, "On the effect of the internal friction on fluids on the motion of pendulums", Camb. Phil. Trans. IX.

TAKAGI, M. et al, 1983, "On the precision of various hydrodynamic solutions of two-dimensional oscillating bodies", Int. Workshop on Ship and Platform Motions, Berkeley, pp. 450-466.

Takagi, M. et al, 1985, "A comparison of methods for calculating the motion of a semi-submersible", J. Ocean Eng., Vol. 12, pp. 45-97.

TAN, S.G. and de Boom, W.C., 1981, "The wave-induced motion of a tension leg platform in deep water", Proc. Offshore Tech. Conf., Paper OTC 4074.

TASAI, F., 1959, "On the damping force and added mass of ships in heaving and pitching", Report, Res. Inst. Appl. Mech., Kyushu Univ., Vol. 7, No. 26.

TELSLE, J.G. and Noblesse, F., 1986, "Numerical evaluation of the Green function of water wave radiation and diffraction", J. Ship Res., Vol. 30, No. 2, pp. 69-84.

THORNE, R.C., 1953, "Multipole expansions in the theory of surface waves", Proc. Camb. Phil. Soc., Vol. 49, pp. 707-716.

TIMMAN, R. and Newman, J.N., 1962, "The coupled damping coefficients of symmetric ships", J. Ship Res., No. 4, Vol. 5, pp. 34-55.

TRIANTAFYLLOU, A.W., 1982, "A consistent hydrodynamic theory for moored and positioned vessels", J. Ship Res., Vol. 26, pp. 97-105.

TUNG, C.C. and Huang, N.E., 1976, "Interaction between waves and currents and their influence on fluid forces", BOSS '76, Trondheim, Norway.

URSELL, F., 1949a, "On the heaving motion of circular cylinders on the surface of a fluid", Quart. J. Mech. & Appl. Math., Vol. 2, pp. 213-231.

Ursell, F., 1949b, "On the rolling motion of circular cylinders on the surface of a fluid", Quart. J. Mech. & Appl. Math., Vol. 11, Part 3, pp. 335.

Ursell, F., 1950, "Surface waves on deep water in the presence of a submerged circular cylinder, II", Proc. Camb. Phil. Soc., Vol. 46, pp. 153-158.

Ursell, F., 1953, "Short surface waves due to an oscillating immersed body", Proc. Royal Soc., Ser. A, Vol. 220, pp. 90-103.

Ursell, F., 1968, "On head seas travelling along a horizontal cylinder", J. Inst. Maths & Appl., Mech., Vol. 4, pp. 414-427.

Ursell, F., 1975, "The refraction of head seas by a long ship", J. Fluid Mech., Vol. 67, pp. 689-703.

Ursell, F., 1981, "Irregular frequencies and motion of floating bodies", J. Fluid Mech., Vol. 105, pp. 143-156.

WANG, S. and Wahab, R., 1971, "Heaving oscillation of twin cylinders in a free-surface", J. Ship Res., Vol. 15, No. 1, pp. 33.

WEHAUSEN, J.V. and Laitone, E.V., "Surface waves", Handbuck der Physik, Vol. 9, pp. 446-778, Springer, Berlin.

WENDLAND, W.L., 1983, "Boundary element methods and their asymptotic convergence", Theor. Acoustics & Num. Tech., pp. 135-216, Springer-Verlag.

WICKERS, J.E.W. and Sluijs, M.F. van, 1979, "The influence of waves on the low-frequency hydrodynamic coefficients of moored vessels", Proc. Offshore Tech. Conf., Paper OTC 3625.

Wickers, J.E.W., 1982, "On the low-frequency surge motions of vessels moored in high seas", Proc. Offshore Tech. Conf., Paper OTC 4437.

Wickers, J.E.W. and Huijsmans, R.H.M., 1984, "On the low-frequency hydrodynamic damping forces acting on offshore moored vessels", Proc. Offshore Tech. Conf., Paper No. 4813.

Wickers, J.E.W., 1986, "Progress in computer simulations of SPM moored vessels", Proc. Offshore Tech. Conf., Paper OTC 5175.

WU, X.J., 1985, "A hybrid 3D-strip method for evaluating surge coefficients of full shaped ships", Boundary Element VII, Vol. 2, pp. 9.3-9.12, Springer-Verlag.

Wu, X.J., 1986, "A two-dimensional source-dipole method for seakeeping analysis of ships and offshore structures", CADMO 86, Washington DC, pp. 223-235, Springer-Verlag.

Wu, X.J. and Price, W.G., 1986a, "A shallow draft theory and its application in computing motions and wave loads on shallow draft offshore structures", CADMO 86, Washington DC.

Wu, X.J. and Price, W.G., 1986b, "An extended form of strip theory applicable to drydock like sections", J. Int. Ship. Prog., Vol. 33, pp. 204-210.

Wu, X.J. and Price, W.G., 1986c, "Behaviour of offshore structures with partially trapped free-surface water regions", Proc. 1st OMAE Speciality Symp. Offshore & Arctic Frontiers, New Orleans, pp. 255-262.

Wu, X.J. and Price, W.G., 1986d, "Modified techniques for motion predictions of offshore structures", International Symposium on Advances in Offshore Technology, Amsterdam, pp. 201-224.

Wu, X.J. and Price, W.G., 1986e, "An equivalent box approximation to predict irregular frequencies in arbitrarily-shaped three-dimensional marine structures", J. Appl. Ocean Res., Vol. 8, No. 4, pp. 223-231.

Wu, X.J. and Price, W.G., 1986f, "Resonant waves in fluid-structure interaction problem involving a free-surface", Int. Conf. Vibration Problems in Eng., Xi'an, pp. 439-446.

Wu, X.J., 1987, "An interior integral equation method for water wave radiation and diffraction problems", 2nd Int. Workshop Water Waves & Floating Bodies, Univ. Bristol, pp. 143-150.

Wu, X.J. and Price, W.G., 1987, "A multiple Green's function expression for the hydrodynamic analysis of multi-hull structures", J. Appl. Ocean Res., Vol. 9, No. 2, pp. 58-66.

Wu, X.J. and Price, W.G., 1989, "Solution approximation to the horizontal plane motions of full-bodied slender marine structures", J. Int. Ship. Prog., Vol. 36, pp. 237-282.

YEUNG, R.W., 1982, "Numerical methods in free-surface flows", Ann. Rev. Fluid Mech., Vol. 14, pp. 395-442.

YONEYA, T. and Yoshida, K., 1983, "The dynamics of tension leg platform in waves", Tech. Bull. Nippon Kaiji Kyokai, Vol. 1, pp. 30-39.

YUE, D.K.P., Chan, H.S. and Mei, C.C., 1978, "A hybrid element method for diffraction of water waves by three-dimensional bodies", Int. J. Num. Meth. Eng., Vol. 12, 245-266.

ZIENKIEWICZ, O.C., Bettess, P. and Kelly, D.W., 1978, "The finite element method for determining fluid loading on rigid structures, two- and three-dimensional formulations", Chapter 4, Numerical Methods in Offshore Engineering, Editors: O.C. Ziekiewicz et al, John Wiley & Sons, pp. 141.

ZHAO, R. and Faltinsen, O.M., 1988, "Wave-current interaction effects on large volume structures", BOSS '88.

An equivalent box approximation to predict irregular frequencies in arbitrarily-shaped three-dimensional marine structures

XIONG-JIAN WU

Ship Hydrodynamics Laboratory, Shanghai Jiao-Tong University, Shanghai, China, presently at Brunel University, Uxbridge, Middlesex UB8 3PH, England

W. G. PRICE

Department of Mechanical Engineering, Brunel University, Uxbridge, Middlesex UB8 3PH, England

An 'equivalent box technique' is developed to derive an analytical solution for the approximate predictions of the irregular frequencies associated with a source or a mixed source-dipole distribution method analysis of an arbitrarily-shaped three-dimensional (3D) marine structure which is free surface piercing. Both analytical and numerical examples are given to confirm the validity and accuracy of the present formulation. By means of this approximation irregular frequencies are known *á priori* to the numerical computation and therefore it becomes possible to avoid 3D calculations around these discrete irregular frequencies.

INTRODUCTION

The singularity distribution method[1] based on a boundary integral equation with a Green's function expression[2] is one of the most powerful theoretical tools in the field of marine hydrodynamics, but unfortunately is partially defective due to the existence of irregular frequencies.[2] That is, when the method is applied to a free surface piercing structure oscillating in calm water or excited by an incident wave, such a method fails to give correct solutions at discrete 'irregular frequencies' due to mathematical failure because the resulting integral equation takes the form of the Fredholm integral equation of the second kind and this has no unique solutions at these irregular frequencies. This has been previously pointed out by John[2] who showed that the irregular frequencies are the eigen-frequencies of an interior eigenvalue problem.[3] Two possible approaches may be conceived to tackle this irregular frequency problem. That is

(i) to adopt an alternative technique or some prescription which erases the irregular frequencies, or
(ii) to predict the irregular frequencies precisely and then simply avoid the 3D computation around these discrete frequencies and so greatly reduce computing time.

Efforts have been focused mainly on 2D cases to develop remedies[1] to eliminate the irregular frequency. An effective method, amongst the many proposals is a 2D non-analytical deep water Green's function given by Ogilvie and Shin.[4] This method was confirmed numerically by Takagi.[5] However, at present there is no parallel procedure for twin or multihull sections when both serious resonant wave effects (physical) and an irregular frequency influence (computational) can arise together, as well as no general treatment applicable to 3D structures.

Accepted October 1985. Discussion closes December 1986.

As to the second approach, analytical solutions to predict the occurrence of irregular frequencies are only available for limited simple geometries,[3] such as a rectangular section,[6] a rectangular box[7] and a vertical circular cylinder.[8] Regrettably, for a more realistic marine structure of arbitrary geometry irregular frequencies are not known before a numerical computation commences and this may produce difficulties in the subsequent numerical procedures if such a frequency is encountered.

The present paper adopts the second approach to solve the irregular frequency problem in which the arbitrary 3D marine structure geometry is represented by a box of equivalent dimensions to the original, i.e. the 'equivalent box assumption'. By this means an empirical approximation is deduced to predict the occurrence of irregular frequencies.

BASIC THEORY

Within the bounds of linear theory, the wave-structure interaction problem is governed by the following set of equations.[3] Namely,

$$\left.\begin{aligned} &\nabla^2\phi = 0 && \text{in the fluid domain } V \\ &\frac{\partial\phi}{\partial z} - \nu\phi = 0 && \text{on } z = 0, \text{ the still free surface } F \\ &\frac{\partial\phi}{\partial z} = 0 && \text{on the seabed} \\ &\frac{\partial\phi}{\partial n} = v_n && \text{on the body mean wetted surface } S_w \end{aligned}\right\} \quad (1)$$

and the radiation condition

$$\lim_{R\to\infty} \sqrt{R}\left(\frac{\partial\phi}{\partial R} - i\nu\phi\right) = 0$$

0141-1187/86/040223-09 $2.00

where ϕ is the time-independent complex amplitude of the velocity potential $\phi e^{-i\omega t}$; $\nu = \omega^2/g$ and ω denotes the wave frequency, n is a unit outward normal on the body surface and v_n is the normal component of the velocity on the body surface. In a Cartesian coordinate system with x-y axes lying in the still water surface plane and the z axis positive upwards, the horizontal distance R between a field point $P(x, y, z)$ and a point on the body surface $Q(\xi, \eta, \zeta)$ is given by $\{(x-\xi)^2 + (y-\eta)^2\}^{1/2}$.

By means of the Green's theorem the wave-structure interaction problem results in an integral equation[1] in the mixed source-dipole distribution form

$$2\pi\phi(P) - \int\!\!\!\!\!\!-_{S_w} \phi(Q)\frac{\partial G(P,Q)}{\partial n_Q}\,dS = -\int_{S_w} G(P,Q)\,v_n(Q)\,dS \tag{2}$$

or in the source distribution form

$$-2\pi\sigma(P) + \int\!\!\!\!\!\!-_{S_w} \sigma(Q)\frac{\partial G(P,Q)}{\partial n_P}\,dS = v_n(P), \tag{3}$$

where both the points P and Q are on the body surface, σ is the source strength, $G(\ )$ is the Green's function and $\int\!\!\!\!\!\!-$ denotes the principal value surface integral.

The integral equations (2) and (3) are representative of the Fredholm integral equation of the second kind which breaks down at an infinite number of discrete 'irregular frequencies' when applied to a free-surface-piercing marine structure. It was John[2] who pointed out that these irregular frequencies are the eigenfrequencies of an image interior eigenvalue problem defined by the equations

$$\left.\begin{aligned} &\nabla^2\bar{\phi} = 0 \qquad \text{in the interior domain } \bar{V}\\ &\frac{\partial\bar{\phi}}{\partial z} - \nu\bar{\phi} = 0 \quad \text{on the interior free surface } \bar{F}\\ &\text{and}\\ &\bar{\phi} = 0 \qquad \text{on the body mean wetted surface } S_w \end{aligned}\right\} \tag{4}$$

where $\bar{\phi}$ denotes an image interior velocity potential.

In addition to these conditions Wu and Price[3] derived a supplementary condition to determine the influence of irregular frequencies in a particular mode of body motion, i.e. surge, sway, heave, roll, pitch or yaw in addition to flexible modes of oscillation. For practical applications this supplementary condition can be simply described in the following manner. That is 'at an irregular frequency a singular behaviour may not occur in a mode of body motion which is of opposite symmetry to the interior potential solution $\bar{\phi}$'. Since this statement is confirmed and illustrated elsewhere[3] a repetition of the discussion in the present analysis is omitted.

INTERIOR EIGEN SOLUTION FOR A RECTANGULAR BOX

For a rectangular box of length L, beam B and draft h, the exact eigen solution[7] of the interior problem given in equation (4), may be written as

$$\bar{\phi}_{pm} = \sin\left[\frac{p\pi}{L}(x - L/2)\right]\sin\left[\frac{m\pi}{B}(y - B/2)\right] \sinh[k(z+h)] \tag{5}$$

for $|x| \leqslant L/2$, $|y| \leqslant B/2$, $-h \leqslant z \leqslant 0$; $p = 1, 2, \ldots, q, \ldots$ and $m = 1, 2, \ldots, n, \ldots$. The irregular frequencies are given by

$$\omega_{pm} = [gk \coth(kh)]^{1/2} \tag{6}$$

with

$$k = \pi\left[\left(\frac{p}{L}\right)^2 + \left(\frac{m}{B}\right)^2\right]^{1/2}$$

Corresponding to the supplementary condition as stated in the foregoing section the possible bodily oscillatory modes influenced by the irregular frequencies are listed in Table 1. The predictions in Table 1 are confirmed by the numerical calculation presented by Inglis and Price.[7]

Furthermore, Wu and Price[3] found that amongst the infinite set of irregular frequencies, a dominant influence in the calculated hydrodynamic coefficients arises from the frequencies ω_{p1} ($p = 1, 2, \ldots$) and ω_{1m} ($m = 1, 2, \ldots$) and therefore these may be referred to as the 'principal irregular frequencies'.

In addition to the rectangular box, analytical solutions of equation (4) may be obtained for a circular tank,[8] a sector of a circular tank and a horizontal triangular prism[3] and these solutions are summarised in the Appendix.

AN 'EQUIVALENT BOX TECHNIQUE'

The derivation of a closed general analytical expression to predict the occurrence of the irregular frequencies for an arbitrarily-shaped 3D body is most likely impossible. To overcome this theoretical difficulty an *equivalent box assumption* is now introduced taking advantage of the previous solution for a rectangular box. That is, 'in order to evaluate irregular frequencies, an arbitrarily 3D body may be represented by a rectangular box of "equivalent" length, beam and draft with the *same displacement volume* as the original structure'.

Based on this assumption the irregular frequencies (i.e. the eigenfrequencies of equation (4)) of an arbitrary body geometry may be expressed by an equivalent box formula

$$\omega_{pm} = [gk \coth(kh_e)]^{1/2}, \tag{7}$$

with $k = \pi\left[\left(\frac{p}{L_e}\right)^2 + \left(\frac{m}{B_e}\right)^2\right]^{1/2}$ for $p = 1, 2, \ldots$ and $m = 1, 2, \ldots$, where L_e, B_e and h_e are the equivalent length, beam and draft.

In naval architecture and offshore engineering, it is well-known that the properties of a marine structure heavily rely on the ratios of its main dimensions and some in-

Table 1. Modes affected by irregular frequencies for a rectangular box

m	p = 2q − 1	p = 2q
	Mode	Mode
2n − 1	Heave	Surge, pitch
2n	Sway, roll	Yaw

dependent form coefficients.[9] Since the irregular frequency is a singular phenomenon associated with a peculiar interior standing wave[2] defined by equation (4), it must depend on some typical geometric coefficients as well. By choosing the aspect ratio of length to beam L/B and three independent form coefficients, namely, the waterplane coefficient $C_w = A_w/LB$, the midsection coefficient $C_m = A_m/Bh$ and the central longitudinal section coefficient $C_c = A_c/Lh$ (where A_w, A_m and A_c are the areas of the waterplane, the midsection and the central longitudinal section of the marine structure respectively, and the characteristic length L, beam B and draft h may be defined by the relevant intersecting lines of the three characteristic planes), the equivalent dimensions may be expressed in the following forms

with

$$\left.\begin{aligned} L_e &= \beta_1(\beta_0)^{\alpha_1}L \\ B_e &= \beta_2(\beta_0)^{\alpha_2}B \\ h_e &= \nabla/(L_eB_e) \\ \alpha_1 &= L^2/(L^2+B^2) \\ \alpha_2 &= B^2/(L^2+B^2) \\ \beta_0 &= (C_w)^{c_0} \\ \beta_1 &= (C_c)^{c_1} \\ \beta_2 &= (C_m)^{c_2} \end{aligned}\right\} \quad (8)$$

where ∇ is the displacement volume whilst the empirical 'correction coefficients' c_0, c_1 and c_2 are assumed expressed as

$$c_0 = 3/4,$$

$$c_1 = \left[1 + 6\left|\frac{L-B}{L+B}\right| \ln(p)\right] \Big/ 8 \quad (9)$$

$$c_2 = \left[1 + 6\left|\frac{L-B}{L+B}\right| \ln(m)\right] \Big/ 8$$

It is obvious that as the geometry of a structure tends to a rectangular box, the coefficients $C_w \to 1$, $C_c \to 1$ and $C_m \to 1$, and the equivalent box formulation of equation (7), reduces to the same as the exact solution for a rectangular box of equation (6). This indicates that in the limiting case the present formula is consistent with the exact solution for a real box.

Since such expressions are constructed based on the equivalent box assumption and the main parameters of the marine structure, there is no strict theoretical justification for their forms. However, no previous alternative approximation exists and from a practical viewpoint the present approximation is found to work.

RESULTS

To assess the accuracy of the values and distribution of the irregular frequency predicted by the equivalent box formula, a comparative study was conducted on a variety of 3D body geometries for which the characteristics of the irregular frequencies are determined either analytically from available exact solutions or numerically by 3D computations.

Analytical examples

Tables 2-4 illustrate the predicted non-dimensional values of the irregular frequencies for a circular tank, a sector of a circular tank and a horizontal triangular prism, respectively. These results are obtained from analytical solutions[3] and from the equivalent box approximation given in equation (7). In all the Tables the non-dimensional frequency $\bar{\omega} = \omega\sqrt{B/2g}$, where B denotes the beam of the original structure.

Table 2. Irregular frequencies for a circular tank of radius r_0 and draft h

$h/2r_0$	$\bar{\omega}$, analytical solution from eq. (A2)			
1.0	1.551	1.958	2.266	2.350
0.5	1.564	1.958	2.266	2.350
0.25	1.698	1.990	2.280	2.359
$h/2r_0$	$\bar{\omega}$, approximate solution from eq. (7)			
1.0	1.560	1.962	2.206	2.333
0.5	1.576	1.963	2.206	2.333
0.25	1.726	2.016	2.230	2.350

Table 3. Irregular frequencies for a sector of a circular tank of radius $r_0 = 10$ m, angle $2\alpha = \pi/3$ and draft $h = 0.5$ m ($B = 5.774$)

Method	$\bar{\omega}$		
Exact	2.44	2.50	2.57
Approximate	2.47	2.50	2.55

Table 4. Irregular frequencies and affected modes for a horizontal triangular prism of length L, beam $B = L/2$ and draft $h = B/2$

(a) Analytical solution derived from equation (A9)

$\bar{\phi}$	p = 1	2	3	4
	$\bar{\omega}$	$\bar{\omega}$	$\bar{\omega}$	$\bar{\omega}$
	1.58	1.67	1.77	1.93
y-symmetric	heave	surge, pitch	heave	surge, pitch
	1.99	2.05		
y-antisymmetric	sway, roll	yaw		

(b) Approximate solution derived from equation (7)

m	p = 1	2	3	4
	$\bar{\omega}$	$\bar{\omega}$	$\bar{\omega}$	$\bar{\omega}$
	1.56	1.65	1.78	1.93
1	heave	surge, pitch	heave	surge, pitch
	2.00	2.05		
2	sway, roll	yaw		

For the circular tank of radius r_0 (i.e. $L = B = 2r_0$), three drafts are considered, i.e. $h/2r_0 = 1.0$, 0.5 and 0.25, and Table 2 displays the first four irregular frequencies determined from equation (A2) (see analytical solution in the Appendix) and equation (7). The generally good agreement between the two sets of results implies the validity of the equivalent box formulation over a wide range of body drafts.

Table 3 shows the predicted irregular frequencies for a sector of a circular tank of radius $r_0 = 10$ m, angle $2\alpha = \pi/3$ and draft $h = 0.5$ m. The exact solutions are obtained

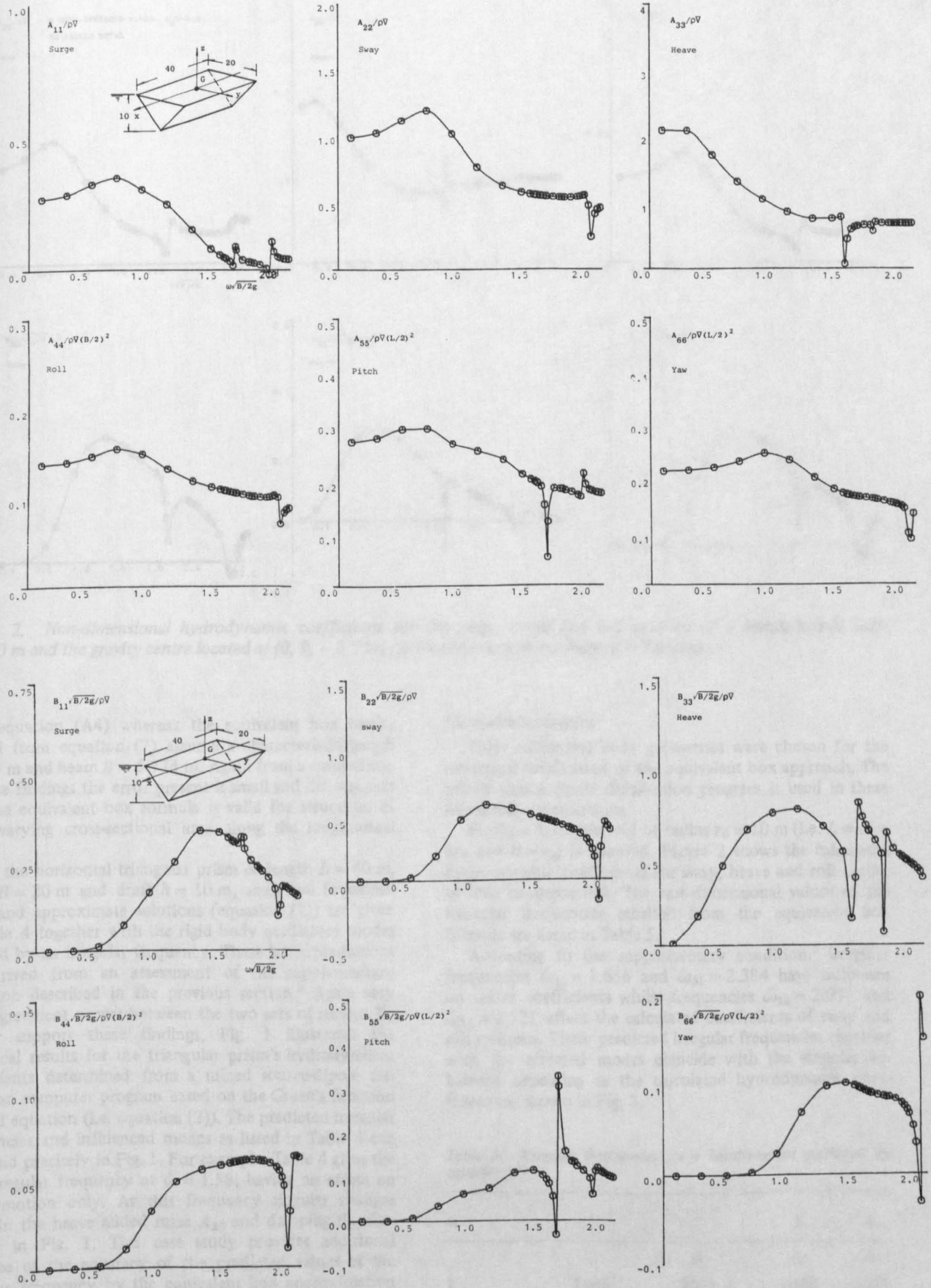

Figure 1. Non-dimensional hydrodynamic coefficients for the six rigid body modes of motion for a horizontal triangular prism with L = 40 m, B = 20 m and h = 10 m. The gravity centre is located at the centroid of its water-plane (A ≡ added mass or moment, B ≡ damping).

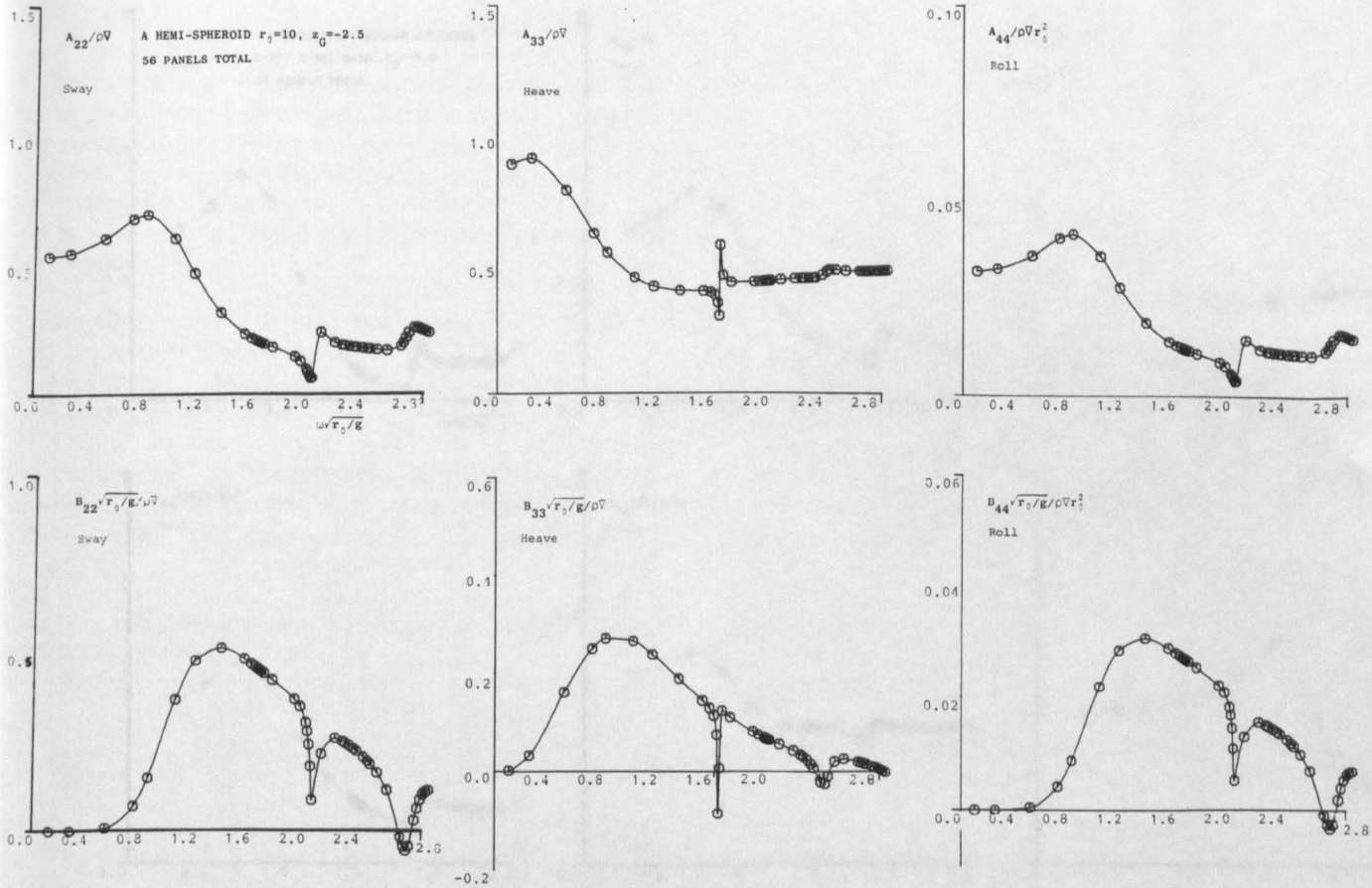

Figure 2. Non-dimensional hydrodynamic coefficients for the sway, heave and roll motions of a hemispheroid with $r_0 = 10$ m and the gravity centre located at (0, 0, − 2.5 m) (A ≡ added mass or moment, B ≡ damping).

from equation (A4) whereas the equivalent box results derived from equation (7) assume a characteristic length $L = 10$ m and beam $B = 5.774$ m. Again from a comparison of these findings the error present is small and this suggests that the equivalent box formula is valid for structures of rapid varying cross-sectional area along the longitudinal axis.

For the horizontal triangular prism of length $L = 40$ m, beam $B = 20$ m and draft $h = 10$ m, analytical (equation (A9)) and approximate solutions (equation (7)) are given in Table 4 together with the rigid body oscillatory modes affected by an irregular frequency. These latter predictions are derived from an assessment of the supplementary condition described in the previous section.[3] Again very good agreement occurs between the two sets of results. To further support these findings, Fig. 1 illustrates the numerical results for the triangular prism's hydrodynamic coefficients determined from a mixed source-dipole distribution computer program based on the Green's function integral equation (i.e. equation (2)). The predicted irregular frequencies and influenced modes as listed in Table 4 can be found precisely in Fig. 1. For example, Table 4 gives the first irregular frequency at $\bar{\omega} = 1.58$, having an effect on heave motion only. At this frequency singular changes occur in the heave added mass A_{33} and damping B_{33} illustrated in Fig. 1. This case study provides additional evidence of the accuracy of the predicted values of the irregular frequency by the equivalent box approximation and the validity of the predicted occurrence rule of the irregular frequency defined by the supplementary condition.

Numerical examples

Three additional body geometries were chosen for the numerical verification of the equivalent box approach. The mixed source-dipole distribution program is used in these numerical computations.

Firstly a hemispheroid of radius $r_0 = 10$ m (i.e. $L = B = 2r_0$ and $h = r_0$) is adopted. Figure 2 shows the calculated hydrodynamic coefficients for sway, heave and roll modes of this hemispheroid. The non-dimensional values of the irregular frequencies resulted from the equivalent box formula are listed in Table 5.

According to the supplementary condition,[3] irregular frequencies $\bar{\omega}_{11} = 1.656$ and $\bar{\omega}_{31} = 2.384$ have influence on heave coefficients whilst frequencies $\bar{\omega}_{12} = 2.015$ and $\bar{\omega}_{14} = 2.721$ affect the calculated coefficients of sway and roll motions. These predicted irregular frequencies together with the affected modes coincide with the singular behaviour appearing in the calculated hydrodynamic coefficients as shown in Fig. 2.

Table 5. Irregular frequencies for a hemispheroid predicted by equation (7)

m \ p	1	2	3	4
	$\bar{\omega}$	$\bar{\omega}$	$\bar{\omega}$	$\bar{\omega}$
1	1.656	2.015	2.384	2.721
2	2.015	2.257	2.545	2.834
3	2.384	2.545	2.760	2.996
4	2.721	2.834	2.996	3.187

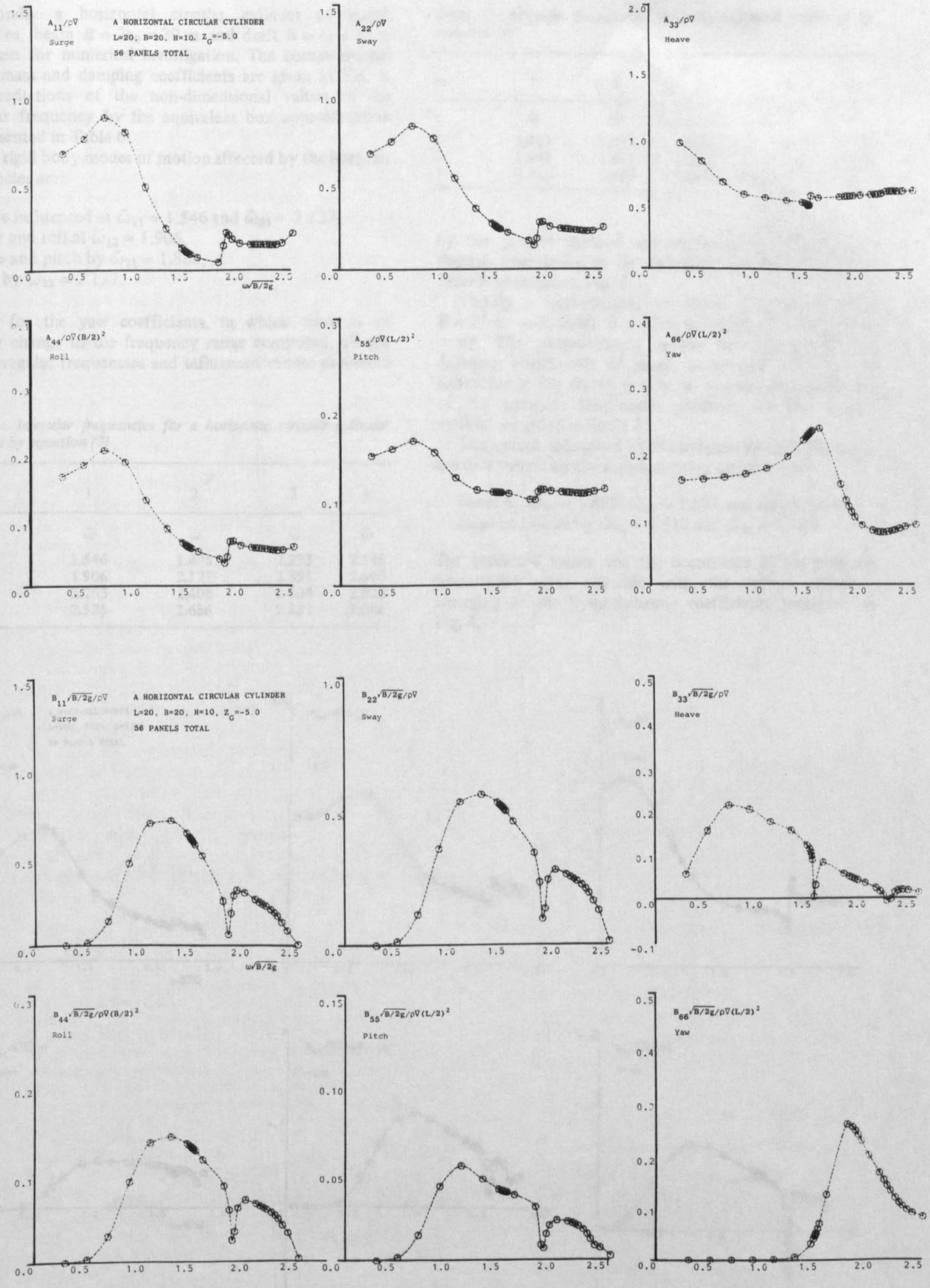

Figure 3. Non-dimensional hydrodynamic coefficients for the six rigid body modes of motions of a horizontal circular cylinder with $L = 20$ m, $B = 2r_0 = 20$ m and $h = r_0 = 10$ m. The gravity centre is located at (0, 0, − 5 m) (A ≡ added mass or moment, B ≡ damping).

Secondly a horizontal circular cylinder of length $L = 20$ m, beam $B = 2r_0 = 20$ m and draft $h = r_0 = 10$ m is chosen for numerical investigation. The computational added mass and damping coefficients are given in Fig. 3. The predictions of the non-dimensional values of the irregular frequency by the equivalent box approximation are presented in Table 6.

The rigid body modes of motion affected by the irregular frequencies are:

heave influenced at $\bar{\omega}_{11} = 1.546$ and $\bar{\omega}_{31} = 2.233$,
sway and roll at $\bar{\omega}_{12} = 1.906$,
surge and pitch by $\bar{\omega}_{21} = 1.888$,
yaw by $\bar{\omega}_{22} = 2.127$.

Except for the yaw coefficients, in which there is no singular change in the frequency range computed, all the other irregular frequencies and influenced modes predicted by the present method are confirmed by the observed singular phenomena in the calculated hydrodynamic coefficients as shown in Fig. 3.

Table 6. Irregular frequencies for a horizontal circular cylinder predicted by equation (7)

m	p 1	2	3	4
	$\bar{\omega}$	$\bar{\omega}$	$\bar{\omega}$	$\bar{\omega}$
1	1.546	1.888	2.233	2.548
2	1.906	2.127	2.393	2.660
3	2.263	2.408	2.604	2.820
4	2.585	2.686	2.833	3.006

Table 7. Irregular frequencies for a half-ellipsoid predicted by equation (7)

m	p 1	2	3	4	5
	$\bar{\omega}$	$\bar{\omega}$	$\bar{\omega}$	$\bar{\omega}$	$\bar{\omega}$
1	1.487	1.512	1.591	1.707	1.843
2	1.943	1.967	2.016	2.084	2.169
3	2.435	2.450	2.476	2.515	2.566

Thirdly a half-ellipsoid of length $L = 100$ m, beam $B = 25$ m and draft $h = 12.5$ is chosen for numerical study. The computational results for added mass and damping coefficients of surge, heave and pitch for the half-ellipsoid are shown in Fig. 4. Non-dimensional values of the irregular frequencies predicted by the present method are listed in Table 7.

The modes influenced by the irregular frequencies which are determined by the supplementary condition are:

heave by $\bar{\omega}_{11} = 1.487$, $\bar{\omega}_{31} = 1.591$ and $\bar{\omega}_{51} = 1.843$
surge and pitch by $\bar{\omega}_{21} = 1.512$ and $\bar{\omega}_{41} = 1.707$

The predicted values and the occurrence of the irregular frequencies again coincide with the abrupt variations emerging in the hydrodynamic coefficients presented in Fig. 4.

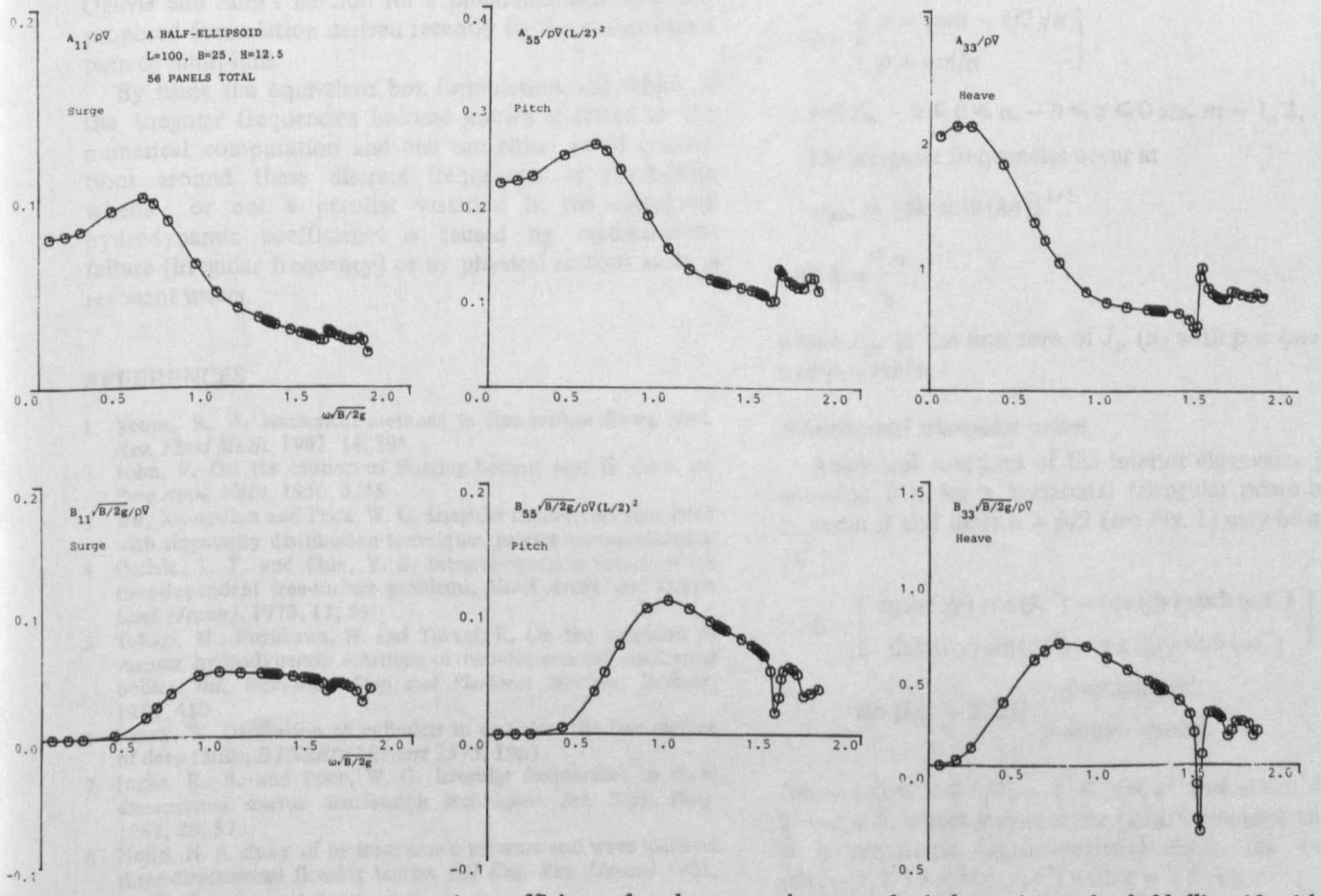

Figure 4. Non-dimensional hydrodynamic coefficients for the surge, heave and pitch motions of a half-ellipsoid with $L = 100$ m, $B = 25$ m and $h = 12.5$ m ($A \equiv$ added mass or moment, $B \equiv$ damping).

FURTHER DISCUSSION AND CONCLUSIONS

An 'equivalent box formula' is presented to predict the irregular frequencies associated with a source or mixed source-dipole distribution method analysis of a 3D mono-hull marine structure. The calculated hydrodynamic coefficients of oscillatory modes of the body motion influenced by an irregular frequency are further determined by the proposed supplementary condition.[3] Both analytical and numerical examples appear to confirm the validity and accuracy of the equivalent box approach for the examples considered.

For a twin or multi-hull offshore structure irregular frequencies encountered in numerical computations are the sum of those of each individual sub-hull. Hence the equivalent box formulation is still valid.

Since the principal irregular frequencies ω_{p1} ($p = 1, 2, \ldots$) and ω_{1m} ($m = 1, 2, \ldots$) have a significant influence on the hydrodynamic coefficients, the density of the occurrence of the irregular frequency may be easily determined from equation (7). Apparently, this density distribution will be high when the aspect ratio of the length to the beam of the body (i.e. L/B), is large. This may imply serious irregular frequency problems for a slender ship or offshore structure at high frequencies commencing from the first irregular frequency ω_{11}. Therefore, the hydrodynamic coefficients at high frequencies produced by a singularity distribution method may be somewhat questionable.

However, the longest irregular wave length must be the same order of the body beam and therefore the 2D strip approximation may be used instead of the 3D computation. In the 2D case, irregular frequencies can be removed by Ogilvie and Shin's method for a mono-hull and by a new proposed formulation derived recently by the authors for a twin or multi-hull.

By using the equivalent box formulation, the values of the irregular frequencies become known *a priori* to the numerical computation and one can either avoid calculations around these discrete frequencies or distinguish whether or not a peculiar variation in the calculated hydrodynamic coefficients is caused by mathematical failure (irregular frequency) or by physical reasons such as resonant waves.

REFERENCES

1 Yeung, R. W. Numerical methods in free-surface flows, *Ann. Rev. Fluid Mech.* 1982, 14, 395
2 John, F. On the motion of floating bodies: part II, *Com. on Pure Appl. Math.* 1950, 3, 45
3 Wu, Xiong-Jian and Price, W. G. Irregular frequencies associated with singularity distribution techniques, private communication.
4 Ogilvie, T. F. and Shin, Y. S. Integral-equation solutions for time-dependent free-surface problems, *Naval Archi. and Ocean Engi. (Japan)*, 1978, 17, 86
5 Takagi, M., Furukawa, H. and Takagi, K. On the precision of various hydrodynamic solutions of two-dimensional oscillating bodies, *Int. Workshop Ship and Platform Motions*, Berkely, 1983, 450
6 Frank, W. Oscillation of cylinders in or below the free surface of deep fluids, *DTNSRDC Report 2375*, 1967
7 Inglis, R. B. and Price, W. G. Irregular frequencies in three dimensional source distribution techniques, *Int. Ship. Prog.* 1981, 28, 57
8 Nojiri, N. A study of hydrodynamic pressure and wave loads on three-dimensional floating bodies. *IHI Eng. Rev. (Japan)* 1981, 14 (2), 6
9 Comstock, J. P. (ed.), *Principle of Naval Architecture* (revised), SNAME, 1967

APPENDIX

Analytical solution of the interior eigenvalue problem (i.e. equation (4)) are available for a circular tank,[8] a sector of a circular tank and a horizontal triangular prism.[3]

A circular tank

For a circular tank of radius r_0, i.e. $L = B = 2r_0$, and draft h the interior eigen solution[8] of equation (4) is given by

$$\bar{\phi}_{pm} = J_p(kr)\begin{bmatrix}\cos(p\theta)\\ \sin(p\theta)\end{bmatrix}\sinh[k(z+h)] \tag{A1}$$

for $r \leqslant r_0$, $0 \leqslant \theta \leqslant 2\pi$, $-h \leqslant z \leqslant 0$; $p = 0, 1, \ldots$ and $m = 1, 2, \ldots$.

The irregular frequencies occur at

$$\omega_{pm} = [gk \coth(kh)]^{1/2} \tag{A2}$$

with $k = \dfrac{x_m}{r_0}$,

where x_m is the mth zero of $J_p(x)$ ($p = 0, 1, \ldots$), the Bessel function of the first kind of order p.

A sector of a circular tank

For a sector of a circular tank with radius r_0, angle 2α and draft h, the solution of the interior velocity potential satisfying equation (4) can be derived as[3]

$$\bar{\phi}_{pm} = J_p(kr)\begin{bmatrix}\cos(p\theta)\\ \sin(p\theta)\end{bmatrix}\sinh[k(z+h)],$$
$$\text{for}\begin{bmatrix}p = (m\pi - \pi/2)/\alpha\\ p = m\pi/\alpha\end{bmatrix}, \tag{A3}$$
$$r \leqslant r_0, -\alpha \leqslant \theta \leqslant \alpha, -h \leqslant z \leqslant 0 \text{ and } m = 1, 2, \ldots$$

The irregular frequencies occur at

$$\omega_{pm} = \{gk \coth(kh)\}^{1/2} \tag{A4}$$

with $k = \dfrac{x_m}{r_0}$,

where x_m is the mth zero of $J_p(x)$ with $p = (m\pi - \pi/2)/\alpha$ or $p = m\pi/\alpha$.

A horizontal triangular prism

Analytical solutions of the interior eigenvalue problem, equation (4), for a horizontal triangular prism of length L, beam B and draft $h = B/2$ (see Fig. 1) may be expressed as[3]

$$\bar{\phi} = \begin{bmatrix}\cosh(\alpha y)\cos(\beta z') - \cos(\beta y)\cosh(\alpha z')\\ \sinh(\alpha y)\sin(\beta z') - \sin(\beta y)\sinh(\alpha z')\end{bmatrix}$$
$$\sin[k(x - L/2)], \quad \begin{matrix}y\text{-symmetric}\\ y\text{-antisymmetric}\end{matrix} \tag{A5}$$

for $-L/2 \leqslant x \leqslant L/2$, $-z' \leqslant y \leqslant z'$ and $0 \leqslant z' \leqslant h$ with $z' = z + h$, where y-symmetric (anitsymmetric) means that $\bar{\phi}$ is symmetric (antisymmetric) about the x-axis, i.e. $\bar{\phi}(x, -y, z') = c\bar{\phi}(x, y, z')$ with $c = 1$ (-1).

To satisfy the boundary conditions in equation (4) the solution requires

$$k = \frac{p\pi}{L} \text{ for } p = 1, 2, \ldots, \tag{A6}$$

$$\alpha^2 - \beta^2 = k^2, \tag{A7}$$

and

$$\alpha \tanh(\alpha h) + \beta \tan(\beta h) = 0, y\text{-symmetric}, \tag{A8}$$

$$\alpha \coth(\alpha h) - \beta \operatorname{cotan}(\beta h) = 0, y\text{-antisymmetric}.$$

The irregular frequencies appear at

$$\omega = \begin{cases} [-g\beta \tan(\beta h)]^{1/2}, y\text{-symmetric}, \\ [g\beta \operatorname{cotan}(\beta h)]^{1/2}, y\text{-antisymmetric}, \end{cases} \tag{A9}$$

where β is obtained by solving equations (A6)–(A8).

APPENDIX 4.2

A multiple Green's function expression for the hydrodynamic analysis of multi-hull structures

XIONG-JIAN WU

Ship Hydrodynamics Laboratory, Shanghai Jiao-Tong University, China; presently at the Department of Mechanical Engineering, Brunel University, Uxbridge, Middlesex, UB8 3PH, UK

W. G. PRICE

Department of Mechanical Engineering, Brunel University, Uxbridge, Middlesex, UB8 3PH, UK

A modified Green's function expression in a multiple function form is developed to evaluate the hydrodynamic coefficients of two-dimensional multi-hull structures floating or fixed in a seaway. Regrettably in conventional singularity methods applied to mono-hulls, twin-hulls, etc., irregular frequencies arise in the numerical analysis. It is shown that when the modified Green's function is used, the numerical analysis is free of irregular frequencies, the numerical accuracy of the results below the lowest irregular frequency is the same as derived from the conventional approach and the physical phenomenon of resonant surface wave interaction is retained in the theory. Results are presented for symmetric and asymmetric twin hull configurations as well as a rectangular mono-hull section heeled to an angle of 15°. A comparison between results evaluated from conventional and modified singularity approaches is also included.

INTRODUCTION

During these recent years interest has been sustained in multi-hull surface piercing floating structures (i.e. catamarans and SWATHs, trimarans, multi-hull semi-submersibles, side wall hovercraft, etc). This has culminated in the building of a large 3500 ton displacement SWATH vessel[1] though several smaller prototypes have been constructed worldwide.[1] Such developments have encouraged extensive research activities, seeking a better understanding and prediction of the behaviour of these multi-hull vessels travelling in a seaway. To do this many hydrodynamic, structural and hydroelastic theories have been proposed,[1] involving both two and three dimensional (2D and 3D) idealisations of the body. This paper however, focusses attention on a method to evaluate fluid-structure interactions arising in multi-hull structures, especially of a twin-hull configuration.

Many different hydrodynamic theories have been developed (for example, the multipole expansions,[2] singularity distributions,[3-6] and null field equations,[7] etc.) to determine the fluid loading on marine structures. Mathematically many of these methods appear effective when discussing simple idealised structures. Recently, a comprehensive numerical investigation was conducted by Takagi *et al.*[8] into the applicability of these theories to more complicated geometric contours associated with realistically shaped marine structures. This study revealed that some approaches produce very poor numerical results. This suggests that some elegantly derived mathematical models may be

(i) accurate mathematically but not necessarily accurate numerically;
(ii) limited in application to well defined idealised shapes (i.e. circular or near circular geometries) rather than general geometric bodies; or
(iii) theoretically incorrect.

It is not the intention of this paper to reiterate such an investigation but to develop a mathematical model which has a practical application.

The multipole expansion approach first developed for mono-hulls by Ursell[2] has been applied by Wang and Wahab[9] to a twin circular cylinder structure oscillating vertically in calm water. Ohkusu[10] developed a large distance approximation applicable to more general twin hull structures even if the distance between the two sub-hulls is small, whereas Lee[11] and Pien and Lee[12] concentrated their efforts on the theoretical predictions and experimental verification of the fluid actions arising in SWATH type hulls. In fact, using a source distribution method,[6,12] they observed two types of singular solutions occurring at certain frequencies. That is

(i) irregular frequencies[13-15] due to an inherent mathematical failure in the formulation arising in the singularity distribution procedure, and
(ii) resonant wave frequencies[16,17] due to standing waves existing between the two hulls.

Both these two kinds of singular solutions cause abrupt variations in the calculated hydrodynamic coefficients and when the two singular phenomena occur at closely spaced frequencies, immediate difficulties are experienced in attempting to distinguish between a real physical phenomenon (ii) and a mathematical abstraction (i).

Accepted January 1986. Discussion closes June 1987.

0141-1187/87/020058-09 $2.00

To remove the troublesome irregular frequency, Pien and Lee[12] imposed an 'artificial lid boundary condition' on the interior free surface of the two hull forms. Their example calculations showed success in eliminating the irregular frequency effect in a mono-hull but the introduction of the lid produced deviations from the results obtained by the original approach in the frequency range below the first irregular frequency value (see Fig. 3d, ref. 12).

For mono-hulls, other methods have been proposed to remove the irregular frequency phenomenon, such as the combined integral equation methods,[18,19] but the approach of Ogilvie and Shin[20] to 2D single hull bodies is of particular relevance to this paper. They overcome this problem by adopting two modified Green's functions, i.e. a symmetric form and an asymmetric form. The symmetric expression only removes difficulties occurring at the irregular frequencies found in the calculation of the hydrodynamic coefficients of symmetric modes of motion of a 2D body with port-starboard symmetry. Their asymmetric expression has been found[8,15] numerically to be a more effective approach to eliminate irregular frequencies in an arbitrarily-shaped 2D mono-hull body.

Ogilvie and Shin's symmetric Green's function was extended by Sayer[21] to the case of finite water depth, and then by Ursell[22] who derived a modified Green's function in a multipole expansion form. By means of this expression Martin[7] introduced the null field equation method from acoustics and this was further extended to a twin-hull problem.[23] In example calculations of simple ellipses, however, Martin found that the null field equation method does not converge for ellipses of beam (B) to draft (h) ratio of orders $B/h < 0.8$ and $B/h > 6.0$. Furthermore, when calculating more realistic geometries Takagi *et al.*[8] reported very poor numerical data by using this approach. Although the null field equation method has the advantage of eliminating the problem of irregular frequency it unfortunately introduces a serious disadvantage of producing non-convergent or incorrect solutions. For realistic marine structures, it is most likely that B/h may be beyond the range 0.8 to 6.0. For example, $B/h < 0.8$ usually holds in a SWATH (catamaran) ship,[5,11,12,16] in general in the bow and stern regions of a vessel, etc. whereas a sea-going barge,[24] a jack-up rig,[25,17] and a dry dock[26] etc., may have $B/h > 6.0$. Therefore, at present, the practical application of the null field equation method may be open to question but this will be discussed elsewhere.[27]

In parallel to these developments, by directly extending Ogilvie and Shin's asymmetric expression, a multiple Green's function expression is proposed for the hydrodynamic analysis of a marine structure with a mono-hull, twin-hull, multi-hull, or to adjacent bodies of differing geometric contours. The method developed and discussed in this paper is shown to eliminate irregular frequencies and to retain numerical accuracy of the calculated hydrodynamic coefficients of multi-hull floating bodies, especially in the frequency range below the first irregular frequency.

THE GREEN'S FUNCTION INTEGRAL EQUATION

When a 2D free-surface piercing marine structure oscillates with frequency ω in calm water or is excited by incident waves of similar frequency, the relationships[28] governing the fluid-structure problem may be expressed as

$$\left.\begin{aligned}
&\nabla^2\phi = 0 && \text{in the fluid domain } V\\
&\frac{\partial\phi}{\partial z} - \nu\phi = 0 && \text{on the calm water surface } z = 0\\
&\frac{\partial\phi}{\partial z} = 0 && \text{on the seabed}\\
&\frac{\partial\phi}{\partial n} = v_n && \text{on the mean body sectional contour } C_w
\end{aligned}\right\} \quad (1)$$

together with the radiation condition

$$\lim_{y\to\pm\infty}\left\{\frac{\partial\phi}{\partial y} \mp i\nu\phi\right\} = 0$$

In these equations, ϕ denotes the time independent amplitude of the velocity potential $\phi e^{-i\omega t}$, v_n is the normal velocity component on the sectional contour, n is a unit normal pointing into the fluid and $\nu = \omega^2/g$ is the wave number. Figure 1 illustrates the chosen Cartesian coordinates $0yz$ with axis $0y$ fixed in the calm water surface and axis $0z$ is positive upwards.

From an application of Green's theorem, it can be shown that the integral equation in a source-dipole distribution approach may be cast into the form[28]

$$\pi\phi(p) + \int_{C_w} \phi(q)\frac{\partial}{\partial n_q}G_0(p,q)\,\mathrm{d}l = \int_{C_w} G_0(p,q)\,v_n(q)\,\mathrm{d}l \quad (2)$$

for 2D modelling of the wetted body sectional contour C_w in which the two points $p(y,z)$ and $q(\eta,\zeta)$ are sited, i.e. $p,\ q \in C_w$. The complementary problem for point $\bar{p}$ interior to C_w, i.e. in $\bar{V}$, is described by the integral equation

$$\int_{C_w} \phi(q)\frac{\partial}{\partial n_q}G_0(\bar{p},q)\,\mathrm{d}l = \int_{C_w} G_0(\bar{p},q)\,v_n(q)\,\mathrm{d}l \quad (3)$$

for $q \in C_w$ and $\bar{p} \in \bar{V}$. In these expressions $G_0(\ )$ denotes the *classical Green's function*[13] satisfying Laplace's equation, the free surface condition, the seabed condition and the radiation condition.

In equations (2) and (3) the operator $\partial/\partial n_q$ signifies an operation on the variable q with parameters p and $\bar{p}$ treated as constants. Therefore if $L_p\{\ \}$ denotes an operator acting only on the variable $\bar{p}$ and $F(p,\bar{p})$ is a suitable but as yet unspecified function, it follows from equation (3) that

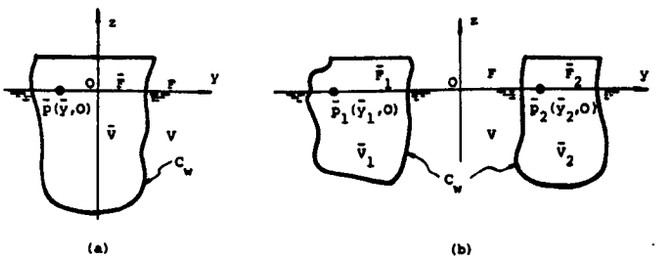

Figure 1. Cartesian co-ordinate system and symbol definitions: (a) a mono-hull section; (b) a twin-hull section

$$\int_{C_w} \phi(q) \frac{\partial}{\partial n_q} [F(p,\bar{p})\, L_{\bar{p}} \{G_0(\bar{p},q)\}]\, \mathrm{d}l$$

$$= \int_{C_w} F(p,\bar{p})\, L_{\bar{p}} \{G_0(\bar{p},q)\}\, v_n(q)\, \mathrm{d}l$$

or defining an *additional Green's function*

$$\tilde{G}(p,q,\bar{p}) = F(p,\bar{p})\, L_{\bar{p}} \{G_0(\bar{p},q)\} \tag{4}$$

then

$$\int_{C_w} \phi(q) \frac{\partial}{\partial n_q} \tilde{G}(p,q,\bar{p})\, \mathrm{d}l = \int_{C_w} \tilde{G}(p,q,\bar{p}) v_n(q)\, \mathrm{d}l \tag{5}$$

Multiplying equation (5) by a chosen constant C and adding it to equation (2) gives

$$\pi\phi(p) + \int_{C_w} \phi(q) \frac{\partial}{\partial n_q} G^*(p,q,\bar{p})\, \mathrm{d}l$$

$$= \int_{C_w} G^*(p,q,\bar{p})\, v_n(q)\, \mathrm{d}l$$

where the *modified Green's function* $G^*(\ )$ is defined as

$$G^*(p,q,\bar{p}) = G_0(p,q) + C\tilde{G}(p,q,\bar{p}) \tag{6}$$

Now equation (3) is valid for any point $\bar{p} \in \bar{V}$. In particular, for a structure of M free-surface piercing sub-hulls with individual interior regions $\bar{V}_1, \bar{V}_2, \ldots, \bar{V}_M$, each of the M points $\bar{p}_l \in \bar{V}_i \in \bar{V}$ $(i = 1, 2, \ldots, M)$ satisfies the equation

$$\int_{C_w} \phi(q) \frac{\partial}{\partial n_q} \tilde{G}(p,q,\bar{p}_l)\, \mathrm{d}l = \int_{C_w} \tilde{G}(p,q,\bar{p}_l)\, v_n(q)\, \mathrm{d}l$$

for $i = 1, 2, \ldots, M$, and the continuation of these M integral equations may be written as

$$\int_{C_w} \phi(q) \frac{\partial}{\partial n_q} \tilde{G}(p,q,\bar{p}_1,\bar{p}_2,\ldots,\bar{p}_M)\, \mathrm{d}l$$

$$= \int_{C_w} \tilde{G}(p,q,\bar{p}_1,\bar{p}_2,\ldots,\bar{p}_M)\, v_n(q)\, \mathrm{d}l$$

where the multiple additional function is given by

$$\tilde{G}(p,q,\bar{p}_1,\bar{p}_2,\ldots,\bar{p}_M) = \sum_{l=1}^{M} C_l \tilde{G}(p,q,\bar{p}_l)$$

It now follows that the previous result in equation (6) may be generalised into the form

$$G^*(p,q,\bar{p}_1,\bar{p}_2,\ldots,\bar{p}_M)$$

$$= G_0(p,q) + \sum_{l=1}^{M} C_l \tilde{G}(p,q,\bar{p}_l)$$

$$= G_0(p,q) + \sum_{l=1}^{M} C_l F(p,\bar{p}_l)\, L_{\bar{p}} \{G_0(\bar{p}_l,q)\} \tag{7}$$

where again this modified Green's function satisfies the equation

$$\pi\phi(p) + \int_{C_w} \phi(q) \frac{\partial}{\partial n_q} G^*(p,q,\bar{p}_1,\bar{p}_2,\ldots,\bar{p}_M)\, \mathrm{d}l$$

$$= \int_{C_w} G^*(p,q,\bar{p}_1,\bar{p}_2,\ldots,\bar{p}_M)\, v_n(q)\, \mathrm{d}l \tag{8}$$

The modified Green's function in equation (7) is the summation of a classical Green's function and multiple operated Green's functions and therefore it may be termed as a *multiple Green's function expression*.

The multiple Green's function integral equation, equation (8), represents an ordinary source-dipole distribution on the mean body sectional contour C_w together with M additional singularities located inside the M free-surface piercing sub-hulls. By suitably choosing the form of singularity, the role of these additional singularity terms is to absorb or cancel the interior resonant wave modes due to irregular frequencies. This has been proved by Ogilvie and Shin[20] in the special case of a mono-hull.

MULTIPLE GREEN'S FUNCTION EXPRESSION

For a body floating in deep water, the classical Green's function $G_0(p,q)$ relating to the potential at point $p = (y,z)$ to a source at $q = (\eta,\zeta)$ on the body contour is given by[13]

$$G_0(p,q) = \frac{1}{2} \ln \left\{ \frac{(y-\eta)^2 + (z-\zeta)^2}{(y-\eta)^2 + (z+\zeta)^2} \right\} + I_1 + iI_2 \tag{9}$$

where the principal value integral

$$I_1 = 2 \int_0^{\infty} \frac{e^{\mu(z+\zeta)}}{\nu - \mu} \cos \mu(y-\eta)\, \mathrm{d}\mu$$

and

$$I_2 = -2\pi e^{\nu(z+\zeta)} \cos \nu(y-\eta)$$

To each hull is allocated an interior point $\bar{p}_l = (\bar{y}_l, 0)$, i.e. $\bar{p}_l \in \bar{F}_l$ with $\bar{F}_l$ being the interior free surface of the lth hull, so that for a mono-hull structure $(M = 1)$ the modified Green's function in equation (7) becomes

$$G^*(p,q,\bar{p}_1) \equiv G^*(y,z;\eta,\zeta;\bar{y}_1,0)$$

$$= G_0(p,q) + C_1\tilde{G}(p,q,\bar{p}_1) \tag{10}$$

whereas for a twin-hull vessel $(M = 2)$ with interior point $\bar{p}_1 = (\bar{y}_1, 0)$ in one hull and $\bar{p}_2 = (\bar{y}_2, 0)$ in the other it follows that

$$G^*(p,q,\bar{p}_1,\bar{p}_2) = G_0(p,q) + C_1\tilde{G}(p,q,\bar{p}_1) + C_2\tilde{G}(p,q,\bar{p}_2) \tag{11}$$

and so on for a multi-hull marine structure with M individual hulls.

The asymmetric modified Green's function expression proposed by Ogilvie and Shin[20] is effective in removing difficulties associated with irregular frequencies in general mono-hull cases as has been successfully used by Takagi *et al.*[8] and Wu and Price[15] in the evaluation of the hydrodynamic coefficients of a variety of single body marine structures with realistic 2D contours. A possible form of the additional Green's function for the present multi-

hull cases may be obtained straightforwardly by modifying and extending Ogilvie and Shin's asymmetric form. That is

$$\bar{G}(p,q,\bar{p}_i) = F(p,\bar{p}_i)\left\{C_{i1}\,\mathrm{sgn}(y-\bar{y}_i)\left[\frac{\partial}{\partial y}G_0(p,q)\right]_{\substack{y=\bar{y}_i\\z=0}} + C_{i2}\left[\frac{\partial}{\partial z}G_0(p,q)\right]_{\substack{y=\bar{y}_i\\z=0}}\right\} \tag{12}$$

for $i = 1, 2, \ldots, M$. For generality, C_{i1}, C_{i2} include the constant C_i and are treated as complex constants and sgn( ) denotes the sign function defined as

$$\mathrm{sgn(a)} = \begin{cases} 1 & \text{for } a > 0 \\ 0 & \text{for } a = 0 \\ -1 & \text{for } a < 0 \end{cases}$$

and the function $F(p,\ \bar{p}_i)$ can be chosen as

$$F(p,\bar{p}_i) = G_0(p,\bar{p}_i) \text{ or } \exp(\nu z - i\nu|y-\bar{y}_i|)$$

Strictly speaking, the sign function, $\mathrm{sgn}(y-\bar{y}_i)$, in equation (12) should be regarded as part of the function $F(p,\bar{p}_i)$.

The present multiple Green's function expression, equations (7) and (12), represents a further generalisation of Ogilvie and Shin's[20] asymmetric modified Green's function relating to mono-hulls. That is, for $i = 1$ and the point $\bar{p}_1 = 0(0,0)$ positioned at the origin, equation (12) reduces to

$$\bar{G}(p,q,0) = \exp(\nu z - i\nu|y|)\left\{C_{11}\,\mathrm{sgn}(y)\left[\frac{\partial}{\partial y}G_0(y,z;\eta,\zeta)\right]_{\substack{y=0\\z=0}} + C_{12}\left[\frac{\partial}{\partial z}G_0(y,z;\eta,\zeta)\right]_{\substack{y=0\\z=0}}\right\} \tag{13}$$

When exchanging the positions of $p(y, z)$ and $q(\eta, \zeta)$ equation (13) is the same as that proposed by Ogilvie and Shin[20] in a source distribution integral equation.

In the case of a twin-hull vessel the multiple Green's function is given in equation (11), whereas the individual terms are of the form

$$\bar{G}(y,z;\eta,\zeta;\bar{y}_1,0) = \exp(\nu z - i\nu|y-\bar{y}_1|)\left\{C_{11}\,\mathrm{sgn}(y-\bar{y}_1)\left[\frac{\partial}{\partial y}G_0(y,z;\eta,\zeta)\right]_{\substack{y=\bar{y}_1\\z=0}} + C_{12}\left[\frac{\partial}{\partial z}G_0(y,z;\eta,\zeta)\right]_{\substack{y=\bar{y}_1\\z=0}}\right\} \tag{14}$$

for position $\bar{p}_1 = (\bar{y}_1, 0)$ in hull I and

$$\bar{G}(y,z;\eta,\zeta;\bar{y}_2,0) = \exp(\nu z - i\nu|y-\bar{y}_2|)\left\{C_{21}\,\mathrm{sgn}(y-\bar{y}_2)\left[\frac{\partial}{\partial y}G_0(y,z;\eta,\zeta)\right]_{\substack{y=\bar{y}_2\\z=0}} + C_{22}\left[\frac{\partial}{\partial z}G_0(y,z;\eta,\zeta)\right]_{\substack{y=\bar{y}_2\\z=0}}\right\} \tag{15}$$

for position $\bar{p}_2 = (\bar{y}_2, 0)$ in hull II.

By a similar procedure for M interior points $\bar{P}_i(\bar{y}_i, 0)$ $(i = 1, 2, \ldots, M)$ the expressions can be easily obtained to account for any number of hulls.

In numerical computations, however, all these individual constants involved in the multiple Green's function expression may simply take an equal complex value, for example, $C = -(1-i)/\nu$.

As pointed out by the authors,[14] irregular frequencies encountered in numerical calculations of a twin or multi-hull structure are the sum of those of each individual sub-hull. Since Ogilvie and Shin demonstrated that a similar additional Green's function can suppress irregular frequencies in a mono-hull structure, the present multiple Green's function with M additional Green's functions related to the M free-surface piercing sub-hulls may suppress all the irregular frequencies.

NUMERICAL TECHNIQUES

Although the problem is theoretically formulated, to determine the fluid actions on realistic marine structure geometries emphasis must be placed on computational techniques and detailed numerical treatment to provide a reasonable solution. Some of the numerical procedures introduced to evaluate the 2D Green's function integral equation together with the present multiple Green's function expression in the solution of the fluid-structure interaction problem in multi-hull structures are now discussed.

Analogous to the discretisation procedure developed by Hess and Smith,[29] the sectional contour C_w is discretised into N elemental lengths, Δl, and correspondingly, the integral equation (8) transforms into a set of N linear equations taking the form

$$\sum_{j=1}^{N} a_{ij}\phi_j = V_i \tag{16}$$

for $i = 1, 2, \ldots, N$. The terms appearing in this set of equations are given by

$$\left.\begin{aligned} a_{ij} &= \pi\delta_{ij} + (1-\delta_{ij})\int_{\Delta l_j}\frac{\partial X_{ij}}{\partial n_j}\,\mathrm{d}l + \frac{\partial}{\partial n_j}(G_{ij}^{\#} - X_{ij})\,\Delta l_j \\ V_i &= \sum_{j=1}^{N} v_{nj}\left[\int_{\Delta l_j} X_{ij}\,\mathrm{d}l + (G_{ij}^{\#} - X_{ij})\,\Delta l_j\right] \end{aligned}\right\} \tag{17}$$

where

$$X_{ij} = \ln\{R_{ij}\} = \ln\{(y_i-y_j)^2 + (z_i-z_j)^2\}^{1/2}$$

$$\delta_{ij} = \begin{cases} 1 & \text{for } i = j \\ 0 & \text{for } i \neq j \end{cases}$$

and v_{nj} is the normal velocity on the jth line element.

In the present study the two elemental integrals in equation (17) are analytically computed for neighbouring elements satisfying the imposed geometric condition $R_{ij} \leqslant 2\Delta l_j$, otherwise (i.e. $R_{ij} > 2\Delta l_j$) these integrals may be approximated simply by the terms $(\partial X_{ij}/\partial n_j)\Delta l_j$ and $X_{ij}\Delta l_j$.

The remaining integrals involved in the evaluation of $G_{ij}^{\#}$ and $\partial G_{ij}^{\#}/\partial n_j$ may be expressed as

$$\int_0^{\infty} e^{\mu(z_j+z)}\begin{Bmatrix}\cos\mu(y_j-y)\\ \sin\mu(y_j-y)\end{Bmatrix}\mathrm{d}\mu = \frac{1}{(y_j-y)^2+(z_j+z)^2}\begin{Bmatrix}-(z_j+z)\\ (y_j-y)\end{Bmatrix} \tag{18}$$

and

$$\int_0^\infty \frac{e^{\mu(z_j+z)}}{\nu-\mu}\begin{Bmatrix}\cos\mu(y_j-y)\\-\sin\mu(y_j-y)\end{Bmatrix}\mathrm{d}\mu=\begin{Bmatrix}Re(I)\\Im(I)\end{Bmatrix} \tag{19}$$

where $Re(\ )$ and $Im(\ )$ denote the real and imaginary components respectively of the principal value integral[6]

$$I=\int_0^\infty \frac{e^{-i\mu(\alpha_j-\bar{\alpha})}}{\nu-\mu}\mathrm{d}\mu$$

$$=e^{-i\nu(\alpha_j-\bar{\alpha})}\{i\pi-E_1[-i\nu(\alpha_j-\bar{\alpha})]\} \tag{20}$$

where $\alpha_j=y_j+iz_j$, $\bar{\alpha}=y-iz$. $E_1(\ )$ is the exponential integral which can be written in a series form.[6] In fact, in equations (18)-(20) the coordinate (y,z) can represent the ith point (y_i,z_i) or the M interior positions $(\bar{y}_i,0)$ $(i=1,2,\ldots,M)$.

There now exists sufficient information for a_{ij} and V_i in equation (16) or (17) to be defined and the determination of ϕ_j $(j=1,2,\ldots,N)$ may be completed. This allows the hydrodynamic added mass coefficients A_{rk} and damping coefficients B_{rk} due to radiation waves and wave exciting forces F_r due to the combination of incident and diffracted waves to be determined for a 2D multi-hull body from the relationships

$$\left.\begin{aligned}A_{rk}&=\frac{\rho}{\omega}\int_{C_w} Im(\phi^k)\,n_r\,\mathrm{d}l\\B_{rk}&=-\rho\int_{C_w} Re(\phi^k)\,n_r\,\mathrm{d}l\\F_r&=-i\omega\rho\int_{C_w}(\phi^0+\phi^7)\,n_r\,\mathrm{d}l\end{aligned}\right\} \tag{21}$$

for $r=2-4$, $k=2-4$. In this equation, $r=2$ denotes a sway motion, $r=3$ a heave motion, and $r=4$ a roll motion; ϕ^0 is the incident wave potential, ϕ^7 is the corresponding diffraction wave potential and ϕ^k $(k=2-4)$ are the radiation potentials of sway, heave and roll modes respectively.

TWIN-HULL COMPUTATIONS

The applicability of any theory relies heavily on its accuracy and practical usage. Takagi *et al.*[8] assessed a variety of mathematical approaches and the evidence presented shows that some theoretical methods produce very poor numerical results when applied to some realistically shaped marine structures. In this paper the proposed mathematical model and the accuracy of the numerical method are judged on two self imposed conditions, namely,

(i) irregular frequencies are eliminated in the frequency range of interest,

(ii) the same numerical accuracy of prediction is achieved as derived from a conventional singularity method (for example, a combination of equations (2) and (9)), especially in the frequency range below the first irregular frequency value since the original method provides accurate solutions in the lower frequency range.

If these two conditions are satisfied, then the proposed method and analysis has a wide range of application.

Twin rectangular cylinders (symmetric)

A sketch of this twin rectangular hull configuration is shown in Figure 2 and represents an idealisation of a drilling platform in transit.[17]

Also illustrated are the sway, heave and roll coefficients calculated by a conventional source-dipole method.[15] Rapid and abrupt variations occur in all the curves describing the coefficients at a number of frequencies and the conclusions deduced in previous studies[14,15,30] are again proved valid. That is, the irregular frequencies occurring in a twin hull structure are the sum of those of each individual hull section. In the present example, the first irregular frequency is predicted[15,30] at $\omega^2B/2g=1.715$, confirming the existence of an irregular frequency and not a wave resonance at this frequency. Such a phenomenon is clearly seen in the sway and heave curves but barely visible in the roll curves. However, by the approximation proposed by Wu and Price,[16] the first resonant wave frequency is predicted at $\omega^2B/2g=1.57$ (i.e. the wave length $\lambda\simeq 2B$), at which large changes in the sway and roll fluid actions are clearly visible. It is interesting to note that at this frequency, no resonant wave effect in heave motion is evident but this result should be compared with those found in the next example. An additional condition governing the appearance of the resonant wave influence has been formulated by the authors and interested readers should refer to Ref. 16 for details.

Figure 3 illustrates the same set of hydrodynamic coefficients but now the results are computed from the modified source-dipole integral equation with a multiple Green's function as described previously. On comparing these results with those in Figure 2, the singular phenomenon at the irregular frequency $\omega^2B/2g=1.715$ has been removed but the resonant wave phenomenon remains although there is a slight shift in frequency to $\omega^2B/2g=1.59$. Apart from the vicinities of these two frequency values, the computational results in all coefficients are exactly the same as those determined by the conventional source-dipole method and can be compared with the predictions presented in Figures 2 and 3.

This example proves to show that for symmetric twin hull cross-sections the present method is successful, satisfying the two imposed conditions introduced prior to the commencement of the computations.

Two different hull sections (asymmetric)

Figure 4 illustrates a two dimensional cross-section consisting of triangular and rectangular hulls. For this configuration, irregular frequencies are predicted[15,30] to occur at $\omega^2B/2g=1.715$ and 2.34, corresponding respectively to the irregular frequencies occurring in a mono-hull rectangular section and a triangular section.

The sway, heave and roll hydrodynamic coefficients determined from a conventional source-dipole method are shown in Figure 4. Variations in the curves are observed at frequencies $\omega^2B/2g=1.66$, 1.785 and 2.34 indicating one resonant wave frequency and two irregular frequencies. The last frequency value coincides exactly with the second predicted irregular frequency value but the first two are slightly different from the first predicted irregular frequency value. It is believed that this is due to overlap in these two ill-conditioning bandwidths occurring in the numerical computations and therefore an interaction effect may cause the deviation.

When the modified approach is used, the irregular frequency phenomenon disappears as shown by the results

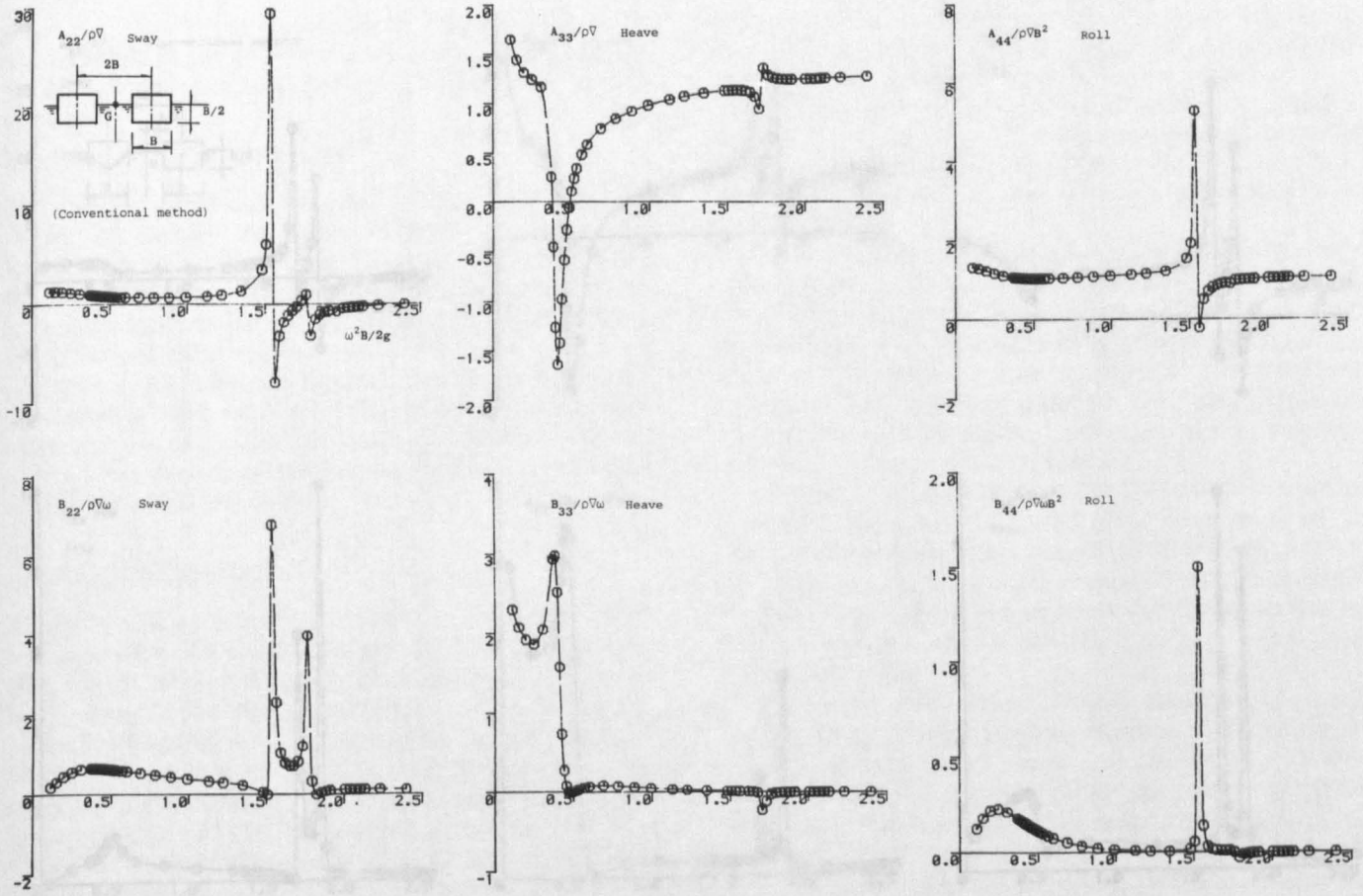

Figure 2. Hydrodynamic coefficients of a twin rectangular hull structure calculated by the conventional method, i.e. equations (2) and (9)

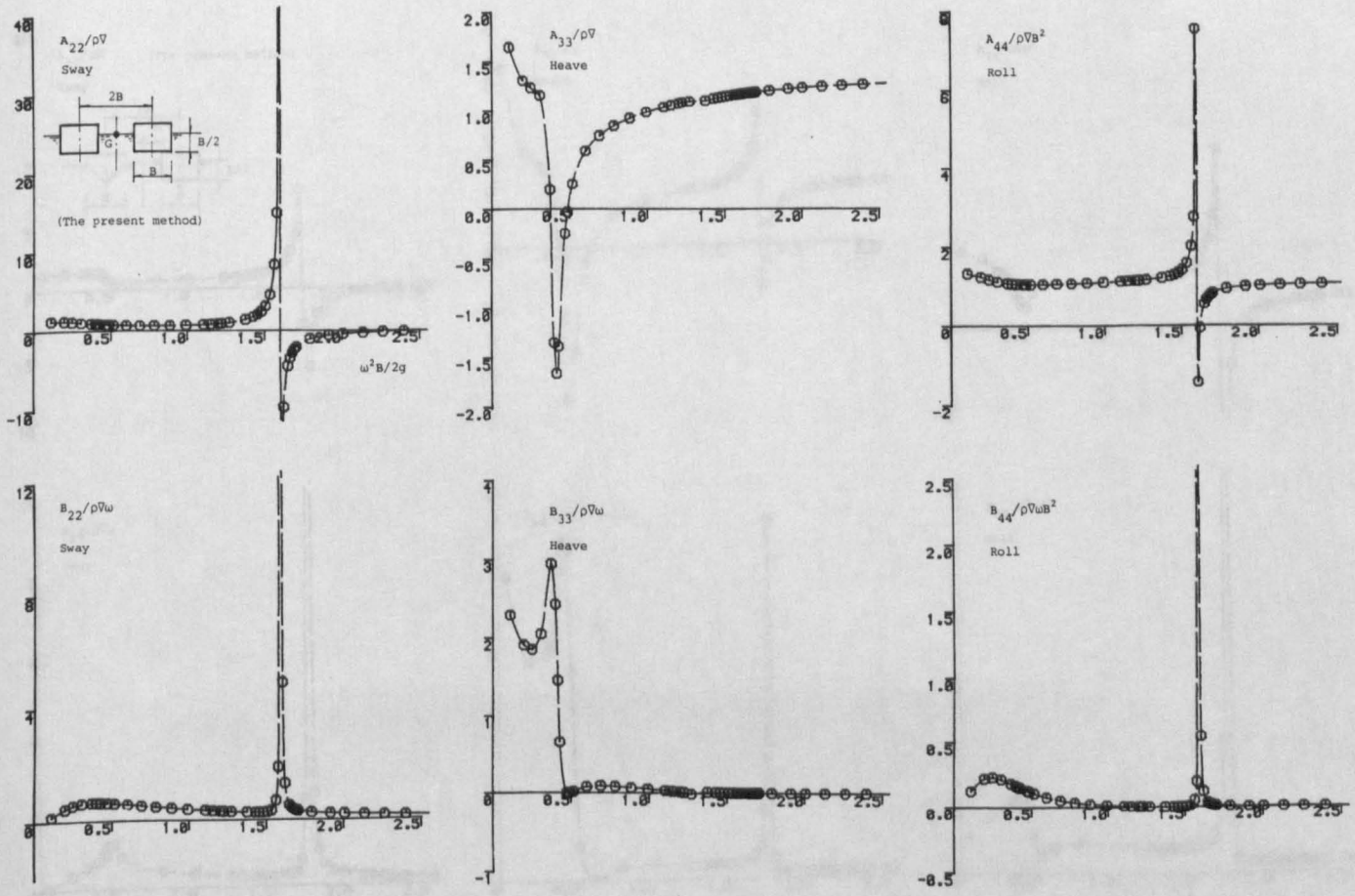

Figure 3. Hydrodynamic coefficients of a twin rectangular hull structure calculated by the present multiple Green's function method

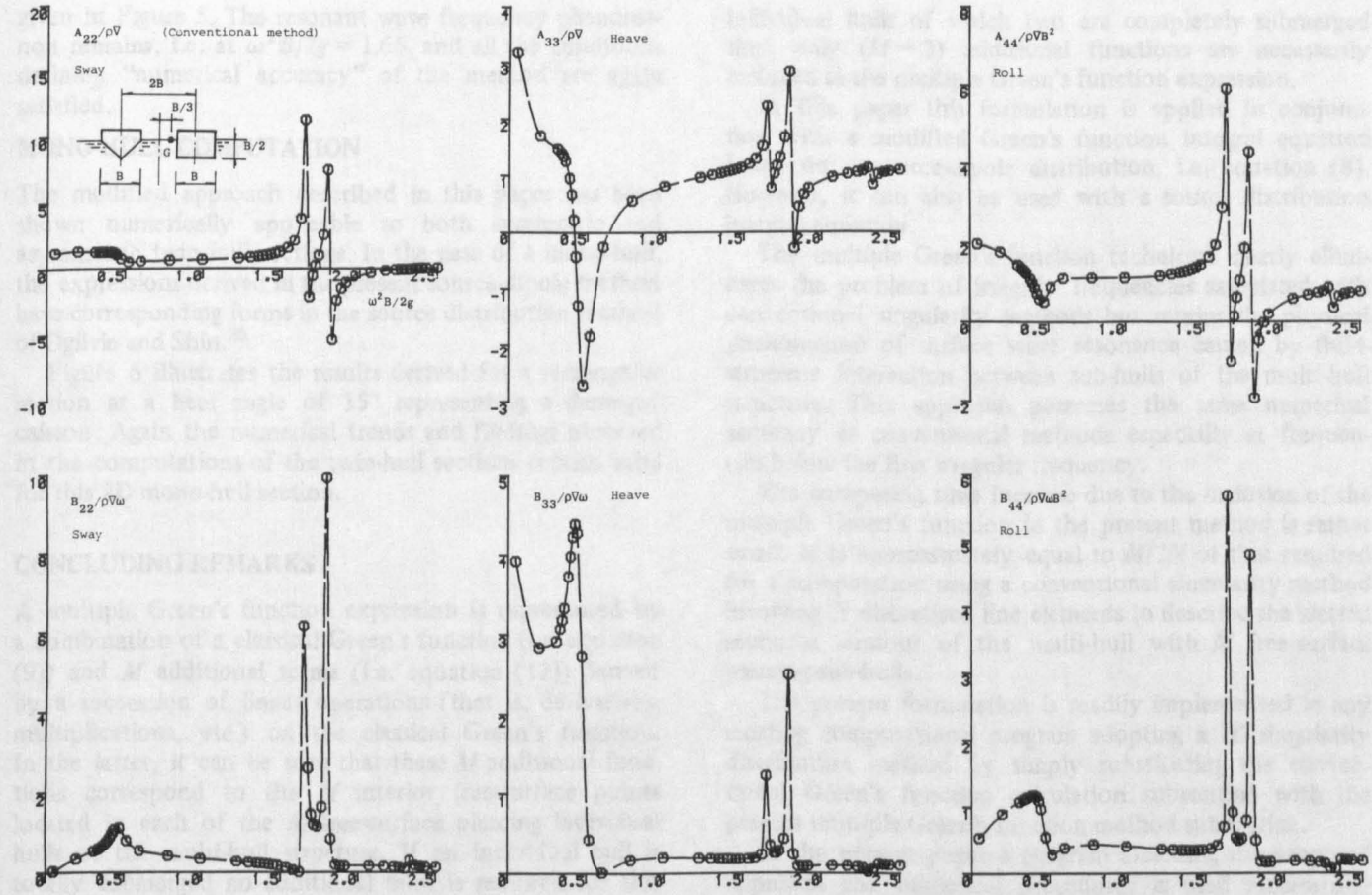

Figure 4. Hydrodynamic coefficients of a twin-hull consisting of a rectangular and a triangular hull calculated by the conventional method, i.e. equations (2) and (9)

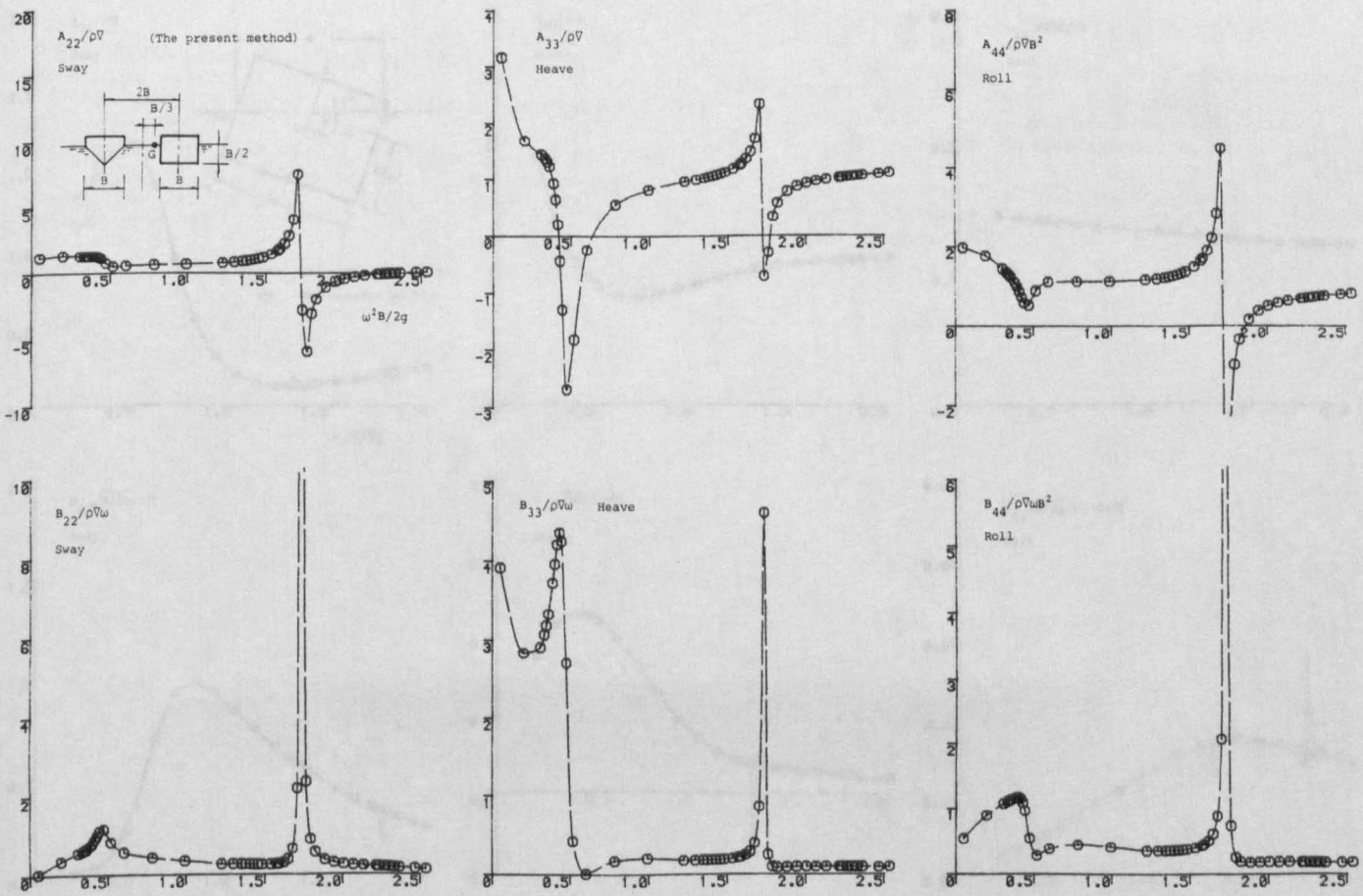

Figure 5. Hydrodynamic coefficients of a twin-hull consisting of a rectangular and a triangular hull calculated by the present multiple Green's function method

given in Figure 5. The resonant wave frequency phenomenon remains, i.e. at $\omega^2 B/2g = 1.66$, and all the conditions defining "numerical accuracy" of the method are again satisfied.

MONO-HULL COMPUTATION

The modified approach described in this paper has been shown numerically applicable to both symmetric and asymmetric twin hull sections. In the case of a mono-hull, the expressions derived in the present source-dipole method have corresponding forms in the source distribution method of Ogilvie and Shin.[20]

Figure 6 illustrates the results derived for a rectangular section at a heel angle of 15° representing a damaged caisson. Again the numerical trends and findings observed in the computations of the twin-hull sections remain valid for this 2D mono-hull section.

CONCLUDING REMARKS

A multiple Green's function expression is represented by a combination of a classical Green's function (i.e. equation (9)) and M additional terms (i.e. equation (12)) derived by a succession of linear operations (that is, derivatives, multiplications, etc.) on the classical Green's function. In the latter, it can be seen that these M additional functions correspond to the M interior free-surface points located in each of the M free-surface piercing individual hulls of the multi-hull structure. If an individual hull is totally submerged no additional term is required for this hull. For example, if a multi-hull body consists of M individual hulls of which two are completely submerged then only $(M-2)$ additional functions are necessarily included in the multiple Green's function expression.

In this paper this formulation is applied in conjunction with a modified Green's function integral equation based on a source-dipole distribution, i.e. equation (8). However, it can also be used with a source distribution integral equation.

The multiple Green's function technique clearly eliminates the problem of irregular frequencies associated with conventional singularity methods but retains the physical phenomenon of surface wave resonance caused by fluid-structure interaction between sub-hulls of the multi-hull structure. This approach possesses the same numerical accuracy as conventional methods especially at frequencies below the first irregular frequency.

The computing time increase due to the inclusion of the multiple Green's function in the present method is rather small. It is approximately equal to $M/2N$ of that required for a computation using a conventional singularity method involving N discretised line elements to describe the wetted sectional contour of the multi-hull with M free-surface piercing sub-hulls.

The present formulation is readily implemented in any existing computational program adopting a 2D singularity distribution method by simply substituting the conventional Green's function calculation subroutine with the present multiple Green's function method subroutine.

In the present paper a program including the proposed approach and numerical procedures is used successfully to study symmetric and asymmetric twin-hull structures

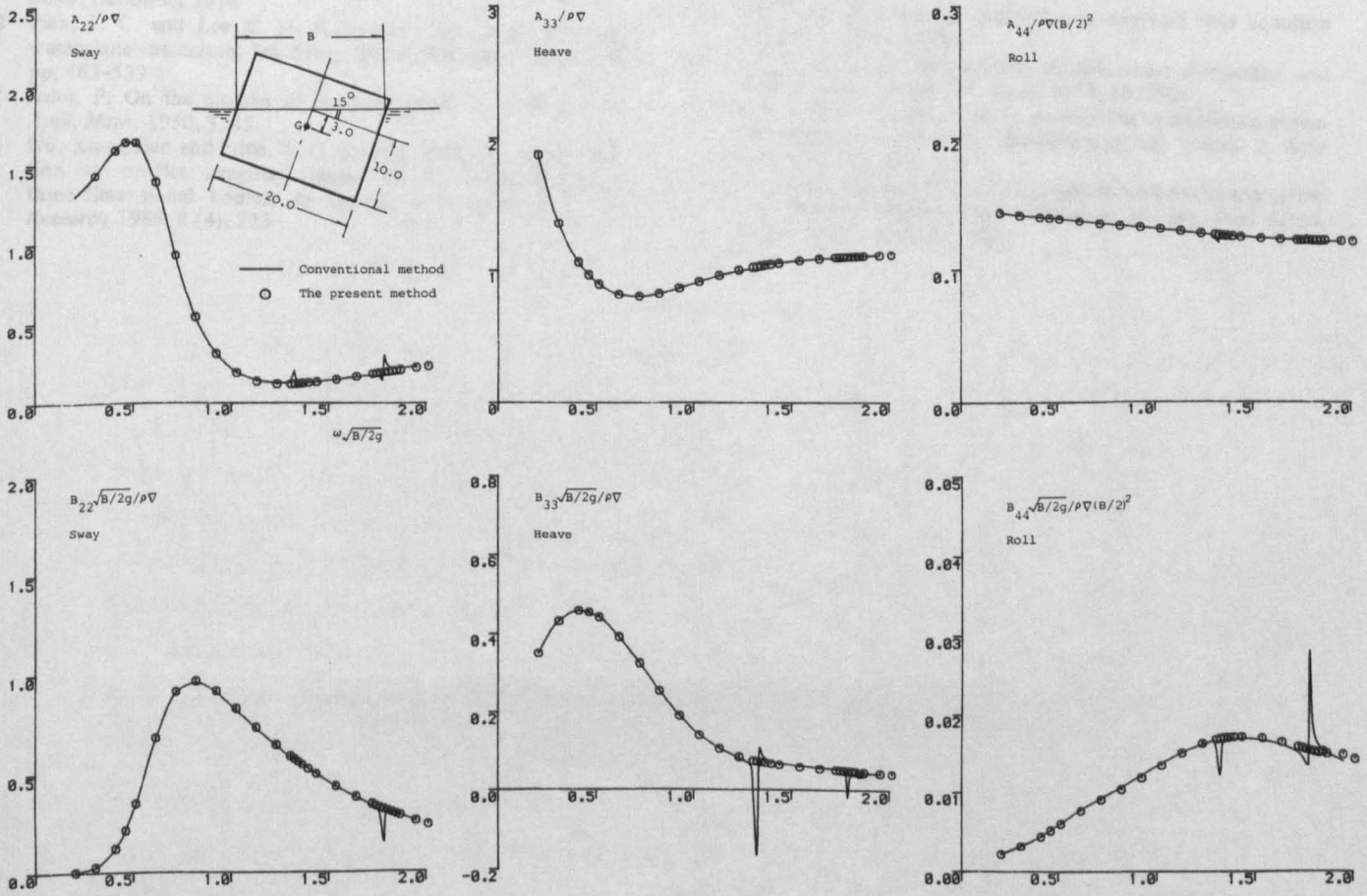

Figure 6. Comparisons between the results by the conventional method (the solid lines) and the present multiple Green's function method (the circular points) for a rectangular hull in 15° of heel

as well as an asymmetric mono-hull body. This technique is easily applied to a multi-hull structure of arbitrarily-shaped 2D cross section and to a problem involving multiple 2D bodies. Detailed results for these two cases will be published elsewhere.

REFERENCES

1 Hightower, J. D., Parnell, L. A., Strickland, A. T. and Warnshuits, P. L. SWATH technology development at the Naval Ocean Systems Centre, *Int. Conf. SWATH Ships and Adv. Multi-Hulled Vessels*, London, April 1985, Paper No. 14

2 Ursell, F. On the heaving motion of a circular cylinder on the surface of a fluid, *Quart. J. Mech. Appl. Math.* 1949, **2**, 218

3 Inglis, R. B. and Price, W. G. A three dimensional ship motion theory-comparison between theoretical predictions and experimental data of the hydrodynamic coefficients with forward speed, *Trans. Roy. Inst. Naval Archi.* 1982, **124**, 141

4 Wu, Xiong-Jian and Price, W. G. A source-dipole distribution procedure for numerical evaluation of wave-structure interaction problems, to be published

5 Price, W. G. and Wu, Y. S. Fluid interaction in multi-hull structures travelling in waves, *2nd Int. Symp. Pract. Design in Shipbuilding*, Tokyo and Seoul, 1983

6 Frank, W. Oscillation of cylinders in or below the free surface of deep fluids, *NSRDC Report 2375*, 1967

7 Martin, P. A. On the null-field equations for water-wave radiation problems, *J. Fluid Mech.* 1981, **113**, 315

8 Takagi, M., Furukawa, H. and Takagi, K. On the precision of various hydrodynamic solutions of two-dimensional oscillating bodies, *Int. Workshop on Ship and Platform Motions*, Berkeley, October 1983, pp. 450–466

9 Wang, S. and Wahab, R. Heaving oscillations of twin cylinders in a free surface, *J. Ship Research* 1971, **15** (1), 33

10 Ohkusu, M. Hydrodynamic forces on multiple cylinders in waves, *Int. Symp. Dynamics Marine Vehicles and Structures in Waves*, London, 1974, pp. 107–112

11 Lee, C. M. Theoretical prediction of motion of small waterplane-area, twin-hull (SWATH) ships in waves, *NSRDC Report 76-0046*, December 1976

12 Pien, P. C. and Lee, C. M. Motion and resistance of a low-waterplane catamaran, *9th Symp. Naval Hydrodynamics*, 1972, pp. 463–539

13 John, F. On the motion of floating bodies, II, *Comm. Pure Appl. Math.* 1950, **3**, 45

14 Wu, Xiong-Jian and Price, W. G. An equivalent box approximation to predict irregular frequencies in arbitrarily-shaped three-dimensional bodies, to appear in *J. Applied Ocean Research* 1986, **8** (4), 223

15 Wu, Xiong-Jian and Price, W. G. Is irregular frequency predictable and solvable? An efficient numerical procedure for hydrodynamic analysis of arbitrary two-dimensional bodies, to be published

16 Wu, Xiong-Jian and Price, W. G. Resonant waves in fluid-structure interaction problems involving a free-surface, *Int. Conf. on Vibration Problems*, Xi'an, June 1986, 439

17 Bishop, R. E. D., Price, W. G. and Wu, Y. A general linear hydroelasticity theory of floating bodies in a seaway, *Phil. Trans. Roy. Soc.* 1986, **A316**, 375

18 Haraguchi, T. and Ohmatsu, S. On an improved solution of the oscillation problem on non-wall sided floating bodies and a new method for eliminating the irregular frequencies, *Trans. West-Japan Soc. Nav. Archi.* 1983, **66**, 9 (in Japanese)

19 Sclavounos, P. D. and Lee, C. H. Topics on boundary-element solutions of wave radiation-diffraction problems, *4th Numerical Hydrodynamics Conf.*, Washington, DC, September 1985

20 Ogilvie, F. and Shin, Y. S. Integral-equation solutions for time-dependent free-surface problems, *J. Soc. Nav. Archi. Japan* 1978, **143**, 41

21 Sayer, P. An integral-equation method for determining the fluid motion due to a cylinder heaving on water of finite depth, *Proc. Roy. Soc.* 1980, **A372**, 93

22 Ursell, F. Irregular frequencies and the motion of floating bodies, *J. Fluid Mech.* 1981, **105**, 143

23 Martin, P. A. Integral-equation methods for multiple-scattering problems II. Water waves, *Quart. J. Mech. Appl. Math.* 1985, **1**, 119

24 Wu, Xiong-Jian and Price, W. G. Motion predictions of seagoing barges in offshore operations, *Offshore Operations Symp.*, ETCE, New Orleans, 23-27 February 1986, 83

25 Wu, Xiong-Jian and Price, W. G. A method to analyse shallow draft offshore structures with six modes of motion, *5th Int. Symp. on Offshore Mechanics and Arctic Engineering (OMAE)*, Tokyo, 13–18 April 1986, ASME Paper No. OMAE-937, 476

26 Wu, Xiong-Jian and Price, W. G. Behaviour of offshore structures with partially trapped free-surface water regions, *Offshore Mechanics and Arctic Engineering (OMAE) Speciality Symp.*, ETCE, New Orleans, 23-27 February 1986, ASME Paper No. OMAE-184, 255

27 Wu, Xiong-Jian. On the limitation of the null field equation method, to be submitted

28 Mei, C. C. Numerical methods in water-wave diffraction and radiation, *Ann. Rev. Fluid Mech.* 1978, **10**, 393

29 Hess, J. L. and Smith, A. M. O. Calculation of nonlifting potential flow about arbitrary three-dimensional bodies, *J. Ship Research* 1964, **8** (2), 22

30 Wu, Xiong-Jian and Price, W. G. Irregular frequencies associated with singularity distribution techniques, *Report, Dept Mech. Eng.*, Brunel University, 1984

APPENDIX 4.3.

SECOND INTERNATIONAL WORKSHOP ON WATER WAVES AND FLOATING BODIES
UNIVERSITY OF BRISTOL, U.K., 16-19 MARCH 1987

AN INTERIOR INTEGRAL EQUATION METHOD FOR WATER WAVE RADIATION AND DIFFRACTION PROBLEMS

by

Xiong-Jian Wu

Ship Hydrodynamics Laboratory, Shanghai Jiao-Tong University,China;
presently at Brunel, The University of West London, Uxbridge, Middlesex
UB8 3PH, U.K.

1. INTRODUCTION

The Green function integral equation governing the water wave-structure interaction problem can be expressed in an exterior, surface or interior integral equation form. Conventionally, in the field of marine hydrodynamics the surface integral equation is always employed in numerical computation because of the diagonally dominant property of the resultant matrix equation and sufficient experiences gained in practical applications. When an interior integral equation is adopted, the kernal function is never singular. However, according to Mei [1] the interior integral equation has not been used in water wave problems perhaps due to the following reasons:

(i) the resultant matrix equation would no longer be diagonally dominant,

(ii) the choice of the interior field points could be too arbitrary.

An effort to apply the interior integral equation has been made by Martin [2] who introduced from acoustics a null field equation method based on the original interior integral equation. Unfortunately, divergent solutions were found for both thin and wide elliptical sections. It seems that the derived null field equation may be valid only for circular sections and slightly perturbed geometries based on a semi-circle or some other simple geometries corresponding to the chosen basis of series functions. These limitations of the null field equation approach have been well discussed in electromagnetics, optics and acoustics (for example, by Bates et al, Phil. Trans. Royal Soc., 1977; van den Berg et al, J. Opt. Soc. Am., 1979; etc.).

In the present paper theoretical basis and numerical techniques to apply the interior integral equation to general geometric forms of ships and offshore structures are described.

2. INTEGRAL EQUATION AND DIAGONAL DOMINANT PROPERTY

The Green function integral equation governing the radiation or diffraction wave potential $\phi e^{-i\omega t}$ can be expressed as

$$\begin{Bmatrix} 4 \\ 2 \\ 0 \end{Bmatrix} \pi\phi(P) - \int_{S_w} \phi(Q) \frac{\partial G(P,Q)}{\partial n_Q} dS = - \int_{S_w} v_n(Q)\, G(P,Q)\, dS \quad \text{for } P(x,y,z) \in \begin{cases} D \\ S_w \\ \bar{D} \end{cases} \tag{1}$$

These three forms in eq. (1) may be referred to as the exterior, the surface and the interior integral equations corresponding to the locations of the field point P outside the body mean wetted surface S_w (i.e. in the exterior fluid domain D), on S_w and inside S_w (i.e. in the interior domain $\bar{D}$). The Green function has the form (Wehausen & Laitone, 1960):

$$G(P,Q) = 1/r_{PQ} + H(P,Q;k) = 1/\{(x-\xi)^2+(y-\eta)^2+(z-\zeta)^2\}^{1/2} + H(P,Q;k) \tag{2}$$

As far as the surface integral equation is concerned the Green function possesses a 1/r singularity for the case $(x,y,z) = (\xi,\eta,\zeta)$.

Rewrite eq. (1) approximately in a discretised form (for i = 1,2,...N) as†

$$\alpha\phi(Q_i) - \sum_{j=1}^{N} \phi(Q_j) \int_{\Delta S_{Q_j}} \frac{\partial}{\partial n_{Q_j}} (G(P_i,Q_j) - \delta_{ij}/r_{P_iQ_j})\, dS = - \sum_{j=1}^{N} v_n(Q_j) \int_{S_{Q_j}} G(P_i,Q_j)\, dS \tag{3}$$

with $\delta_{ij} = \begin{cases} 1 & \text{for } i = j \\ 0 & \text{for } i \neq j \end{cases}$

and define the SELF-INDUCED CONTRIBUTION FACTOR

$$\alpha = \begin{Bmatrix} 4\pi \\ 0 \end{Bmatrix} - \int_{\Delta S_{Q_i}} \frac{\partial}{\partial n_{Q_i}} (1/r_{P_iQ_i})\, dS \quad \text{for } P_i \in \begin{cases} D \text{ (neighbourhood of } S_w) \\ \bar{D} \text{ (any positions)} \end{cases} \tag{4}$$

For $r \to 0^{\pm}$, that is, P_i tends to Q_i from the exterior or the interior domain, α becomes 2π which is identical with the second form of eq. (1). For simplicity, a circular flat panel ΔS_{Q_i} is chosen together with a field point P_i of local coordinats $(0,0,\bar{z})$ as illustrated in Fig. 1. It can be readily derived that

$$\alpha = \begin{Bmatrix} 4\pi \\ 2\pi \\ 0 \end{Bmatrix} - 2\pi\, \mathrm{sign}(\bar{z}) \left(1 - \frac{|\bar{z}|}{\sqrt{a^2+\bar{z}^2}}\right) \quad \text{for } P_i \in \begin{cases} D \text{ (neighbourhood of } S_w) \\ S_w \\ \bar{D} \text{ (any positions)} \end{cases} \tag{5}$$

Values of α versus the non-dimensional distance $\bar{z}/a$ are shown in Fig. 2. It is apparent that the self-induced contribution factor α varies continously and smoothly from $0 \to 2\pi \to \gamma < 4\pi$ as the field point P_i moves from a far interior location, via the body surface S_w, to the exterior region neighbouring to the body surface. This conclusion holds for any arbitrary polygonal panels.

This discussion implies that if all the interior field points are chosen such that $|\bar{z}|$ is small the resultant matrix equation of the interior integral equation retains a similar diagonally dominant property to the surface integral equation approach.

† For P_i located in the exterior region not close to the body surface S_w, the first term in eq. (3) should be written as $\alpha\phi(Q_i) + 4\pi\{\phi(P_i) - \phi(Q_i)\}$.

3. CHOICE OF THE INTERIOR FIELD POINTS

As long as all the interior field points are located close to the body mean wetted surface S_w the resultant matrix equation of the interior integral formulation has the numerical advantage of diagonal domination. In practical numerical computation, all chosen interior control points make up an interior surface $\bar{S}$ which is parallel to the body surface S_w and with a scale reduction factor C_s slightly less than 1.0 (i.e. $C_s = 1.0 - \varepsilon$ for ε being a small positive value). In the two-dimensional case, a scale reduction factor value $C_s = 0.95$ implies that the area enclosed by the interior contour is about 90% of the cross-sectional area.

In such a manner all these interior points can be automatically produced by a computational programme suite ("HYDROINT") in terms of the same input data file for the computer package based on the surface integral equation technique.

4. NUMERICAL EXAMPLES

Extensive numerical applications of the present interior integral equation method to various ship forms and complicated offshore structures have been conducted to verify the proposed approach. Two examples are displyed in the present paper. Fig. 3 shows the calculated sway, heave and roll added mass and damping coefficients for a ship section. The two sets of data obtained from the surface and the interior integral equation techniques coincide very well. Since the ordinary Green function is used irregular frequencies occur when these computed hydrodynamic coefficients exhibit abrupt variations due to mathematical failures (cf Wu and Price, First Workshop, 1986 and J. Applied Ocean Res., Oct. 1986). The irregular frequencies appearing in the interior integral equation calculation are higher than those related to the surface integral equation formulation because of a reduced area of the interior free-surface bounded by the chosen artificial interior surface. However, when a modified Green function [3] is adopted there exist no irregular frequency effects. This may be confirmed by data given in Fig. 4. In Fig. 4 hydrodynamic coefficients for a rectangular section derived from the surface and the interior integral equations by means of the modified Green function are presented. Excellent agreement between the two formulation calculations can be observed and there is no mathematical failure due to irregular frequency problem. In addition to the similar numerical solution stability and accuracy the computing time required for the surface and the interior integreal equations is nearly the same.

5. CONCLUSIONS

(i) The resultant matrix equation of the interior integral equation can retain diagonal dominant feature if all the interior field points are arranged close to the body wetted surface.

(ii) It is proposed to locate these interior control points on an artificial interior surface which is close and parallel to the body surface.

(iii) In contrast with the null field equation method which seems free of irregular frequency effect but may have divergent solutions for more complicated geometries in practical applications, the interior integral equation itself can not eliminate difficulties associated with irregular frequency problem in a higher frequency range but it may be applicable to arbitrary ship forms and offshore structure geometries.

(iv) In combination with the modified Green function the present interior integral equation approach can remove irregular frequency influence and thus may be applied to a wider range of wave frequencies as well as body geometries.

(v) Numerical example studies confirm that the present method can be performed in a totally same manner as the conventional surface integral equation with the same input data, similar numerical stability indicated by associated values of a condition number, a similar degree of numerical accuracy achieved in nearly the same computer time.

REFERENCES

1. Mei, C.C. "Numerical methods in water-wave diffraction and radiation", Ann. Rev. Fluid Mech., Vol. 10, 1978, pp. 393-416.
2. Martin, P.A. "On the null-field equations for water wave radiation problems", J. Fluid Mech., Vol. 113, 1981, pp.315-332.
3. Wu, X.J. and Price, W.G. "A multiple Green function expression for the hydrodynamic analysis of multi-hull structures", J. Applied Ocean Res., Vol. 9, No.2, 1987, pp. 58-66.

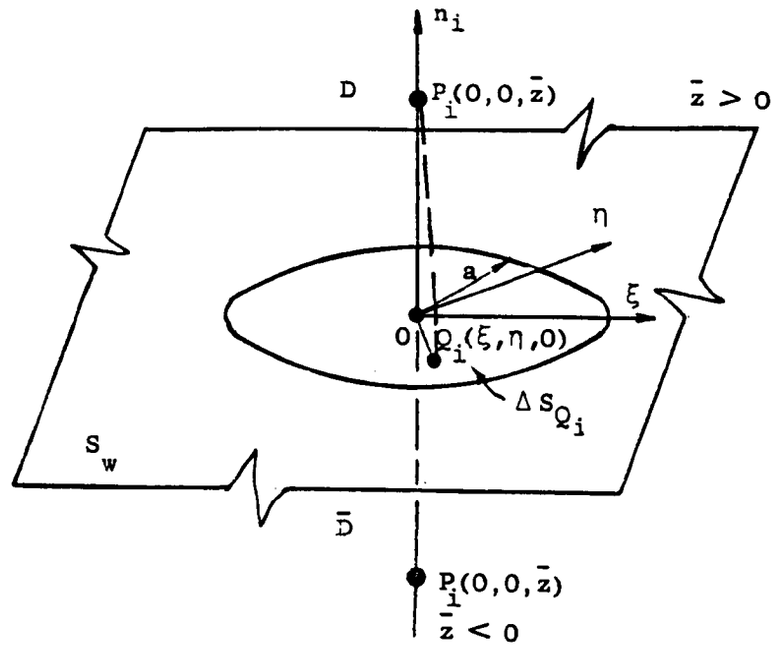

Fig. 1 A circular flat panel on the body wetted surface S_w together with a field point $P_i(0,0,\bar{z})$ exterior (i.e. $\bar{z} > 0$) or interior (i.e. $\bar{z} < 0$) to the body surface. a is the radius of the panel.

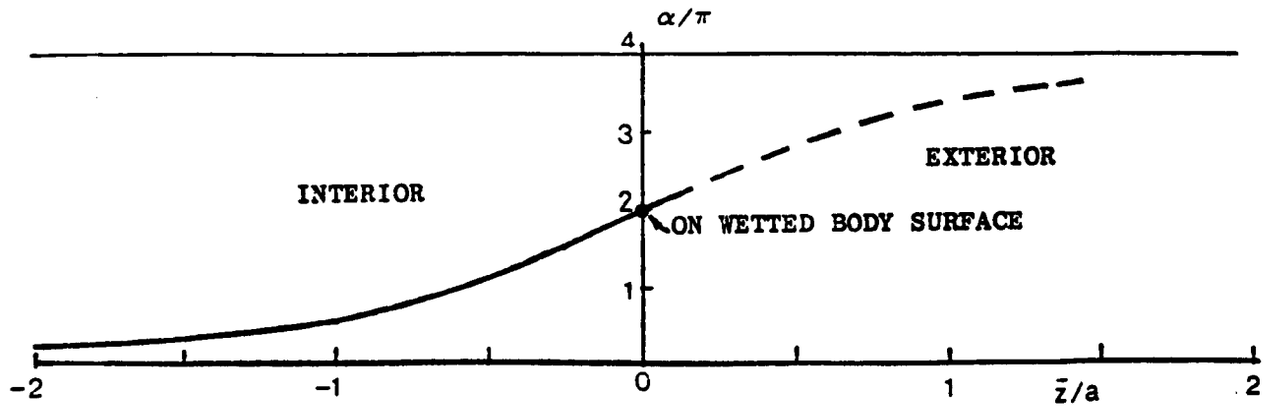

Fig. 2 Values of the self-induced contribution factor versus the distance between the field point P_i and a circular panel ΔS_{Q_i} of radius a calculated from eq. (5).

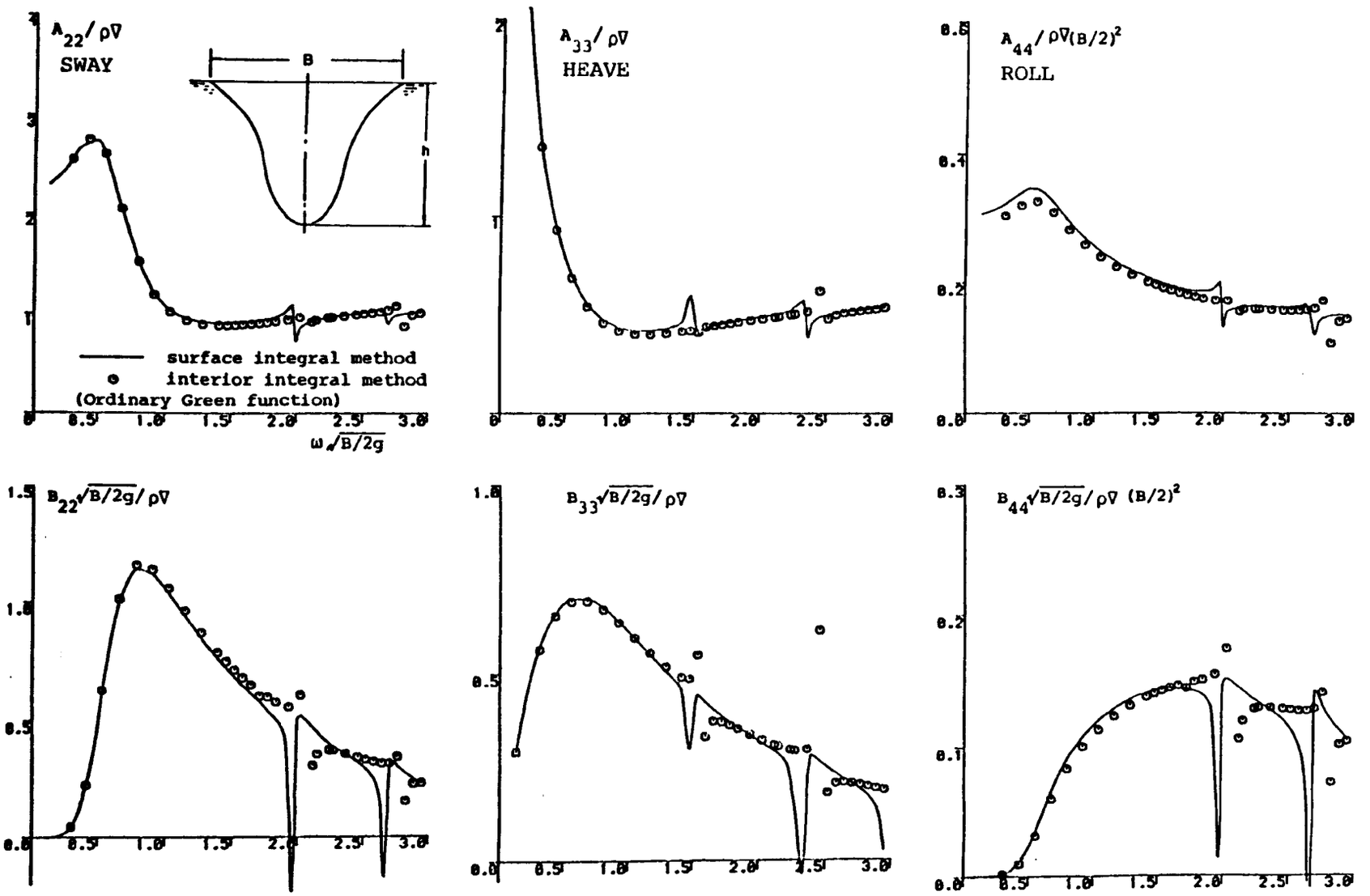

Fig. 3 Comparison between results from the surface and the interior integral equation methods (ordinary Green function).

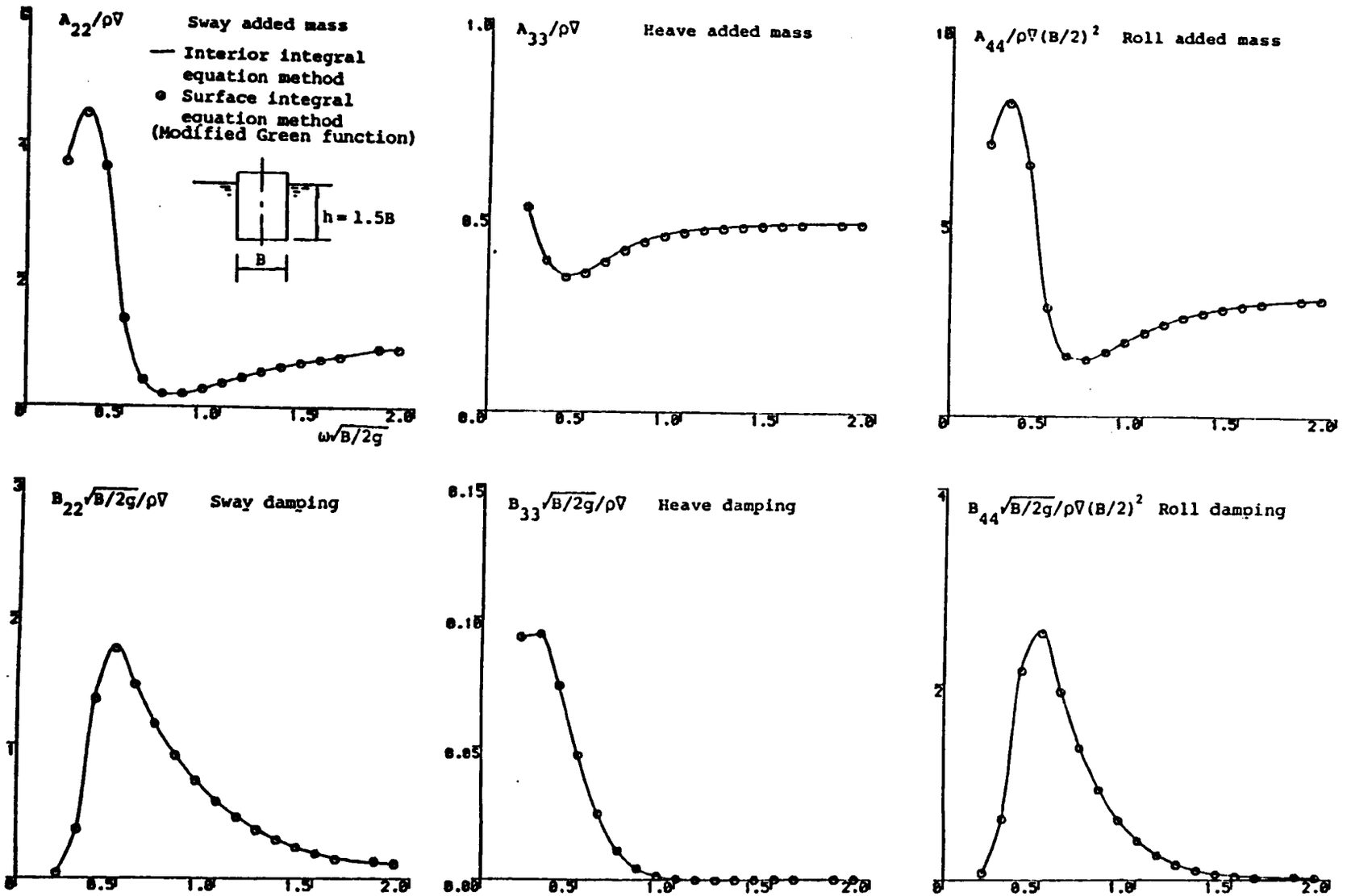

Fig. 4 Sway, heave and roll added mass and damping coefficients for a rectangular section of B/h = 2/3.

SOLUTION APPROXIMATIONS TO THE HORIZONTAL PLANE MOTIONS OF FULL-BODIED SLENDER OR SHALLOW DRAFT MARINE STRUCTURES

Xiong-Jian Wu*),**) and W.G. Price**)

*) *Ship Hydrodynamics Laboratory, Shanghai Jiao-Tong University, China*
**) *Department of Mechanical Engineering, Brunel, The Univ. of West London, United Kingdom*

Int. Shipbuild. Progr., 36, no. 407 (1989) pp. 237-282

Received : June 1988
Accepted: June 1988

On the basis of an order estimate analysis [1,2] approximate solutions to the horizontal plane motions (i.e. surge, sway, yaw) are derived for full-bodied slender and/or shallow draft floating marine structures excited by sinusoidal waves of long wavelength. These solutions are intended for use in the early stages of design and are obtained from analytical expressions (when the body is of a simple geometric form) or by computing simple expressions requiring only modest computing resources.

For the structures and wave conditions investigated it is shown that the contributions of the radiation forces and diffraction forces associated with the surge motion are higher order smaller quantities than the Froude-Krylov force and for sway and yaw motions these forces partially cancel one another leaving a residue of order smaller than the now dominant Froude-Krylov force component. The resulting approximate solutions of the motion predictions of a wide range of typical offshore structures are compared with experimental data and more traditional theoretical approaches incorporating contributions from radiation and diffraction force components. Satisfactory agreement is found not only at long wavelengths but also in shorter waves,

confirming the practical applicability of the approximations to describe the responses of full-shaped slender bodies, submerged slender bodies, shallow draft slender bodies and three-dimensional shallow draft structures such as a triangular deck of a jack-up rig.

1. Introduction

Many structures and vessels used in offshore operations, marine transport and in the servicing of offshore platforms, etc., possess forms described as

(a) slender, defined by the ratios of length L and beam B (i.e. $L/B >> 1$) and length to draft h, ($L/h >> 1$);
(b) shallow draft ($B/h >> 1$).

An additional feature to (a) and/or (b) is the fullness of the cross-sectional shape of the body. That is the structure has a relatively long parallel midbody with a midsection coefficient of order 1.0. The block coefficient C_b ($= \nabla/L\ Bh$, ∇ represents the volume displacement) is large and the hull is referred to as "full-bodied".

On the basis of the slenderness of the body, slender body theory [1,2] and strip method techniques [3] have been developed to evaluate the fluid actions (i.e. hydrodynamic coefficients, wave loads, etc.) associated with ship-like bodies travelling in waves. For barges, which are a typical group of "full-bodied slender structure", several practical, theoretical and experimental investigations into the hydrodynamic characteristics, motion behaviour and structural responses have been reported [4-9]. In particular, Wu and Price [8,9] find that it is surprisingly effective to derive approximate solutions of the horizontal plane motions (i.e. surge, sway and yaw) of the structures by including only the Froude-Krylov force contributions in the analysis, ignoring the radiation and wave exciting diffraction forces. It was shown that this approach greatly reduces computational effort without significantly decreasing the accuracy of the solution. Furthermore, this type of

approximation appears valid for a variety of three-dimensional shallow draft offshore structures of various waterplane geometries such as a circular dock [10], a triangular jack-up rig [9] and a square platform [10], etc. In these cases, comparisons between predictions and experimental data show good agreement confirming the intuitive approach, but a theoretical basis for the proposed approximate solutions has not been fully justified.

In a study of the surge motion of slender ships, Grim [11] introduced a similar simplification to the surge exciting force, representing it by a Froude-Krylov contribution only. However, in the present study, based on the slenderness parameter [1,2] or shallow draft parameter [9], a method is developed providing rational approximations to the solutions of all the horizontal plane motions for a full-bodied slender vessel or shallow draft structure excited by sinusoidal waves of long wavelength. If further the vessel is both slender and of shallow draft, the proposed approximate solutions may be of a higher degree of accuracy.

It is shown that for long wavelengths, the diffraction force due to the incident sinusoidal wave acting on a restrained full-bodied slender vessel and the radiation force arising from the body oscillatory sway or yaw motion are of the same order of magnitude as the Froude-Krylov force. The first two components are of a form which nearly cancel one another out, contributing a combined influence of much smaller magnitude than the now dominant Froude-Krylov component to the wave forces exciting the sway and yaw motions (as well as surge motion).

Comparisons of predictions from the proposed approach, two- and three-dimensional methods and experimental data illustrate the validity of the approximate solutions. The latter are demonstrated to be applicable and accurate in waves of long wavelength and retain considerable accuracy even when applied to waves of shorter length.

2. General mathematical formulation

For an arbitrary shaped three-dimensional rigid structure excited by sinusoidal waves of amplitude ζ_a, frequency ω, wave number k and heading angle β (= 180^o, head waves), the total linear velocity potential

Φ describing the structure-wave interaction may be represented by a summation of all the potential components ϕ^j. These are associated with the bodily motions of surge, sway, heave, roll, pitch, yaw (i.e. $X_j = X_{ja}\, e^{-i\omega t}$, j = 1,2,...,6 respectively), the diffraction potential ϕ^7, and the incident wave potential ϕ^0. That is

$$\Phi(x,y,z;t) = \phi\, e^{-i\omega t} = \left(\phi^0 + \phi^7 + \sum_{j=1}^{6} X_{ja}\, \phi^j\right) e^{-i\omega t} \tag{1}$$

with

$$\phi^0 = -\frac{i\, g\, \zeta_a}{\omega}\, W(z)\, e^{ik(x\cos\beta + y\sin\beta)} \tag{2}$$

where

$$W(z) = \begin{cases} e^{kz} & \text{for infinite water depth, } d = \infty \\ \dfrac{\cosh k(z+d)}{\cosh kd} & \text{for finite water depth, } d \end{cases}$$

and k satisfies the relationship

$$\left.\begin{matrix} k \tanh kd \\ k \end{matrix}\right\} = \nu = \frac{\omega^2}{g} \quad \text{for} \quad \begin{matrix} d \neq \infty, \\ d = \infty. \end{matrix}$$

The unknown velocity potentials ϕ^j (j = 1,2,...,7) can be solved using the Green's function integral equation (cf. [12]).

$$2\pi\, \phi(P) - \int_{S_w} \phi(Q)\, \frac{\partial G(P,Q)}{\partial n_Q}\, dS = -\int_{S_w} v_n(Q)\, G(P,Q)\, dS \tag{3}$$

where G(P,Q) denotes the appropriate Green's function, P(x,y,z) and $Q(\xi,\eta,\zeta)$ are two points on the wetted body surface S_w, and the normal velocity

$$v_n = \begin{cases} -i\omega n_j & \text{for } j = 1,2,...,6 \\ -\partial\phi^0/\partial n & \text{for } j = 7. \end{cases}$$

Here the unit normal vector

$$\vec{n} = (n_1, n_2, n_3)$$
$$\vec{n} \times (x - x_G,\ y - y_G,\ z - z_G) = (n_4, n_5, n_6)$$

and coordinates (x_G, y_G, z_G) denote the centre of gravity G defined in a suitable right-hand axis system with origin placed at amidships.

Let us assume that the velocity potential solutions ϕ^j exist and can be determined. This allows the added mass coefficient A_{rj} (j,r = 1,2,...,6) damping coefficient B_{rj} and diffraction wave force F_r^7 to be evaluated from the expressions [2]

$$\omega^2 A_{rj} + i\omega B_{rj} = -\int_{S_w} i\omega\rho\phi^j n_r \, dS \tag{4}$$

or

$$\begin{cases} A_{rj} = \frac{\rho}{\omega}\int_{S_w} \mathrm{Im}(\phi^j)\, n_r \, dS \\ B_{rj} = -\rho\int_{S_w} \mathrm{Re}(\phi^j)\, n_r \, dS \end{cases} \tag{5}$$

and

$$F_r^7 = -i\omega\rho\int_{S_w} \phi^7 n_r \, dS = -\rho\int_{S_w} \phi^r \frac{\partial\phi^0}{\partial n} \, dS. \tag{6}$$

The Froude-Krylov force is given by

$$F_r^0 = -i\omega\rho\int_{S_w} \phi^0 n_r \, dS. \tag{7}$$

In these equations, ρ denotes the fluid density and the real and imaginary parts of the complex potential amplitude ϕ^j are denoted by Re(•), Im(•) respectively.

The equation of motion describing the behaviour of the vessel in the sinusoidal seaway may be expressed in the form (cf. [9])

$$\sum_{j=1}^{6} [(M_{rj} + A_{rj}) \ddot{X}_j + (B_{rj} + B_{vrj}) \dot{X}_j + C_{rj} X_j] = (F_r^0 + F_r^7) e^{-i\omega t} \tag{8}$$

for r = 1,2,...,6. In this expression M_{rj} is the generalised mass, C_{rj} is the hydrostatic coefficient and B_{vrj} is a term introduced to describe the damping contribution due to viscosity, eddy making etc. The latter plays a significant role in depressing the magnitudes of the motions at the resonance frequencies.

Equation (8) may be rewritten in the form

$$\sum_{j=1}^{6} (-\omega^2 M_{rj} X_{ja}) - (F_r^H + F_r^S) = (F_r^0 + F_r^7) \tag{9}$$

where the term

$$F_r^H = \sum_{j=1}^{6} [\omega^2 A_{rj} + i\omega (B_{rj} + B_{vrj})] X_{ja} \tag{10}$$

represents the radiation force amplitude and the term

$$F_r^S = - \sum_{j=1}^{6} C_{rj} X_{ja} \tag{11}$$

describes the hydrostatic restoring force amplitude. As a simplification to the subsequent analysis for the horizontal plane motions, but with no loss of generality, it is assumed that the viscous damping term $B_{vrj} = 0$ in Equations (8) and (10).

For simplicity, let us assume that a single mode of motion $X_r(t)$ can exist, uncoupled from the remaining five motions. Thus from Equation (9) the motion amplitude can be expressed in the simplified form

$$X_{ra} = (F_r^0 + F_r^7 + F_r^H + F_r^S)/(-\omega^2 M_{rr}) =$$
$$= (F_r^0 + F_r^S)/(-\omega^2 M_{rr}) + F_r^B/(-\omega^2 M_{rr}) \qquad (12)$$

with the body induced force $F_r^B = F_r^H + F_r^7$, for each r = 1,2,...,6. Here the absolute value of the real motion amplitude is denoted by

$$|X_{ra}| = \begin{cases} X_a \text{ for } r = 1, \text{ surge amplitude} \\ Y_a \text{ for } r = 2, \text{ sway amplitude} \\ Z_a \text{ for } r = 3, \text{ heave amplitude} \\ \phi_a \text{ for } r = 4, \text{ roll amplitude} \\ \theta_a \text{ for } r = 5, \text{ pitch amplitude} \\ \psi_a \text{ for } r = 6, \text{ yaw amplitude} \end{cases}$$

and if the study is restricted to surge, sway and yaw motions, the hydrostatic restoring forces $F_j^S = 0$ (j = 1,2,6).

For the typical full-bodied slender structures under investigation, a two-dimensional strip theory formulation provides a more practical approach to evaluate the potentials than the three-dimensional version represented by Equation (3). That is, Equation (3) can be replaced by the equation [12]

$$\pi \phi(p) + \int_{C_w} \phi(q) \frac{\partial G(p,q)}{\partial n_q} \, d\ell = \int_{C_w} v_n(q) \, G(p,q) \, d\ell \qquad (13)$$

where G(p,q) is the appropriate two-dimensional Green's function, p(y,z) and q(η,ζ) are two points on the sectional contour $C_W(x)$ located at the longitudinal coordinate x. Thus the surface integral over the wetted surface S_W in Equations (4-7) can be substituted by integration of the sectional quantities over the longitudinal length, i.e.

$$\int_{S_W} (\cdot)\, dS = \int_{-L/2}^{L/2} dx \int_{C_W(x)} (\cdot)\, d\ell \simeq \sum_{n}^{N} \left[\int_{C_W(X_n)} (\cdot)\, d\ell\right] \Delta X_n \tag{14}$$

where N denotes the number of longitudinal divisions of the body.

3. Solution approximation based on slenderness

3.1. *The slenderness parameter*

The theory developed to describe the hydrodynamic analysis and the motions of slender, rigid, ship-like bodies in waves is well established [1,2,13,14). The body has port and starboard symmetry and the theory is based on a small parameter $\epsilon = B/L << 1$, denoting the slenderness of the body. The draft h is of the same order of magnitude as the beam such that $h/B = O(1)$ or $h/L = O(\epsilon)$. In general the non-dimensional coordinates of the centre of gravity and centre of buoyancy, i.e. $(x_G/L, y_G/L, z_G/L)$ and $(x_b/L, y_b/L, z_b/L)$ respectively are of order ϵ. The generalised normal components n_1 and n_4 are of similar order, i.e. $O(\epsilon)$, whilst the remaining normal components are treated as of order O(1).

For wavelengths λ comparable to the body length L, i.e. $L/\lambda = O(1)$ or $kL = O(1)$, the orders of magnitudes of the geometric quantities used to describe a slender marine structure are summarised in Table 1.

In the present paper, the water depth is assumed to be of order $d/\lambda = O(1)$ and this implies a "deep water" case, i.e. $d = \infty$ and $k = \nu$. However, the body draft related dimensions always remain an order ϵ or smaller such that $kh = 2\pi(h/L)/(\lambda/L) \simeq O(\epsilon)$ or smaller and the free surface condition

TABLE 1. Orders of main dimensions of a slender body

Surface	L/λ	B/λ	h/λ	Area	n_1	n_2	n_3	n_4	n_5	n_6	$(z_b-z_G)/L$
S_w	1	ϵ	ϵ	ϵ	ϵ,1*)	1	1	ϵ	1	1	ϵ

*) Applicable to the body with flat or blunt ends.

$$\frac{\partial \phi}{\partial z} - \nu\phi = 0 = \frac{\partial \phi}{\partial (z/h)} - (kh)\,\phi. \tag{15}$$

In the inner region this result can be replaced by a first approximation with respect to ϵ and Equation (15) is replaced by the rigid boundary condition

$$\frac{\partial \phi}{\partial z} = 0. \tag{16}$$

Thus, orders of magnitude of various potential components in Equation (1) and force components given by expressions (6,7,10,11) can be estimated based on Newman's analysis for a slender body in waves [1,2].

Table 2 provides estimates of the orders of magnitudes of each force component; that is, the inertia or body mass force F_j^M, the hydrostatic restoring force F_j^S, the Froude-Krylov force F_j^0, the radiation force F_j^H and the diffraction force F_j^7 acting on the structure. In the last column the total body induced force $F_j^B = F_j^H + F_j^7$ is listed and this information is deduced from the data given in the table as will be subsequently explained. Thus, under the specified conditions $L/\lambda = O(1)$, $B/\lambda = O(\epsilon)$ and $h/\lambda = O(\epsilon)$ it is observed that

(i) In an analysis of surge motion, the hydrostatic restoring force F_1^S is zero; the radiation and diffraction forces are both of order $\epsilon^4 \ln \epsilon$ (or ϵ^3 if the slender body has flat or blunt ends), whilst the inertia force F_1^M and the Froude-Krylov force F_1^0 are of order ϵ^2. The latter two components provide the dominant contributions to the total surge force.

TABLE 2. Orders of various forces on a slender body at wave length $L/\lambda = O(1)$

Mode	j	Mass F_j^M	Rest. F_j^S	F-K F_j^0	Radiation F_j^H	Diffraction F_j^7	$F_j^H+F_j^7= F_j^B$ ***)
Surge	1	ϵ^2	0	ϵ^2	$\epsilon^4 \ln\epsilon, \epsilon^3$*)	$\epsilon^4 \ln\epsilon, \epsilon^3$*)	$\epsilon^4 \ln\epsilon, \epsilon^3$*)
Sway	2	ϵ^2	0	ϵ^2	ϵ^2	ϵ^2	ϵ^3
Heave	3	ϵ^2	ϵ	ϵ	$\epsilon^2 \ln\epsilon$	$\epsilon^2 \ln\epsilon$	$\epsilon^2 \ln\epsilon$
Roll	4	ϵ^4	ϵ^3	ϵ^3	ϵ^4	ϵ^4	ϵ^4
Pitch	5	ϵ^2	ϵ	ϵ	$\epsilon^2 \ln\epsilon$	$\epsilon^2 \ln\epsilon$	$\epsilon^2 \ln\epsilon$
Yaw	6	ϵ^2	0	ϵ^2	ϵ^2	ϵ^2	ϵ^3

*) See the note in Table 1.

***) Results in this column are *derived* in Section 3.

(ii) For sway and yaw motions, all the forces are of order ϵ^2 except the hydrostatic forces when $F_2^S = 0 = F_6^S$.

(iii) In the heave (j = 3), roll (j = 4) and pitch (j = 5) modes the contributions from F_j^0 and F_j^S dominate all other force components. However, due to the resonance behaviour inherent in these motions, at or near a resonance frequency the contributions from F_j^M, F_j^H and F_j^7 can play an important role.

On the basis of Table 2 we shall assess the influence and the contributions of the various loading components in the determination of the *surge*, *sway* and *yaw* responses described by the simple, uncoupled expressions assumed in Equation (12).

3.2. *Surge motion*

From Equation (12) and Table 2, the surge motion amplitude (r = 1) is given by

$$X_{1a} = F_1^0/(-\omega^2 m) + F_2^B/(-\omega^2 m) \simeq F_1^0/(-\omega^2 m) + O\left(\epsilon^2 \ln \epsilon\right)$$

where $m = M_{11} = M_{22} = M_{33}$ is the mass of the body. Since $F_1^0/(-\omega^2 m)$ is of order 1 and the remaining term is of order ϵ or smaller, the first approximation of the surge motion of a slender marine structure can be expressed as

$$X_{1a} = F_1^0(-\omega^2 m) \simeq O(1). \tag{17}$$

Thus it can be concluded that to the first approximation in ϵ, the surge motion of a slender body is solely determined by the inertia and the Froude-Krylov forces as given in Equation (17).

It may be further shown that the coupling effect due to the pitch motion on the surge motion is of order ϵ provided that the pitch motion amplitude is of O(1). Therefore, to a first approximation this may be neglected and the previous conclusion resulting from Equation (17) remains valid for these coupled motions.

3.3. *Sway motion*

From Equation (12), the sway motion amplitude may be written as

$$\begin{aligned} X_{2a} &= F_2^0/(-\omega^2 m) + F_2^B/(-\omega^2 m) = \\ &= X_{2a}^* + F_2^B/(-\omega^2 m) = \\ &= O(1) + \{O(1) \text{ or smaller}\}. \end{aligned} \tag{18}$$

To simplify the analysis, it is assumed that the full-bodied structure has a uniform cross-sectional shape of area A along its length and a

volume displacement ∇. Thus it follows from Equations (2) and (7) that

$$X_{2a}^{*} = F_2^{0}/(-\omega^2 m) = \{-i\omega\rho \int_{S_w} \phi^0 n_2 \, ds\}/(-\omega^2 \rho \nabla) =$$

$$= i\zeta_a \sin(\bar{L})/\bar{L} \int_{C_w} e^{kz} \sin(ky \sin\beta) n_2 \, d\ell/kA =$$

$$= i\zeta_a \sin\beta \sin(\bar{L})/\bar{L} [1 + O(\epsilon)] =$$

$$= O(1) \tag{19}$$

since ky, kz, n_1 are of order ϵ, n_2 is O(1) and $\bar{L} = (kL \cos\beta)/2$.

From Equations (6), (2) and (4) the diffraction force

$$F_2^{7} = -\rho \int_{S_w} \phi^2 \frac{\partial \phi^0}{\partial n} \, dS =$$

$$= i\omega\rho\zeta_a \int_{S_w} \phi^2 (n_3 + i \sin\beta \, n_2 + i \cos\beta \, n_1) e^{kz} e^{ikz\cos\beta} \times$$

$$\times e^{iky\sin\beta} \, dS =$$

$$= i\zeta_a \sin\beta \int_{-L/2}^{L/2} e^{ikx\cos\beta} \, dx \int_{C_w(x)} (\omega\rho \, i\phi^2 n_2) \, d\ell \, [1 + O(\epsilon)] =$$

$$= i\zeta_a \sin\beta \int_{-L/2}^{L/2} [-\omega^2 a_{22}(x) - i\omega b_{22}(x)] e^{ikx\cos\beta} \, dx \, [1 + O(\epsilon)] =$$

$$= -i\zeta_a \sin\beta \sin(\bar{L})/\bar{L} (\omega^2 A_{22} + i\omega B_{22}) [1 + O(\epsilon)] =$$

$$= -(\omega^2 A_{22} + i\omega B_{22}) X_{2a}^{*} [1 + O(\epsilon)] =$$

$$= -(F_2^{H}/X_{2a}) X_{2a} [1 + O(\epsilon)] =$$

$$= O(\epsilon^2) O(1) [1 + O(\epsilon)] =$$

$$= O(\epsilon^2)$$

and the radiation force

$$F_2^H = (\omega^2 A_{22} + i\omega B_{22}) X_{2a} =$$
$$= (\omega^2 A_{22} + i\omega B_{22}) \{X_{2a}^* + F_2^B/(-\omega^2 m)\} =$$
$$= O(\epsilon^2).$$

The combination of the radiation and the diffraction forces yields

$$F_2^B = F_2^H + F_2^7 = -(\omega^2 A_{22} + i\omega B_{22}) X_{2a}^* O(\epsilon) +$$
$$+ F_2^B (\omega^2 A_{22} + i\omega B_{22})/(-\omega^2 m)$$

or

$$F_2^B = -(\omega^2 A_{22} + i\omega B_{22}) X_{2a}^* O(\epsilon)/\{1 + (\omega^2 A_{22} + i\omega B_{22})/(\omega^2 m)\} =$$
$$= O(\epsilon^3) \qquad (20)$$

and

$$F_2^B/(-\omega^2 m) = O(\epsilon^3)/O(\epsilon^2) = O(\epsilon),$$

since $X_{2a}^* = O(1)$ and both $(\omega^2 A_{22} + i\omega B_{22})$ and $(\omega^2 m)$ are of order ϵ^2.

Consequently, the sway motion amplitude given in Equation (18), can be rewritten as

$$X_{2a} = X_{2a}^* + F_2^B/(-\omega^2 m) = X_{2a}^* + O(\epsilon) \qquad (21)$$

and the results from this analysis imply that:

(i) Although the individual radiation and diffraction force components are each of order ϵ^2 (see Table 2), these largely cancel one another and their combination is of a higher order, i.e. ϵ^3, as given in Equation (20).

(ii) To the first approximation in ϵ, the sway motion of a full-bodied slender vessel given in Equation (21) can be expressed by

$$X_{2a} = F_2^0/(-\omega^2 m) \tag{22}$$

provided that the coupling effect due to the roll motion can be ignored.

(iii) It can be shown that the coupling effect due to the roll motion on the sway motion amplitude is a higher order small quantity provided that the roll motion amplitude is of order 1 and therefore its influence may be neglected. Thus, the first approximation given in Equation (22) is valid for the roll-coupled sway motion of a full-shaped slender structure in long wavelengths.

3.4. *Yaw motion*

Before extending the previous arguments to a discussion of the evaluation of the yaw motion, it is worthwhile to estimate the likely magnitude of the moment of inertia coefficient required in such a calculation. For simplicity, the moment of inertia about an axis perpendicular to the longitudinal axis of a uniform slender cylindrical body of length L and cross-sectional area A is given by

$$M_{66} = \frac{\rho L^3 A}{12} = m\left(\frac{L}{2\sqrt{3}}\right)^2 = m(K_{zz})^2 \tag{23}$$

where the yaw radius of gyration is

$$K_{zz} = L/2\sqrt{3}\,. \tag{24}$$

For a more realistic full-bodied slender marine structure, the value of the yaw radius of gyration K_{zz} is probably of a similar magnitude such that

$$\left(K_{zz} - \frac{L}{2\sqrt{3}}\right) / L = O(\epsilon) \tag{25}$$

and the longitudinal coordinate of the centre of gravity measured from amidships satisfies the condition

$$x_G/L = O(\epsilon). \tag{26}$$

In fact, for a cylindrical body of uniform cross-section with no trim the centre of gravity is at amidships so that $x_G = 0$.

The Froude-Krylov force associated with the yaw motion is

$$\begin{aligned} F_6^0 &= -i\omega\rho \int_{S_w} \phi^0 n_6 \, dS = \\ &= -i\omega\rho \int_{S_w} \phi^0 \{(x - x_G) n_2 - y n_1\} \, dS = \\ &= -i\omega^2 \zeta_a m I \sin\beta \{1 + O(\epsilon)\} = \\ &= O(1) \end{aligned} \tag{27}$$

where

$$I = \int_{-L/2}^{L/2} \frac{(x - x_G)}{L} e^{ikx\cos\beta} \, dx. \tag{28}$$

Following the previous arguments together with a strip method approximation it may be shown that

$$X^*_{6a} = F_6^{\,0}/(-\omega^2 M_{66}) =$$

$$= F_6^{\,0}/(-\omega^2 m K_{zz}^{\,2}) =$$

$$= i \zeta_a \sin \beta \frac{I}{K_{zz}^{\,2}} [1 + O(\epsilon)] = O(1) \tag{29}$$

$$F_6^{\,7} = -i \omega \rho \int_{S_w} \phi^7 n_6 \, dS =$$

$$= -\rho \int_{-L/2}^{L/2} (x - x_G) \, dx \int_{C_w(x)} \phi^2 \frac{\partial \phi^0}{\partial n} \, d\ell \, [1 + O(\epsilon)] =$$

$$= -i \zeta_a I \sin \beta \, (\omega^2 A_{22} + i \omega B_{22}) \, [1 + O(\epsilon)] =$$

$$= - (\omega^2 A_{22} + i \omega B_{22}) X^*_{6a} K_{zz}^{\,2} \, [1 + O(\epsilon)] =$$

$$= O(\epsilon^2) \tag{30}$$

and

$$F_6^{\,H} = (\omega^2 A_{66} + i \omega B_{66}) X_{6a} =$$

$$= (\omega^2 A_{22} + i \omega B_{22}) I_1 X_{6a} \, [1 + O(\epsilon)] =$$

$$= (\omega^2 A_{22} + i \omega B_{22}) K_{zz}^{\,2} \{X^*_{6a} + F_6^{\,B}/(-\omega^2 m K_{zz}^{\,2})\} \times$$

$$\times [1 + O(\epsilon)] =$$

$$= O(\epsilon^2) \tag{31}$$

since from Equations (25) and (26)

$$K_{zz}^{\,2}/I_1 = 1 + O(\epsilon)$$

where

$$I_1 = \int_{-L/2}^{L/2} \frac{(x - x_G)^2}{L}\, dx =$$

$$= L^2 \left\{ \frac{1}{12} + \left(\frac{x_G}{L} \right)^2 \right\}. \qquad (32)$$

A combination of Equations (30) and (31) results in the following expressions:

$$F_6^B = F_6^H + F_6^7 =$$

$$= -(\omega^2 A_{22} + i\omega B_{22}) \{ K_{zz}^2 X_{6a}^* O(\epsilon) + F_6^B [1 + O(\epsilon)]/(-\omega^2 m) \}$$

or

$$F_6^B = -(\omega^2 A_{22} + i\omega B_{22}) K_{zz}^2 X_{6a}^* O(\epsilon)/\{1 + (\omega^2 A_{22} + i\omega B_{22})/$$

$$/(\omega^2 m)\} =$$

$$= O(\epsilon^3) \qquad (33)$$

since K_{zz} and X_{6a}^* are O(1) whilst $(\omega^2 A_{22} + i\omega B_{22})$ and $(\omega^2 m)$ are $O(\epsilon^2)$.

Thus for the yaw motion, Equation (12) can be rewritten as

$$X_{6a} = X_{6a}^* + O(\epsilon) =$$

$$= F_6^0/(-\omega^2 M_{66}) + O(\epsilon) =$$

$$= O(1). \qquad (34)$$

Therefore, in line with the conclusions for the sway motion, the yaw motion of a slender structure of a full-bodied form or of nearly uniform cross-section can be predicted by the following first approximation

$$X_{6a} = F_6^0/(-\omega^2 \, m \, K_{zz}^2) \tag{35}$$

with contributions of order ϵ neglected.

3.5. *Analytical formulations*

On the basis of the approximation derived for the surge, sway and yaw motions of a full-bodied slender structure, analytical expressions describing these motions may be deduced for vessels of simple geometries.

3.5.1. *Rectangular barge*

For this case, the amplitude of surge (r = 1), sway (r = 2) and yaw (r = 6) motions are respectively described by the expressions

$$\left.\begin{matrix} X_{1a}/\zeta_a \\ X_{2a}/\zeta_a \end{matrix}\right\} = \left\{\begin{matrix} \cos\beta \\ \sin\beta \end{matrix}\right\} i \frac{\sin\bar{L}}{\bar{L}} \frac{\sin\bar{B}}{\bar{B}} \left(\frac{1 - e^{-kh}}{kh}\right) \tag{36}$$

$$\frac{X_{6a}}{k\,\zeta_a} = \frac{1}{(k\,K_{zz}^2)} \left(\frac{1 - e^{-kh}}{kh}\right) \left\{\left(\frac{L}{B}\right) \left[\left(\cos\bar{L} - \frac{\sin\bar{L}}{\bar{L}}\right)\bar{L} + \right.\right.$$

$$\left.\left. - 2i \frac{x_G}{L} \frac{\sin\bar{L}}{\bar{L}}\right] \sin\bar{B} - \left(\frac{B}{L}\right) \sin\bar{L} \left(\cos\bar{B} - \frac{\sin\bar{B}}{\bar{B}}\right)/\bar{B}\right\} \tag{37}$$

where $\bar{B} = (kB \sin\beta)/2$.

Although the previous results are derived from the condition $L/\lambda = O(1)$ and the data given in Table 2, nevertheless, it is interesting to speculate on the asymptotic behaviour of these analytical expressions. This is not strictly valid, but from the results presented it may be deduced that

(i) At very long wavelengths, the magnitudes of the amplitude of surge and sway responses tend to $\cos\beta$ and $\sin\beta$ respectively since both the limits of $\frac{\sin \bar{L}}{\bar{L}}$ and $\frac{\sin \bar{B}}{\bar{B}}$ are 1.0. These amplitudes decrease as the wavelength decreases, reaching zero values when

$$\frac{kL}{2}\cos\beta = \frac{L}{\lambda}\pi\cos\beta = \pi \quad \left(\text{i.e. } \frac{L}{\lambda}\cos\beta = 1.0\right)$$

or

$$\frac{kB}{2}\sin\beta = \frac{B}{\lambda}\pi\sin\beta = \pi \quad \left(\text{i.e. } \frac{B}{\lambda}\cos\beta = 1.0\right).$$

For smaller wavelengths, the amplitudes of the motion exhibit fluctuations of reducing magnitude.

(ii) The phases of these motions remain nearly constant, although changes of sign occur at short wavelengths.

3.5.2. *Circular cylinder*

For a long circular cylinder of uniform semi-cylinder underwater cross-section of radius R_0 and length L, the amplitudes of surge and sway motions are given by

$$X_{1a}/\zeta_a = i\cos\beta\,\frac{\sin \bar{L}}{\bar{L}}\,\{4\sin(kR_0\sin\beta)/[\pi(kR_0)^2\sin\beta] - C_1\} \quad (38)$$

$$X_{2a}/\zeta_a = i\,\frac{\sin \bar{L}}{\bar{L}}\,C_2 \quad (39)$$

with

$$\left.\begin{matrix} C_1 \\ C_2 \end{matrix}\right\} = \frac{4}{\pi kR_0}\int_0^{\pi/2} \begin{matrix} \cos\theta\cos \\ \sin\theta\sin \end{matrix} (kR_0\sin\beta\sin\theta)\, e^{-kR_0\cos\theta}\, d\theta$$

and the amplitude of yaw motion is

$$\frac{X_{6a}}{k\zeta_a} = \frac{I}{k K_{zz}^2} C_2 \tag{40}$$

with I given in Equation (28).

4. Submerged full-bodied slender structure

As an extension of the analysis described in the previous section, a study of the motions of submerged slender structures excited by waves is now considered. The body of length L, width B, height h is at an intermediate average submergence $T = (H_1 + H_2)/2$ where H_1 is the depth of the uppermost surface and $H_2 = H_1 + h$. This submergence depth is chosen such that the effects of wave resonance occurring in the water region above the body are negligible. The orders of magnitude of the main geometric features are the same as those given in Table 1 and the order of kT is assumed to be of $O(\epsilon)$ but this is not strictly defined and has some degree of arbitrariness.

4.1. *The orders of various forces*

Based on the reasoning given in Section 3.1, orders of magnitudes of the force components can be estimated for a typical submerged slender body. These are displayed in Table 3 and are defined with respect to the slenderness parameter $\epsilon = B/L$.

For the three horizontal motions of surge, sway and yaw, the estimates of these force components are the same as those for the free surface piercing slender body shown in Table 2. Therefore, the derived formulae, approximation solutions and conclusions deduced in Section 3 are valid for the submerged slender body. Moreover, by employing a similar agreement to the one used in the derivation for the sway modes in Section 3.3, it can be shown that a large cancellation effect also takes place in the evaluation of the heave motion for the submerged slender

TABLE 3. Orders of various forces on a submerged slender body of submergence T at wavelength $L/\lambda = O(1)$

Mode	j	Mass F_j^M	Rest. F_j^S	F-K F_j^0	Radiation F_j^H	Diffraction F_j^7	$F_j^H+F_j^7=$ $= F_j^{B***)}$
Surge	1	ϵ^2	0	ϵ^2	$\epsilon^4 \ln\epsilon, \epsilon^{3*)}$	$\epsilon^4 \ln\epsilon, \epsilon^{3*)}$	$\epsilon^4 \ln\epsilon, \epsilon^{3*)}$
Sway	2	ϵ^2	0	ϵ^2	ϵ^2	ϵ^2	ϵ^3
Heave	3	ϵ^2	0	ϵ^2	$\epsilon^2 \ln\epsilon$	$\epsilon^2 \ln\epsilon$	ϵ^3
Roll	4	ϵ^4	$\epsilon^3, \epsilon^{4**)}$	$\epsilon^3, \epsilon^{4**)}$	ϵ^4	ϵ^4	ϵ^4
Pitch	5	ϵ^2	$\epsilon^3, \epsilon^{4**)}$	ϵ^2	$\epsilon^2 \ln\epsilon$	$\epsilon^2 \ln\epsilon$	ϵ^3
Yaw	6	ϵ^2	0	ϵ^2	ϵ^2	ϵ^2	ϵ^3

*) See the note in Table 1.

**) Applicable when $(z_b - z_G)/L = O(\epsilon^2)$.

***) Results in this column are *derived* in Section 4.

body. This reduces the combined contribution of the radiation and diffraction forces (each of order $\epsilon^2 \ln \epsilon$) to order ϵ^3 and the dominant forces in the heave motion are the inertia and the Froude-Krylov components, both of order ϵ^2. This implies that to a first approximation in ϵ the heave motions may be expressed as:

$$X_{3a} = F_3^0/(-\omega^2 M_{33}) + O(\epsilon) = \\ = O(1). \tag{41}$$

In the determination of the heave an pitch motions of a slender body using strip theory, the pitch related hydrodynamic quantities are predicted from information associated with the heave motion. For the submerged body case, the pitch restoring force is given by

$$F_5^S = -C_{55} X_{5a} =$$
$$= -\rho g \nabla (z_b - z_G) X_{5a} =$$
$$= O(\epsilon^{2+n})$$

for $(z_b - z_G)/L = O(\epsilon^n)$. Assuming $(z_b - z_G)/L = O(\epsilon)$ or smaller it follows that, F_5^S is of order ϵ^3 or smaller and is a higher order small quantity than the other force components. Again, because of the large cancellation between the radiation and the diffraction forces, their combination is of order ϵ^3. Thus, the inertia and the Froude-Krylov force components of order ϵ^2 dominate the other components permitting a first approximation for the pitch motion to be expressed as

$$X_{5a} = F_5^0/(-\omega^2 m K_{yy}^2) + O(\epsilon) =$$
$$= O(1). \qquad (42)$$

Finally, in the roll mode, the hydrostatic restoring force

$$F_4^S = -C_{44} X_{4a} =$$
$$= -\rho g \nabla (z_b - z_G) X_{4a} =$$
$$= O(\epsilon^{2+n})$$

for $(z_b - z_G)/L = O(\epsilon^n)$. Adopting the previous assumption for $(z_b - z_G)/L = O(\epsilon)$ and $F_4^S = O(\epsilon^3)$ it follows that F_4^S and F_4^0 dominate the other force components, all of order ϵ^3.

If $(z_b - z_G)/L$ is assumed of $O(\epsilon^2)$, $F_4^S = O(\epsilon^4)$ and it can be shown that F_4^0 becomes of $O(\epsilon^4)$ as well. Thus all the force components for the roll modes are of the same order, ϵ^4, and therefore no simplified solution to the roll motion can be deduced.

The theoretical proof for the heave and pitch modes is similar to those presented in Sections 3.3 and 3.4 for the sway and yaw motions of a free surface piercing slender body and therefore are not repeated. As an example of a typical submerged structure used in offshore engineering, a long rectangular cylinder is considered and the heave and pitch motions solution approximations are now discussed.

4.2. *Heave motion*

Starting from Equation (7), it can be shown that for a long, submerged rectangular cylinder the Froude-Krylov force is defined by

$$F_3^0 = -\zeta_a \, gk \, (\rho \, L \, Bh) \, e^{-kT} \, \frac{\sinh (kh/2)}{(kh/2)} \, \frac{\sin \bar{L}}{\bar{L}} \, \frac{\sin \bar{B}}{\bar{B}} = O(\epsilon^2) \quad (43)$$

and the heave amplitude, given by Equation (12), may be expressed in the form

$$X_{3a} = X_{3a}^* + F_3^B/(-\omega^2 \, m) = O(1) \quad (44)$$

where

$$\begin{aligned} X_{3a}^* &= F_3^0/(-\omega^2 \, m) = \\ &= \xi_a \, e^{-kT} \, \frac{\sinh (kh/2)}{(kh/2)} \, \frac{\sin \bar{L}}{\bar{L}} \, \frac{\sin \bar{B}}{\bar{B}} = \\ &= \zeta_a \, e^{-kT} \, \frac{\sin \bar{L}}{\bar{L}} \, [1 + O(\epsilon)] = \\ &= O(1). \end{aligned} \quad (45)$$

From Equations (6), (2) and (4), the diffraction force can be written as

$$\begin{aligned} F_3^7 &= -\rho \int_{S_w} \phi^3 \, \frac{\partial \phi^0}{\partial n} \, dS = \\ &= \zeta_a \, e^{-kT} \, \frac{\sin \bar{L}}{\bar{L}} \int_{C_w} \omega \, \rho \, i \, \phi^3 \, n_3 \, d\ell \, [1 + O(\epsilon)] = \\ &= - (\omega^2 \, A_{33} + i \, \omega \, B_{33}) \, X_{3a}^* \, [1 + O(\epsilon)] = \\ &= O(\epsilon^2 \ln \epsilon) \end{aligned} \quad (46)$$

whilst the radiation force is given by

$$F_3^H = (\omega^2 A_{33} + i\omega B_{33}) X_{3a} =$$
$$= (\omega^2 A_{33} + i\omega B_{33}) [X_{3a}^* + F_3^B/(-\omega^2 m)] =$$
$$= O(\epsilon^2 \ln \epsilon). \tag{47}$$

A combination of Equations (46) and (47) yields

$$F_3^B = -(\omega^2 A_{33} + i\omega B_{33}) X_{3a}^* O(\epsilon)/[1 + (\omega^2 A_{33} + i\omega B_{33})/(\omega^2 m)] =$$
$$= O(\epsilon^3) \tag{48}$$

since

$$X_{3a}^* = O(1), (\omega^2 m) = O(\epsilon^2) \text{ and } (\omega^2 A_{33} + i\omega B_{33}) = O(\epsilon^2 \ln \epsilon).$$

From Equation (44) the heave amplitude is expressible in the form

$$X_{3a} = X_{3a}^* + O(\epsilon) \tag{49}$$

or to the first approximation in ϵ as

$$X_{3a} = F_3^0/(-\omega^2 m)$$

giving

$$X_{3a}/\zeta_a = e^{-kT} \frac{\sinh(kh/2)}{(kh/2)} \frac{\sin \bar{L}}{\bar{L}} \frac{\sin \bar{B}}{\bar{B}}. \tag{50}$$

4.3. *Pitch motion*

In pitch motion, the submerged rectangular cylinder is excited by a Froude-Krylov force component given from Equation (7) in the form

$$F_5^0 = -i\omega\rho \int_{S_w} \phi^0 n_5 \, dS =$$

$$= -i g \zeta_a (\rho L Bh) e^{-kT} \frac{\sin \bar{B}}{\bar{B}} \left\{ V \cos\beta \frac{\sin \bar{L}}{\bar{L}} + i k I \frac{\sinh (kh/2)}{(kh/2)} \right\}$$

$$= \omega^2 \zeta_a m I [1 + O(\epsilon)] =$$

$$= O(\epsilon^2) \tag{51}$$

where

$$V = \{e^{kh/2} [k (-H_1 - z_G) - 1] + e^{-kh/2} [k (H_2 + z_G) + 1]\}/(kh)$$

and I is given in Equation (28).

The hydrodynamic restoring force is given by

$$F_5^S = -C_{55} X_{5a} =$$

$$= -\rho g \nabla (z_b - z_G) X_{5a} =$$

$$= O(\epsilon^3) \tag{52}$$

and corresponding to Equation (12), we may define a modification pitch amplitude

$$X_{5a}^* = (F_5^0 + F_5^S)/(-\omega^2 M_{55}) =$$

$$= F_5^0 [1 + O(\epsilon)]/(-\omega^2 m K_{yy}^2) =$$

$$= i \zeta_a e^{-kT} \frac{\sin \bar{B}}{\bar{B}} \left\{ V \frac{\cos\beta}{k} \frac{\sin \bar{L}}{\bar{L}} + i I \frac{\sinh (kh/2)}{(kh/2)} \right\} [1 + O(\epsilon)] =$$

$$= -\zeta_a e^{-kT} \frac{I}{K_{yy}^2} [1 + O(\epsilon)] =$$

$$= O(1). \tag{53}$$

The adoption of a similar reasoning to the one discussed in Section 3.4, i.e. Equations (23-26) assumes the radius of gyration for pitch K_{yy} to satisfy the relationship

$$\left(K_{yy} - \frac{L}{2\sqrt{3}}\right) /L = O(\epsilon) \tag{54}$$

giving

$$K_{yy}^{\ 2}/I_1 = 1 + O(\epsilon)$$

where I_1 is defined in Equation (32) with $x_G = 0$.

In terms of a strip method, Equation (6) for the pitch diffraction force can be rewritten as

$$\begin{aligned} F_5^{\ 7} &= -i\,\omega\,\rho \int_{S_w} \phi^7\, n_6\, dS = \\ &= \rho \int_{-L/2}^{L/2} (x - x_G)\, dx \int_{C_w(x)} \phi^3\, \frac{\partial \phi^0}{\partial n}\, d\ell\, [1 + O(\epsilon)] = \\ &= -\zeta_a\, e^{-kT}\, I\, L \int_{C_w} \omega\,\rho\, i\, \phi^3\, n_3\, d\ell\, [1 + O(\epsilon)] = \\ &= (\omega^2\, A_{33} + i\,\omega\, B_{33})\, \zeta_a\, e^{-kT}\, I\, [1 + O(\epsilon)] \end{aligned} \tag{55}$$

whilst the radiation force is

$$\begin{aligned} F_5^{\ H} &= (\omega^2\, A_{55} + i\,\omega\, B_{55})\, X_{5a} = \\ &= (\omega^2\, A_{33} + i\,\omega\, B_{33})\, I_1\, X_{5a}\, [1 + O(\epsilon)] = \\ &= (\omega^2\, A_{33} + i\,\omega\, B_{33})\, K_{yy}^{\ 2}\, \{X_{5a}^* + F_6^{\ B}/(-\omega^2\, m\, K_{yy}^{\ 2})\} \times \\ &\qquad \times [1 + O(\epsilon)]. \end{aligned} \tag{56}$$

The addition of Equations (55) and (56) gives

$$\begin{aligned} F_5^{\ B} &= F_5^{\ H} + F_5^{\ 7} = \\ &= (\omega^2 A_{33} + i\,\omega\, B_{33})\, K_{yy}^{\ 2}\, X_{5a}^*\, O(\epsilon)/\{1 + (\omega^2 A_{33} + i\,\omega\, B_{33})/(\omega^2\, m) \\ &= O(\epsilon^3) \end{aligned}$$

since X^*_{5a} and K_{yy} are of order 1 and $(\omega^2 A_{33} + i\,\omega B_{33})$ and $(\omega^2 m)$ are of order ϵ^2.
Thus, the pitch motion is given by

$$X_{5a} = X^*_{5a} + O(\epsilon) =$$
$$= O(1). \tag{57}$$

Therefore, it follows that to the first approximation a long, submerged rectangular cylinder excited in pitch motion by sinusoidal waves of long wavelength is described by the expression

$$X_{5a}/k\,\zeta_a = F_5^0/(-\omega^2 m K_{yy}^2 K \zeta_a) =$$
$$= \frac{-1}{(k K_{yy})^2} e^{-kT} \frac{\sin \bar{B}}{\bar{B}} \left\{ I \frac{\sinh (kh/2)}{(kh/2)} - i V \frac{\cos \beta}{K} \frac{\sin \bar{L}}{\bar{L}} \right\}. \tag{58}$$

5. Shallow draft slender body

A shallow draft slender marine structure [9] is categorised by its dimensions of length L, maximum lateral beam B and draft h. Again the slenderness of the body is denoted by the parameter $\epsilon = B/L$ whilst the shallow draft feature is expressed by the relationship $h/B = O(\epsilon)$. That is, the magnitude of the draft is an order ϵ smaller than the beam and an order ϵ^2 smaller than the length.

Figure 1a illustrates a general shallow draft structure of wetted surface S_W. The orders of magnitude of the dimensions and generalised normal components n_r $(r = 1,2,...,6)$ are given in Table 4. Figure 1b shows a more specific shallow draft structure (e.g. a barge) which is dominated by a large flat or nearly flat bottom surface S_b and has vertical or nearly vertical end surfaces S_e and side walls S_s. The orders of magnitude of its dimensions and generalised normal components are listed in Table 5. For these shallow draft structures in waves of wavelength comparable to their body length L, i.e. $L/\lambda = O(1)$, it follows that $B/\lambda = O(\epsilon)$ and $h/\lambda = O(\epsilon^2)$.

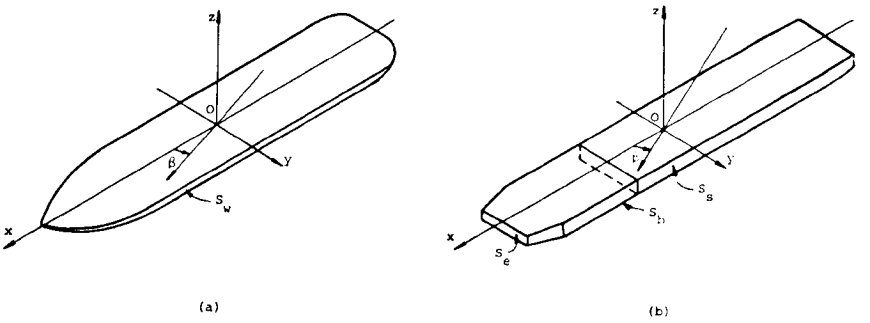

Figure 1. Schematic illustration of a shallow draft slender body:
(a) with a smooth wetted surface S_w;
(b) with a nearly flat bottom surface S_b and nearly vertical end surfaces S_e and side walls S_s.

TABLE 4. Orders of main dimensions of a shallow draft slender body of smooth wetted surface

Surface	L/λ	B/λ	h/λ	Area	n_1	n_2	n_3	n_4	n_5	n_6
S_w	1	ϵ	ϵ^2	ϵ	ϵ^2	ϵ	1	ϵ	1	ϵ

TABLE 5. Orders of main dimensions of a shallow draft slender body of a flat bottom S_b, nearly vertical end surfaces S_e and side walls S_s

Surface	L/λ	B/λ	h/λ	Area	n_1	n_2	n_3	n_4	n_5	n_6
S_e	1	ϵ	ϵ^2	ϵ^3	1	ϵ	ϵ^2	ϵ^2	ϵ	ϵ
S_s	1	ϵ	ϵ^2	ϵ^2	ϵ	1	ϵ	ϵ	ϵ	1
S_b	1	ϵ	ϵ^2	ϵ	ϵ^2	ϵ	1	ϵ	1	ϵ

TABLE 6. Orders of magnitudes of various forces on a shallow draft slender body

Mode	j	Mass F_j^M	Rest. F_j^S	F-K F_j^0	Radiation F_j^H	Diffraction F_j^7	$F_j^H+F_j^7=$ $=F_j^{B***)}$
Surge	1	ϵ^3	0	ϵ^3	$\epsilon^6 \ln\epsilon, \epsilon^{9/2}$†)	$\epsilon^6 \ln\epsilon, \epsilon^{9/2}$†)	$\epsilon^6 \ln\epsilon, \epsilon^{9/2}$†)
Sway	2	ϵ^3	0	ϵ^3	ϵ^4	ϵ^4	ϵ^5
Heave	3	ϵ^3	ϵ	ϵ	$\epsilon^2 \ln\epsilon$	$\epsilon^2 \ln\epsilon$	$\epsilon^2 \ln\epsilon$
Roll	4	ϵ^5	ϵ^3	ϵ^3	ϵ^4	ϵ^4	ϵ^4
Pitch	5	ϵ^3	ϵ	ϵ	$\epsilon^2 \ln\epsilon$	$\epsilon^2 \ln\epsilon$	$\epsilon^2 \ln\epsilon$
Yaw	6	ϵ^3	0	ϵ^3	ϵ^4	ϵ^4	ϵ^5

†) Applicable to bodies of geometric properties listed in Table 5.
***) Results in this column are *derived* in Section 5.

By analogy to the order analysis described in Section 3, Table 6 illustrates the estimated orders of magnitudes of the individual force components associated with the six rigid body motions of a slender, shallow draft structure. In comparison with the data presented in Table 2 for a slender body it is seen that

(i) for a slender, shallow draft body the inertia force components are an order smaller;

(ii) the additional restriction of shallow draft does not alter the orders of the fluid force components for heave, pitch and roll motions since these are strongly dependent on the bottom surface area or the waterplane area;

(iii) changes in the fluid force components for surge, sway and yaw motions arise because these horizontal modes depend on the

projected area of the wetted body surface onto the vertical plane. (For the types of bodies under consideration this is dominated by the contributions from the side walls and ends).

For the surge mode, both the inertia and the Froude-Krylov force components are of order ϵ^3 and the radiation and diffraction components are much smaller, of order $\epsilon^6 \ln \epsilon$. Hence, the latter two force components are an order $\epsilon^3 \ln \epsilon$ (or $\epsilon^{3/2}$ for a body with flat vertical ends) smaller than the former two components and, to the first approximation, the surge motion expression given in Equation (17) remains valid, i.e.

$$X_{1a} = F_1^0/(-\omega^2 m) + O\begin{pmatrix}\epsilon^3 \ln \epsilon \\ \epsilon^{3/2}\end{pmatrix} \simeq$$
$$= O(1). \tag{59}$$

For the sway or yaw mode, both the radiation and diffraction forces are of order ϵ^4 and these are an order ϵ smaller than the inertia and Froude-Krylov components. Moreover, since the shallow draft body is assumed slender, the cancellation process described in Section 3 between the radiation and the diffraction forces remains and the combination of these two components produces an overall contribution of $O(\epsilon^5)$ which is of $O(\epsilon^2)$ smaller than the Froude-Krylov force. Hence, the neglect of these contributions to the wave forces leads to errors of order ϵ^2 in the predictions of the sway or yaw motions of a shallow draft slender body, namely,

$$X_{ja} = F_j^0/(-\omega^2 M_{jj}) + O(\epsilon^2) =$$
$$= O(1) \qquad \text{for } j = 2 \text{ or } 6. \tag{60}$$

Thus, it may be concluded that when a slender body is of shallow draft, the motion approximations for the surge, sway and yaw motions using only the Froude-Krylov force components will provide satisfactory estimates.

6. Three-dimensional shallow draft body

In addition to the three kinds of slender marine structures, discussed in Sections 3-5, a three-dimensional shallow draft body is now investigated. For this structure the length and beam (maximum width) are of the same order, i.e. $L/\lambda = O(1) = B/\lambda$ and the draft h to length ratio is defined by the small parameter $\epsilon = h/L$. Orders of magnitude of the main geometric particulars of these structures are displayed in Table 7.

TABLE 7. Orders of main dimensions of a three-dimensional shallow draft body

Surface	L/λ	B/λ	h/λ	Area	n_1	n_2	n_3	n_4	n_5	n_6
S_w	1	1	ϵ	1	ϵ	ϵ	1	1	1	ϵ

6.1. *Motion approximation*

Because the draft of the structure is small, in long waves the replacement of the free surface condition (Equation (15)) by the rigid boundary condition (Equation (16)) in the inner region is valid. The application of the three-dimensional formulae in Equations (2-12) allows estimates of the orders of magnitudes of the various force components acting on the three-dimensional body to be determined. These are listed in Table 8. It can be seen that for the six rigid body modes the inertia forces are of order ϵ and the hydrostatic restoring forces are either zero (surge, sway, yaw) or O(1) (heave, roll, pitch). For surge, sway and yaw modes the Froude-Krylov forces are of order ϵ and these together with the inertia forces dominate the radiation and diffraction forces which are estimated to be of order ϵ^2.

Thus, the uncoupled motion Equation (12) may be written in the form

TABLE 8. Orders of magnitudes of various forces on a three-dimensional shallow draft body

Mode	j	Mass F_j^M	Restoring F_j^S	F-K F_j^0	Radiation F_j^H	Diffraction F_j^7	$F_j^H+F_j^7=$ $=F_j^{B***})$
Surge	1	ϵ	0	ϵ	ϵ^2	ϵ^2	ϵ^2
Sway	2	ϵ	0	ϵ	ϵ^2	ϵ^2	ϵ^2
Heave	3	ϵ	1	1	1	1	1
Roll	4	ϵ	1	1	1	1	1
Pitch	5	ϵ	1	1	1	1	1
Yaw	6	ϵ	0	ϵ	ϵ^2	ϵ^2	ϵ^2

***) Results in this column are *derived* in Section 6.

$$X_{ja} = F_j^0/(-\omega^2 M_{jj}) + O(\epsilon) \qquad \text{for } j = 1,2,6 \qquad (61)$$

and to first approximation in ϵ reduces to

$$X_{ja} = F_j^0/(-\omega^2 M_{jj}) \qquad \text{for } j = 1,2,6. \qquad (62)$$

6.2. *Analytical formulation*

On the basis of the simple, uncoupled approximation given in Equation (62), analytic formulae are available for three-dimensional shallow draft structures of simple waterplane geometry. Some of these have been derived and applied by the authors based on previous intuitive findings rather than on the theoretical evidence given in the present paper. Here, only results are quoted for the following four simple geometries.

6.2.1. *A circular dock*

The surge (or sway) motion of a shallow draft dock of radius R_0 and draft h can be formulated from Equation (62) in the form [10]

$$X_{1a}/\zeta_a = i \left(\frac{1 - e^{-kh}}{kh}\right) \frac{2 J_1 (kR_0)}{kR_0} \tag{63}$$

where $J_1(\cdot)$ is the Bessel function of the first kind of order 1.

6.2.2. *An elliptic dock*

The surge and sway motions of an elliptic dock of major and minor axes a and b respectively, i.e. L = 2a and B = 2b, and a shallow draft h, can be expressed as [15]

$$\frac{X_{ja}}{\zeta_a} = \frac{F_j^0}{-\omega^2 m} = i \left(\frac{1 - e^{-kh}}{kh}\right) \frac{2}{k a b} \sum_{n=0}^{\infty} (-1)^n \times$$

$$\times \begin{cases} b A_1^{(2n+1)} Ce_{2n+1}(\beta,q) Mc_{2n+1}^{(1)} (\xi_0,q) \\ a B_1^{(2n+1)} Se_{2n+1}(\beta,q) Ms_{2n+1}^{(1)} (\xi_0,q) \end{cases} \quad \text{for } j = \begin{cases} 1 \\ 2 \end{cases} \tag{64}$$

with $q = \frac{k^2 c^2}{4}$, $c^2 = a^2 - b^2$ and $\xi_0 = \frac{1}{2} \ln \frac{a + b}{a - b}$.

Here $Ce_m(\cdot)$ and $Se_m(\cdot)$ are the even and odd Mathieu functions of the first kind of integral order of period π (for m = 2n) or 2π (for m = 2n+1) whilst $Mc_m^{(j)}(\cdot)$ and $Ms_m^{(j)}(\cdot)$ are the even and odd modified Mathieu functions of the j-th kind of integral order of period πi (for m = 2n) of $2\pi i$ (for m = 2n+1). The terms $A_1^{(2n+1)}(q)$ and $B_1^{(2n+1)}(q)$ are the coefficients of the first term in the expansion forms of $Ce_{2n+1}(v,q)$ and $Se_{2n+1}(v,q)$ relating to the characteristic numbers a_{2n+1} and b_{2n+1} (see for example Abramowitz and Stegun [16]).

6.2.3. *A triangular platform*

A floating jack-up rig may be idealised as a shallow draft equilateral triangular platform [9,17]. For this body with side length B, the first order approximations describing the surge and sway motions deduced from Equation (62) are given by [9]

$$\left.\begin{matrix} X_{1a}/\zeta_a \\ X_{2a}/\zeta_a \end{matrix}\right\} = \frac{4}{\sqrt{3}\,kB}\,\frac{1-e^{-kh}}{kh}\left[\left\{\begin{matrix} 1/2 \\ \sqrt{3/2} \end{matrix}\right\}\frac{\sin\alpha_1 - i(1-\cos\alpha_1)}{\alpha_1} + \right.$$

$$+\left\{\begin{matrix} 1/2 \\ \sqrt{3/2} \end{matrix}\right\}\frac{\sin\alpha_2 - i(1-\cos\alpha_2)}{\alpha_2} +$$

$$\left.+\left\{\begin{matrix} -1 \\ 0 \end{matrix}\right\}\frac{(\cos\alpha_3 - i\sin\alpha_3)\sin\alpha_4}{\alpha_4}\right] \qquad (65)$$

where

$$\left.\begin{matrix} \alpha_1 \\ \alpha_2 \end{matrix}\right\} = \frac{\sqrt{3}}{2}\,kB\,(\cos\beta \mp \sin\beta/\sqrt{3})$$

$$\alpha_3 = \frac{\sqrt{3}}{2}\,kB\cos\beta$$

$$\alpha_4 = \frac{1}{2}\,kB\sin\beta.$$

6.2.4. *A rectangular platform*

For a three-dimensional shallow draft rectangular platform [10] the analytical formulations for the surge, sway and yaw motions are the same as those for a slender rectangular cylinder given in Equations (36) and (37).

7. Numerical studies

To verify the previous theoretical findings several numerical studies on full-bodied slender structures and shallow draft structures were performed. Where appropriate the derived analytic formulae for the surge, sway and yaw motions were compared with results derived from more sophisticated two-dimensional and three-dimensional numerical approaches as well as experimental data.

7.1. *Full-bodied slender structures*

A *rectangular cylinder* of length L = 100 m, beam B = 20 m and draft h = 10 m was adopted in this study. These dimensions denote a structure of block coefficient C_b = 1.0, L/B = 5.0 and h/B = 0.5, satisfying the assumptions adopted in the theory described in Section 3.

A comparison of predictions was performed based on the following three numerical approaches (Figures 2-4):

(i) A two-dimensional Green's function method using a modified Green's function which is free of irregular frequencies when applied to mono, twin and multi-hulled bodies [18,19]. In the computation the cross-sectional contour of the body (see Figure 2) is subdivided into 16 segments. Calculated results are denoted by hollow circular points.

(ii) A fully three-dimensional Green's function method [9,19] is used and the mesh arrangement in these computations involves 96 panels as shown in Figure 3. These predictions are represented by solid circular points.

(iii) The present approximate solutions given in Equations (36) and (37) are denoted by solid lines.

The calculated sway motion responses excited by unit amplitude regular waves approaching from the direction of beam seas ($\beta = 90^o$) to

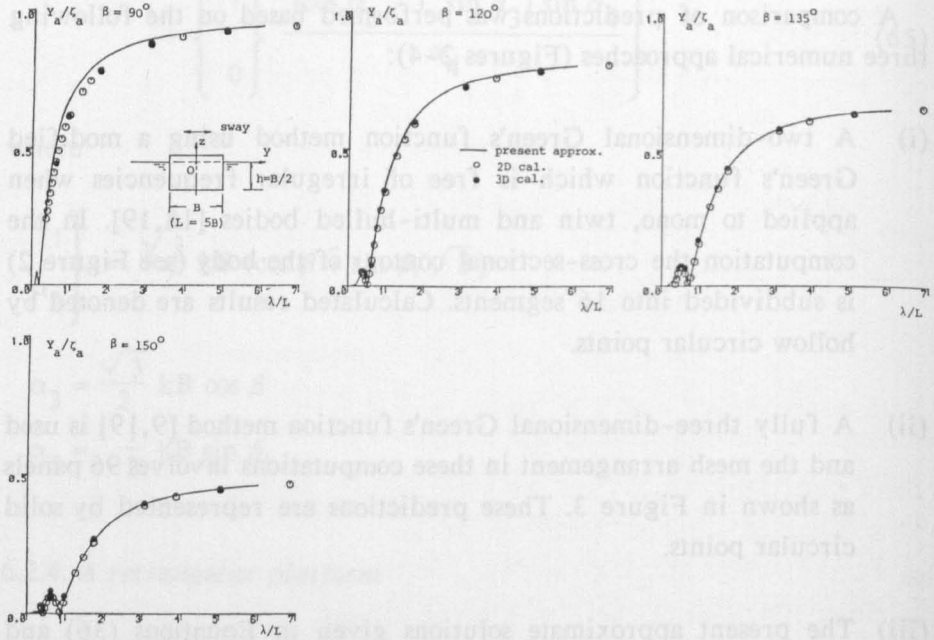

Figure 2. Sway responses of a rectangular cylinder of dimensions h = B/2 and L = 5B for comparison between the 2D and 3D Green's function integral equation method calculations and the present analytical approximation.

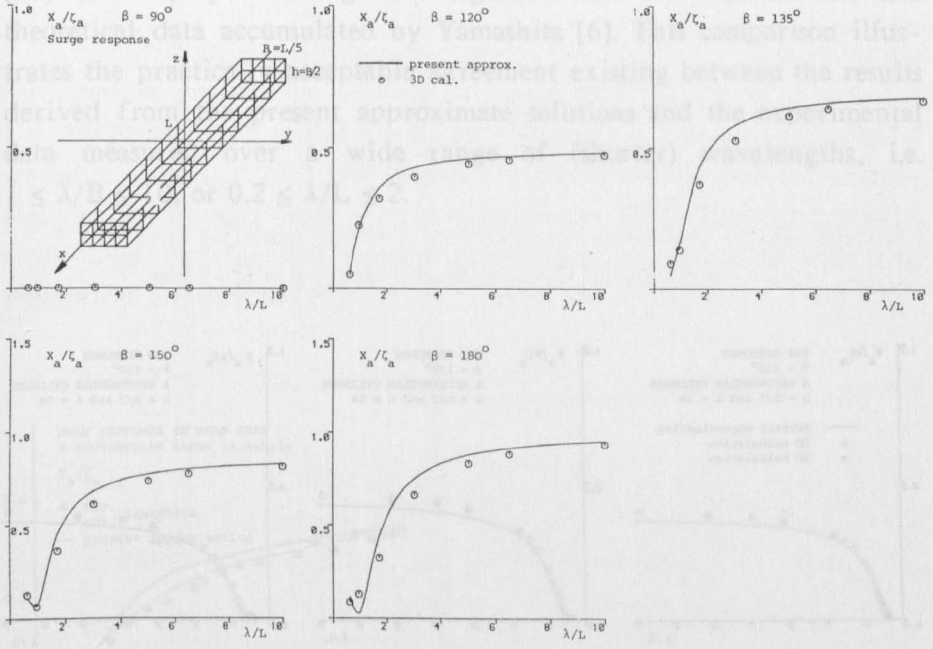

Figure 3. Surge responses of a rectangular cylinder of dimensions h = B/2 and L = 5B for comparison between the 3D Green's function integral equation method calculations and the present analytical approximation.

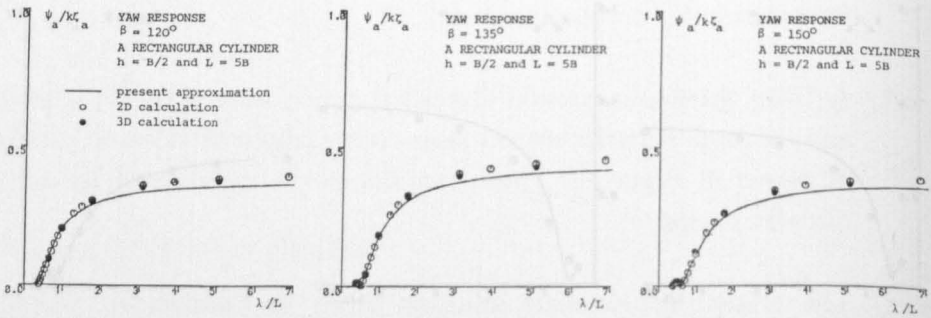

Figure 4. Yaw responses of a rectangular cylinder of dimensions h = B/2 and L = 5B for comparison between the 2D and 3D Green's function integral equation method calculations and the present analytical approximation.

bow seas (β = 120°, 135° and 150°) are shown in Figure 2. The data derived from the three approaches show good correlation at each heading. In Figure 3, the surge responses are displayed together with the results from the three-dimensional calculation. Good correlation can be observed for wave lengths $\lambda/L \leq 2$ and $\lambda/L \geq 5$. At wavelengths around $\lambda/L \simeq 3.0$, a deviation of approximately 10% exists.

Figure 4 illustrates the yaw motion responses in bow seas. Excellent agreement exists between the three numerical methods for wavelengths less than 2L whilst at longer wavelengths a small but constant deviation exists between approaches (i), (ii) and (iii).

To further verify the present method and to illustrate its range of applicability, a second example involving a barge model of dimensions L = 24.8 m, B = 5 m and h = 2 m was considered. The predictions of the sway motion in beam seas by the analytical expression of Equation (36) are displayed in Figure 5 together with the experimental and theoretical data accumulated by Yamashita [6]. This comparison illustrates the practically acceptable agreement existing between the results derived from the present approximate solutions and the experimental data measured over a wide range of (shorter) wavelengths, i.e. $1 \leq \lambda/B \leq 10$, or $0.2 \leq \lambda/L \leq 2$.

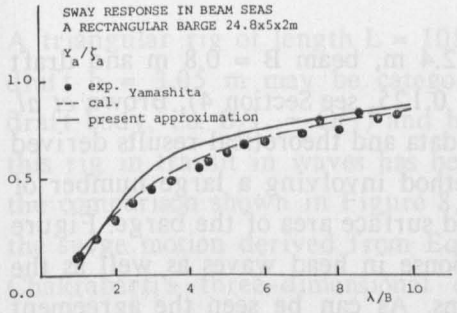

Figure 5. Sway response of a rectangular barge 24.8 × 5 × 2 m in beam seas.

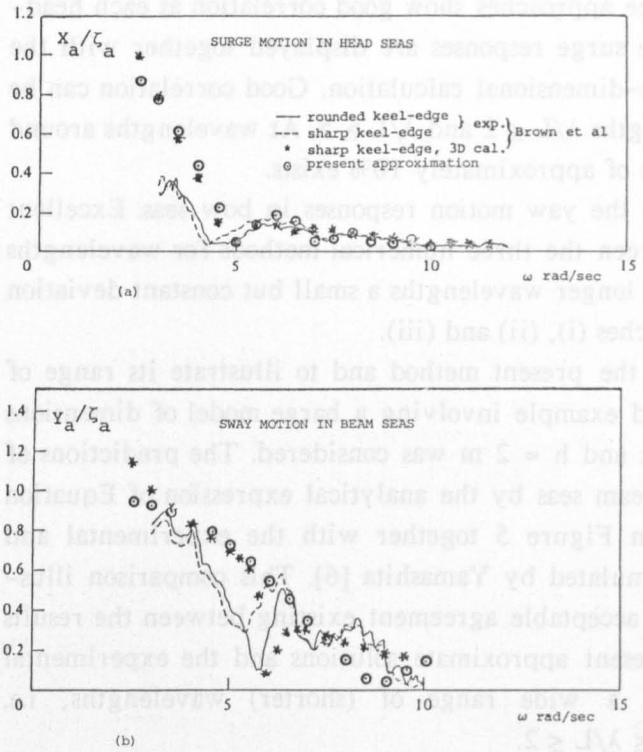

Figure 6. Surge and sway responses of a barge model of length L = 2.4 m, width B = 0.8 m and draft h = 0.105 m.

7.2. *Shallow draft slender bodies*

For a barge model of length L = 2.4 m, beam B = 0.8 m and draft h = 0.105 m (i.e. B/L = 0.33, h/B = 0.125, see Section 4), Brown *et al.* [7] present wave tank experimental data and theoretical results derived from a three-dimensional source method involving a large number of panel elements to discretise the wetted surface area of the barge. Figure 6a shows the data for the surge response in head waves as well as the present analytical solution predictions. As can be seen the agreement between the theoretical results is very satisfactory and this conclusion is extended to the sway motion comparison illustrated in Figure 6b.

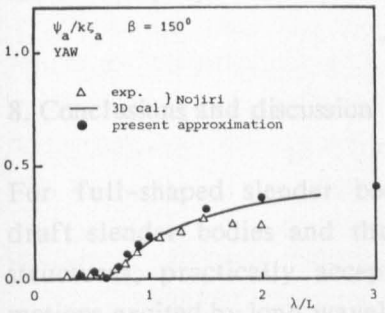

Figure 7. Yaw response at wave heading 150^0 of a shallow draft barge with dimensions 3.0 × 0.75 × 0.015 m for comparison between the present analytical approximation and the theoretical and experimental data given by Nojiri.

To complement this comparative study, the amplitude of yaw motion for a shallow draft barge is shown in Figure 7. The barge of dimensions L = 3.0 m, B = 0.75 m and h = 0.015 m is excited by regular sinusoidal waves at a heading $\beta = 150^0$. Figure 7 includes results from the analytical expressions and those presented by Nojiri [20]. Good agreement is again seen between the present predictions, experimental data and theoretical predictions [20].

7.3. *Three-dimensional shallow draft bodies*

A triangular rig of length L = 108 m, maximum width B = 124 m and draft h = 3.05 m may be categorised as a three-dimensional shallow draft body, i.e. B/L ~ O(1) and h/L or h/B ~ O(ϵ). The behaviour of this rig in transit in waves has been studied previously [17] and from the comparison shown in Figure 8, the present analytical predictions of the surge motion derived from Equation (65) correlate very well with Chakrabarti's three-dimensional diffraction theory calculations and experimental data [17] in the range of wavelengths $0.70 \leq \lambda/L \leq 6.4$. This agreement provides preliminary confirmation of the accuracy of

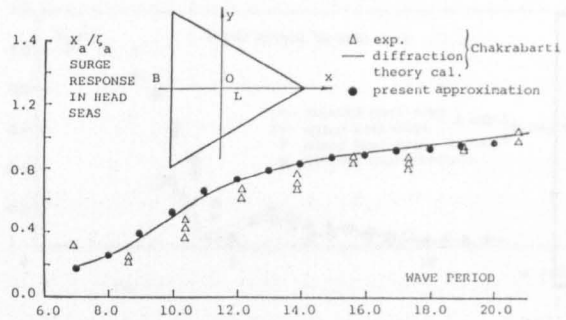

Figure 8. Surge response of a triangular platform of length L = 108 m, width B = 124.6 m and draft h = 3.05 m.

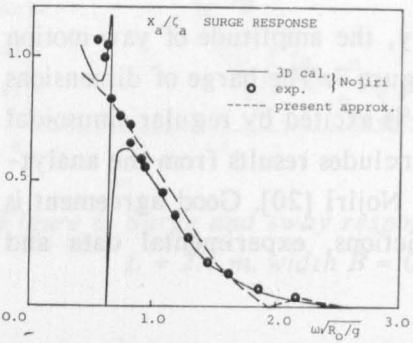

Figure 9. Surge response of a circular dock.

the proposed approximations to determine the horizontal motions of this type of structure.

Another interesting example of a three-dimensional body is a circular dock of radius R_0 and draft $h = R_0$ [10,20]. The analytical predictions for the surge (or sway) motion obtained from Equation (63) are displayed in Figure 9. The data extend over the frequency range $0.3 < \omega\sqrt{(R_0/g)} < 3.0$, i.e. $0.09 < kR_0 < 9.0$ and agree favourably with the experimental data but show no abrupt variation in the vicinity

$\omega \sqrt{(R_0/g)} = 0.64$ as occurs in Nojiri's three-dimensional source method calculation [20].

8. Conclusions and discussion

For full-shaped slender bodies, submerged slender bodies, shallow draft slender bodies and three-dimensional full-shaped shallow draft structures, practically acceptable predictions of the horizontal plane motions excited by long wavelength, sinusoidal waves can be determined from simplified approximate solutions. These are derived from an analysis based on an extension of existing order estimate theory [1,2]. The study shows that

1. To a first order approximation only the Froude-Krylov forces need be considered when determining the surge, sway and yaw motions of the structures considered because

   (a) each of the radiation and diffraction force components is of a higher order small quantity than the Froude-Krylov force component and/or
   (b) the combination of the radiation and diffraction force components partially cancel one another leaving a higher order small quantity force component.

2. The previous statements are found valid

   (i) for full-shaped slender bodies in surge motion because of (a) and in sway and yaw motions because of (b);
   (ii) for slender bodies in surge motion because of (a);
   (iii) for full-shaped submerged slender bodies in heave and pitch because of (b) — but these motions are not the main focus of this study;
   (iv) for full-shaped shallow draft slender bodies in surge motion because of (a) and in sway and yaw motions because of (a) and (b);

(v) for three-dimensional full-bodied shallow draft structures in surge, sway and yaw motions because of (a).

3. The restriction to structures described as "full-bodied" or "full-shaped" is imposed to ensure the exemption of strong coupling effects from resonant heave, roll and pitch motions. This restriction may not be as severe as assumed in the paper.

4. For some full-bodied structures of simple geometry, analytical formulae are presented to describe the horizontal motions.

5. The applicability and accuracy of the proposed analytical formulations are confirmed by comparisons with experimental data and results derived from sophisticated two- and three-dimensional mathematical models. The latter require fine descriptions of the wetted surface area of the structure and involve a significant amount of computer usage. From the limited evidence presented, the approximate solutions are shown to produce results in good agreement with the other sources of comparable data, but at a greatly reduced cost and effort.

6. Some of the conclusions reached in this study confirm those deduced by the authors when investigating the predictions of the horizontal motions of two- and three-dimensional shallow draft marine structures [9,10]. The assumptions adopted previously appear very reasonable and valid in the light of the findings of this study.

7. Although the analysis is based on the assumption of long wavelengths, from the evidence of the numerical examples its application may possibly extend over a wider range of frequencies than considered, allowing more probable wave conditions to be assessed.

8. The four types of full-bodied structures investigated are idealisations of typical marine structures used in offshore operations and services. Therefore, the findings of this paper should be of practical use especially in the early stages of design.

References

[1] Newman, J.N., The theory of ship motions, *Adv. in Appl. Mech.*, Vol. 18 (1978), pp. 221-283.

[2] Newman, J.N., *Marine hydrodynamics*, The MIT Press, 1977.

[3] Salvesen, N., Tuck, E.O., and Faltinsen, O., Ship motions and sea loads, *Trans. SNAME*, Vol. 78 (1970), pp. 250-287.

[4] Szajnberg, R., Greiner, W., Chen, H.H.T., and Rawstron, P., Practical design approaches for the analysis of barge performance in offshore transportation and launching operations, *Trans. SNAME*, Vol. 88 (1980), pp. 195-223.

[5] Kaplan, P., Jiang, C-H, and Bentson, J., 'Hydrodynamic analysis of barge-platform system in waves', RINA Spring Meetings, April 1982, Paper No. 8.

[6] Yamashita, S., Motions of a box-shaped floating structure in regular waves, *IHI Engng. Rev.*, Vol. 14, No. 2 (1981), pp. 21-30.

[7] Brown, D.T., Eatock Taylor, R., and Patel, M.H., Barge motions in random seas — a comparison of theory and experiment, *J. Fluid Mech.*, Vol. 129, pp. 385-407.

[8] Wu, Xiong-Jian and Price, W.G., 'Motion predictions of sea-going barges in offshore operations', Proc. of Offshore Operations Symp. (ASME), New Orleans, Feb. 1986, pp. 83-88.

[9] Wu, Xiong-Jian and Price, W.G., 'The behaviour of shallow draft offshore structures and service vessels in deeper water', Proc. of RINA Int. Symp. on Development in Deeper Waters, London, Oct. 1986, Paper No. 18.

[10] Wu, Xiong-Jian and Price, W.G., 'A method to analyse shallow draft offshore structures with six modes of motion', Proc. of 5th OMAE Symp. (ASME), Tokyo 1986, pp. 476-482.

[11] Grim, O., Surging motions and broaching tendencies in a severe irregular sea, *Deutschen Hydrographischen Zeitschrift*, Vol. 16 (1963).

[12] Wu, Xiong-Jian and Price, W.G., An extended form of strip theory applicable to dry dock like sections, *Int. Shipbuild. Progr.*, Vol. 33, No. 387 (1986), pp. 204-210.

[13] Ogilvie, T.F., 'Workshop on slender-body theory, Part 1: Free-surface effects', Report No. 162, Univ. Michigan, Dept. Naval. Arch. and Marine Engng., 1974.

[14] Ogilvie, T.F., Singular perturbation problems in ship hydrodynamics, *Adv. in Appl. Mech.*, Vol. 17 (1977), pp. 92-187.

[15] Wu, Xiong-Jian and Price, W.G., 'Water waves around an elliptical cylinder or a flat plate, Part 1: Diffraction problem, Part 2: Radiation problems', Brunel Univ., 1987.

[16] Abramowitz, M. and Stegun, I.A., *Handbook of Mathematical Functions*, Dover Publ., New York.

[17] Chakrabarti, S.K., 'Wave interaction with a triangular barge', Proc. 5th OMAE Symp. (ASME), Tokyo 1986, pp. 455-460.

[18] Wu, Xiong-Jian and Price, W.G., A multiple Green's function expression for the hydrodynamic analysis of multi-hull structures', *J. Appl. Ocean Res.*, (1987), pp. 58-66.

[19] Wu, Xiong-Jian and Price, W.G., 'Modified theoretical techniques for motion predictions of offshore structures', WEMT Symp. on Advances in Offshore Technology, Amsterdam, Nov. 1986, pp. 201-224.

[20] Nojiri, N., A study of hydrodynamic pressure and wave loads on three-dimensional floating bodies, *IHI Engng. Rev.*, Vol. 14, No. 2 (1981), pp. 6-20.

A NEW SHALLOW DRAFT APPROACH :

I. THE THREE DIMENSIONAL THEORY AND ITS COMPUTATIONAL APPLICATIONS

Xiong-Jian Wu

Ship Hydrodynamics Laboratory, Shanghai Jiao-Tong University, China; presently at Brunel, The University of West London, Uxbridge, Middlesex UB8 3PH, U.K.

W.G. Price

Brunel, The University of West London, Uxbridge, Middlesex UB8 3PH, U.K.

SUMMARY This paper summarises a new shallow draft theory incorporated with an efficient computer algorithm for the hydrodynamic analysis and motion and loads predictions of mono-, twin- and multi-hulled shallow draft offshore structures excited by sea waves. This method provides a considerable saveing in computing time but still remains a high degree of numerical accuracy.

The applicability of this approach to structures of finite volume of displacement is illustrated by studies on both mono-hull structures and a semi-submersible in transit. These complement previous investigations on mono-hull structures[1,2]. From these extensive investigations, the advantages arising from the approach are clearly shown and the predicted responses agree favourably with the available experimental data, thus providing a measure of validity of the proposed shallow draft theory.

1. INTRODUCTION

A jack-up rig in transit, an ocean plant or floating port, an OTEC barge, crane and transportation barges, dredger vessels, semi submersible and TLP platform in transit, etc., all have the common geometric features of shallow draft. That is,

(i) the aspect ratio of beam B to draft h is large, i.e. $B/h >> 1$,

(ii) the bottom surface of the vessel is nearly flat and provides the dominant contribution to the total wetted body surface area,

(iii) in addition, a large number of these structures may have small or intermediate aspect ratio of length L to beam B.

Because of these characteristics, in general, the hydrodynamic analysis and evaluations of motions and wave loadings necessitate the use of large computer programs based on three dimensional (3D) mathematical models and a large number of panel discritisation to obtain convergent or accurate numerical solutions. These require much computing effort and time. Alternatively, 2D mathematical models may be adopted incorporating suitable 3D corrections[3]. Furthermore, for both 2D[3] and 3D[4] cases an empirical viscous damping term is usually introduced into the analysis so that reasonable predictions of roll response at resonance may be achieved but this is not the focus of the present study.

For a shallow draft structure the draft value may be the same order of the wave height. Therefore, the linear wave theory calculation over an idealised mean wetted body surface is not strictly applicable and the nonlinearity is obviously of certain importance, especially for the oscillatory modes in the horizontal plane, i.e. surge, sway and yaw motions. Moreover,considerable discrepencies of predicted hydrodynamic coefficients have been reported by Berhault[5] for a shallow draft rectangular barge of dimensions 120x4ox2.43m when applying various theoretical models or different programs based on the same theoretical method. Since more complicated or sophisticated theoretical approaches are not necessarily more accurate, why not devise a simplified practical model of less complexity, similar accuracy, higher efficiency and better applicability with which individually developed software packages can be more identical and errors of resultant solutions may be readily estimated.

From the point of view of structural strength, wave loads of a shallow draft vessel in the vertical plane, i.e. those related to the heave, roll and pitch motions and vertical distortion modes, are of ultimate importance.

These require that an applicable new approach is able to describe necessary details of the vertical motion modes in a high degree of accuracy and provide general information of the horizontal motion modes with an acceptable accuracy. Some twenty years ago MacCamy[6] proposed a shallow draft method appropriate to analyse the heave motion of a 2D flat plate. This zero-draft or flat ship theory was extended by Kim[7] to an elliptical plate heaving and pitching in calm water of infinite depth, whilst Maeda[8] analysed the behaviour of square and circular plates heaving and pitching in finite water depth. Unfortunately, due to the inbuilt assumptions in thses methods, relative analyses were not strictly applicable to realistic floating shallow draft marine structures of finite displacement volume and were unable to predict motion responses of surge, sway and yaw. To overcome these disadvantages a new shallow draft approach has been proposed by Wu and Price[1,2] based on a simple modified assumption drawn from considerations of the realistic physical phenomena. It is capable of predicting six rigid body modes of a mono-hull shallow draft structure or more if flexible modes analysis is required. These progressive developments are shown in Figure 1.

This paper summarises the brief theoretical approach of the proposed 3D shallow draft theory and describes the related numerical procedure adopted, the efficient computer algorithm and program suite developed to takle problems associated with various shallow draft structures and contains further extended applications to a semi-submersible in transit.

2. GENERAL 3D LINEAR WAVE THEORY FORMULATION

Based on linear wave theory, the radiation velocity potential ϕ^j associated with a marine structure performing oscillatory motion in the modes j = 1 (surge), j = 2 (sway), j = 3 (heave), j = 4 (roll), j = 5 (pitch), j = 6 (yaw) and the diffracted wave potential ϕ^7, related to the incident sinusoidal wave potential ϕ^o, may be shown[1,2] to satisfy the Green's function integral equation

$$2\pi\phi^j(P) - \int_{S_w} \phi^j(Q) \frac{\partial G_o(P,Q)}{\partial n_Q} dS = - \int_{S_w} v_n^j(Q)\ G_o(P,Q)\ dS \qquad (1)$$

for j = 1,2,...,7. In this expression P(x,y,z), Q(ξ,η,ζ) represent two points on the mean wetted body surface S_w, $\vec{n} = (n_1,n_2,n_3)$ denotes the outward unit normal to the wetted surface and $(\vec{r} - \vec{r}_G)x\vec{n} = (n_4,n_5,n_6)$ where $\vec{r} = (x,y,z)$ and the subscript G indicates the centre of gravity. The normal velocity

$$v_n^j = \frac{\partial \phi^j}{\partial n} = \begin{cases} -i\omega n_j & \text{for } j = 1,2,\ldots,6 \\ -\partial\phi^o/\partial n & \text{for } j = 7 \end{cases} \qquad (2)$$

where ω denotes the frequency of oscillation and the Green's function may be expressed in the form

$$G = I_o + I_1 + iI_2$$

with

$$I_o = 1/r + 1/r_1$$

$$I_1 = -\nu e^{\nu(z+\zeta)}\{\pi[H_o(\nu R) + Y_o(\nu R)] + 2\int_o^{-\nu(z+\zeta)} \frac{e^s\, ds}{(s^2+\nu^2R^2)^{1/2}}\}$$

$$I_2 = 2\pi\nu e^{\nu(z+\zeta)} J_o(\nu R) \qquad (3)$$

for infinite water depth[9] and

$$I_o = C\, Y_o(kR)$$

$$I_1 = 4\sum_{m=1}^{\infty} \frac{\mu_m^2+\nu^2}{(\mu_m^2+\nu^2)d-\nu} \cos\mu_m(z+d)\cos\mu_m(\zeta+d)\, K_o(\mu_m R)$$

$$I_2 = -C\, J_o(kR)$$

$$C = \frac{2\pi(\nu^2-k^2)}{(k^2-\nu^2)d+\nu} \cosh k(z+d)\cosh k(\zeta+d) \qquad (4)$$

for finite water depth[9], d, as $R \neq 0$.

In these expressions Y_o, J_o, K_o denote the appropriate Bessel functions, H_o denotes the Struve function of order zero, $R = \{(x-\xi)^2+(y-\eta)^2\}^{1/2}$, $r = \{R^2+(z-\zeta)^2\}^{1/2}$, $r_1 = \{R^2+(z+\zeta)^2\}^{1/2}$, k satisfies the equation

$$k\tanh(kd) = \nu = \omega^2/g \qquad (5)$$

and μ_m is the mth positive root of the equation

$$\mu_m \tan(\mu_m d) + \nu = 0 \qquad (6)$$

3. 3D SHALLOW DRAFT THEORY

To deal with realistic shallow draft marine structures with finite volume of displacement as shown in Figure 2, the present shallow draft approach[1,2] represents an extended and modified version of the previous flat ship theories[6-8] capable of analysing real shallow draft bodies rather than flat plates and predicting horizontal motions as well as vertical oscillatory modes. To achieve thses improvements, the present new shallow draft method adopts a simple but self-consistent assumption that:

The radiation and diffraction wave potentials are evaluated on a flat surface S_o with realistic values of the normal velocity components in the vertical direction. The resultant radiation and diffraction wave forces are cooperated with the Froude-Krylov forces exerted by an incident wave upon the mean wetted body surface S_w.

The surface S_o located on the still water surface z = 0 is an approximation to the total mean wetted body surface S_w of the shallow draft structure. In other words, the vertical side wall area is ignored when calculating radiation and diffraction wave potentials but the effect of a small finite value of draft is taken into account.

On the surface s_o (z = 0, ζ = 0) it follows that

$$\partial G/\partial n = \partial G/\partial z \; n_z = -\partial G/\partial z \qquad \text{on } s_o \tag{7}$$

which together with the free surface condition

$$\partial G/\partial z = \nu G \qquad \text{on } z = 0 \tag{8}$$

gives the result

$$\partial G/\partial n = -\nu G \qquad \text{on } s_o \tag{9}$$

Substituting this expression into eq.(1), the shallow draft Green's function integral equation describing the modes j=1,2, ...,7 reduces to

$$4\pi\phi^j(P) + \nu\int_{s_o} \phi^j(Q)\; G(P,Q)\; dS = -\int_{s_o} v_n^j(Q)\; G(P,Q)\; dS \tag{10}$$

with

$$v_n^j = \begin{cases} -i\omega n_j & \text{for } j = 1,2,\ldots,6 \\ -\partial\phi^o/\partial n\big|_{z=-h} & \text{for } j = 7 \end{cases}$$

The change of the constant coefficient of the first term on the left-hand side from 2π in eq. (1) to 4π in eq. (10) is due to the contribution of the term $1/r_1$ included in the Green's function since on s_o (where z = 0) the elemental surface integral of $\partial(1/r_1)/\partial n$ at a point Q = P is equal to -2π.

Eq. (10) requires no derivative evaluation of the Green's function, G, and the shallow draft Green's function can be expressed in much simpler forms with components

$$I_o = 2/R$$
$$I_1 = -\nu\pi\{H_o(\nu R) + Y_o(\nu R)\} \tag{11}$$
$$I_2 = 2\pi\nu\, J_o(\nu R)$$

for infinite water depth and

$$I_o = C\, Y_o(kR)$$
$$I_1 = 4\sum_{m=1}^{\infty} \frac{\mu_m^2+\nu^2}{(\mu_m^2+\nu^2)d-\nu} \cos^2(\mu_m d)\, K_o(\mu_m R) \tag{12}$$
$$I_2 = -C\, J_o(kR)$$
$$C = \frac{2\pi(\nu^2-k^2)}{(k^2-\nu^2)d+\nu} \cosh^2(kd)$$

for finite water depth.

Solving for the unknown velocity potentials ϕ^j $(j = 1,2,\ldots,7)$ allows the added mass coefficients (A_{rj}), damping coefficients (B_{rj}) and wave exciting forces (F_r) to be determined from the expressions

$$A_{rj} = \frac{\rho}{\omega}\int_{S_o} \mathrm{Im}(\phi^j)\, n_r\, dS \tag{13}$$

$$B_{rj} = -\rho\int_{S_o} \mathrm{Re}(\phi^j)\, n_r\, dS \tag{14}$$

for $r = 1,2,\ldots,6$ and $j = 1,2,\ldots,6$, and

$$F_r = -i\omega\rho\int_{S_w} \phi^o\, n_r\, dS - i\omega\rho\int_{S_o} \phi^7\, n_r\, dS \tag{15}$$

for $r=1,2,\ldots,6$. In eq. (15) the first term represents the Froude-Krylov force contribution and the other term the contribution from the diffraction potential.

Since these hydrodynamic actions are now theoretically known, it can be shown that the equation of motion representing the jth displacement

$$X_j(t) = X_{ja}\, e^{-i\omega t} \tag{16}$$

may be expressed in the form

$$\sum_{j=1}^{6}\{(M_{rj}+A_{rj})\ddot{X}_j + (B_{rj}+B_{vrj})\dot{X}_j + C_{rj}X_j\} = F_r\, e^{-i\omega t} \tag{17}$$

where M_{rj} denotes the generalised mass, B_{vrj} represents a viscous damping contribution[3,4] which is set to zero in the present study, and C_{rj} is the restoring coefficient. It is now a straightforward procedure to determine the amplitudes X_{ja} and the pressure distribution

$$p = -\rho\, \partial\phi/\partial t = i\omega\rho(\phi^o + \phi^7 + \sum_{j=1}^{6} X_{ja}\phi^j)$$
$$\simeq i\omega\rho(\phi^o + \phi^7 + \sum_{j=3}^{5} X_{ja}\phi^j) \tag{18}$$

and if required the bending moments and shearing forces[10] experienced by the shallow draft marine structure.

4. NUMERICAL FORMULATION

By discretising the wetted surface s_o by N panels of elemental area Δs, eq. (10) may be replaced by N simultaneous linear equations of the form

$$\sum_{m=1}^{N} \phi_m^j \{4\pi \delta_{rm} + \nu \int_{\Delta s_m} (G_{rm} - \frac{2\delta_{rm}}{R_{rm}}) \, dS\} = -\sum_{m=1}^{N} v_{rm}^j \int_{\Delta s_m} G_{rm} \, dS \qquad (19)$$

for $r = 1,2,\ldots,N$, and

$$\delta_{rm} = \begin{cases} 1 & \text{for } r = m \\ 0 & \text{for } r \neq m \end{cases}$$

To solve eq. (19) requires the evaluation of the elemental integral of the Green's function which may be approximated by

$$\int_{\Delta s_m} G_{rm} \, dS \simeq \{G_{rm} - \frac{2}{R_{rm}} + 2k \, \ell n(kR_{rm})\} \Delta s_m + 2 \int_{\Delta s_m} \frac{ds}{R_{rm}} - 2k \int_{\Delta s_m} \ell n(kR_{rm}) ds \qquad (20)$$

On the right-hand side the first term is regular everywhere in the fluid domain and is easily calculated using polynomial expansions for the special functions. To retain high numerical accuracy and to reduce as far as possible the total number of panel elements N, the first integral term on the right-hand side is computed by an analytical expression relating two nearby points. Namely,

$$\int_{\Delta s_m} \frac{dS}{R_{rm}} = \begin{cases} \sum_{k=1}^{N_a} \{\dfrac{Z_k}{(X_k^2 + Y_k^2)^{1/2}} \ell n \, F(\theta)\}_{\theta_k}^{\theta_{k+1}} & \text{for } R_{rm} \leq 2\sqrt{\Delta s_m} \\ \Delta s_m / R_{rm} & \text{elsewhere} \end{cases} \qquad (21)$$

where

$$F(\theta) = \left| \frac{(X_k^2+Y_k^2)^{1/2} - (X_k \cos\theta + Y_k \sin\theta)}{X_k \sin\theta - Y_k \cos\theta} \right|$$

and as shown in Fig. 3 , N_a is the total number of apices in the mth elemental panel with parameters

$$X_k = \xi_{k+1} - \xi_k, \quad Y_k = \eta_{k+1} - \eta_k,$$

$$Z_k = (\xi_{k+1} - \bar{x})(\eta_k - \bar{y}) - (\xi_k - \bar{x})(\eta_{k+1} - \bar{y}), \text{ for } k = 1,2,\ldots,N_a$$

and $\xi_{N_a+1} = \xi_1$, $\eta_{N_a+1} = \eta_1$. The local coordinates of the kth apex with respect to the local origin $C_m(x_m, y_m, 0)$ are $A_k(\xi_k, \eta_k)$ whilst $C_r(\bar{x}, \bar{y}, 0)$ is the local coordinates of C_i with respect to C_m. θ_k is the angular position of the kth apex as shown in Figure 3.

Finally the remaining integral can be evaluated from the expression

$$\int_{\Delta s_m} \ell n(kR_{rm}) \, dS \simeq \begin{cases} \Delta s_m (\ell n \, k\sqrt{\Delta s_m/\pi} - 1/2) & \text{for } R_{rm} = 0 \\ \Delta s_m \, \ell n(kR_{rm}) & \text{for } R_{rm} \neq 0 \end{cases} \qquad (22)$$

5. HORIZONTAL MOTIONS

Because of the assumptions introduced into the present shallow draft theory, the equations of motion describing surge (j = 1), sway (j = 2) and yaw (j = 6) reduce from the general expressions given in equations (13-17) to

$$X_{ra} = F_r/(-\omega^2 M_{rr}) = i\rho \int_{S_w} \phi^o \, n_r \, dS/(\omega M_{rr}) \tag{23}$$

giving a response amplitude operator

$$|X_{ra}|/\zeta_a = \rho \left| \int_{S_w} \phi^o \, n_r \, dS \right| / (\omega M_{rr} \zeta_a) \tag{24}$$

where ζ_a denotes the amplitude of the sinusoidal incident wave.

Further simplifications to eq. (24) may be achieved for structures with simple side walls which can be modelled by a series of flat plates or if the geometry of the structure can be described by analytical expressions, i.e. circular cylinders, rectangular barges , etc.

For a circular cylinder of radius R_o and not large draft h floating in deep water, the complex surge amplitude can be given by[2]

$$X_{1a}/\zeta_a = e^{i\pi/2} \, \frac{4(1 - e^{-\nu h})}{\nu h} \, \frac{\int_0^{\pi/2} \sin(\nu R_o \cos\theta)\cos\theta \, d\theta}{\pi \nu R_o}$$

$$= i \, \frac{1 - e^{-\nu h}}{\nu h} \, \frac{2 J_1(\nu R_o)}{\nu R_o} \tag{25}$$

where J_1 denotes the Bessel function of the first kind of order one.

For a rectangular barge of length L, beam B and draft h (Figure 2) floating in deep water, the respective surge, sway and yaw motion responses can be expressed as[1]

$$\left.\begin{matrix} X_{1a}/\zeta_a \\ X_{2a}/\zeta_a \end{matrix}\right\} = e^{i\pi/2} \left\{\begin{matrix} 1/\sin\beta \\ 1/\cos\beta \end{matrix}\right\} \frac{1 - e^{-\nu h}}{\nu h} \, \frac{\sin(\ell \cos\beta)}{\ell}$$

$$\cdot \frac{\sin(b \sin\beta)}{b} \, , \tag{26}$$

$$X_{6a}/\nu\zeta_a = e^{i\pi} \, \frac{1 - e^{-\nu h}}{\nu^3 K_{zz}^2 LBh} \Big\{ 2\sin(\ell \cos\beta)$$

$$\cdot \left[\frac{B \cos(b \sin\beta)}{\nu \sin\beta} - \frac{2\sin(b \sin\beta)}{(\nu \sin\beta)^2} \right]$$

$$- 2 \sin(b \sin\beta) \left[\frac{L \cos(\ell \cos\beta)}{\nu \cos\beta} \right.$$

$$\left. - \frac{2 \sin(\ell \cos\beta)}{(\nu \cos\beta)^2} \right] \Big\} \tag{27}$$

where $\ell = L/2$, $b = B/2$ and K_{zz} denotes the radius of gyration of yaw about the vertical axis oz, and β is the heading angle between the Ox-axis of the structure and the incoming sinusoidal waves ($\beta = 180^{\circ}$, head seas).

Further analytical expressions for a triangular platform of length L, beam B and draft h in surge, sway and yaw motions can also be derived. For example, in deep water the surge and sway motion amplitudes are given by the complex forms [11]

$$\left.\begin{matrix} X_{1a} \\ X_{2a} \end{matrix}\right\} = \frac{4}{\sqrt{3}} \frac{1 - e^{-\nu h}}{(\nu B)(\nu h)} \left(\left\{ \begin{matrix} 1/2 \\ \sqrt{3}/2 \end{matrix} \right\} \frac{\sin\alpha_1 - i(1 - \cos\alpha_1)}{\alpha_1} \right.$$

$$+ \left\{ \begin{matrix} 1/2 \\ -\sqrt{3}/2 \end{matrix} \right\} \frac{\sin\alpha_2 - i(1 - \cos\alpha_2)}{\alpha_2}$$

$$\left. + \left\{ \begin{matrix} -1 \\ 0 \end{matrix} \right\} \frac{(\cos\alpha_3 - i \sin\alpha_3) \sin\alpha_4}{\alpha_4} \right) \qquad (28)$$

where

$$\left.\begin{matrix} \alpha_1 \\ \alpha_2 \end{matrix}\right\} = \frac{\sqrt{3}}{2} \nu B \, (\cos\beta \mp \sin\beta / \sqrt{3})$$

$$\alpha_3 = \frac{\sqrt{3}}{2} \nu B \cos\beta$$

$$\alpha_4 = \frac{1}{2} \nu B \sin\beta$$

Applications of these derived analytical formulas will be discussed in Section 7.

6. COMPUTATIONAL PACKAGE

The numerical examples to be presently discussed were calculated using a 3D shallow draft diffraction suite of programs (X.J. Wu, 1984) which were derived by modifying a general 3D diffraction suite of programs (X.J. Wu, 1983). The computational programs include the following features:

(i) an automatic mesh generator to provide the input data file describing the discretised body surface;

(ii) the analytical evaluation of the simple source terms together with the generation of the geometric and hydrostatic information;

(iii) producing information on velocity potentials, hydrodynamic coefficients, wave exciting forces, etc for chosen wave headings and each required wave frequency;

(iv) all data are stored in link files to ease manipulation, enabling predictions of responses, wave loads etc to be quickly performed.

By suitably structuring the suite of programs, a highly efficient and time saving procedure was constructed which greatly benefits the user to perform complicated computations.

7. APPLICATIONS TO SHALLOW DRAFT STRUCTURES

An extensive series of calculations have been undertaken to verify the practical applicability of the present shallow draft theory and some examples are presented. Motion response amplitudes for surge, sway, heave, roll, pitch and yaw, i.e. $|X_{ja}|$ for j = 1-6, are denoted by X_a, Y_a, Z_a, θ_a, ϕ_a and ψ_a respectively whilst the wave length by λ.

7.1 A jack-up rig in transit

Matsumoto et al[12] investigated the behaviour of a rectangular rig model in transit in regular waves Figure 4 illustrates the structure having dimensions

$L = 1.5m$, $B = 1.5m$, $h = 0.1075m$, $KG = 0.17m$,
$K_{xx} = 0.447m$, $K_{yy} = 0.433m$, $K_{zz} = 0.615m$

where K_{xx} etc denote radii of gyration and KG the distance between keel and centre of gravity.

Preliminary calculations have been presented elsewhere[2] and improved motion predictions are shown in Figure 5. Matsumoto et al's experimental and 3D calculation data[12] are compared with those determined by the proposed shallow draft theory. Satisfactory agreement is shown to exist between the sway motion data for beam seas ($\beta = 90^o$) and bow seas ($\beta = 150^o$) but large deviations in the yaw predictions arise . However, the latter motion amplitude is very small and the differences are therefore of only minor importance. Excellent agreement exists between the experimental data and the heave and pitch predictions and reasonable agreement occurs in the roll motion responses excited by beam waves. It is seen that the ordinary 3D method[12] slightly over estimates the resonant roll response whereas the present calculation slightly under estimates the experimental values.

7.2 Barge of intermediate length

Brown et al[13] performed model experiments on a rectangular barge of dimensions

$L = 2.4m$, $B = 0.8m$, $h = 0.105m$

and calculated the motion responses by a 3D source method utilizing the panel description of the wetted body surface shown in Figure 6a. Since side walls of small area are involved a rather fine discretisation using a large number of panels becomes necessary. However, applying the present shallow draft theory to evaluate the radiation and diffraction potentials no side walls are included and therefore a much coarser panel mesh as shown in Figure 6b may be sufficient to achieve the required numerical accuracy.

As illustrated in Figure 7, good agreement is observed between the present method computation(by analytical solutions for the surge and sway motions and numerical predictions for the heave, roll and pitch motions) and Brown et al's 3D source method calculation and experimental data (the solid line for the rounded keel-edge barge and the dash line for the sharp keel-edge model).

This study using a simpler mathematical model has produced results of equivalent accuracy to those obtained from a much more complicated model, but the demands on computing effort have been greatly reduced.

In this example study no yaw motion prediction is presented for lack of relative experimental data[13]. Therefore, an additional comparison between the present prediction and available model testing data for a similar rectangular barge (L = 3.0m, B = 0.75m and h = 0.015m)[1] is shown in Figure 8. Again, reasonable agreement is confirmed between the present analytical results from eq. (27) and the published 3D source method calculation and experimental data[14].

7.3 A circular dock

To verify the validity of the present approach to predict the horizontal motion of circular platforms as given by eq. (25), a circular dock of radius R_o (i.e. $B = 2R_o$) and draft $h = R_o$ is chosen. Analytical prediction of the surge motion of the dock is given in Figure 9 by the dash line whereas the 3D source method results and experimental measurements[14] by the solid line and circular points respectively. The present predictions take very little computer time and these seem to agree favourably with the experimental data.

7.4 A triangular platform

Recently Chakrabarti[15] reported model experimental data and theoretical computations for a triangular platform modelling a triangular jack-up rig or deck in a wet tow. This provides another typical shallow draft structure configuration to check the proposed shallow draft theory.

A theoretical study applying the present method to such a model of dimensions of length L = 118m, B = 124.6m and h = 3.05m as illustrated in Figure 10 has been performed[11] and main results are quoted here. The analytical results for the surge motion amplitude of the structure from eq. (28) are denoted by solid circular points in Figure 11. It can be seen that the present analytical predictions correlate well with the experimental data and retain the same degree of accuracy as a 3D diffraction theory calculation[15]. This further verifies the validity of the present horizontal motion predictions for mono-hull shallow draft marine structures.

Furthermore, the numerically computed heave motion response in head seas is given in Figure 12. In this calculation, the flat plate S_o approximating the real wetted body surface S_w is subdivided into a total of 22 panels (i.e. 11 panels for the port half of S_o). Figure 12 apparently indicates the excellent correlation of the present heave motion prediction with Chakrabarti's data.

These example studies including various waterplane geometries of shallow draft structures, i.e. rectangular (aspect ratio ranging from 1 - 4), circular and triangular areas, may imply the theoretical validity, numerical accuracy and computational efficiency of the proposed shallow draft theory in analysing mono-hull shallow draft marine structures.

7.5 A semi-submersible in transit

Previous applications of the shallow draft theory have been restricted to mono-hull structures. To assess the possible extended applicability of the method to multi-hulled offshore structures in transit, further study on a twin-hull semi-submersible in transit is now presented.

The semi-submersible model adopted was the subject of a previous investigation by Takaki et al[16] and its main particulars are as follows

L = 2.23m, h = 0.06m, pontoon beam B = 0.24m,
pontoon central distance B_c = 0.74m,
displacement W = 59.76kg,
KG = 0.133m, K_{xx} = 0.42m, K_{yy} = 0.622m.

The general configuration of this semi-submersible model is illustrated in Figure 13. To determine the radiation and diffraction forces, the mean wetted body surface of the semi-submersible is approximated by a pair of parallel flat plates 2.23x0.24m. Computed heave, roll and pitch responses of the structure excited by regular waves are given in Figure 14 and these seem to agree reasonably with the experimental evidence[16]. This limited study suggests that the shallow draft theory may be extended to predict heave, roll and pitch motions of multi-hulled offshore structures in a wet tow or transit operation.

8. CONCLUSIONS

Existence of a large group of shallow draft vessels and offshore structures necessitates the development of a shallow draft theory for motion and wave loading predictions of these realistic marine structures. By further extension of the previous flat ship approach a new shallow draft theory has been derived and applied to various shallow draft structures.

The present study reveals that

(i) The proposed shallow draft method enables realistic motion predictions to be determined with confidence for mono-hull shallow draft marine structures with finite volume of displacement.

(ii) According to the basic assumption for the evaluation of the radiation and diffraction forces the wetted surface contribution from the small side walls is neglected and the total mean wetted body surface is restricted to an approximate flat surface S_o without any curvature. Consequently, no small area panels exist in the discretisation and this is useful to obtain stable numerical solution of the matrix formulation required in the numerical procedure. Thus a much coarser mesh arrangement of the wetted body surface may achieve necessary convergence and accuracy of the solution but produce a great saving in computational effort. In addition, both the shallow draft integral equation and Green's function become much simpler, enabling a further reduction of required computing time. Therefore, the shallow draft approach achieves the same numerical accuracy as the more complicated conventional 3D methods but with a significant reduction in coputing time.

(iii) The simple expression or possible analytical formulas for the prediction of horizontal motions are easily understood, redily usable and reliable to apply. In fact, it implies that due to the mutual cancellation effect of multiple factors existing in shallow draft body motions, a simple formulation may reasonably predict horizontal motions of shallow draft marine structures.

(iv) The efficient computer algorithm developed from the shallow draft theory is of practical use in the analysis of motions and sea loads, etc, and in the preliminary design of shallow draft ships and offshore structures.

(v) Limited application indicates the possible extension of the proposed shallow draft theory to predict the heave, roll and pitch motions of multi-hulled offshore structures in transit.

This paper is the revised and enhanced version of the paper titled "A shallow draft theory and its applications in computing motions and wave loads of shallow draft marine structures" read in the CADMO '86 Conference (International Conference on Computer Aided Design, Manufacture and Operation in the Marine and Offshore Industries), Washington DC, September 1986, by inclusion of various example applications of the proposed shallow draft theory.

REFERENCES

1. Wu, Xiong-Jian and Price, W.G. "Motion predictions of sea-going barges in offshore operations", Proc. Offshore Operations Symposium (ASME), New Orleans, Feb. 1986, pp. 83-88.
2. Wu, Xiong-Jian and Price, W.G. "A method to analyse shallow draft offshore structures with six modes of motion", Proc. 5th OMAE Symposium (ASME), Tokyo, April 1986, pp. 476-482.
3. Kaplan, P., Jiang, C.W. and Bentson, J. "Hydrodynamic analysis of barge-platform systems in waves", RINA Spring Meetings, Paper No. 8, 1982.
4. Standing, R.G. "Applications of wave diffraction theory", Int. J. Numerical Method in Engineering, Vol. 13, 1978, pp. 49-72.
5. Berhault, C. "Comparison of the main numerical methods in water wave diffraction and radiation", Inst. Francais du Petrole, Paris, 1978.
6. MacCamy, R.C. "On the heaving motion of cylinders of shallow draft", J. Ship research, Vol. 5, Dec. 1961, pp. 34-43.
7. Kim, W.D. "On the forced oscillations of shallow draft ships", J. Ship Research, Vol. 7, Oct. 1963, pp. 7-18.
8. Maeda, H. "On the hydrodynamic forces for shallow draft ships in shallow water", Naval Archi. and Ocean Eng. (Japan), Vol. 19, 1981, pp. 54-67.
9. Wehausen, J.V. and Laitone, E.V. "Surface Waves", Handbuch der Physik, Band 9, 1960, pp. 446-778, Springer-Verlag, Berlin.
10. Salvesen, N., Tuck, E.O. and Faltinsen, O. "Ship motions and sea loads", Trans. SNAME, Vol. 78, 1970, pp. 250-287.
11. Wu, Xiong-Jian and Price, W.G. "The behaviour of offshore structures and service vessels of shallow draft in deep water", Proc. RINA Int. Symposium on Developments in Deeper Waters, London, Oct. 1986, Paper No. 18.
12. Matsumoto, N., Koterayama, W. and Moriyama, A. "Motion of an elevating-deck ocean structure while closing with sea bottom in regular waves", Trans. West-Japan Soc. Naval Architects, No. 63, March 1982, pp. 135-149 (in Japanese).
13. Brown, D.T., Eatock Taylor, R. and Patel, M.H. "Barge motions in random seas - a comparison of theory and experiment", J. Fluid Mech., Vol. 129, 1983, pp. 385-407.
14. Nojiri, N. "A study of hydrodynamic pressure and wave loads on three-dimensional floating bodies", IHI Engineering Review (Japan), Vol. 14, No. 2, April 1981, pp. 6-20.
15. Chakrabarti, S.K. "Wave interaction with a triangular barge", Proc. 5th OMAE Symposium (ASME), Tokyo, April 1986, pp. 455-460.
16. Takaki, M., Arakawa, H. and Tasai, F. "On the oscillations of semi-submersible catamaran hull at shallow draft", Trans. West-Japan Soc. Naval Architects, No. 42, May 1971, pp. 115-130 (in Japanese).

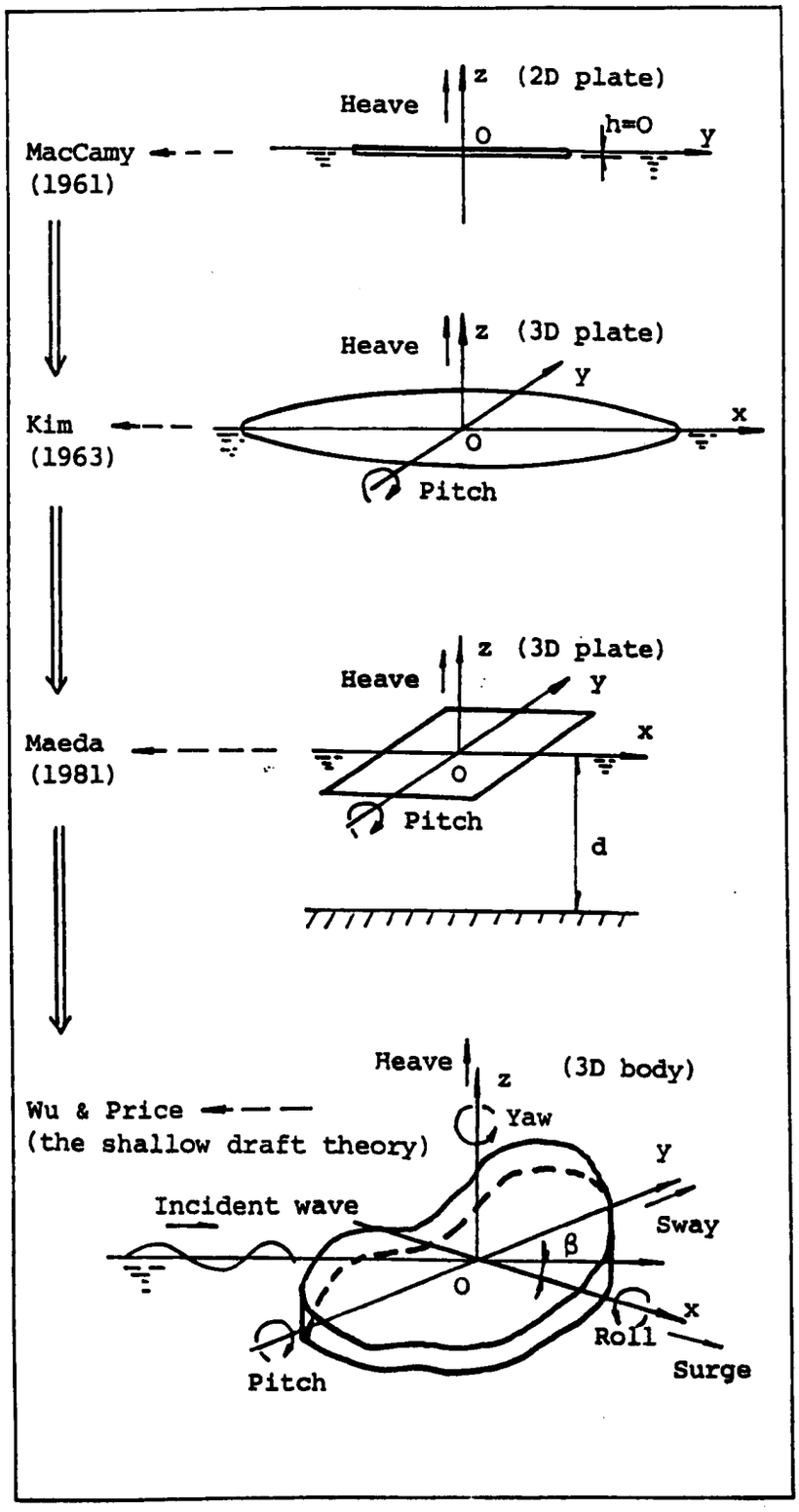

Fig. 1 The development chart of the shallow draft theory.

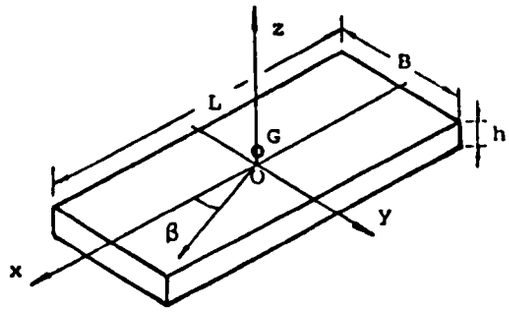

Fig. 2 A shallow draft structure.

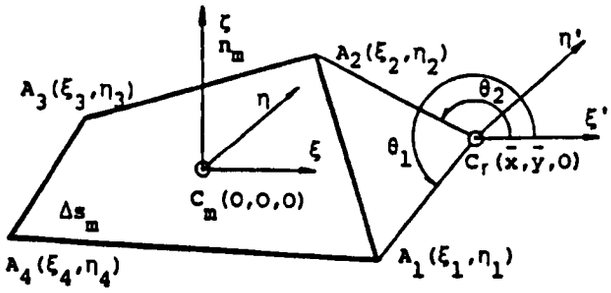

Fig. 3 Definitions of symbols related to the mth panel and the rth point.

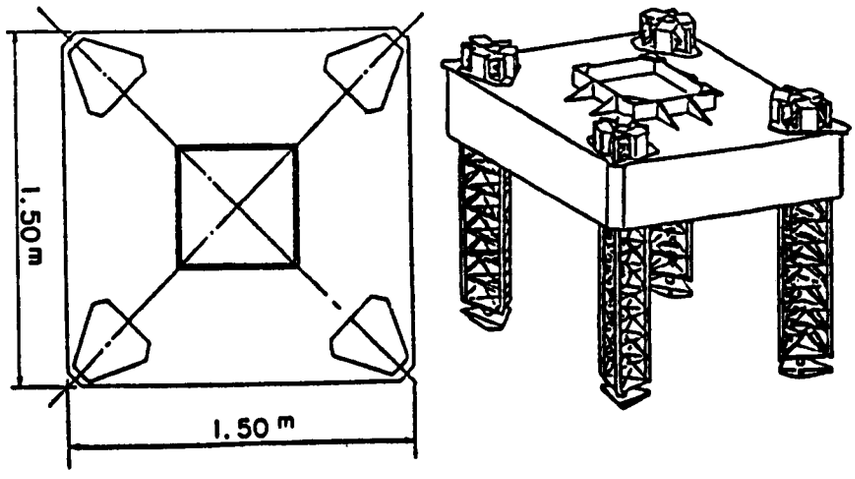

Fig. 4 A rectangular jack-up rig model.

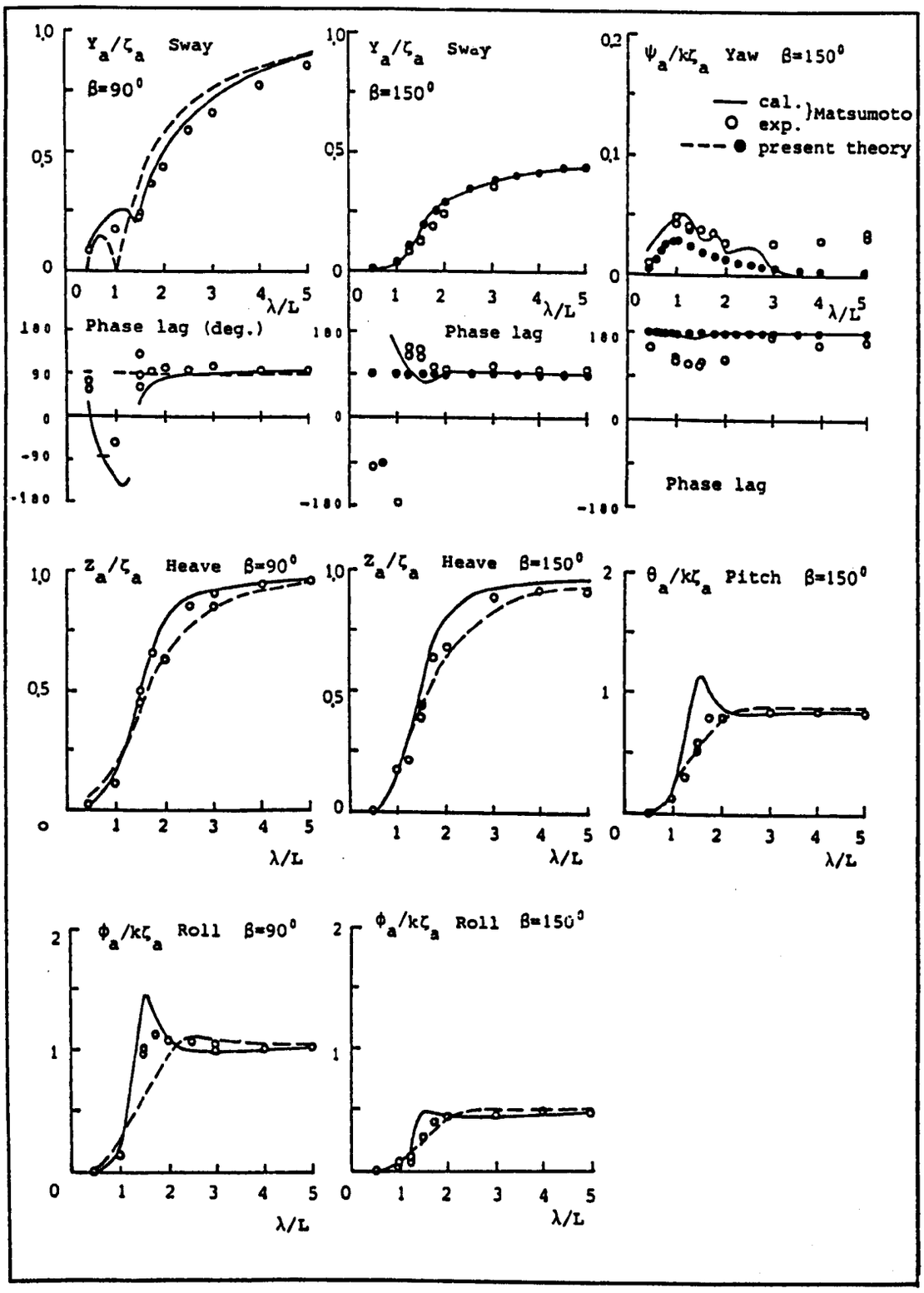

Fig. 5 Motion responses of the rectangular jack-up rig model in transit with Length L = 1.5m, beam B = 1.5m and draft h = 0.1075m.

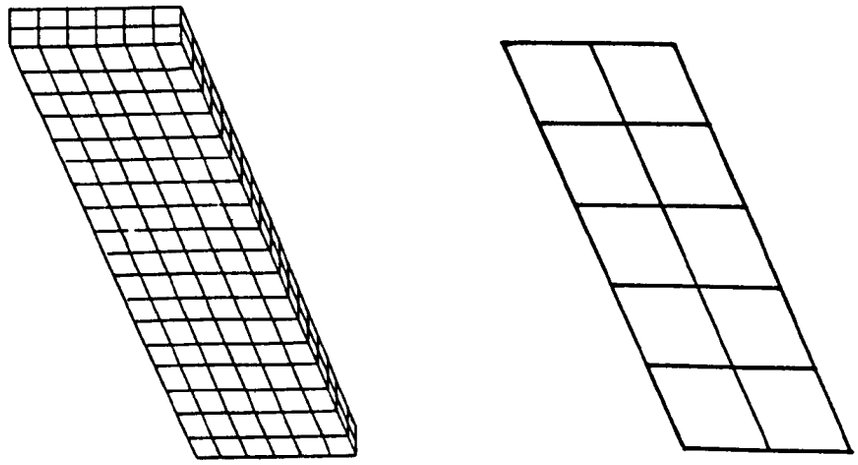

(a) (b)

Fig. 6 Discretisation of a quadrant of the barge wetted surface (2.4x0.8x0.105m):
(a) the 3D source method used by Brown et al;
(b) the present method.

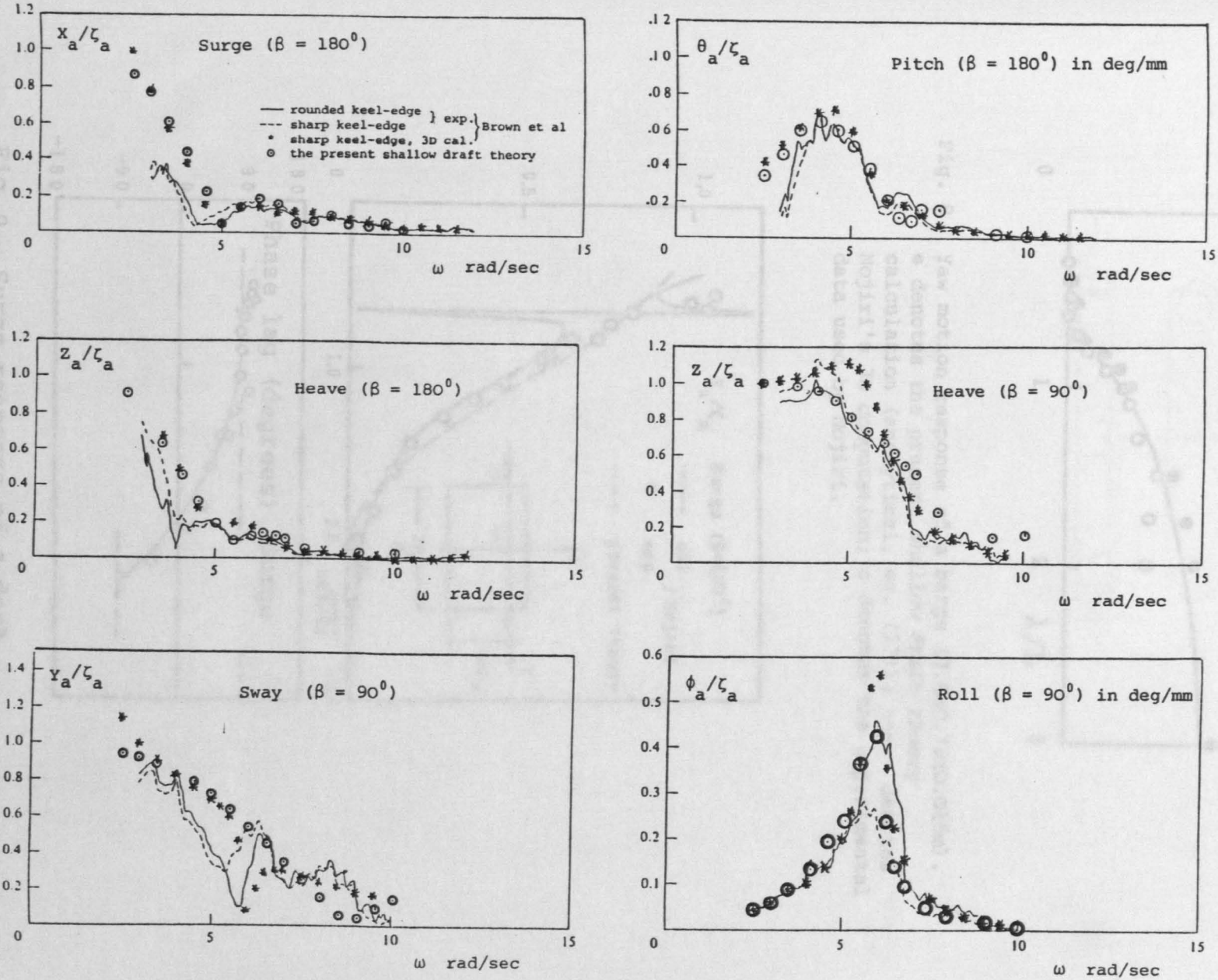

Fig. 7 Motion amplitude operators of a barge of length L= 2.40m, breadth B=0.80m and draft h=0.105m. ⊙ denotes the present shallow draft theory calculation; * denotes Brown et al's 3D source method calculation; —— and ---- denote Brown et al's experimental results for barges of rounded and sharp keel respectively.

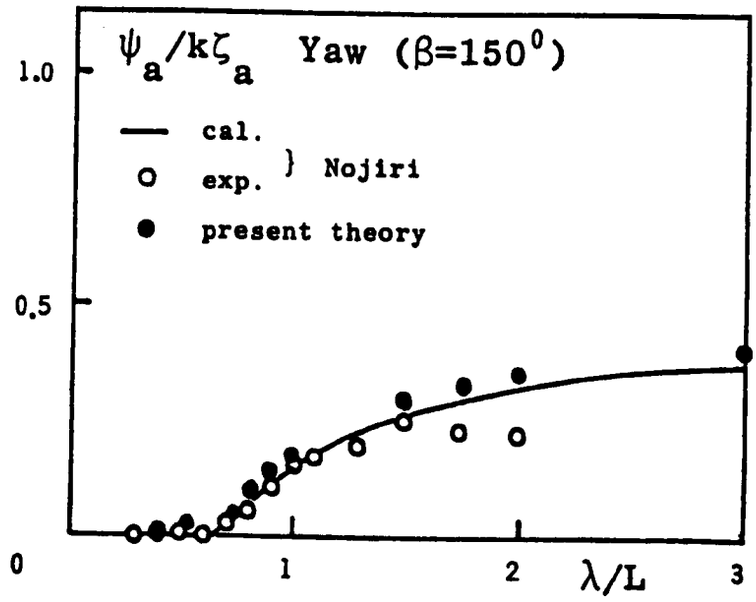

Fig. 8 Yaw motion response of a barge (3.0x0.75x0.015m). • denotes the present shallow draft theory calculation (analytical, eq. (27)); ——— denotes Nojiri's 3D computation; o denotes the experimental data used by Nojiri.

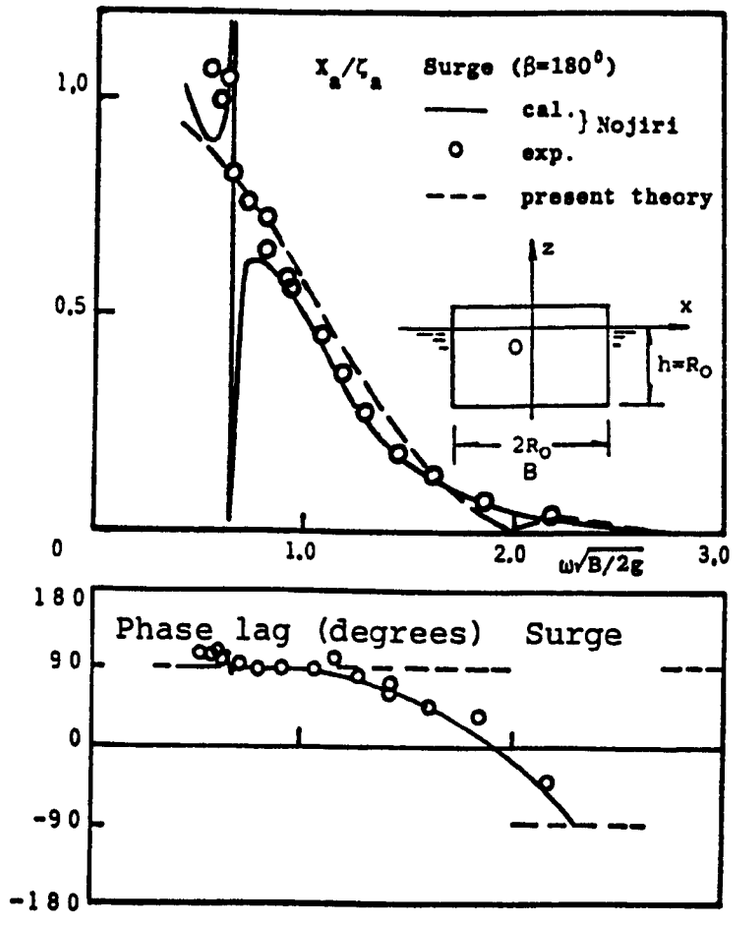

Fig. 9 Surge response of a dock.

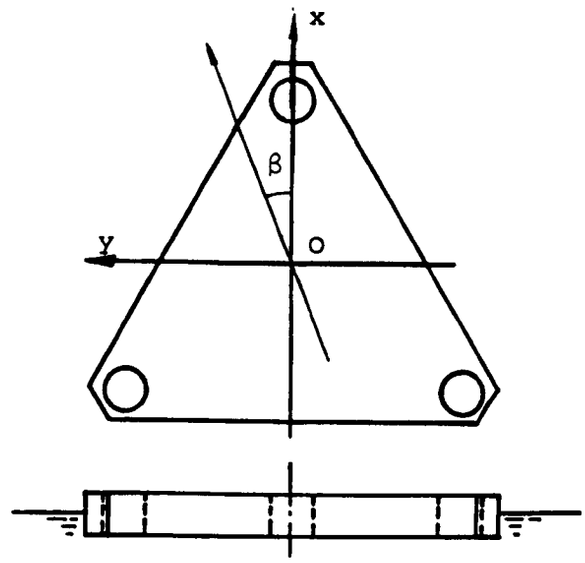

Fig. 10 A triangular platform.

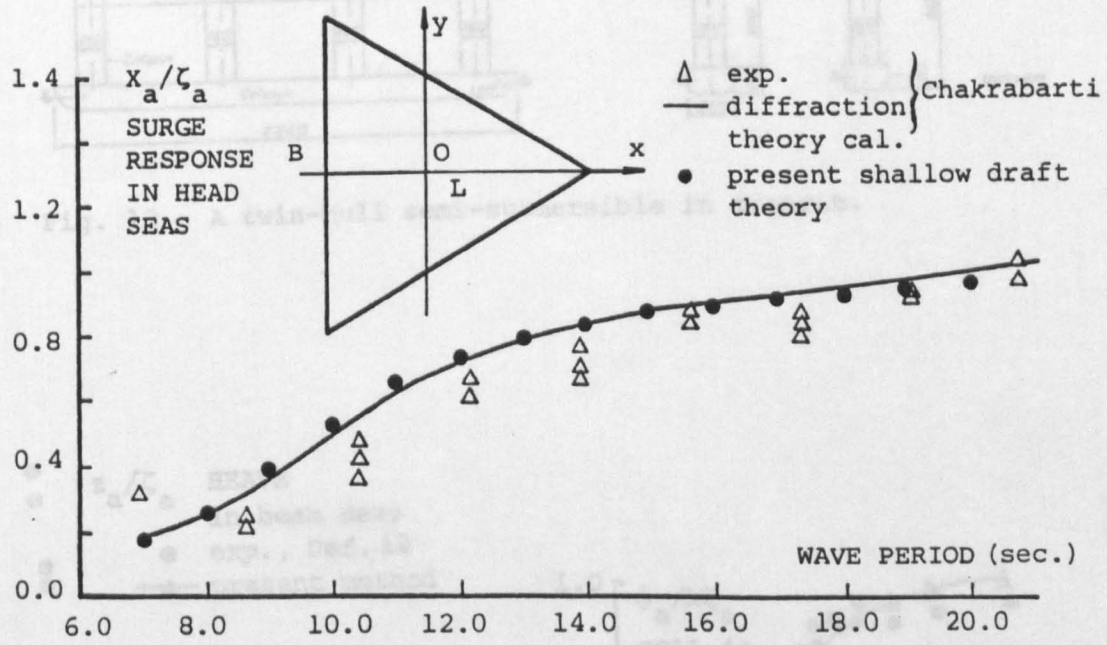

Fig. 11 Surge response of a triangular platform of length L = 108m, width B = 124.6m and draft h = 3.05m.

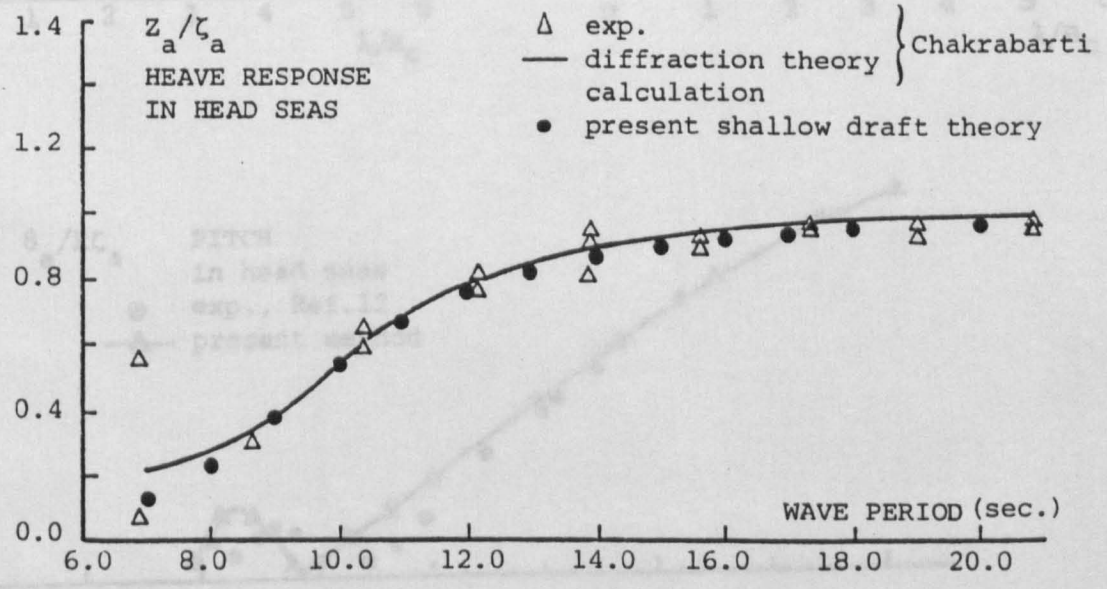

Fig. 12 Heave response of a triangular platform of length L = 108m, width B = 124.6m and draft h = 3.05m.

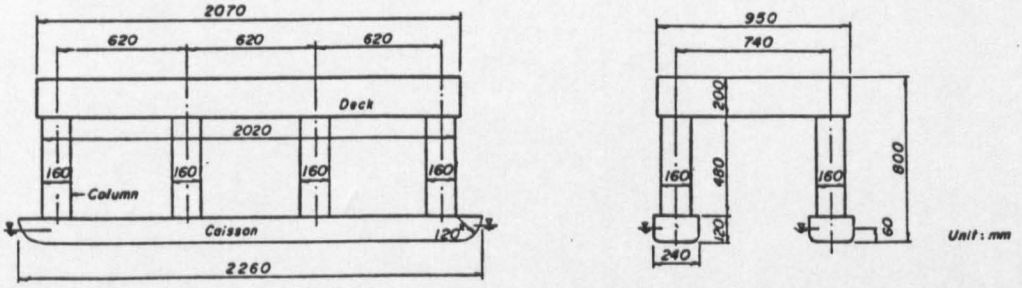

Fig. 13 A twin-hull semi-submersible in transit.

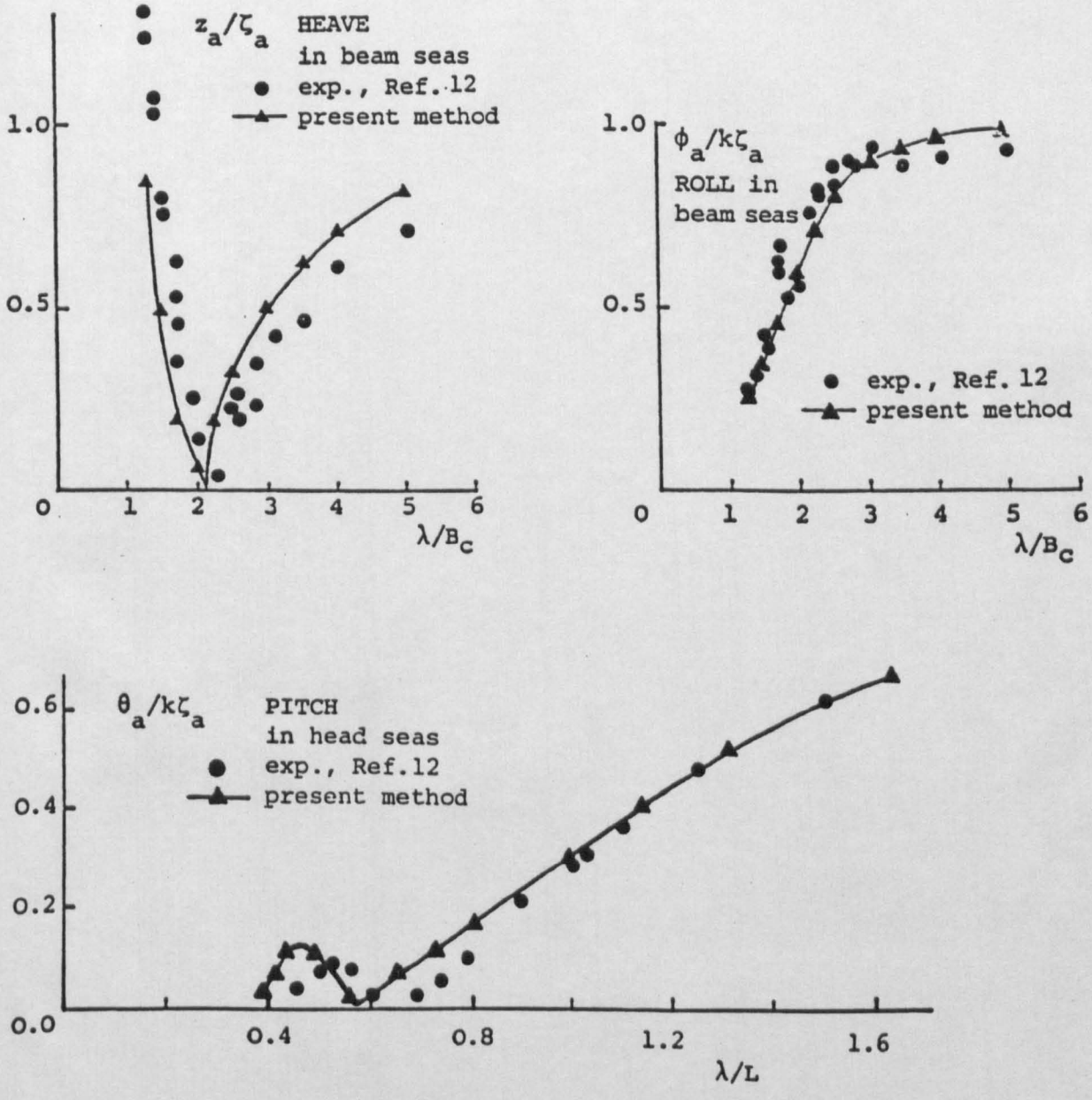

Fig. 14 Heave, roll and pitch responses of the semi-submersible in transit.